

WP2 – Deliverable 2.11

Report on the regional hydrogeology of the three study areas

Paris Basin – France
Lusitanian Basin – Portugal
Ebro Basin – Spain

Release Status: Final version

Edited by Frédéric Mathurin and Mark Wilkinson

Authors: Frédéric Mathurin, Julio Carneiro, Julio López-Gutiérrez, Catarina Matos and Ivan Moreno.

Date: September 2023

Filename and Version: D2.11_Regional_Hydrogeological_Systems_Final

Project ID Number: 101022664

PilotSTRATEGY (H2020- Topic LC-SC3-NZE-6-2020 - RIA)

1. Document History

1.1 Location

This document is stored in the following location:

Filename	D2.11_Regional_Hydrogeological_Systems_Final
Location	https://pilotstrategy.eu/about-the-project/work-packages/geo-characterisation/Task2.6_Hydrogeology

1.2 Revision History

This document has been through the following revisions:

Version No.	Revision Date	Filename/Location stored:	Brief Summary of Changes
Version 0	July 25 th , 2023		Initial draft
Version 1	August 7 th , 2023		Edited MW, WP leader
Version 2	August 14 th , 2023		Edited FM, task leader, Proof reading, all co-authors
Pre-final version	Spetember 22 th , 2023		Minor comments from Coordination review
Final Version	September 24 th , 2023		Final deliverable

1.3 Authorisation

This document requires the following approvals:

AUTHORISATION	Name	Signature	Date
WP Leader	Mark Wilkinson	MW	7 Aug 2023
Project Coordinator	Fernanda de Mesquita Lobo Veloso	F.MLV	22 Sept 2023

1.4 Distribution

This document has been distributed to:

Name	Title	Version Issued	Date of Issue
		Public report	25/09/2023

© European Union, 2023

No third-party textual or artistic material is included in the publication without the copyright holder's prior consent to further dissemination by other third parties.

Reproduction is authorised provided the source is acknowledged.

Mathurin F., Carneiro, J., López-Gutiérrez, J., Matos, C., Moreno, I. and Wilkinson, M., 2023. Deliverable 2.11 – Report on the regional hydrogeology of the three study areas: Paris Basin (France), Lusitanian Basin (Portugal) and Ebro Basin (Spain). EU H2020 PilotSTRATEGY project 101022664, 147 pp.

Disclaimer

The information and views set out in this report are those of the author(s) and do not necessarily reflect the official opinion of the European Union. Neither the European Union institutions and bodies nor any person acting on their behalf may be held responsible for the use which may be made of the information contained therein.



2. Executive summary

This deliverable is part of the geo-characterization work package (WP2) of PilotSTRATEGY and focuses on the regional hydrogeological systems of each of the three regions selected for full characterization of the storage complex, in the Paris Basin (onshore France), the Lusitanian Basin (offshore Portugal) and the Ebro Basin (onshore Spain). The report provides a description of the regional aquifers (permeable units) within each studied onshore sedimentary basin from the target reservoir to the surface. When the targeted reservoir is located offshore, the review uses the onshore hydrogeological system as a proxy for the offshore storage area.

Based on current knowledge and available data, this document presents the geological, structural and hydrogeological characteristics of the hydrogeological units within the prospect areas, and focuses on their geographical extent, regional flow, and their hydrodynamic properties. The thermal and hydrogeochemical characteristics of the fluids and societal use of the hydrogeological units are also documented. The characterization of the aquitards (semi-permeable units) and aquicludes (confining units) is considered – whenever enough data exists – within each studied sedimentary basin in order to get an overview of the 3D hydrosystems of interest.

The availability of hydrogeological data and related information varies from region to region and is usually dependant on the regional development and the past use of the underground natural resources. Societal use or management of the hydrogeological system for underground energy or groundwater resources has resulted in exploration projects, the drilling of wells and data acquisition, which contribute to the knowledge of the regional hydrogeological system. The knowledge of the regional hydrosystem varies greatly according to the complexity of the system, the depth of the hydrogeological units and the location (onshore or offshore).

In the Paris Basin, the regional hydrogeological system includes all geological formations from the Dogger reservoir (middle Jurassic) to the outcropping Paleogene sedimentary deposits. In the prospect area, located near the center of the sedimentary basin, the 2000 m thick hydrosystem is made up of a succession of thick aquifers units – many of which are multilayer aquifers – and aquicludes/aquitards units. Five major aquifer units are present, from the bottom to the surface: (i) the Dogger (Bathonian and Callovian) limestones, which are the target reservoir for CO₂ storage, (ii) the Oxfordian (Lusitanian) limestones and/or sandstones, the Early Cretaceous sandy (iii) Neocomian and (iv) Albian aquifers and the (v) Paleogene aquifer composed of the undifferentiated Lutetian, Saint Ouen and Champigny limestones. The Tithonian limestones and the Late Cretaceous Chalks, generally considered as productive aquifer units in the border of the basin – i.e. where the formations crop out to the surface (unconfined aquifer) – are considered as aquitard units in the center of the sedimentary basin due to low permeability. The aquiclude units, namely the (i) Callovo – Oxfordian argillites to marls, (ii) the Kimmeridgian marls to clayey limestone, (iii) the Barremo-Aptian argillites to sandy marl, (iv) the Ypresian argillites and (v) Late Eocene and Oligocene marls, delimit and separate vertically the main aquifers within the basin.

Broadly, the available data and existing studies differentiate the Jurassic deep saline aquifers from the Cretaceous and Paleogene freshwater aquifers. The historical development of geothermal resources in the Paris metropolitan region, combined with oil exploration in the center of the basin provide a large set of hydrogeological information in the deepest formations of interest. The high demand for water prompted the historical use of the fresh groundwater resource in the Paris metropolitan region and has provided large hydrogeological insights. In that respect, each aquifer unit has been the object

of a detailed description, taking into account the specific hydrogeological features of the multi-layer aquifers and the vertical drainage processes within the relatively thin-to-moderately thick aquiclude/aquitard units at the sedimentary basin scale.

The information about the hydrogeological system enables the definition of the conceptual boundaries of the storage site and the storage complex in the PilotSTRATEGY study area. The prospective storage pilot site is composed of the reservoir (*Oolithe Blanche*, Comblanchian and *Dalle Nacrée* formations) and the Callovo-Oxfordian caprock (marls) as the primary reservoir-seal unit. The boundaries of the French prospect area, defined as the prospect area of the storage site, shall be extended to define the storage complex. Laterally, the different oil field concessions surrounding the PilotSTRATEGY study area shall be included within the storage complex in order to consider the associated past and ongoing production and injection activities within the reservoir in dynamic models (to be addressed in WP3). Although relatively remote from the prospect area, the occurrence of subvertical faults, which intersect both the Jurassic and Cretaceous formations, require the uppermost boundary of the storage complex to be extended to the Late Barremian and Aptian clayey and marly formations, underlying the Albian aquifer (Early Cretaceous). The Barremo-Aptian aquiclude unit (ultimate seal), together with the underlying aquifers (secondary reservoirs) and aquitard/aquiclude units (secondary seals), contribute to ensure the safety of the CO₂ storage site by preventing any impact on the Albian aquifer, which is the deepest and nearest strategic freshwater aquifer from the target reservoir in the center of the Paris basin.

In the Lusitanian Basin, the target reservoir for the CO₂ storage pilot is located offshore, at a distance of 18 to 20 km from the coastline. A description of the onshore hydrogeological features has been made to understand the interaction between the reservoir (the Torres Vedras Group, and Aptian/Albian siliciclastic sedimentary sequence) and any aquifers, aquitards, and aquicludes that may overlie it offshore.

The structural complexity of the Lusitanian basin, influenced by salt diapirism, normal faulting throughout the Mesozoic, and reactivation during the Alpine orogeny, resulted in several sub-basins. In a subdivision of the Mesozoic, groundwater is produced from multiple locally and regionally important freshwater aquifers. This report describes only those Cretaceous and Tertiary aquifers that are present in the coastal area, not because of any risk imposed by CO₂ storage (to be addressed in WP5) but because their characteristics should be similar to those of the offshore site. Aquifers in the Quaternary formations, which are locally important, were not analysed since they cannot provide insight to the offshore storage site.

Accordingly, the aquifer systems described are: i) the Aveiro Cretaceous aquifer system; ii) the Figueira da Foz aquifer and; iii) the Louriçal aquifer. In every case, they are multilayered aquifer systems, in which groundwater abstraction is conducted from multiple productive layers ranging from the Aptian/Albian siliciclastic deposits that are the lateral equivalents of the offshore reservoir, to the Upper Cretaceous (Coniacian-Santonian) Upper Coarse Sandstones. The Louriçal multilayered aquifer encompasses an even longer sequence, extending from the Aptian/Albian up to the Miocene.

The Aveiro Cretaceous aquifer is, by and large, the best well studied aquifer in the north sector of the Lusitanian basin, with two higher salinity aquifer layers (Base aquifer and Intermediate aquifer) in Aptian/Albian deposits; these are separated from a lower salinity productive Main aquifer in top Aptian/Albian to Late Cretaceous strata. The differences in groundwater salinity between the Base, Intermediate and Main aquifers are explained by the aquitard properties of clay layers that have been described at the base and top of the Intermediate sequence.

These Cretaceous aquifers are topped by the Aveiro Sandstones and Clays Formation (Upper Cretaceous), a thick layer with aquiclude properties that provides excellent sealing capacity and that, at least locally in the Lourical aquifer, is overlaid by a Paleogene sequence that also acts as an aquitard.

Hydraulic parameters and productivity data were gathered for the multilayered aquifer systems, although usually not in enough detail to distinguish the relative importance of each productive layer, as wells are usually screened in multiple productive layers. Nevertheless, these values are highly relevant, given the almost complete absence of hydraulic data about the offshore Early Cretaceous. Regrettably, it was not possible to identify any published or publicly available data about the properties of aquitards and aquicludes.

The general sequence of the Cretaceous aquifers is confirmed in the three aquifers described, although the quality of the data for the Figueira da Foz and the Lourical aquifers does not allow the differentiation of the Base, Intermediate and Main aquifers. Overall, the sequence seems to be replicated in the petroleum exploration boreholes in the offshore part of the north Lusitanian basin.

Regarding the definition of the storage complex, the onshore hydrogeological system provides three relevant considerations: i) the need to confirm offshore, the existence of the intraformational clay layers that onshore act as aquitards to the Base, Intermediate and Main aquifers. This will have implications for the modelling of the storage complex and for the design of the CO₂ storage pilot; ii) carefully assess the hydraulic role of the Cacém formation in the offshore, since its onshore lateral equivalent (the Costa de Arnes Limestones) in some instances acts as a productive groundwater layer (when at shallow depths and near to the outcropping areas), while in other instances as an aquiclude (specially at higher depths, closer to the coastline). Both onshore groundwater wells and offshore petroleum exploration boreholes show that the base of the formation has a higher clay and marly content, granting it better qualities as a seal. The lateral evolution of this formation to the offshore is essential to understand its role as the primary seal to the offshore reservoir; iii) the Upper Cretaceous Sandstones and especially the Aveiro Sandstones and Clays formation, play an important role to define the storage complex, and overall to guarantee the safety of the CO₂ storage site, with the former providing an important secondary reservoir in case of leakage from the Torres Vedras Group, and the latter having excellent capacity as a secondary seal. Their integration (if confirmed with the same characteristics offshore) in the storage complex is highly recommended.

In the Ebro Basin, the interest is focused on the deep Triassic hydrogeological system. The top of the Triassic is 850 m deep at the crest of the Lopín structure (Upper Triassic) and the storage formation (Lower Triassic) depth ranges between 1250 m and 2000 m. The Triassic system is hydraulically disconnected from the regional hydrogeological upper system that is Lower Jurassic to Cenozoic in age. The only exception is at the discharge zone of the Triassic strata, located 90 km to the NE of the Lopín structure, where vertical ascending flow is interpreted. No water uses are identified in the Triassic system, as the main exploited aquifers in the area are the carbonate Jurassic formations (Lias and Dogger).

The target reservoir aquifer corresponds with the Buntsandstein facies B1 (*Aranda* formation) and B2 (*Carcalejos* formation), which are sandstones and conglomerates, with an average thickness of 127 m. The primary top seal is the Röt facies (*Rané* formation), 5 - 98 m thick, which is shales, marls and anhydrite at the top of the Buntsandstein facies. There are two additional seals: 1) Muschelkalk M2 facies, a local seal of evaporites and shales, whose thickness in the Ebro basin ranges between 17 and 323 m; 2) Keuper facies (regional caprock) of shales, salts and anhydrite. For the whole basin the thickness varies from 15 to 895 m. In the Lopín-1 borehole these secondary seals are 445 m thick.

With respect to the structural features, the overall gravimetric-seismic modelling supports the interpretation of the Lopín structure as a succession of horsts and grabens, where the faults that limit those structures only affect the Paleozoic basement, Buntsandstein and Muschelkalk, but do not dissect the regional caprock of the Keuper facies.

With respect to the flow of the Triassic hydrogeological system, an existing numerical model (Feflow variable density transient model) shows that fresh water is not commonly found at depth greater than 500 m. These results are in line with the data obtained in oil drilling. From 500 to 1000 m, salinity reaches a pseudo-stationary regime and no important variations are expected. Additionally, considering the mineralogy of Units B1 and B2, which are dominated by quartz, feldspar and muscovite, the high salinities found in the Buntsandstein storage formation, where no evaporite lithologies are present, only can be explained if the transit period of the fluids is extremely long, as concluded from the numerical model. This scenario implies that the injected CO₂ plume would barely travel towards the discharge zone, located about 90 kilometers NE, in the discharge area, close to Lérida (Lleida) city.

In the Ebro basin, a total of six aquifers are present in the prospect area, from the base to the top: 1) Triassic Buntsandstein; 2) Triassic Muschelkalk 1; 3) Triassic Muschelkalk 3; 4) Subliassic-Rhaetic; 5) Jurassic Liassic-Malm; 6) Quaternary fluvial-alluvial deposits. Five aquicludes from the base to the top are: 1) Triassic – Röt facies (primary seal); 2) Triassic – Muschelkalk 2 (local seal); 3) Triassic – Keuper facies (regional seal); 4) Lower Lias – Anhydrite 5) Upper Malm (Jurassic) – Lacustrine marls. At a regional scale, the whole Cenozoic is considered as an aquitard, since it is a succession of medium to low permeability layers. Nevertheless, at a local scale, there may exist small and very poor aquifers that were exploited in the past by means of shallow handmade wells, associated with thin transmissive detrital layers. No groundwater masses are defined in those areas where Cenozoic sediments are predominant and where the Jurassic aquifer is too deep to be exploited.

The Spanish storage site considered in the project is mainly composed of the reservoir Buntsandstein facies B1 (*Aranda* formation) and B2 (*Carcajejos* formation) plus the Röt facies (*Rané* formation) shales, marls and anhydrite as the reservoir seal unit. The boundaries of the storage complex shall include the regional extended seal formation (Keuper facies) and the interpreted discharge zone of the Triassic system (from the numerical Feflow model), located 90 km NE away from the Lopín structure, in the direction of the groundwater flow. With respect to the occurrence of subvertical faults in the storage site, they do not dissect the Keuper facies that is the ultimate seal unit in the Spanish prospect area, preventing potential impact on the Jurassic aquifer that is the main strategic aquifer in this sector of the Ebro basin.

In the framework of the objective of the PilotSTRATEGY project, the detailed hydro-geo-characterization presented in this report provides the hydrogeological context taking into account the specificities of each region. This background information and the definition of the conceptual boundaries of the storage complexes supply qualitative and quantitative insights and general guidance to be considered in the dynamic modeling (WP3), the detection of environmental impact and associated risks (WP5) and possibly the social acceptance (WP6). These complementary work packages will contribute, in turn, to the preparation of the legal and technical proposals for the deployment of pilot facilities.

Table of Contents

1. Document History	2
1.1 Location	2
1.2 Revision History	2
1.3 Authorisation	2
1.4 Distribution	2
2. Executive summary	4
3. Introduction	11
4. Material and Method	12
5. Paris Basin – France	14
5.1 Overview of the Paris Basin	15
5.2 Main aquifers, aquitards and aquicludes of the Paris Basin	17
5.3 Dogger formations	21
5.3.1 Geological features of the formations	21
5.3.2 Distribution and extent of the aquifer, aquitard and aquiclude units	22
5.3.3 Hydrogeological properties	25
5.3.4 Features of the pristine fluid	29
5.3.5 Occurrence of faults	30
5.3.6 Societal use of the formation in the study area.	30
5.4 Malm formations	32
5.4.1 Geological features of the formation	32
5.4.2 Distribution and extent of the aquifer, aquitard and aquiclude units	33
5.4.3 Hydrogeological properties	36
5.4.4 Features of the groundwater	38
5.4.5 Occurrence of faults	39
5.4.6 Societal uses of the formation.....	39
5.5 Early Cretaceous formations	40
5.5.1 Geological features of the formation	40
5.5.2 Distribution and extent of the aquifer, aquitard and aquiclude units	41
5.5.3 Hydrogeological properties of the aquifer	43
5.5.4 Features of the groundwater	48
5.5.5 Occurrence of faults	50
5.5.6 Societal uses of the formation.....	50

5.6	Late Cretaceous formations	51
5.6.1	Geological features of the formation	51
5.6.2	Distribution and extent of the aquifer, aquitard and aquiclude units	52
5.6.3	Hydrogeological properties of the aquifer	53
5.6.4	Groundwater composition	55
5.6.5	Occurrence of faults (if any)	56
5.6.6	Societal uses of the formations	56
5.7	Paleogene formations	57
5.7.1	Geological features of the formation	57
5.7.2	Distribution and extent of the aquifer, aquitard and aquiclude units	60
5.7.3	Hydrogeological properties of the aquifer	60
5.7.4	Groundwater composition	62
5.7.5	Occurrence of faults	62
5.7.6	Societal uses of the formation.....	63
6.	Portugal – Lusitanian Basin	64
6.1	Overview of the Lusitanian Basin	66
6.1.1	General sedimentary sequence.....	67
6.1.2	Aquifer systems in the north sector of the Lusitanian basin.....	69
6.2	Aveiro Cretaceous aquifer System – O2.....	72
6.2.1	Geological features of the aquifer.....	72
6.2.2	Hydrogeological properties of the aquifer	75
6.2.3	Features of the groundwater	79
6.2.4	Conceptual model and occurrence of faults	81
6.3	Figueira da Foz – Gesteira aquifer system (O7).....	82
6.3.1	Geological features of the aquifer.....	82
6.3.2	Hydrogeological properties of the aquifer	83
6.3.3	Groundwater composition	85
6.3.4	Conceptual model and occurrence of faults	86
6.4	Louriçal aquifer system (O29).....	86
6.4.1	Geological features of the formation	87
6.4.2	Hydrogeological properties of the aquifer	88
6.4.3	Groundwater composition	91
6.4.4	Conceptual model and occurrence of faults	91
7.	Spain – Ebro Basin	93

7.1	Overview of the Ebro Basin	96
7.2	Hydrogeology of the Triassic system	98
7.2.1	Buntsandstein formation: the target reservoir	101
7.2.2	Muschelkalk M1 formation	122
7.2.3	Muschelkalk M3 formation	127
7.3	Jurassic Formations.....	131
7.3.1	Geological features of the formation	131
7.3.2	Hydrogeological properties	131
7.3.3	Features of the groundwater	133
7.3.4	Occurrence of faults	134
7.3.5	Societal uses of the formation.....	135
7.4	Cenozoic and Quaternary formations – a multilayer detrital aquifer	136
7.4.1	Geological features of the formations	136
7.4.2	Hydrogeological properties	137
7.4.3	Occurrence of faults	138
7.4.4	Societal uses of the formation.....	138
7.5	Aquicludes in the Ebro Basin	139
8.	Hydrogeological boundaries of the storage sites and storage complexes	141
8.1	Storage complex in the Paris Basin.....	142
8.2	Storage complex in the Lusitanian Basin	144
8.3	Storage complex in the Ebro Basin	146
8.4	Conclusion	147
9.	References.....	148

3. Introduction

The European project “CO₂ Geological Pilots in Strategic Territories” (PilotSTRATEGY project) aims to prepare legal and technical documents for the deployment of pilot facilities for geological storage of CO₂ in deep saline aquifers in five industrial regions in Southern and Eastern Europe. The legal and technical proposals will rely on multidisciplinary aspects, including a detailed geo-characterization, static and dynamic modeling, detection of environmental impact and associated risks and social acceptance, and taking into account the specificities of each region. The studied regions were selected after detailed screening of multiple storage sites in the European STRATEGY CCUS project. Three regions were selected for full characterization of the storage complex – in France, Portugal and Spain, respectively – and two regions for enhancement of knowledge on the existing storage capacity – in Poland and Greece.

Within work package (WP) 2, the geo-characterisation of each of the prospective regions will result in a 3D multidisciplinary characterisation of the storage site and storage complex, i.e. including the reservoir, the overlying caprocks, and the surrounding area. This deliverable focuses on the current knowledge of the regional hydrogeological system of each of the three most promising regions, located in the Paris Basin (onshore area; France), the Lusitanian Basin (offshore area; Portugal) and the Ebro Basin (onshore area; Spain).

The hydrogeological description aims to document the characteristics of the regional aquifers (permeable units), focusing on their geological characteristics and geographical extent, as well as their respective hydrogeological, hydrodynamic, thermal and hydrogeochemical properties. Whenever enough data exists, aquitards (semi-permeable units) and aquicludes (confining units) within each studied sedimentary basin are also characterized. The review covers both the deep geological formations and the intermediate-to-shallow formations. For the onshore reservoirs, this will provide a complete understanding of the regional flow and potential discharge or recharge of fluids within and/or between the different hydrogeological units within the hydrosystem, from the target reservoir to the surface. When the targeted reservoir is located offshore, the review uses a nearby onshore area as a proxy to gather knowledge about the hydraulic properties from the shallower onshore aquifers that can be of use in characterising the deeper offshore CO₂ storage reservoir.

The regional hydrogeological systems are presented individually and cover a more or less large number of aquifers, aquitards and aquicludes in the different study areas. The current level of knowledge of the hydro-properties of the Mesozoic-Cenozoic sedimentary basins depends on the location of the site (i.e. whether onshore or offshore), the level of groundwater usage that prompted previous hydrogeological studies and the amount of associated existing data. Moreover, the poor or high level of hydrogeological connections and the existence of complex geological structures within the sedimentary basins may result in more or less complex local hydrogeological systems, with the same sedimentary formation defining different hydrogeological basins. From the perspective of deploying pilot facilities for geological storage of CO₂, the definition of the storage site and storage complex are discussed for each region, integrating the understanding of the regional hydrosystems and the gaps identified in the current knowledge.

4. Material and Method

The regional hydrogeological system is described from the compilation of studies carried out at the sedimentary basin scale (e.g. geothermal potential) or as part of various local studies (e.g. oil prospecting, hydrogeological studies). Relying on public reports, PhD thesis and scientific articles, this report summarizes the current state of hydrogeological knowledge in the three regions of study. Only public data and public studies are reported and listed in the bibliography.

The geological formations making up the onshore sedimentary basins or the basin sectors close to the proposed offshore CO₂ storage pilot were the subject of an in-depth literature review with respect to the main features of the aquifer, aquitard and aquiclude units, generally organized around four main components:

- the general geometry, extent and petrophysical properties of the each formation: top depth, thickness, occurrence of fractures/faults, porosity, permeability;
- hydrodynamic characteristics: the hydraulic head, direction of groundwater flow, recharge area, discharge area, hydrostatic behavior, transmissivity and hydrostatic behavior of the aquifer;
- features of the fluid: temperature, salinity, chemical composition;
- societal use and anthropogenic features: existence of wells/boreholes, geothermal facilities, oil and gas concessions, exploitation of the groundwater.

Data quality and quantity in each of the three studied areas varies considerably, which is reflected in the approach undertaken in each of the regions. The Paris Basin, which has seen oil production and geothermal exploitation, has much more detailed information about deep geological formations than the onshore Ebro and Lusitanian basins. Furthermore, the CO₂ storage pilot in the Portuguese Lusitanian basin is located offshore, where no data about the hydrogeological behavior exists (except from one oil exploration borehole – see PilotSTRATEGY Deliverable D2.7 (Wilkinson, 2023)). Accordingly, all the data used in this report for the Portuguese area are indirect information from the onshore geological formations that are thought to compose the CO₂ storage complex, located more than 20 km away in a structurally complex sedimentary basin.

With respect to the general extent of the aquifers, aquicludes and aquitards in the sedimentary basin, the characterization relies on the interpretation of available cross-sections, well logs, geophysics and correlation between wells in the basin and the extended area of interest. Petrophysical properties (porosity, permeability) are from the inversion of borehole resistivity measurements and/or measured on rock samples taken by core sampling in productive wells. However, only geological horizons deemed to be interesting (i.e. for exploration and production) were considered, involving a potential bias in the dataset of the deepest formations – when data exist.

The hydrodynamic properties of the aquifers, such as the static level of the water table that reflects its natural regional flow, were characterized using static pressure measurements and hydraulic head measurements. Static pressure measurements are usually less precise for oil wells in deep formations. Maps of isostatic level of the water table were generally produced using pressure values in geothermal wells and piezometric levels in strategic aquifers for fresh water supply. The transmissivity values across the formation were retrieved from flow tests, including short formation tests during drilling and long duration aquifer/reservoir production tests after drilling. Overall, transmissivity is mainly studied at a local scale (i.e. well scale). For aquifers with large datasets, average transmissivity values were retrieved from existing dynamic (hydrogeological) models. When not possible, a simple

comparison with the permeability values (and net productive thickness) inferred from well tests were used to define the order of magnitude of the regional transmissivity in the formation of interest. Overall, only a few hydrodynamic values were available for the aquitards or aquicludes, which are of lower industrial or societal interest. Within the sedimentary basins of interest, only the Callovian-Oxfordian argillites and clayey marls (aquiclude) have been characterised in – specific regions of – the Paris Basin, for underground storage purposes of gas (i.e. as the caprock of the facility) and nuclear wastes (i.e. as a natural confining barrier).

The fluid temperature, salinity and composition can vary substantially at the basin scale. Temperature measurements were obtained either by in situ measurements (bottom hole temperature), surface measurements from production wells at the regional scale, or by estimation based on an approximate geothermal gradient for the formation at the basin scale. The temperature, salinity and chemical measurements come mainly from water wells and geothermal boreholes (if any) in the basin. The salinity values retrieved from oil well results are generally chloride anions analyses in the water phase, an approximation of the salinity. Such approximation remains valid for aquifer with water of Na-Cl type, but can deviate from the total salinity (Total Dissolved Solid) for water with other dominant major ions. Moreover, most of the wells (i.e. oil, geothermal and water wells) pump from the uppermost part of the aquifer, preventing a consideration of any vertical salinity gradient – induced by density gradients – in thick aquifer formations.

The understanding of the main aquifers, aquitards and aquicludes, as well as their associated hydro-properties, are presented by geological epoch from the bottom to the top of the formations, meaning from the Middle Jurassic to the Paleocene in the Paris and Lusitanian Basins and from the Triassic to the Neogene in the Ebro basin.

5. Paris Basin – France

The study area of the PilotSTRATEGY project in France is located onshore in the Paris sedimentary basin, 55 km southwest of Paris city in the Ile de France region, called the Paris metropolitan region hereafter (Figure 5-1a). The area of interest is located in the southeastern part of the Brie plateau, on and nearby the Grandpuits-Bailly-Carrois county, near Nangis county (Figure 5-1c). The valley of the Marne River and the valley of the Seine River delimit the Brie area to the north (e.g. cities of Meaux) and the south (e.g. city of Melun), respectively (Figure 5-1c). The central part of the sedimentary basin is beneath the Brie area.

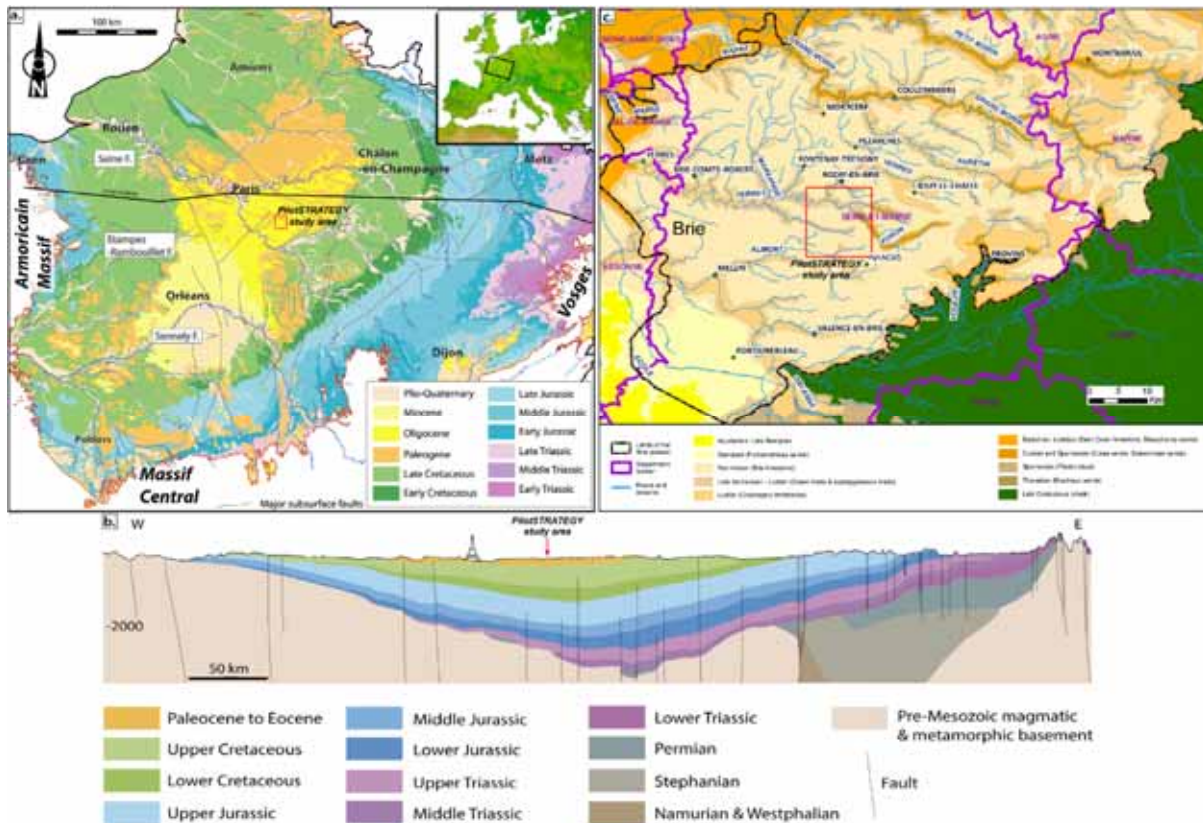


Figure 5-1. (a) geological overview of the Paris Basin featuring the major subsurface faults and (b) West-East cross section of the sedimentary basin (modified from Delmas et al. (2002) by Mas et al., (2022)). (c) geological overview of the Brie plateau (modified from Bellier (2013)).

Since the late 1950's, the Oil & Gas and geothermal prospecting have provided a large amount of geoscientific data in the center of the Paris Basin. The Brie area has been an area of significant oil exploration, with no less than 103 boreholes that intersected the entire hydrosystem down to the Dogger and Triassic formations. Although the activity has progressively slowed down since the 1980s, some wells are still in production. Since the 1970's, the deployment of geothermal energy in the Paris metropole contributed to further deep drilling (110 boreholes) in a new area of the sedimentary basin. The data acquired from geothermal production testing and geothermal doublets complemented the knowledge of the hydrodynamic properties of the deep saline aquifers gained from the oil exploration. Over the same period, the rapid population growth and industrialization of the Paris metropolitan region increased pressure on the water demand for domestic, industrial and agricultural water supply. The exploitation of the abundant groundwater resources in the Paris Basin, in freshwater aquifers, contributed to the economic development of the metropolitan region. The subsequently introduced

monitoring and regulation policy, when applied to the strategic groundwater resources, contributed to the regional knowledge of the intermediate to shallow freshwater aquifers.

The historical development of the Paris region and the progressive drilling of the boreholes make it possible to build an overall or comparative vision of the key features of the hydrogeological system at the regional-to-basin scale. The long lifespan (> 20 years) of certain oil wells and geothermal wells contributes to the confidence of the estimation the hydro properties and their relative stability over time in the Dogger aquifer, considered here as the main target reservoir for prospective CO₂ storage in the Paris Basin. Although the amount of data available for the deep aquifers is particularly noteworthy at the basin scale, most of the existing data were however collected in the uppermost part of the aquifers. The measurements in the lower part of the deep aquifers are generally too seldom to define general trends at the basin scale. Moreover, shallower (i.e. intermediate) geological formations were considered of lower interest in terms of energy or water supply potential at the time of drilling of the deep boreholes. Accordingly, only summary information exists regarding some of the intermediate hydrogeological units, even now.

5.1 Overview of the Paris Basin

In north of France, the Paris Basin is a large subsiding zone triggered by lithospheric cooling and gravitational loading mechanisms during the Permian-Triassic, initiated after the Variscan orogeny in northern Europe (Dewolf and Pomerol, 2005). The quasi – continuous sedimentation since the Mesozoic period contributed to form an intracratonic sedimentary basin. The Paris Basin, lying over a Paleozoic Variscan basement, is a sub-circular structure with an approximate radius of 350 km (110 000 km²) and made of a maximum thickness of about 3km of indurated sediments in its central part (Figure 5-1), located in the Brie area (40 km east from Paris). The sedimentary basin extends northwards below the English Channel.

The main sedimentary basin is delimited by Paleozoic outcrops, including the Armorican Massif at the western border, the Massif Central to the South-West, the Morvan to the South-East and the Vosges at the eastern border (Figure 5-1a). The basin is bordered by a deep (up to 5 km) basin with sedimentary deposits of Stephanian (Carboniferous) and Permian age on the easternmost boundary (Figure 5-1b). The present-day geometry of the basin, with its characteristic distribution of the outcrops in concentric rings, is attributed to the major uplift and erosion stages associated with the subsequent Pyrenean and Alpine compression, initiated during the Late Cretaceous.

The structures of the Paris Basin are complex because of inheritance from the successive Mesozoic extensional (i.e. Alpine Tethys, Atlantic Ocean and Bay of Biscay) and compressional Late Cretaceous-Cenozoic Pyrenean and Alpine orogenies (Mégnyen et al., 1980; Robin, 1995; Guillocheau et al., 2000). The basin was affected by the reactivation of Variscan faults at different geological periods (Graciansky and Jacquin, 2003; Andre, 2003). Among the regional faults, six major fault structures propagated both laterally and vertically through the entire sedimentary pile of the basin, including the (i) North-West to South-East Bray and Bouchy/Manoue faults, the (ii) East-West Vittel and (iii) Metz faults and the North-South (iv) Sancerre/Loire, (v) Sennely and (vi) Saint-Martin-de-Bossenay faults (Figure 5-2). These major faults, together with minor faults (Figure 5-1b), divided the sedimentary basin into several blocks (Figure 5-2) which locally-to-regionally affected the lateral continuity of the sedimentary layers and thus the extent of the aquifers. The PilotSTRATEGY study area is on the central block of the basin delimited to the North by the Bray – Vittel fault zone, to the west by the Seine –

Sennely fault zone and to the East by the Sillon houiller – Saint-Martin-de-Bossenay fault zone (Figure 5-2). At a regional scale, the Bouchy/Malnoue faults run in the Paris Region through the Brie area and separates the central block to the South-West, from the Rheno-Hercynian block to the North-East (Figure 5-2).

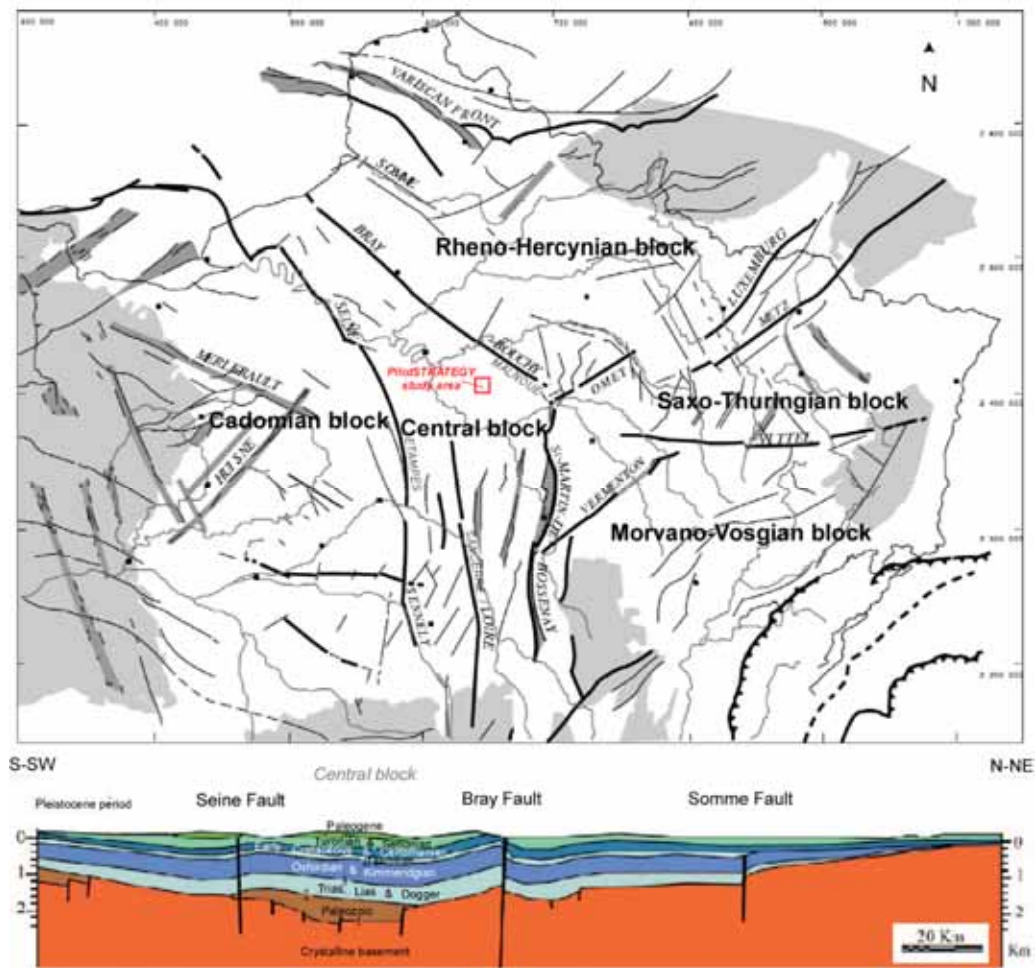


Figure 5-2. Regional subsurface faults structuring the five main blocks of the Paris Basin, map (top; adapted from Guillocheau et al. (2000)) and S-SW – N-NE vertical transect in the North of the basin (bottom; adapted from ANDRA, (2005)). The vertical exaggeration of the transect is a factor 10.

The stratigraphic sequence and the lithological features of the sediments in the Paris Basin form, along a vertical profile, an alternation of permeable layers (aquifer) separated from each other by impermeable layers (aquicludes) or semi-permeable layers (aquitards). Such a setting results in a complex multi-layered aquifer system made of more than one hundred aquifers and aquitards at the basin scale (Roux, 2006) when including the many different shallow and local unconfined aquifers.

The shallow unconfined aquifers are closely controlled by local characteristics, topography and streams and rivers, so that an exhaustive description of the shallow hydrosystem at the scale of the Paris Basin would result in an very long list of local mono-layer aquifers and aquitards. Hence, for a review of the Paris Basin hydrosystem suitable for the PilotSTRATEGY project, the following subchapters focus primarily on the main confined and unconfined aquifers, aquicludes and aquitards identified beneath the study area.

5.2 Main aquifers, aquitards and aquicludes of the Paris Basin

The Paris Basin is a series of sedimentary strata overlying pre-Triassic bedrock and bounded by rocks deformed in the Hercynian orogeny. Most of the groundwater resource comes from sedimentary formations of the Mesozoic, Tertiary and sometimes Quaternary eras (Figure 5-1c). The geology and morphology of these different layers, distributed on a basin-scale regularly in successive layers, delineate the different hydrogeological components of the Paris Basin.

In the region of interest, the top of the pre-Triassic bedrock, located along the western border of the basin, reaches up to 2930 m.b.s.l. and is overlaid by thick Keuper (Triassic) sandstones, i.e. 380 to 480 m thick (Figure 5-3). The Keuper sandstones are generally composed of two main fluvial bodies known as (i) the Donnemarie Sandstones lower body (coarse sandstone and conglomerate deposits) and (ii) the Chaunoy Sandstones upper body (finer sandstones). The uppermost Triassic (Rhaetian) consists of marls and dolomites, which continue into the Lias (Early Jurassic), where an alternation of clays or marls with clayey and often dolomitic limestones are found. Apart from the more clayey Liassic, the Jurassic sediments are dominated by carbonate platform facies, with limestones and marly carbonates commonly associated with clays. In the Lower Cretaceous, the sedimentation becomes more detrital with a return to carbonate in the Upper Cretaceous in the form of an alternation of limestone and chalk, then essentially chalky. The Paleogene is characterized by both detrital and carbonate sedimentation. This general lithological trend is summarized on the stratigraphic log of the Paris Basin (Figure 5-4).

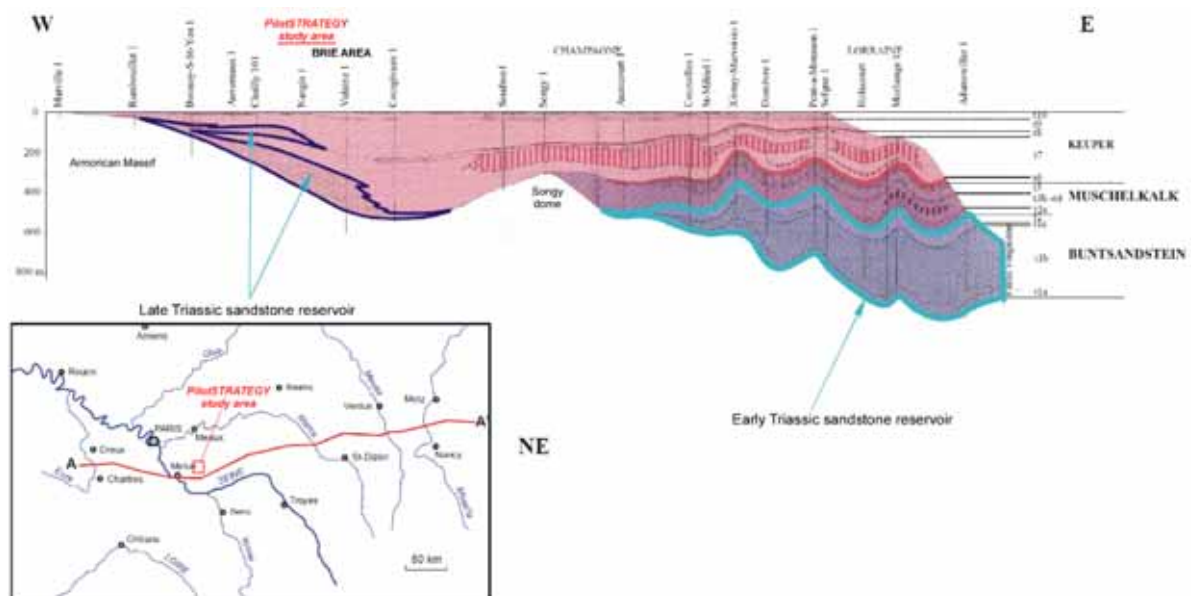


Figure 5-3. West-East cross-section of Triassic reservoirs in the Paris Basin (adapted from Mégnien et al.(1980)).

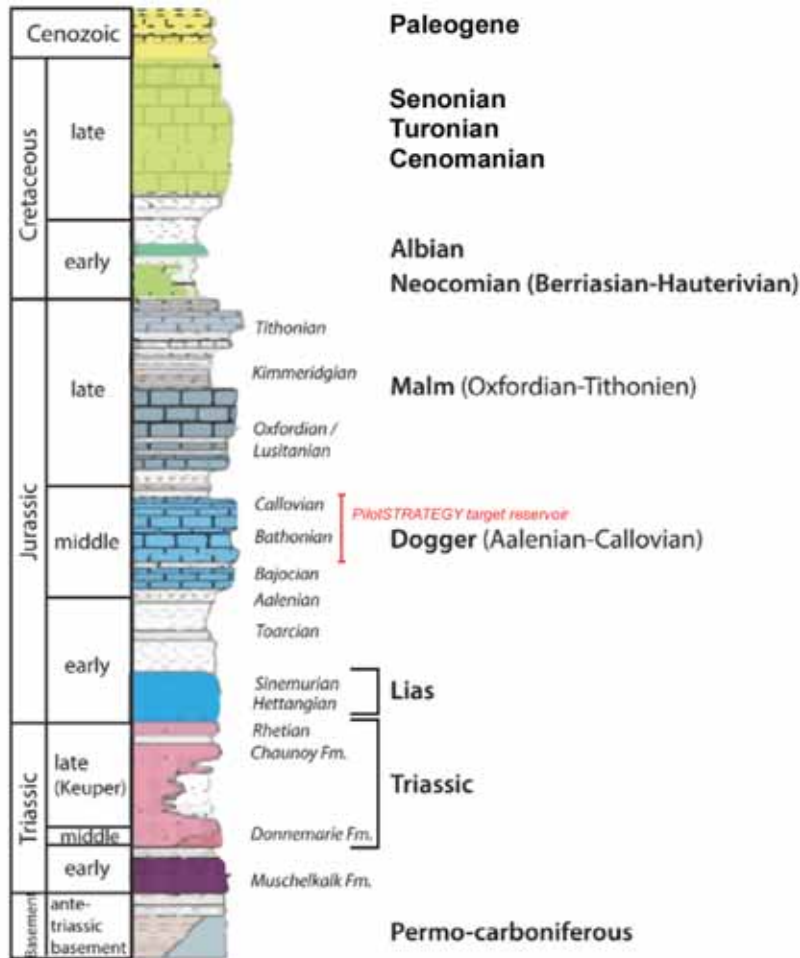


Figure 5-4. Stratigraphic and lithologic log of the Paris Basin with the major aquifers (colored) and aquitards (white) (adapted from Mas et al. (2022), after Delmas et al. (2002)).

The multilayered Paris Basin features many hydrogeological units: up to 15 geological formations with potential aquifer properties; up to 6 formations with potential aquitard properties and up to 17 geological formations with potential aquiclude properties (Table 5-1).

Table 5-1. Simplified lithostratigraphy and main aquifer, aquitard and aquiclude formations in the Paris Basin.

Geological period		Age	Aquifer formations	Aquitard formations	Aquiclude formations
Paleogene	Oligocène	Rupelain	Brie limestone		Marl Green Clay
	Late Eocene	Priabonian	Champigny limestones (multilayered aquifer)		Supra-gypsum marl Marl
	Mid Eocene	Lutetian	Lutetian coarse limestone	Marls and gravels	
	Early Eocene	Ypresian	Ypresian sand		Plastic clay
Cretaceous	Late Cretaceous	Senonian - Turonian	Turonian - Senonian chalk*	Chalk and gravel	
		Cenomanian		Chalk	Marly chalk - grey chalk
	Early Cretaceous	Albian	Albian clayey - gravel/sand		Gault Clay
		Late Barremian - Aptien			Clay - clayey-marl
		Hauterivian - Early Barremian	Neocomian/Wealdian gravel/sand		
		Valangian - Berrasian			Clay - clayey-marl
Jurassic	Malm	Tithonian	Early Tithonian limestone*	Purbeckian limestone Early Tithonian limestone	Tithonian marl
		Kimmeridgian			Marl - marly limestone
		Oxfordian to Kimmeridgian	Lusitanian limestone, sandstone		
		Oxfordian			Clay - clayey-marl
	Dogger	Callovian			Clay - clayey-marl
		Callovian-Bathonian	Dogger limestone		Marl
		Bajocian - Aallenian	Dogger limestone	Clayey limestone - marl	
	Lias	Toarcian - Pliensbachian			Clayey marl
		Sinemurian - Hettangian	Lias limestone, dolomite, sandstone		Anhydrite clays, marls and shales
	Trias	Late Trias	Keuper	Rhetian : marine sandstone,	
Chaunoy continental sandstone					
Middle Trias			Donnemie conglomerat and continental sandstone		

Unlike the Portuguese and Spanish sites, which both study the potential of Triassic sandstones, the reservoir of interest in the Paris Basin was focused on the Dogger limestones at an early stage of the project. Accordingly, this report focuses mainly from the Dogger limestones (reservoir) to the uppermost-unconfined aquifer in the Paris Basin. This includes most of the major confined aquifers, aquitards, and aquicludes that are widespread within the basin. The hydrosystem above the target

reservoir is highly influence by the hydro-properties, regional flow and hydraulic connections between the main aquifers – identified at basin scale –, including from the surface to the reservoir at the scale of the Paris Basin:

- the Paleogene multilayered aquifers: Lutetian, Saint Ouen and Champigny limestones and the uppermost Brie limestones;
- the Late Cretaceous chalks: Turonian and Senonian formations
- the Early Cretaceous sands: Neocomian (« Wealden »), Albian formations
- the Malm (Upper Jurassic) limestones and/or sandstones: Oxfordian (Lusitanian) and Tithonian formations;
- the Dogger (Middle Jurassic) limestones: main reservoir in this study.

It is noteworthy that some of the main aquifers listed above can be locally absent, poorly permeable or undifferentiated as single aquifers in certain parts of the basin. Such specific cases within the sedimentary strata of the PilotSTRATEGY study area are specified in the following subchapters, where the sequence of geological formations is further specified.

While a detailed description of the Triassic and Liassic aquifers and aquitards is out of the scope of this report, the deepest aquifers and aquitards of the basin are however considered with respect to their connection with the overlying Dogger limestone aquifers. The role of regional fault zones, which can connect aquifers, will be discussed qualitatively as the precise geographical extent of the tectonic structures and their quantitative impact on the hydrosystem remain poorly known.

5.3 Dogger formations

The Dogger (Middle Jurassic) platform is one of the deepest aquifers of the sedimentary basin. The platform is underlain by alternating limestones or dolomites with marlstones (Early Jurassic), and is overlaid by the Callovian and Oxfordian claystone and marls (Late Jurassic). Limestones dominate the Dogger formations, which form one of the main oil reservoirs in the Paris Basin, sourced from the organic-rich claystones of the Lias (Espitalie et al., 1987). The Dogger formations is the major deep aquifer and thus the prime reservoir for geothermal projects in the Paris area since the 1970's. Since 2005, the Dogger limestones have been studied by industrial and/or scientific consortiums to select and assess sites in the Paris Basin where geological storage of CO₂ could be tested at pilot scale (10³ – 10⁶ tons of CO₂ stored). Among the different projects, the ANR-GéoCarbone-PICOREF project (i.e. “Pléageage du CO₂ dans des Reservoirs géologiques En France”) focused partly on the characterization of the Dogger formations in the southeastern part of the Brie area (Champagne Region), located on the eastern part of the extended area of the sector prospected for the French site in the PilotSTRATEGY project. Therefore, the Dogger formations have been widely explored in the central part of the sedimentary basin and partly characterized in the Brie area.

As part of the Dogger formation is the target reservoir for the French site, the Dogger aquifer is subject to a thorough hydrogeological review, at both the basin and the regional scale. The Callovian marls, composing the upper part of the Dogger formations (Table 5-2), are shortly introduced in this subchapter (5.3.1), whereas their hydrogeological properties are described in the next chapter, together with the Oxfordian marls (i.e. Callovo-Oxfordian argillites/marls) as they both form the main caprock of the Dogger reservoir.

5.3.1 Geological features of the formations

The Dogger platform is present over the whole basin and approximately corresponds to the sequence of middle Jurassic limestones. There are six main geological formations (Table 5-2), the *Dalle Nacrée* (Early Callovian); the Comblanchian limestones (Late Bathonian); the *Oolithe Blanche* (Late Bathonian); the limestones with *Pholadomya* fossils (marly limestones; Late Bathonien to Late Bajocian); the marls with *Ostrea acuminata* fossils (Late to Early Bajocian) and the crinoidal limestones (Early Bajocian).

The Dogger formations has an average thickness of 200 m, with a maximal thickness (up to 400 m) beneath the Brie area and a progressive thinning to nothing in the north towards Cambrai and in the west towards Angers (Figure 5-1). The geological features in the Early Callovian to Middle Bathonian limestones were addressed in the PilotSTRATEGY Deliverable 2.7 – Conceptual Geological Models Report (Wilkinson, 2023; Bordenave and Issautier, 2023) and are therefore not described here. In the PilotSTRATEGY study area, the lateral facies variations are small compared to the vertical facies variations. Accordingly, the vertical facies distribution defines the framework of the complex lithostratigraphic platform, which results hydrogeologically in alternating sequences of aquifer, aquitard and aquiclude units with depth (Figure 5-5).

Table 5-2. Simplified lithostratigraphy of the Dogger formations in the Paris Basin (adapted from Mégnién et al., (1980)). The color code specifies the overall hydrogeological properties of the formation: aquifer (blue), aquitard (light blue) and aquiclude (white).

Geological period	Chronostratigraphy	Lithological domains	Dominant lithology
Dogger	Late Callovian	Callovian marls	marl
	Middle Callovian		
	Early Callovian	<i>Dalle Nacrée</i>	limestone
	Late Bathonian	Comblanchian limestones	
	Middle Bathonian	<i>Oolithe Blanche</i>	
	Middle Bathonian	Limestones with <i>Pholadomya</i> fossils	marly limestone
	Late Bathonian		
	Late Bajocian		
	Early Bajocian	Marls with <i>Ostrea acuminata</i> fossils	marl
	Aalenian	Early Bajocian	Limestones with entroque fossils
Aalenian		Black marls with <i>Lytoceras jurense</i>	marls
		Black marls with <i>Hildoceras bifrons</i>	

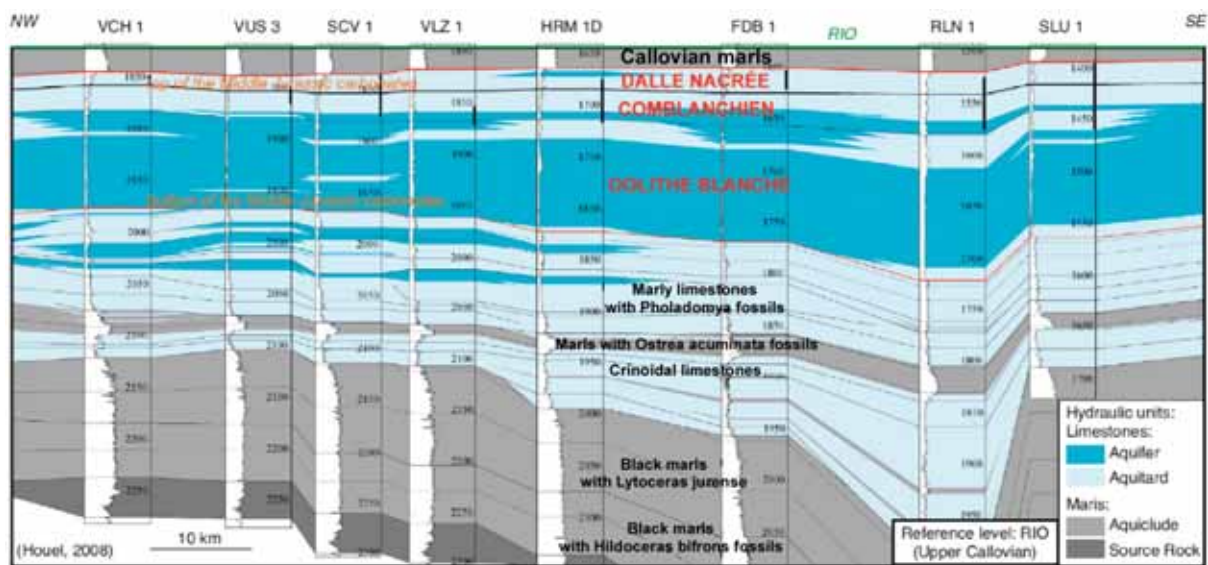


Figure 5-5. Example of distribution of the main formations and potential aquifer, aquitard and aquiclude units based on well correlation profiles and relative porosity of the Dogger carbonates in the PICOREF study area, located 5 – 10 km South-East from the PilotSTRATEGY study area (adapted from Houel, (2008) after Delmas et al., (2010)).

5.3.2 Distribution and extent of the aquifer, aquitard and aquiclude units

In the Paris metropolitan region, the “main aquifer”, which is also the main reservoir for oil and geothermal production, is mainly located in the Callovian-Bathonian limestone formations, i.e. the *Oolithe Blanche*, *Comblanchian* and *Dalle Nacrée* formations (Figure 5-5). The Bajocian limestones may act locally as minor aquifers, but are generally regarded only as potential secondary reservoirs for geothermal production due to the lower thickness of the high porosity layers (Figure 5-5) and progressive decrease of permeability with depth as a result of compaction and cementation processes

(Roux, 2006). Accordingly, within the Bajocian formations the alternation of limestones and marly limestones and the *marls with Ostrea acuminata* fossils are defined as aquitards and aquicludes, respectively (Figure 5-5).

The uppermost Dogger formation, namely the Callovian claystones/marls, are the first aquiclude overlying the Dogger aquifer and thus the lower part of the caprock of the prospective storage site. In the PilotSTRATEGY study area, the bottom of the Callovian claystone and marls reaches a depth up to 1730 m.b.s.l, with an estimated thickness of about 30 m based on stratigraphic logs of existing wells.

Regarding the Callovian-Bathonian limestones, most of the past studies focused on their geo- and hydro-properties, with a major interest for the *Dalle Nacrée* and Comblanchian formations for oil exploration, and for the Comblanchian and the *Oolithe Blanche* formation for geothermal production. In fact, to avoid the contamination of geothermal brines by oil, geothermal boreholes are cemented down to the base of the *Dalle Nacrée* formation (Lopez et al., 2010). This common interest of the different Callovian-Bathonian formations has provided a large dataset, which enabled a relatively good understanding of the hydro-properties to better refine the successive overlay of the aquifer and aquitard units within the “main Dogger aquifer”.

In the central part of the basin, the area regarded as a geothermal reservoir formation (temperature > 50 °C) lies between 1500 to a maximum of almost 2000 m.b.s.l. near Coulommiers and stretches over 15,000 km² area (Figure 5-6). Beneath the PilotSTRATEGY study area, the top of the main aquifer was locally estimated as 1680 – 1765 m.b.s.l from seismic interpretation (Wilkinson, 2023; Bordenave and Issautier, 2023). These estimates are in line with mapping of the top of the Dogger limestone platform at basin scale (Figure 5-6).

The overall thickness of the Callovian-Bathonian formations varies from 100 to 150 m in the central part of the basin (Figure 5-7). Among the permeable layers of the Dogger formations, the *Dalle Nacrée* formation, also defined as the roof of the Dogger limestone platform, generally displays a low to intermediate porosity but a good permeability (Delmas et al., 2010). In the PilotSTRATEGY study area, the total thickness of the Callovian limestones ranges from 12 to 20 meters from seismic interpretation (Wilkinson, 2023; Bordenave and Issautier, 2023). These results are in line with the total thickness of 10 – 28 m reported in the PICOREF study area (Delmas et al., 2010), which is near the PilotSTRATEGY study area. The Comblanchian limestones are predominantly composed of oncoidal packstone, wackstone and some mudstone. Geologists have considered this formation as an aquitard unit (dominantly semi-permeable properties) in the PilotSTRATEGY study area (Fleury et al., 2011; Wilkinson, 2023; Bordenave and Issautier, 2023). The total thickness of the Comblanchian formation is thus locally comparable to the *Dalle Nacrée* formation, with a thickness estimated between 10 and 25 m, and thus thinner than estimated (40 m) in the PICOREF study area (Delmas et al., 2010). The *Oolithe Blanche* formation is mainly composed of grain-supported limestones (grainstones, packstones) with abundant ooids, peloids and bioclastic debris, and is the main aquifer unit of the Bathonian formation (Wilkinson, 2023; Bordenave and Issautier, 2023). The *Oolithe Blanche* formation is the most porous and most massive formation of the Bathonian platform, with an estimated total thickness – together with the *limestones with Pholadomya fossils* – ranging from 130 to 210 m in the PilotSTRATEGY study area (Wilkinson, 2023; Bordenave and Issautier, 2023). For comparison, the total thickness of the *Oolithe Blanche* formation (alone) was estimated as 70 – 80 m in the PICOREF study area (Delmas et al., 2010).

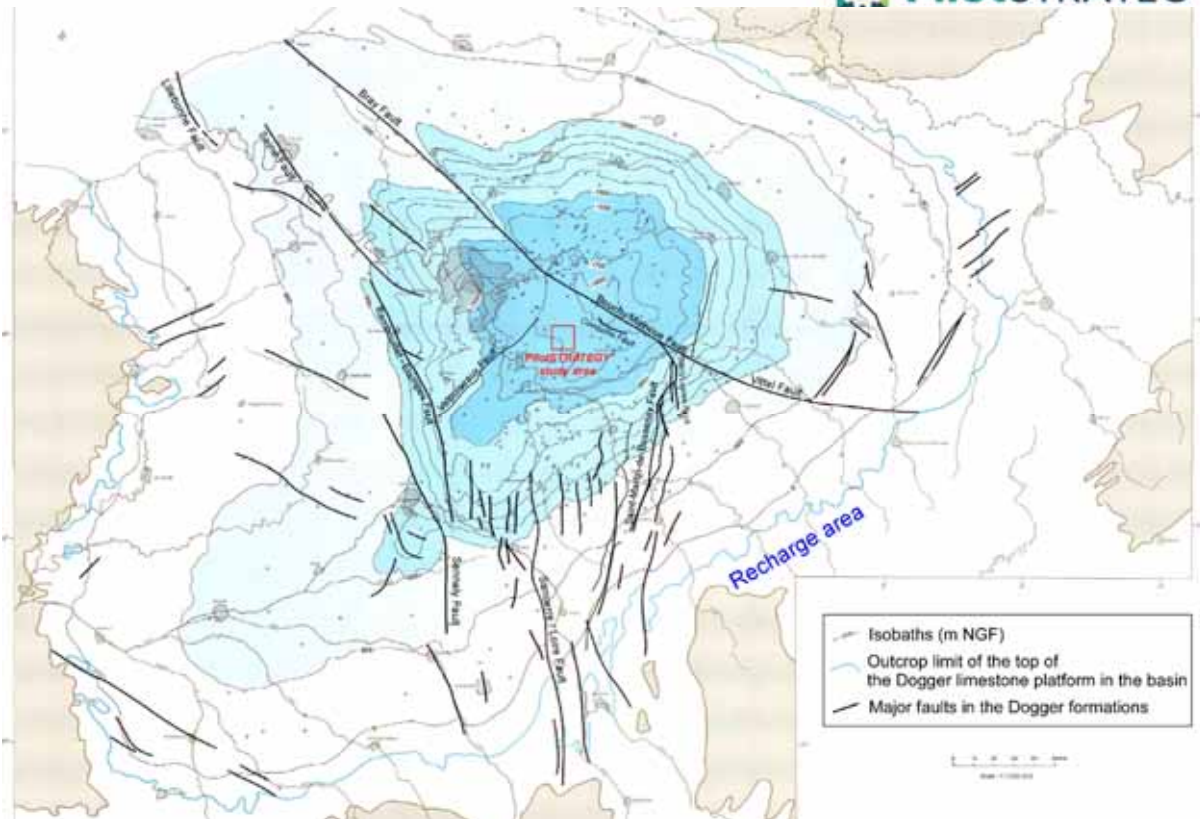


Figure 5-6. Map of the isobaths and outcrop limit of the top of the Callovian-Bathonian limestones (i.e. Dalle Nacrée, Camblanchian limestones and Oolithe Blanche) in the Paris Basin (Housse and Maget, 1976). Major subvertical faults identified in the Dogger limestone platform are reported.

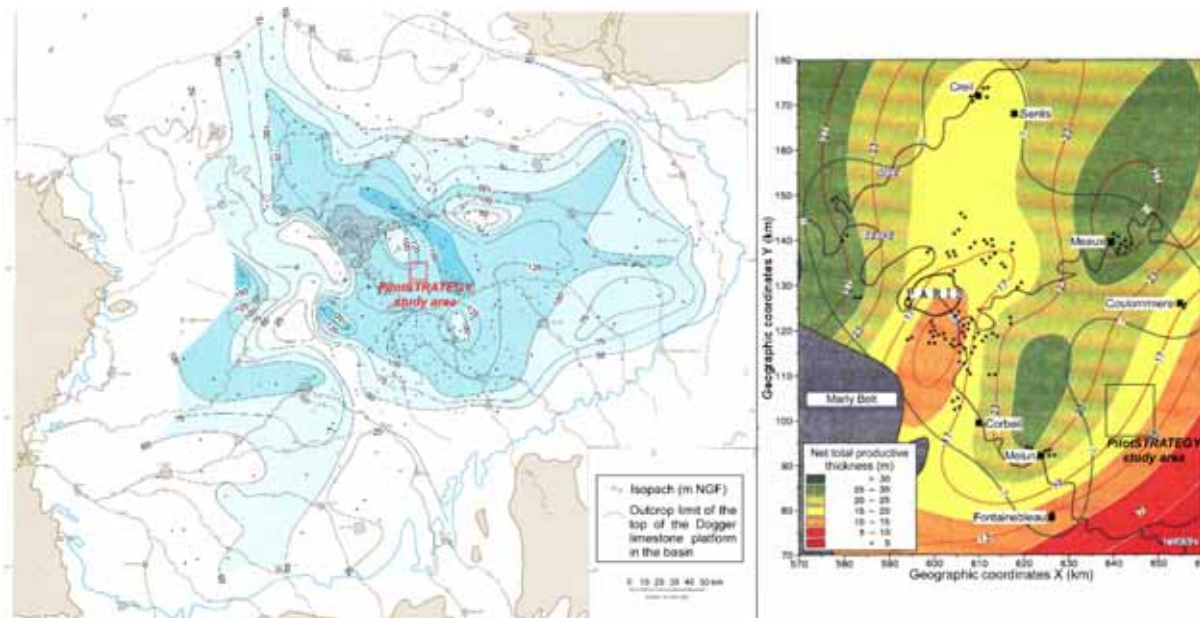


Figure 5-7. Maps of isopachs of the Callovian-Bathonian limestones in the central part of the Paris Basin: total thickness (left; Housse and Maget (1976)), b) net total productive thickness (right; Rojas et al. (1989)).

The effective thickness of the aquifer units within the Callovian-Bathonian limestones remains challenging to estimate both at the basin scale and at the sector scale because of the complex platform geometry. An estimate of the total thickness of a formation does not distinguish the cumulative

thickness of aquifer from aquitard within that formation. In the Callovian-Bathonian limestones, the *Dalle Nacrée* and the Comblanchian limestones formations are both known to contain alternating aquifer and aquitard units (e.g. Figure 5-5). The thickness of the alternating aquifer and aquitard units within these two formations varies laterally to a significant extent in the central part of the basin (Figure 5-7), as observed in the PICOREF study area (Figure 5-5).

Experience gained from the production of geothermal wells has revealed high vertical and lateral variability in the hydrogeological characteristics of the aquifers. Many studies have concluded that the high porosity and permeability horizons from which most water production is sourced accounts only for a minor part (i.e. 10 – 20%) of the total thickness of the Bathonian limestone formations. The net total productive thickness is commonly estimated as 15 – 20 m in the metropolitan Paris area (Rojas et al., 1989; Lopez et al., 2010). This net productive thickness is distributed within strong vertical stratification, with successive alternation of thin (metric to sub-metric thickness) highly permeable layers and thin-to-thick sub-horizontal layers with low permeability (e.g. Figure 5-8). The multiplicity of the highly permeable layers confers to the Bathonian limestone formations its aquifer properties at the basin scale. However, the lack of lateral continuity between geothermal wells in the central part of the Paris Basin prevents a generalized description of the most productive layers from being made. Due to the lack of wells intersecting the entire Middle-to-Late Bathonian formations, the estimation of the net total productive thickness remains uncertain in the PilotSTRATEGY study area. Interpolation of the net total productive thickness suggests a local average value between 13 and 21.5 m (Figure 5-7).

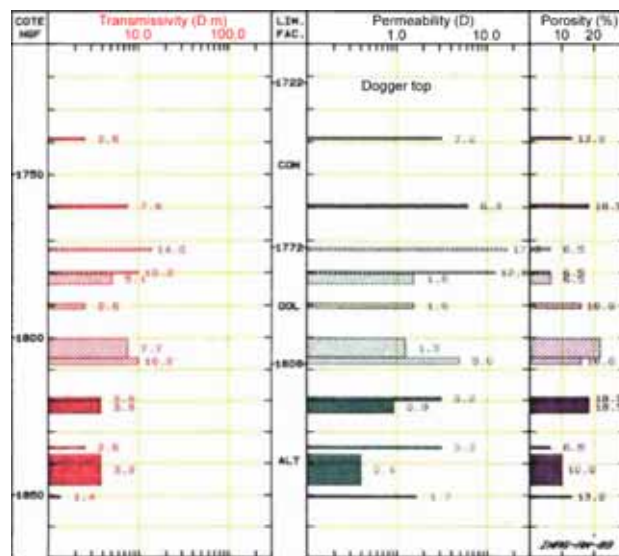


Figure 5-8. Vertical structure of the productive layer in the Dogger aquifer (adapted from Rojas et al., (1989)): permeability in Darcys (left) and porosity in % (right) in the production well of the geothermal doublet located in Meaux-Beauval (southwest of the Brie area).

5.3.3 Hydrogeological properties

At a basin scale, the groundwater in the Dogger aquifer flows naturally from the East and South-East to the North-West of the Paris Basin and toward the South-West along the Loire River (Figure 5-9a). The flow velocity has been estimated as 0.1 to 1 m/year, depending on the zone of the aquifer (Wei, 1986; Gonçalves, 2003; Brosse et al., 2010). The Callovian-Bathonian limestones recharge from the outcrop at the periphery of the Paris Basin (Figure 5-6) and discharge in and beyond the English Channel.

At a regional scale, the water table of the aquifer forms a natural concave-upwards surface around the PilotSTRATEGY study area (hydraulic head ≤ 140 mNGF; 'Nivellement Général de la France' or French ordnance datum), meaning that groundwater may naturally flow from Fontainebleau (hydraulic head > 180 mNGF) and Coulommiers (hydraulic head > 160 mNGF) toward the prospect area (Figure 5-9b). The understanding of the regional flow is however partly influenced by limited data and/or wells between the study area and the Paris Metropolitan area. In the PilotSTRATEGY study area, the regional flow velocity was estimated to be in the lower end of the range 0.10 – 0.40 m/year.

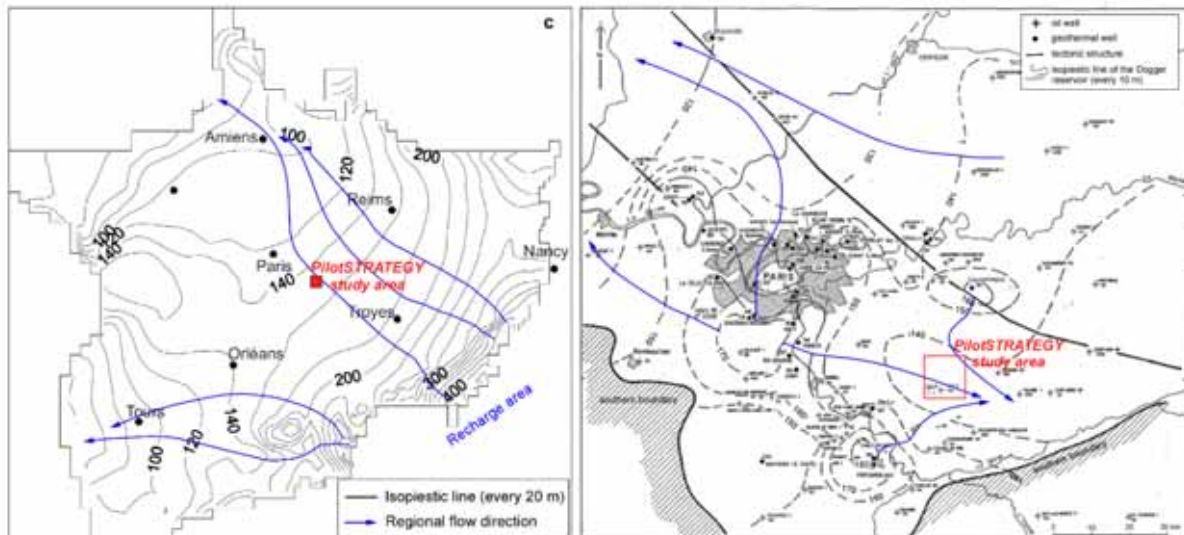


Figure 5-9. Piezometric map of the Dogger aquifer in the Paris Basin (left; Gonçalvès, (2003)) and in the central part of the Paris Basin (right; adapted from Aubertin and Ballin (1984)).

In the area of interest, the aquifer formations recharge from the outcrops located in the southeast part of the sedimentary basin (Burgundy region), i.e. situated nearly 130 km away from the PilotSTRATEGY study area. From the salinity of the groundwater coupled with the low natural flow rates, a partial recharge from the underlying Triassic aquifer is suspected in the central part of the basin based on geochemical studies (Matray and Fontes, 1990; Matray et al., 1994; Worden and Matray, 1995; Innocent et al., 2021). At the basin scale, Wei (1990) calculated the recharge from the outcrop of the formation and from the Triassic aquifer as 65 and 35 %, respectively.

Analyses of available porosity-permeability data of the Callovian-Bathonian limestones showed, at sample scale, variable trends from one formation to another in the nearby PICOREF study area (Delmas et al., 2010). In general, the highest matrix porosities were measured in the *Oolithe Blanche* formation. The most permeable formations are the *Dalle Nacrée* and the *Comblanchien* macroporous limestones (representating the oil-bearing levels), whereas the microporous *Oolithe Blanche* limestones had locally very low permeability (Figure 5-10a). This finding must be seen in relative terms, as the petrophysical characteristics of the *Oolithe Blanche* limestones were known from a more limited number of samples (Figure 5-10d). Overall, the permeability of the Callovian-Bathonian limestones is relatively isotropic at the sample scale, independent of the rock texture.

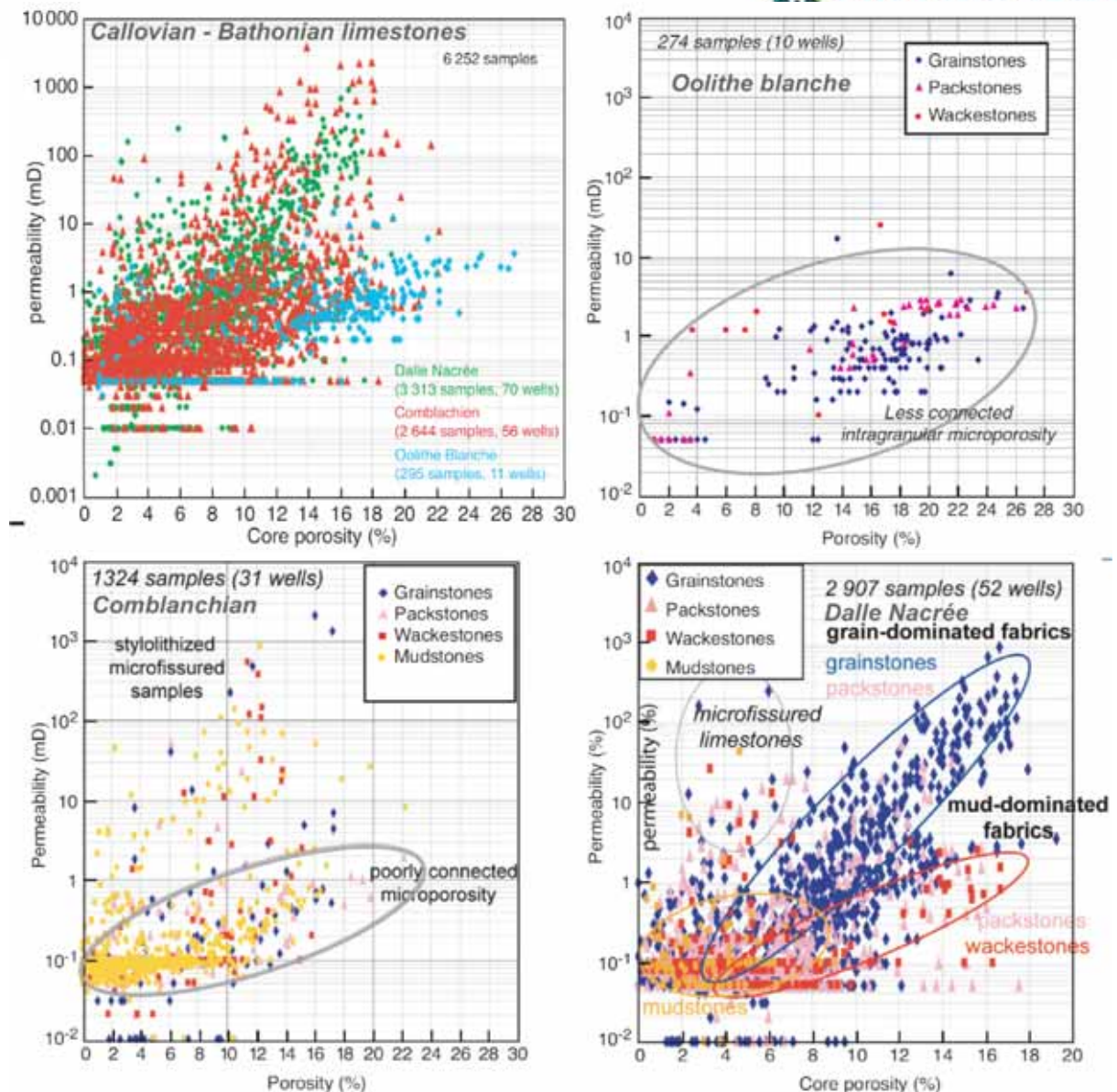


Figure 5-10. Porosity-permeability cross-plot in the PICOREF study area (adapted from Delmas et al., (2010)): a) three formations of the Middle Jurassic; b) Dalle Nacrée with textural interpretation of the rock fabrics; c) Comblanchian limestones with textural interpretation of the rock fabrics; d) Dalle Nacrée with textural interpretation of the rock fabrics.

More specifically, the *Dalle nacrée* has a large range of porosity (0 – 19%) and permeability (0.01 – 1000 mD). Three main groups could be differentiated in the porosity-permeability distribution, related to the texture of the rock fabric (Delmas et al., 2010). In the upper part of the formation, the petrophysical properties of the grain-dominated fabrics (grainstone and packstones) followed a typical calcarenite law, reaching porosity and permeability values up to 16% and 1000 mD, respectively (Figure 5-10). Conversely, the mud-dominated fabrics (packstones, wackestones and mudstones) in the lower part of the formation have a large porosity range but overall low permeability values (< 1 mD). The microfissured and microstylolithized limestones (independent of texture) were characterized by a low porosity (< 10%) and a high permeability (< 200 mD).

The Comblanchian limestones have a large porosity (0 – 22%) and permeability (0.01 – 3800 mD) range (Figure 5-10) controlled by the rock fabric. Lime muds have a large porosity range (0 – 24%) but overall

very low permeabilities (< 10 mD). In comparison, wackestone-packstones and grainstones have higher permeability values (10 mD – 1 000 mD) but still large porosity ranges. Higher permeabilities measured in some mud dominated fabrics (wackestone-packstone) were associated with microfissures or stylolites (Delmas et al., 2010).

The porosity of the *Oolithe Blanche* ranged from 1 to 26.8% (mean: 14.5%), whereas the permeability, measured on horizontal plugs, ranged from 0.1 to 2 mD (Figure 5-10). The low permeabilities compared to the porosities were related to the absence of macro-connected porosity, independent of the sediment fabric. In micrite the porosity is restricted to both micro-porosity which is not sufficiently connected to provide good permeability (Delmas et al., 2010).

The porosity values of the Callovian-Bathonian formations from the PICOREF study area are consistent with previously reported values (Castro et al., 1998; André et al., 2007). However, the permeability of the local *Oolithe Blanche* formation contrasts sharply with the flow rates of geothermal doublets in the Bathonian limestones (50 – 600 m³/h; mean: 270 m³/h) in which 50 to 70% of the production flow generally comes from the *Oolithe Blanche* limestones (Rojas et al., 1989; Lopez et al., 2010). The influence of fracturing, commonly observed in the limestones, would explain at least part of the large discrepancy between the core permeability and permeability at reservoir scale (Rojas et al., 1989). Permeability at a regional scale is generally considered to be one to three orders of magnitude higher (depending on the formation), due to the influence of open fractures and dissolution channels (Rojas et al., 1989). Dezayes (2007) reported in the PICOREF project that between 20% and 30% of fractures in the *Dalle Nacrée* and Comblanchien were found to be open, whereas 75 % were open in the *Oolithe Blanche* in limestone quarries located in Burgundy. The role of fractures must therefore be properly characterised in the *Oolithe Blanche*, to properly model the flow properties at the scale of the formation.

Horizontal transmissivity of the Dogger limestone, estimated from geothermal well testing, varies between 2Dm (Darcy – metres) and 110 Dm, with an average value of about 40 Dm ($\approx 4 \times 10^{-4}$ m²/s) in the Paris metropolitan area (Figure 5-11). The transmissivity is generally slightly higher than the average value beneath the Brie area (45 – 60 Dm), with highly favorable properties near Meaux (north of the PilotSTRATEGY study area). The values of relative transmissivity, taking into account the dynamic fluid viscosity, suggest high permeabilities in the southern part of the Brie area in the Comblanchian and *Oolithe Blanche* formations (Figure 5-11). Based on the productivity of geothermal wells, sub-vertical fractures significantly influence the anisotropy of the hydraulic properties of the limestones. Rachez (2007) showed that fractures connecting sedimentary layers (inter-layer fractures) increase the connection within the fractured media and this minimizes the anisotropy within the reservoir. The role of fractures within sedimentary layers (intra-layer fracture) has a lower impact than inter-layer fractures in terms of flow in the Bathonian formations. However, no direct information was available about sub-vertical fractures.

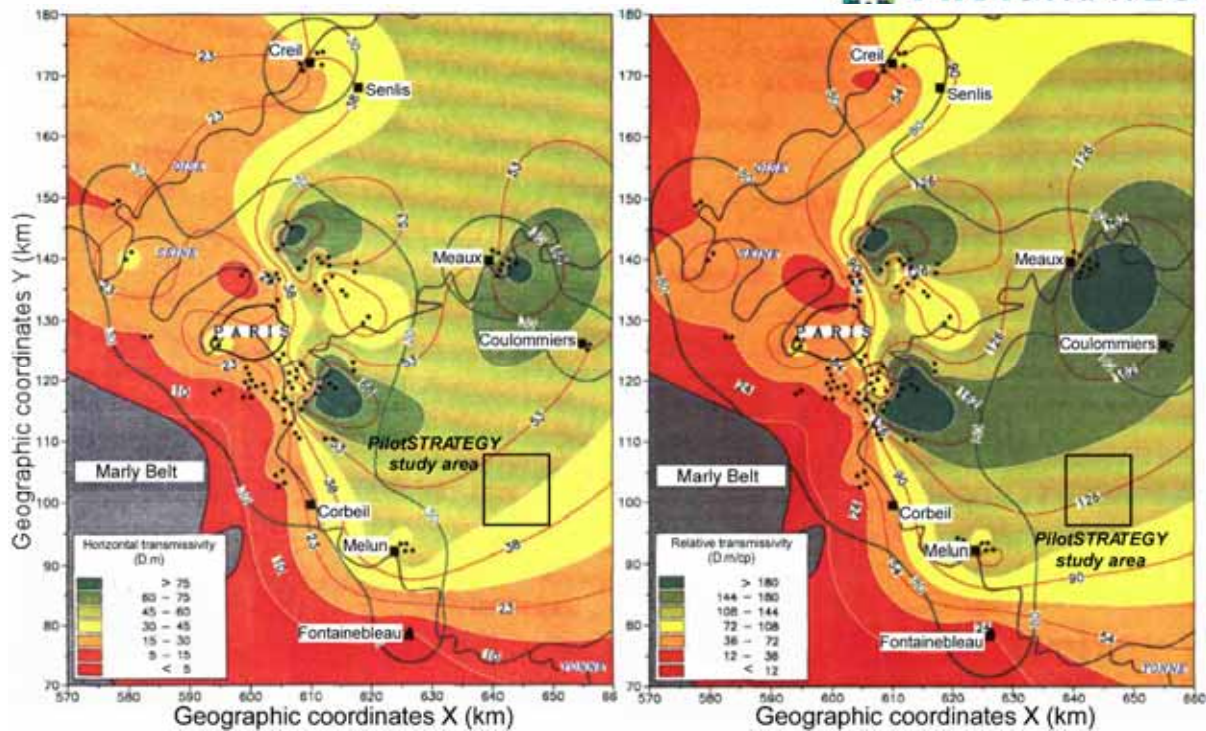


Figure 5-11. Contour maps of horizontal transmissivity of the Bathonian formations (adapted from Rojas et al., (1989)): horizontal transmissivity (left); relative horizontal transmissivity considering the dynamic flow velocity (right). The western low transmissivity area corresponds to the “Marly Belt”, with poor reservoir properties due to its higher marl content.

5.3.4 Features of the pristine fluid

Rojas et al. (1989) compiled and discussed the most comprehensive chemical analyses of geothermal fluids. Groundwater temperature and salinity are the lowest close to the outcrops – e.g. in the south of the Paris Basin (Fontainebleau, Corbeil; Figure 5-12) – due to dilution by meteoric waters in the recharge areas. The salinity progressively increases in the Dogger aquifer towards the center of the basin. The mineralization of the groundwater is of sodium-chloride type, with a salinity ranging from 5.8 to 35 g/l and temperatures ranging from 47 to 85°C in the center of the basin (Figure 5-12). The most saline and the warmest groundwater are located in the topographic troughs (Meaux, Coulommiers; Figure 5-12), which contain brine waters (> 30 g/l). A comparison of the fluid composition of the Callovian-Bathonian formations (Dogger) and the Keuper aquifers (Trias), concluded that there is a common origin to the salinity, derived from salts and brines from Triassic evaporitic deposits (Matray and Fontes, 1990; Matray et al., 1994; Worden and Matray, 1995). A vertical upflow of brine groundwater through the sub-vertical Bray and Bouchy/Malnoue faults expels the Triassic brine into the Dogger formation. The cross-formational flow process would explain the occurrence of brine in the northern part of the Brie area (Meaux) as well as slight sulphate enrichment identified locally in the Dogger aquifer (Wei, 1986; Michard and Bastide, 1988; Wei et al., 1990; Maget, 1991).

As the PilotSTRATEGY study area is located in the southeastern part of the Brie-sub-basin (East of Melun), groundwater of intermediate salinity (17 – 23 g/l) and an average temperature around 75°C is expected in the Dogger aquifer (Figure 5-12). While the expected salinity range (17.5 – 23 g/l) is confirmed by productive oil wells from the surrounding petroleum concessions, the expected temperature is slightly lower (60-65° C; measured in 2012) than extrapolated by Rojas et al. (1989).

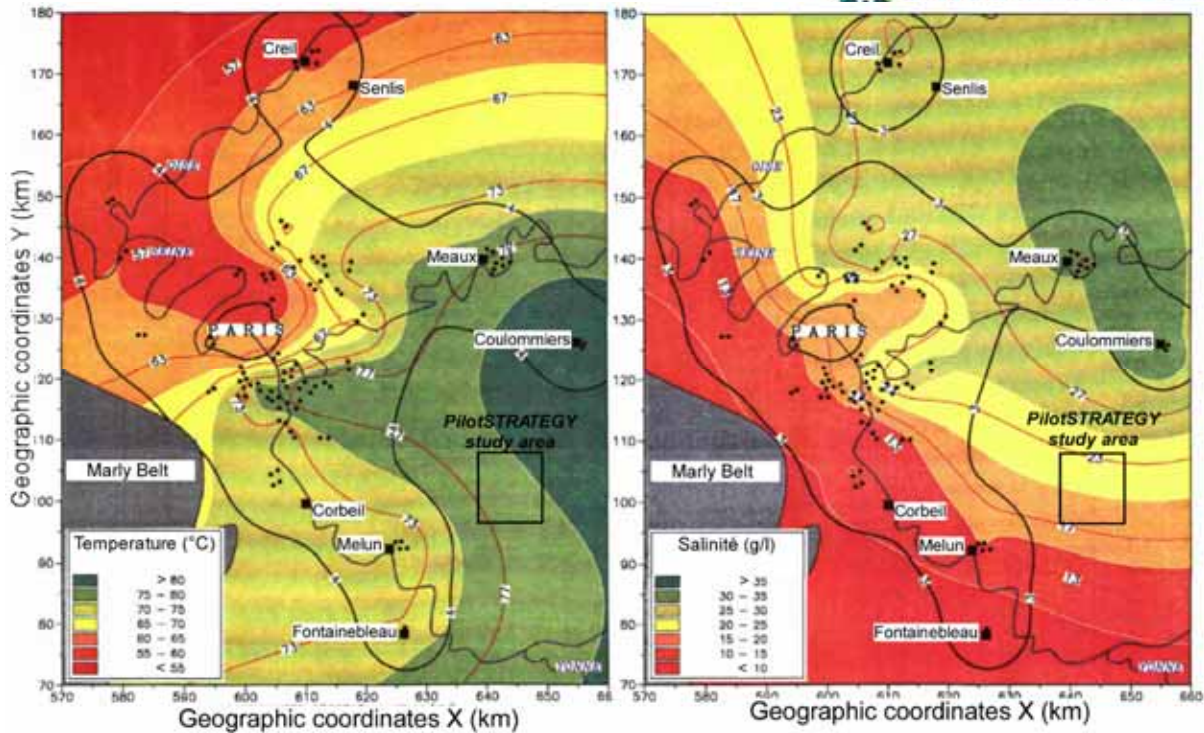


Figure 5-12. Contour map of temperature (left) and salinity (right) of the fluid at the top of the Bathonian formations (Rojas et al., 1989).

5.3.5 Occurrence of faults

The major faults in the nearby PilotSTRATEGY study area are the Bray and the Bouchy/Malnoue faults, which extend eastwards and southeastwards with the Vittel fault and the Saint Lupien / Saint-Martin-de-Bossenay faults, respectively (Figure 5-6). The Bray and Bouchy/Malnoue faults are located several kilometres north of the prospect area, the upper right corner of the PilotSTRATEGY study area being located a minimum of 15 km from the faults. The minor Conquillie fault, of moderate extent, is 12.5 km (minimum distance) to the east of the study area, whereas the minor Valpuseaux fault is located ca. 8 km (minimal distance) west of the study area (Figure 5-6). Based on seismic reprocessing performed in the PICOREF project, Bouchy/Malnoue and the Conquillie faults cut the Triassic formations (Brosse et al., 2010). The major Bray fault, and by analogy the Malnoue faults, are suspected to act as a preferential vertical path for cross-formational flow. Such flow has been identified qualitatively, i.e. from geochemical studies and conceptual interpretation (Matray et al., 1994; Worden and Matray, 1995; Gonçalvès, 2003). However, the hydro-properties of the regional faults remain unknown. Within the multi-layered aquifer-aquitard system of the Paris Basin, Gonçalvès (2003) considered the Bray fault to be porous and applied a vertical flow along the fault by enhancing the vertical permeability by one order of magnitude along the structure within the aquitards and aquicludes.

5.3.6 Societal use of the formation in the study area.

The PilotSTRATEGY study area is surrounded by many concessions producing oil from the *Dalle Nacrée* and Comblanchian formations (Figure 5-13). No geothermal production is known in the study area, the nearest geothermal doublets are located more than 10 km from the prospect area. The Dogger aquifer is not part of any current protected zone for water supply in the extended area of study. The SEIF 1-1 well is the only well currently operating in the study area in the Dogger. This well is used

exclusively for the injection of industrial water resulting from the production of fertilizer, only after recycling and treatment of the water in compliance with the criteria imposed by the competent authorities. Accordingly, the SEIF 1-1 well and the petroleum concessions are therefore the current main societal use of the Callovian-Bathonian formation in the broad area of interest. The numerous wells are subject to monitoring of their commissioning, use (i.e. production / injection) and abandonment.

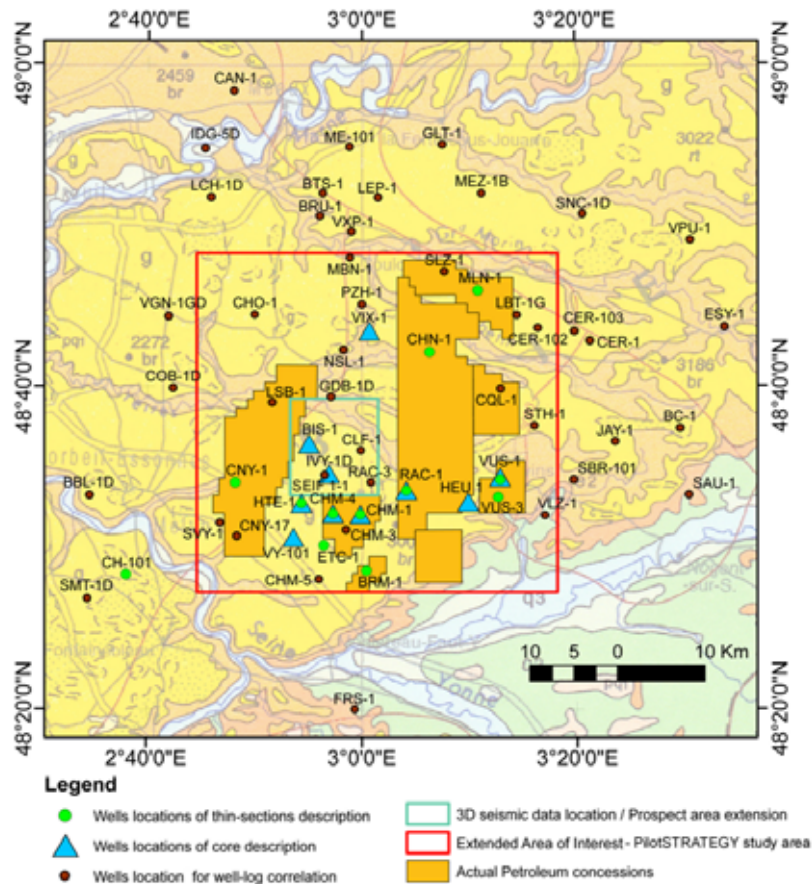


Figure 5-13. Map of the actual Petroleum concessions exploiting the Dalle Nacrée and Comblanchian limestones (adapted from PilotSTRATEGY Deliverable 2.7 Conceptual Geological Models Report; Wilkinson (2023); Bordenave and Issautier, 2023).

5.4 Malm formations

The Malm (Late Jurassic) formations overlay the Dogger aquifer (i.e. target reservoir) with thick layers of Oxfordian argillites-to-marls. A major limestone platform, known as the Lusitanian limestones in the Paris Basin, separates the Oxfordian marly formations from the thick Kimmeridgian marly formations. The upper part of the Malm, the Tithonian formations, are composed of limestone alternating with marl layers. Although the stratigraphy is relatively well known, few hydrogeological and hydrodynamic data are available to characterize the Malm formations, including the aquifer units.

The limited interest in hydrocarbon exploration in the 1970s, and the massive geothermal exploitation of the Dogger aquifer from the 1980s onwards restricted the exploration of the Lusitanian aquifer in the past. The knowledge of the aquifer described here are retrieved from the few geothermal wells drilled in the Lusitanian limestones in the 1980's. The hydro-properties of the Callovo-Oxfordian aquiclude/caprock have been widely studied by ANDRA, the French national radioactive waste management agency, at the underground research laboratory (URL) in Bures to the east of the Paris Basin (https://radioactivity.eu.com/radioactive_waste/underground_bure_lab). ANDRA is continuously investigating the argillite/marl units, as it is likely to become the host rock for the future disposal site for highly radioactive long-lived nuclear waste in France. Most of the hydro-properties reported in this sub-chapter provide only order of magnitude estimates of the parameters in the PilotSTRATEGY study area, as the data were only available from relatively distant areas.

5.4.1 Geological features of the formation

The Malm formations consist mainly of argillites, marls and limestones layers, with local occurrences of sandstone. There are three formal ages (time) and stages (rock) within the Malm: the Oxfordian, Kimmeridgian and Tithonian (Table 5-3). However, geologists working in the Paris Basin defined the "Lusitanian" as the limestones with ammonite fossils located between the Oxfordian and Kimmeridgian marls. The term "Lusitanian" has since been widely used by the oil industry and hydrogeologists working in the basin as an informal 'age' term. Within the geological time scale, the Lusitanian formation includes the Argovian, Rauracian and Sequanien domains from the middle Oxfordian to the earliest Kimmeridgian (Table 5-3). The Lusitanian includes mainly the Middle to Late Oxfordian, although the stratigraphic limit includes the thin layer of clayey limestones with Planula fossils, which is part of the Early Kimmeridgian. Likewise, the Tithonian formations are subdivided into two units to differentiate the Early Tithonian and the Purbeckian (Late Tithonian) formations and the associated evolution of limestone facies. The five classical stratigraphic domains in the Paris Basin are used hereafter, i.e. Early Oxfordian, Lusitanian, Kimmeridgian, Early Tithonian and Purbeckian (Table 5-3).

Table 5-3. Simplified lithostratigraphy of the Malm formations in the Paris Basin, defining the Purbeckian and Lusitanian formations – and the associated lithological domains – specific to the Paris Basin (adapted from Bouniol and Magnet (1983)). The color code specifies the overall hydrogeological properties of the geological formation: aquifer properties (blue), aquitard properties (light blue) and aquiclude properties (white).

Geological period	Chronostratigraphy	Lithological domains	Classical stratigraphy	Dominant lithology
Malm	Late Tithonian	Purbeckian	Purbeckian	Limestone, alternating with calcareous marl layers
	Early Tithonian		Early Tithonian	
	Late Kimmeridgian	Sequanian	Kimmeridgian	Marl and clayey limestone
	Early Kimmeridgian			Marl and clayey limestone
	Late Oxfordian		Rauracian	Lusitanian
	Middle Oxfordian	Argovian	Limestone	
	Early Oxfordian		Early Oxfordian	Clayey limestone to marl
				Marl

With respect to the general lithostratigraphy, the Early Oxfordian is mainly composed of marls. The base of the Lower Oxfordian is characterized by a thin transitional zone between the Callovian and Lower Oxfordian marls, with local intercalation of thin limestones, and a significant change in clay mineralogy (Pellenard et al., 1999; Yven et al., 2007; Lerouge et al., 2011). The Lusitanian, dominantly composed of limestones, corresponds to sedimentation cycles that have many common stratigraphic features with those of the Dogger limestone formations (Bouniol, 1985). The Argovian is characterised by silty marls and calcareous clay. The Rauracian is mainly composed of locally gravelly oolitic limestones (grainstone – packstone) and bioclastic limestones (wackstone-packstone), with micritic limestones in the lower part of the formation. The Sequanian varies from oolitic limestones (grainstone, locally packstone) in the lower part to marly-banded limestone (mudstone). The Kimmeridgian is dominated by thick marls with rare intercalation of marly limestone beds. Marine marls and marly limestones dominate the Early Tithonian, whereas the Purbeckian is mainly composed of fine grain limestones and dolomitic limestones.

5.4.2 Distribution and extent of the aquifer, aquitard and aquiclude units

The Malm has a cumulative average thickness of 700 m in the Paris metropolitan area (Castro et al., 1998) and 710 m in the Brie area. The Callovo-Oxfordian argillites and marls form together a thick aquiclude (120 m) in the PilotSTRATEGY study area and the primary caprock of the prospective storage site. With a cumulative thickness of the order of 15 m, the limestone beds within the Callovo-Oxfordian are relatively thin and their occurrence does not compromise the unit as an aquiclude.

The Lusitanian contains the main aquifer(s) within the Malm. The Lusitanian has been studied in the area as a consequence of the unit's geothermal potential (Bouniol and Magnet, 1983; Bouniol, 1985). Three main aquifers were identified, namely the Sequanian sandstones, the Sequanian limestones and the Raurecian limestones (Figure 5-14). The Argovian formations are overall considered as aquiclude in most of the sedimentary basin. Based on a lithological approach, the mapped extent of the three main aquifers units varies significantly both vertically and laterally at the basin scale (Figure 5-14; Figure 5-15).

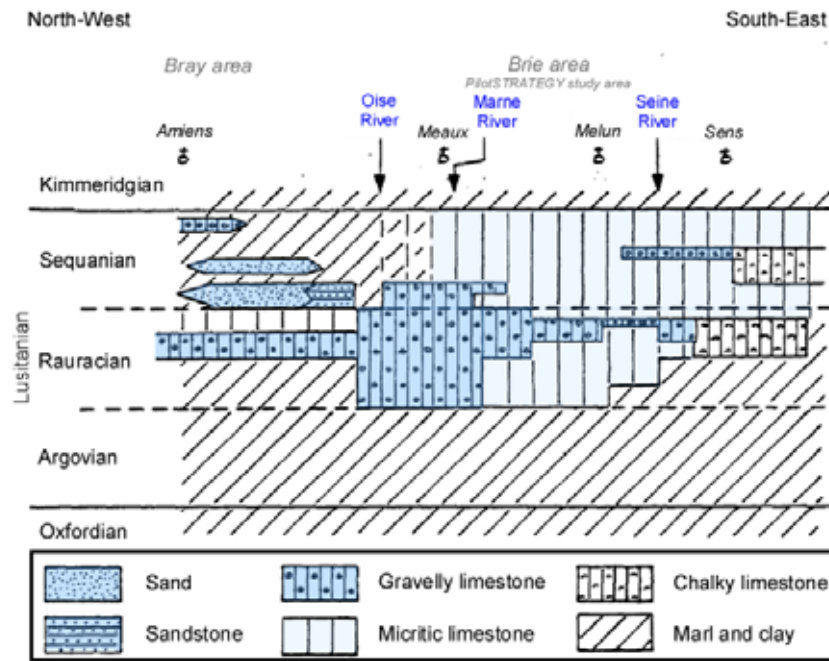


Figure 5-14. Schematic representation of the spatial extent of the lithology and associated hydrogeological properties within the Lusitanian formations along a North-West – South-East transect crossing the Brie area (adapted from Bouniol and Magnet; 1983). The depth and thickness of the gravelly limestone in the Rauracian are relative – i.e. estimated thickness corresponds to cumulative thickness of permeable limestone beds. The main aquifer and aquitard units are colored in blue and light blue, respectively.

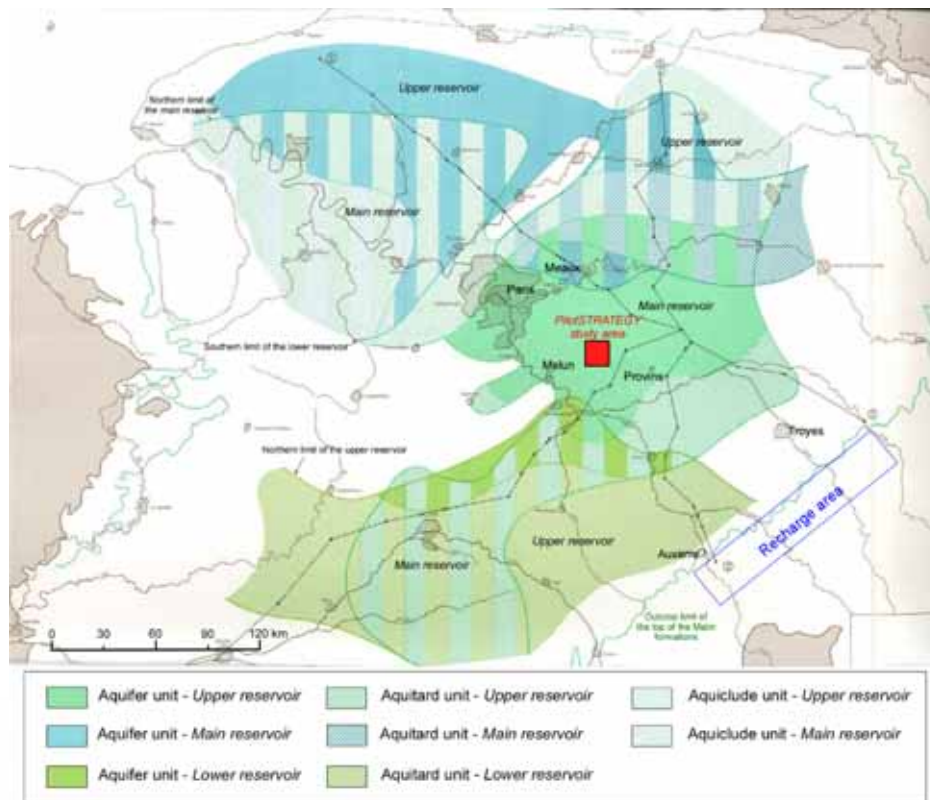


Figure 5-15. Spatial extension and distribution of the three main aquifers within the Lusitanian formation (adapted from Housse and Maget (1976)).

In the Brie area, the Raurecian oolitic to gravelly limestones compose the main aquifer of Lusitanian formation with a maximum vertical extent in the Meaux sector, where the Raurecian limestone are in contact with the overlying Sequanian limestone aquifer (Figure 5-14). In the PilotSTRATEGY study area, the Rauracian formations form tight (cemented) alternation of gravelly/oolitic limestones and compact limestone beds. The Rauracian sequences lower the effective thickness of the main Lusitanian aquifer and make the estimation of effective thickness difficult locally (Bouniol and Magnet, 1983). The Lusitanian reaches a total thickness of up to 285 m in the study area, including a 60 m thick Argovian marly formation and a cumulative thickness of Raurecian and Sequanian limestones of 210 m. The top of the Lusitanian was estimated to be at around 1350 m.b.s.l. (1470 m depth; Figure 5-16), with a maximum effective thickness of slightly lower than 50 m (Caritg et al., 2014).

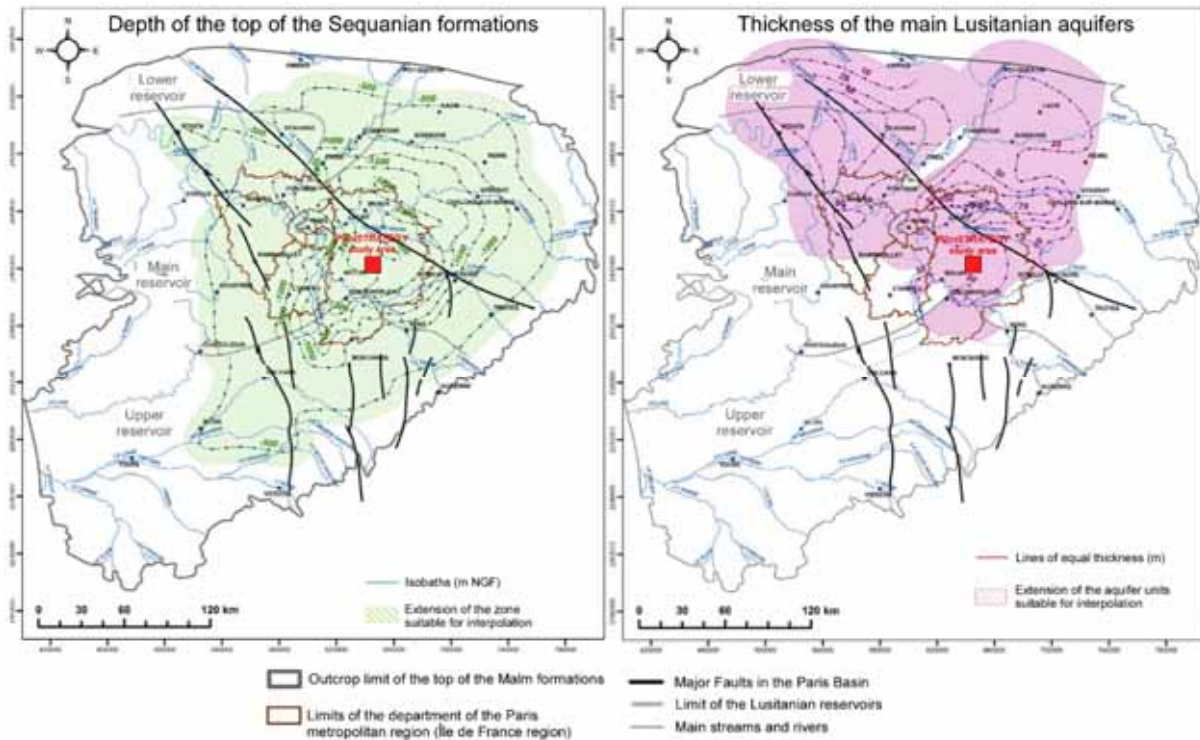


Figure 5-16. Contour maps of (left) the estimated depth (isobaths) of the top of the Lusitanian aquifer and cumulative thickness (right) of the Lusitanian aquifers (adapted from Housse and Maget (1976) after Caritg et al. (2014))

The Kimmeridgian formations are the second major aquiclude of the Malm, with an overall thickness of 150 – 160 m in the PilotSTRATEGY study area.

The Early Tithonian formation presents mixed hydro-properties, with a lower part considered as a thick aquiclude due to the dominant marly facies overlying the Kimmeridgian formations. The upper part of the Early Tithonian and the Purbeckian formations may be considered either as an aquifer or as an aquitard depending on their respective thickness and hydro-properties. In the study area, the upper 65 m of the Early Tithonian formations are marly limestones (total thickness estimated at 135 m) and overlain by the 40 m thick Purbeckian. Although very productive near the outcrop area (basin edge), the Early Tithonian and Purbeckian formations were not historically considered to be a strategic aquifer in the center of the Paris Basin and were therefore poorly characterised in term of the hydro-properties. When found to be an aquifer unit, the high permeability of the (marly) limestones and dolomitic limestones results mainly from fracture permeability.

A lack of data prevents a confident classification of the Early Thitonian and Purbeckian as either aquifer or aquitard on the PilotSTRATEGY study area. Based on a global approach, Housse and Maget (1976) considered the Early Tithonian to be an aquitard and the Purbeckian to be an aquifer in the center of the Paris Basin. However, Wei et al. (1990) and Castro et al. (1998) reported the opposite, with the uppermost Early Tithonian and the Purbeckian formations as an aquifer and an aquitard, respectively. The Andra's quantitative model, developed for the entire Paris Basin, used a median hydraulic conductivity of the Tithonian formations (i.e. upper Early Tithonian and Purbeckian) to an order of 10^{-10} m/s (ANDRA, 2005). This relatively low hydraulic conductivity suggests that both the Upper Early Tithonian and Purbeckian can be regarded as aquitards at a regional scale.

5.4.3 Hydrogeological properties

The Callovo-Oxfordian marls from the Bures Underground Research Laboratory (URL; Meuse / Haute-Marne department; 150 km east from the PilotSTRATEGY study area) are currently buried at a depth 420 to 520 m, with a previous maximum depth of 800 m. The lower burial depth of the sediments in the Bures URL may have resulted in different diagenetic conditions to the center of the Paris Basin, which may affect the local mineralogical and petrophysical properties. The Callovo-Oxfordian marls have a total porosity ranging from 14 % for the most carbonate levels to 19.5% for the clay-rich levels in the URL, with an average total porosity of 18% in homogeneous claystone (Yven et al., 2007). The macroporosity and mesoporosity (intra-aggregate porosity) accounts for 20 – 40% and 60 – 80% of the total porosity, respectively. The microporosity (intraparticle porosity) is lower than 1%. The free water in the Callovo-Oxfordian claystone, located in the inter-platelet porosity, accounts for approximately 75% of the total porosity (Belmokhtar et al., 2018). A large number of hydraulic measurements have been performed in instrumented boreholes (Enssle et al., 2011), including hydraulic tests for the determination of the average hydraulic conductivity at the decimetre scale. The best fit yielded a horizontal hydraulic conductivity of 7×10^{-13} m/s and a vertical hydraulic conductivity of 4×10^{-13} m/s in the Callovo-Oxfordian clay (Enssle et al., 2011). However, the values range from 10^{-14} to 10^{-12} m/s for horizontal hydraulic conductivity and from 10^{-14} to 6×10^{-13} m/s for the vertical hydraulic conductivity (Lasseur et al., 2009).

Few hydrogeological and hydrodynamic data are available for the Lusitanian units, apart from the few geothermal boreholes that reach the aquifer(s) (Figure 5-17). The spatial distribution of the boreholes covers mainly the areas of the three main reservoirs (Figure 5-15) defined by Housse and Maget (1976). However, the geothermal wells drilled east of Paris are mainly located to the north of the Marne River and to the south of the Seine River, thus outside of the Brie area (Figure 5-17). The spatial distribution of the wells prevents the production of a piezometric map of the Lusitanien aquifer at the regional scale around the PilotSTRATEGY study area. The piezometric map calculated at the basin scale (Figure 5-18) indicates a predominant natural flow direction from the South-East to the North-West part of the basin, toward the English Channel along the Seine watershed (Wei et al., 1990; Gonçalves, 2003). Only the southern part of the basin is an exception to this general flow direction, with a preferential path toward the South-West along the Loire watershed (Figure 5-18). Accordingly, the Lusitanian aquifer recharges from outcrops in the southeast part of the basin (the Burgundy region), i.e. situated about 120 km away from the PilotSTRATEGY study area.

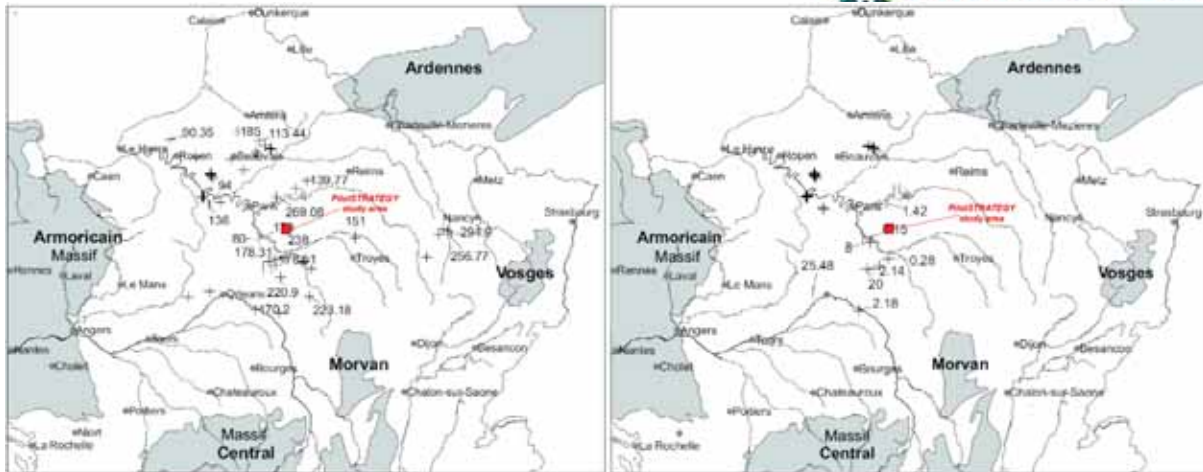


Figure 5-17. Hydraulic head (mNGF; left) and hydraulic conductivity (mDarcy; right) from the main wells (+) tapping the Lusitanian aquifer in the Paris Basin (Gonçalvès, 2003).

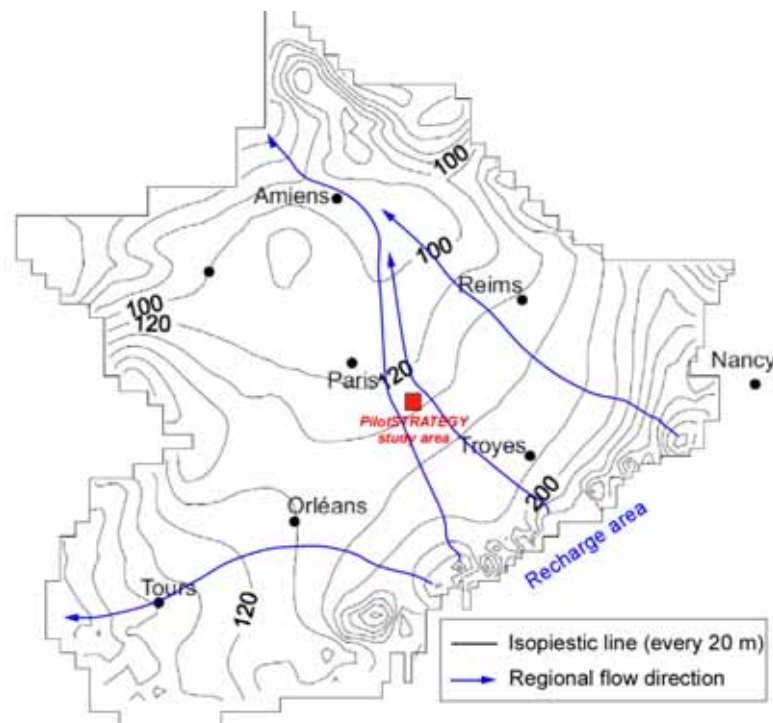


Figure 5-18. Calculated piezometric map of the Lusitanian aquifer in the Paris Basin (Gonçalvès, 2003) and direction of the regional flow.

Petrophysical measurements on core plugs are limited to investigations in a few geothermal wells mainly located North and South of Paris (i.e. off-center from the area of interest). The studied samples of oolitic or bio-oolitic grainstones have undergone minor diagenesis (matrix dissolution, very local cementation) and had a total porosity greater than 10% which is mostly microporosity (Bouniol, 1985). The petrophysical data were complimented by log porosity values back-calculated from well log recovered from 31 oil and 1 geothermal well (Figure 5-19; Caritg et al. (2014)). These give an average log-porosity of the Lusitanian aquifer between 6 and 11 % in the Brie area, with a medium value of 8 to 9 % in the PilotSTRATEGY study area. The highest hydraulic conductivity determined on core sample reached up to 240 mD (2×10^{-6} m/s; Bouniol (1985)). The few tests and measurements carried

out on geothermal boreholes show that the hydraulic conductivity of the Lusitanian aquifer ranges from 1.5×10^{-9} up to 2.45×10^{-6} m/s (Figure 5-17) where fracture permeability prevails (Gonçalvès, 2003). Based on the available data, the average regional flow velocity in the aquifer is estimated to be 5 – 45 cm/year at a regional scale around the extended area of interest.

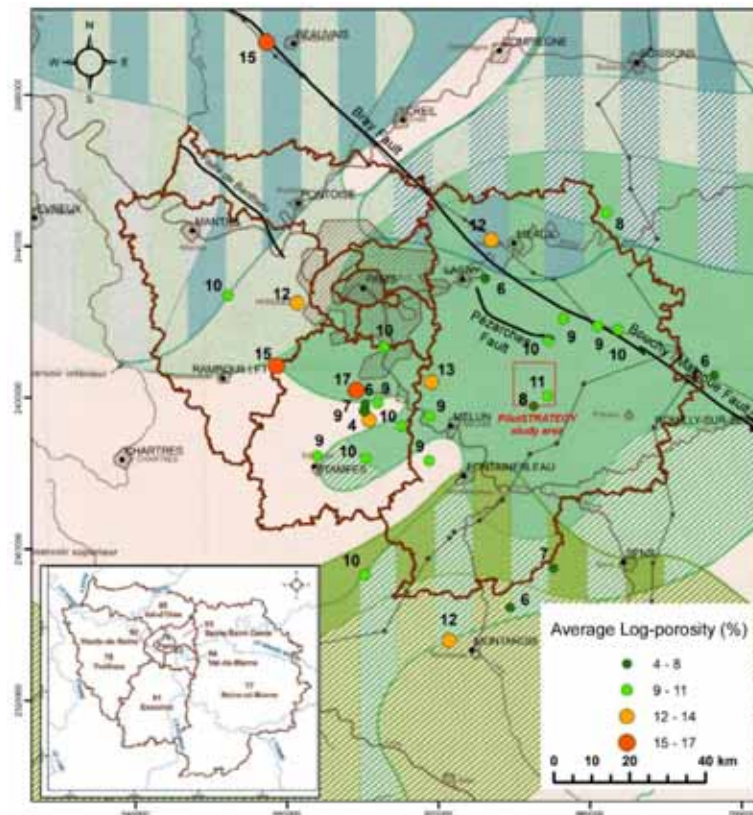


Figure 5-19. Map of the distribution of the log-porosity of the Lusitanian main aquifer / reservoir facies identified by House and Maget (1976).

The hydraulic conductivity measurement on the Kimmeridgian marl is very limited and build upon the research studies led by Andra in the area near its URL, thus some distance from the PilotSTRATEGY study area (Lasseur et al., 2009). The Kimmeridgian marls have a very low and homogeneous hydraulic conductivity, of the order of 10^{-12} m/s, in line with the average values for aquitard in the Paris Basin chosen by Wei et al. (1990).

The value of porosity of the Tithonian limestone selected for the hydrogeological model is around 15% (Seguin et al., 2015). The transmissivity of the Tithonian aquitard (i.e. upper Early Tithonian and Purbeckian) has been measured within the range of 3.5×10^{-6} m²/s to 3.5×10^{-7} m²/s at the border of the basin, where Tithonian limestones (Barrois limestones) crop out at the surface near the Andra URL (cited in Seguin et al., 2015). In the center of the Paris Basin, these values are obviously to be taken as maxima for the more deeply buried Tithonian. At scale of the entire Paris Basin, Andra's hydrogeological quantitative model estimated the hydraulic conductivity of the Tithonian aquitard to be of the order of 10^{-10} m/s (ANDRA, 2005).

5.4.4 Features of the groundwater

The fluids flowing or trapped in the Malm formations are only known for the Lusitanian aquifer in the central part of the Paris Basin. The relatively low salinity of the groundwater in the Lusitanian aquifer, estimated to 2 to 3 g/l (total salinity) in the deepest part of the basin, increases to 5 and 10 g/l along

the natural flow path toward the English Channel (Bouniol and Magnet, 1983). Higher salinity has been measured to the south of Paris (4 – 9.5 g/l), but the lack of data prevents the identification of a regional trend (Bouniol, 1985). The groundwater composition evolves from Na – SO₄ type in the southern and central part of the basin to Na – Cl type in the northwest of the basin, resulting mainly from an enrichment in chloride but constant sulfate concentrations (Housse and Maget, 1976; Bouniol and Magnet, 1983). The Lusitanian aquifer reaches a maximum temperature of 68°C in the central part of the basin and decreases toward the basin edge (Figure 5-20).

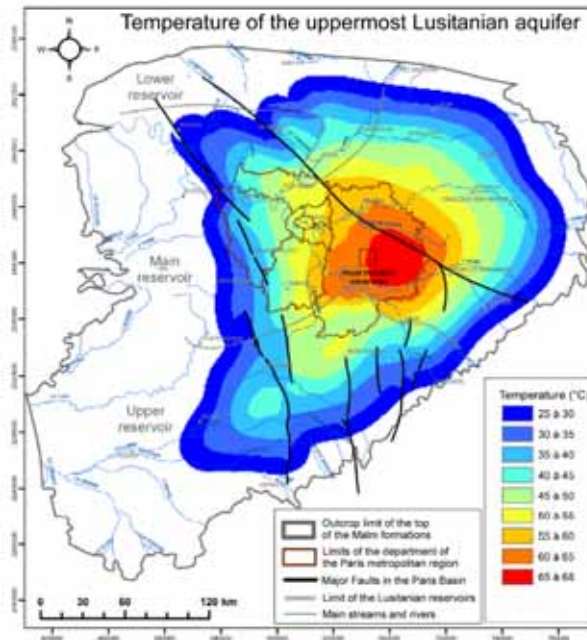


Figure 5-20. Map of the temperature in the Lusitanian aquifer in the center of the Paris Basin (adapted from Housse and Maget (1976) after Caritg et al. (2014)).

As the Lusitanian aquifer in the southern part of the Brie area is only intermediate-to-thin (i.e. effective thickness), the groundwater composition remains unknown on the PilotSTRATEGY study area. The nearest wells drilled in the Lusitanien for geothermal prospecting are located northern to Meaux (40 km), where the effective thickness of the aquifer is at a maximum (Figure 5-20). The average salinity of the groundwater ranges locally from 0.35 to 2 g/l (Bouniol, 1985); the temperature is expected to be around 65°C (Figure 5-20).

5.4.5 Occurrence of faults

The main geological faults in the Lusitanian aquifers includes the major Bouchy/Manoue faults, as already identified in the Dogger formations, and the minor Pézarches fault near the PilotSTRATEGY study area (Figure 5-20). The study area is about 7 km away from the minor Pézarches fault and about 15 km from the major East Malnoue fault. Based on the high salinity contrast between the Dogger (17 – 30 g/l) and the Lusitanian aquifer (2 – 3 g/l) in the center of the basin, it is concluded conceptually that the Bouchy/Malnoue faults do not induce any significant upward flow of groundwater from the Dogger to the Lusitanian aquifer.

5.4.6 Societal uses of the formation

At present, the Lusitanian aquifer and the Tithonian aquitards/aquifers are not exploited for any societal use in the extended study area. Because of its high salinity, the groundwater of the Lusitanian

aquifer cannot be exploited for water supply for human consumption, irrigation or industrial use. Moreover, the successful geothermal exploitation of the Dogger aquifer lowered the interest for the Lusitanian aquifer in the southern Brie area in the past. The Malm aquifer(s) are therefore not subject to any specific regulations in and near the PilotSTRATEGY study area.

5.5 Early Cretaceous formations

The Early Cretaceous formations are alternating unconsolidated sand banks, shale to marl layers of varying nature and thicknesses. The succession of interspersed sand banks forms more or less continuous and connected aquifers considered to be multi-layer aquifer units at the basin scale. A thick layer of marls separates the two main multi-layer aquifers, namely the Wealdan/Neocomian aquifer and the Albian aquifer, in the Lower Cretaceous.

The Early Cretaceous formations are well known thanks to the numerous geothermal and oil wells exploiting the deeper Triassic, Dogger or Lusitanian aquifers as reservoirs. The Albian aquifer has been extensively exploited in the Paris Basin for water supply since the drilling of the first artesian well in 1841 in Paris, and for geothermal exploitation since the 1970's. However, the Neocomian aquifer is more limited as the formation is mainly from studies of low-temperature geothermal potential (e.g. BRGM, 1983; Grenet et al., 1995). Hydrogeological and hydrodynamic properties of the aquifer units are from data retrieved from the water and geothermal wells. Their knowledge remains constrained by the influence of the management policy of the groundwater resource, the impact of over-exploitation of the aquifer and the (narrow) spatial distribution of the wells within the Paris Basin.

5.5.1 Geological features of the formation

The geological synthesis of the Paris Basin of Mégnien et al. (1980) provides an overview of the different facies forming the Early Cretaceous formations (Table 5-4).

Table 5-4. Simplified lithostratigraphy of the Early Cretaceous formations in the Paris Basin, defining the Neocomian and Wealdian formations and the dominant lithology in the Paris Basin (adapted from Mégnien et al. (1980) and Vernoux et al. (1997)). The color code specifies the overall hydrogeological properties of the geological formation: aquifer (blue), aquitard (light blue) and aquiclude (white).

Geological period	Chronostratigraphy	Lithological domains	Classical stratigraphy	Dominant lithology
Early Cretaceous	Late Albian	Albian	Albian	Brienne Marl
	Middle Albian			Gault Clay
				Frécambault Sand
				Tegulines Clay
				Drillons Sand
	Early Albian			Armance Clay
	Green Sand			
	Aptian	Barremo - Aptian	Aptian	plastic clay and sandy marl
	Late Barremian		Barremian	clay
	Early Barremian	sand		
		clay		
	Hauterivien	Neocomian	Wealdan	Perthes Sand
clay				
Châteaurenard Sand				
clay				
Valanginian	Château-Landon Sand			
	clay			
Valanginian	Puiselet Sandstone			
	clay			
	Griselles Sand			
Valanginian	Neocomian	Wealdan	clay	

The Neocomian denotes the lower formations of the Early Cretaceous, from the top Early Barremian downwards (Mégnién et al., 1980; Vernoux et al., 1997). The Neocomian is a continental facies (i.e. Wealdian facies) consisting of a succession of poorly consolidated sand and sandstone layers separated by sandy clay layers with significant lateral and vertical facies variation in the center of the basin (Figure 5-21). The Valanginian clay beds overlay the Tithonian (Jurassic) limestones before transitioning to coarse detrital deposits, poorly classified – locally named the Griselles Sands – which extend over almost the whole Paris Basin. Various Hauterivian sands (fine to medium grain sand) and early Barremian clays, with a prominent sandy bed at the bottom – named the Perthes Sands – complete the Neocomian. The Hauterivian sandy bed does not outcrop on the South-East and East part of the basin, where a limestone facies is present (Figure 5-21).

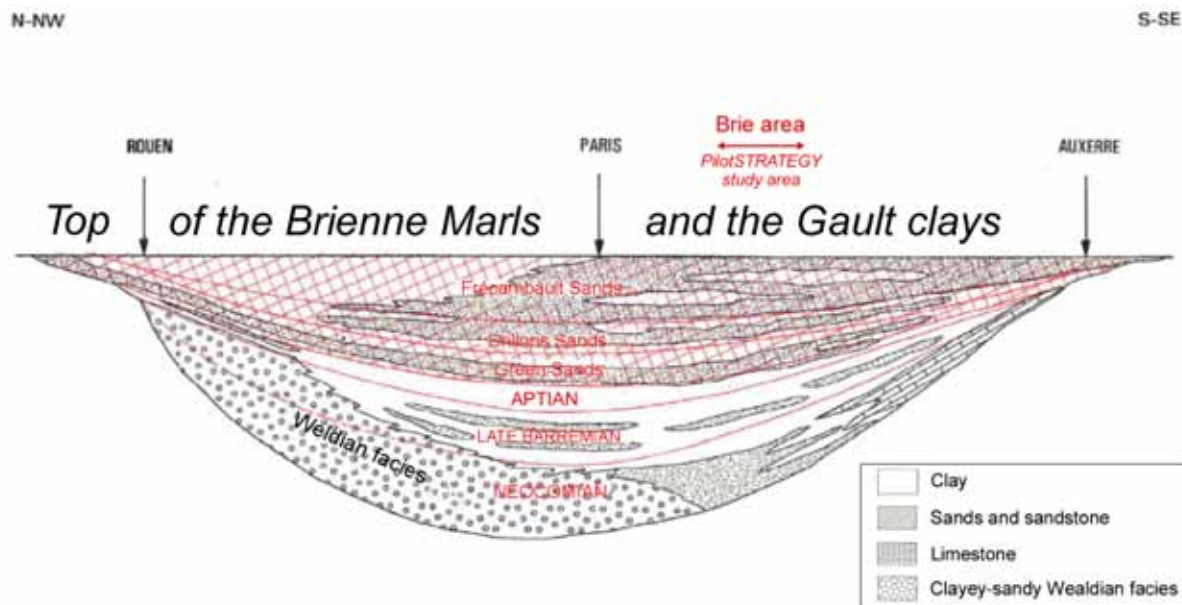


Figure 5-21. Schematic cross-section of the Paris Basin showing the structure of the reservoir in the Lower Cretaceous (after Sarrochi and Levy-Lambert, 1966). Red shading illustrate the distribution of the Albian formations.

The Late Barremian and Aptian clayey and marly beds separate the sandy-clayey Neocomian formation from the sandy-clayey Albian complex. A sandstone layer characterizes the bottom of the Late Barremian formation, before transitioning to clay beds interspersed locally with irregular sand beds (Figure 5-21). The overlying Aptian formation is composed of (fine to coarse grained and glauconitic) sand banks and sandy clay beds in the upper part.

The Early and Middle Albian contains three poorly consolidated sand units, namely the Green Sands (locally clayey – up to 30% glauconite – and consolidated), the Drillons Sands (fine to coarse grains, slightly glauconitic) and the Fréambault Sands (fine grains, slightly glauconitic). The three sand units are interspersed with two main clay layers, namely the Armance Clays (stiff clay, slightly sandy) and the Télugines Clays (slightly sandy clay). These sandy units are overlaid by the Late Albian formations, named the Gault Clays and Brienne Marls. The Gault Clays are composed of plastic, locally glauconitic and slightly sandy clays, topped by Brienne Marls, which are marls with calcareous and glauconitic clays.

5.5.2 Distribution and extent of the aquifer, aquitard and aquiclude units

The Early Cretaceous formations have an average thickness of 330 m in the Paris metropolitan area (Castro et al., 1998) and 355 m in the Brie area. The various poorly consolidated sand banks confer

aquifer properties to part of the Neocomian and (Early and Middle) Albian sediments. The multi-layer Neocomian aquifer, consisting of alternating very fine sand and sandy clay, varies in thickness from 20 to 90 m in the center of the Paris Basin (Mégnyen, 1979; Mégnyen et al., 1980). The sandy banks display generally good permeability, but the layers are relatively discontinuous. In the eastern part of the basin, the marine facies (marl, marly limestone, shell limestone) have fairly low permeability.

Within the Early and Middle Albian, the Frécambault, Drillons and the Green sands aquifers are separated by the Télugines and Armance clays, with thickness varying laterally from ca. 1 to 10 meters. Although of low permeability, the lateral extent and the relatively low thickness of the clay layer suggests that the Télugines or the Armance clays should be considered to be aquitards, possibly allowing vertical drainage within the sandy-clayey Albian aquifer complex.

The Late Barremian and the Aptian sandy-clay formations, which are overall less permeable, lie between the two aquifer units. The Late Barremian and the Aptian sandy-clays can together reach a maximum thickness of 100 m in the center of the basin (70 m thick in the Brie area) conferring aquiclude properties to these formations overall. However, the thickness of Aptian and Barremian clayey beds are not constant and the Aptian clays are interspersed with sand layers, notably in the south of the Brie area (Melun; Seguin et al, 2015). Accordingly, vertical drainage may occur in the areas of the sedimentary basin where the thickness of sandy-clay formations is minimal, conferring locally to regionally aquitard properties to the Late Barremian and the Aptian formations. As a vertical drainage process cannot be excluded between the two main aquifer complexes, the Early Cretaceous formation are considered by some authors as a single hydrodynamic system, namely the Albian-Neocomian complex (Vernoux and Manceau, 2017). The Gault Clays and Brienne Marls (Late Albian) formation separate the Albian aquifer from the Late Cretaceous formation, acting as an aquiclude.

The multi-layer Albian and Neocomian aquifers extend over a large part of the Paris Basin (Figure 5-22), mostly as confined aquifer, covering a global area of about 75,000 km². The depth of the aquifers increases from the outcrops towards the center of the basin, with a maximum depth in the Coulommiers area (Brie area), where the top of the Albian aquifer reaches up to 800 m depth. Based on wells in the PilotSTRATEGY study area, the Neocomian aquifer is about 60 m thick compared to a total thickness of 130 m of the entire Neocomian. The overlying Barremian clayey formations are locally thick – 70 m and 20 m thick of Early Barremian and Late Barremian clays, respectively – and overlain by 55 m thick of dominantly clayey Aptian beds. The Barremo-Aptian clay unit is therefore locally very thick (145 m), suggesting that it will act as an aquiclude between the two Early Cretaceous aquifer units in the PilotSTRATEGY study area. The multi-layer Albian aquifer falls within a 110 m thick sequence and is overlaid by about 40 m of Gault Clays. The larger geographical extent and thickness of the sandy-clayey Albian complex suggests that this is the main Early Cretaceous aquifer within the Paris Basin (Figure 5-22).

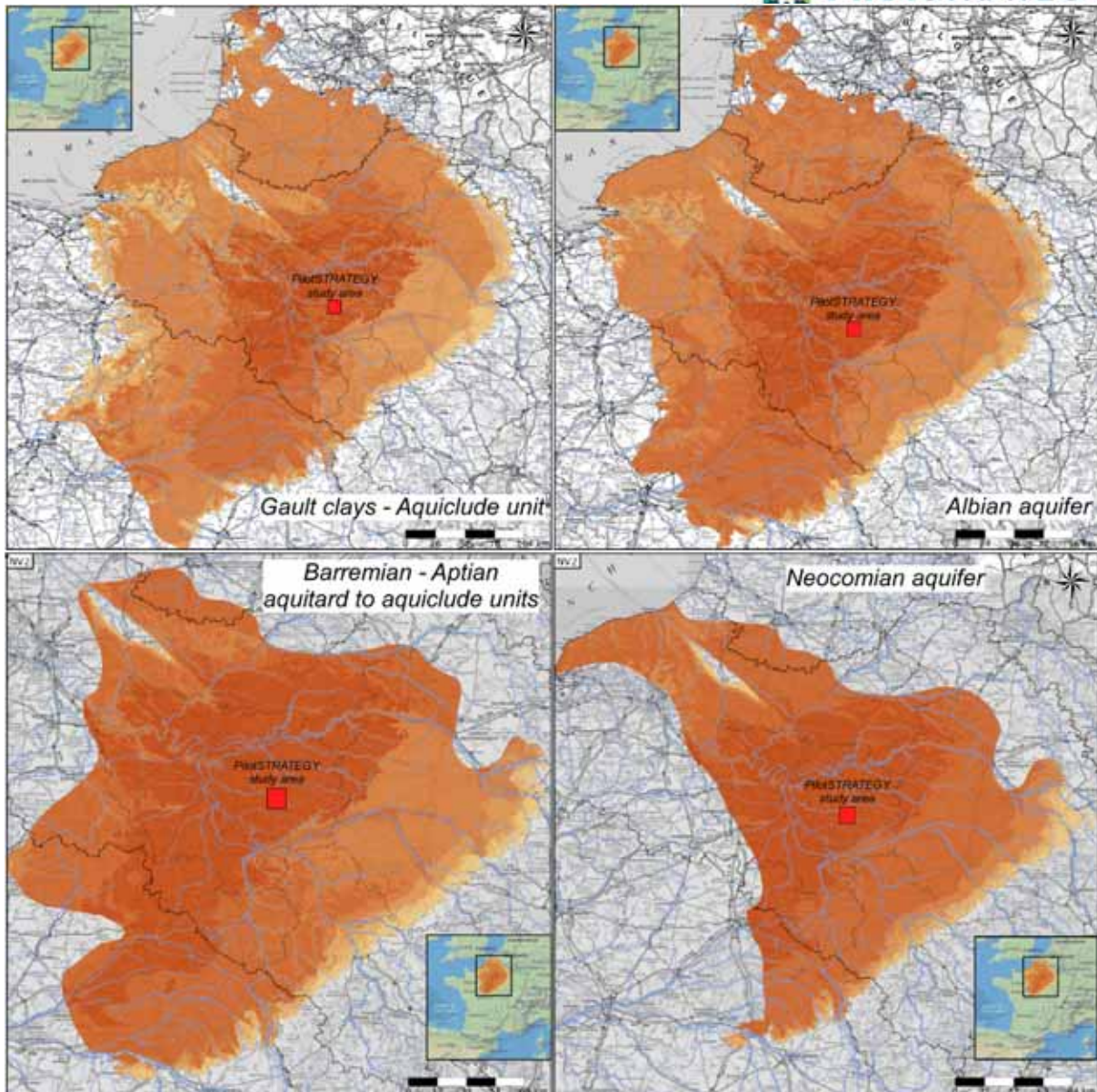


Figure 5-22. Spatial extents of the hydrogeological units of the early Cretaceous (BDLISA, 2023), including the Neocomian aquifer (bottom right), the Late Barremian-Aptian aquitard/aquiclude (bottom left), the Early and Middle Albian aquifer (top right) and the Late Albian/Gault Clays aquiclude (top left).

5.5.3 Hydrogeological properties of the aquifer

Since the first deep wells were drilled in the center of Paris, the Albian aquifer has been considered as an extensive and unique groundwater resource in the Paris metropolitan area due to its large geographical extent, its artesian pressure, and the good quality (low salinity) of the groundwater. The aquifer's most productive zones are detrital facies in the center of the basin. The relatively coarse grain size of the Albian sands (compared to the very fine Neocomian sands) and the lower depth of the aquifer top made the Albian aquifer less expensive to exploit than the Neocomian aquifer. Taken together, these characteristics have led historically to a preferential exploitation of the Albian aquifer. The knowledge of the hydrogeological and hydrodynamic properties of the Albian and Neocomian aquifers are strongly influenced by the historical exploitation and the management policy of the groundwater resource since the 1840's.

The unique properties of the Albian aquifer, notably the artesian pressure in the center of the basin, have led to an ever-increasing number of wells in the Paris metropolitan area as drilling techniques improved in the beginning of the 1920's. Artesian flow and the water table both gradually decreased from the 1840's onwards, under the effect of the growing number of abstracting wells. A management policy was progressively established to limit the over-exploitation of the groundwater resource considered as strategic for the Paris metropolitan region, first by imposing a mandatory drilling permit application for new borehole deeper than 80 m in the 1935's, and by regulating regionally the groundwater volume that could be withdrawn in the 1970's. Following these regulations, the water table level gradually decreased down to -115 m (compared to the reference level) by the early 1970's in the Paris metropolitan area, then increased by 10 m by 1985, before stabilizing in the early 2000's. Since then, the water table has tended to rise again, as a result of a more restrictive management policy.

This historical exploitation in the Paris metropolitan region has significantly impacted the natural regional flow of the Albian aquifer. Before the early 1930's, the groundwater naturally flowed from the east and southeast to the northwest of the Paris Basin (Raoult, 1999; Raoult et al., 1999), along the Somme and the Seine River valleys (Figure 5-23). The exploitation of the aquifer in the Paris metropolitan area caused the appearance of conical piezometric depressions in the center of the basin (Vernoux et al., 1997; Raoult, 1999). Ever since, the groundwater flows towards the Paris metropolitan area in the central part of the basin (Figure 5-23), and thus from the South-East to the North-West in the Brie area.

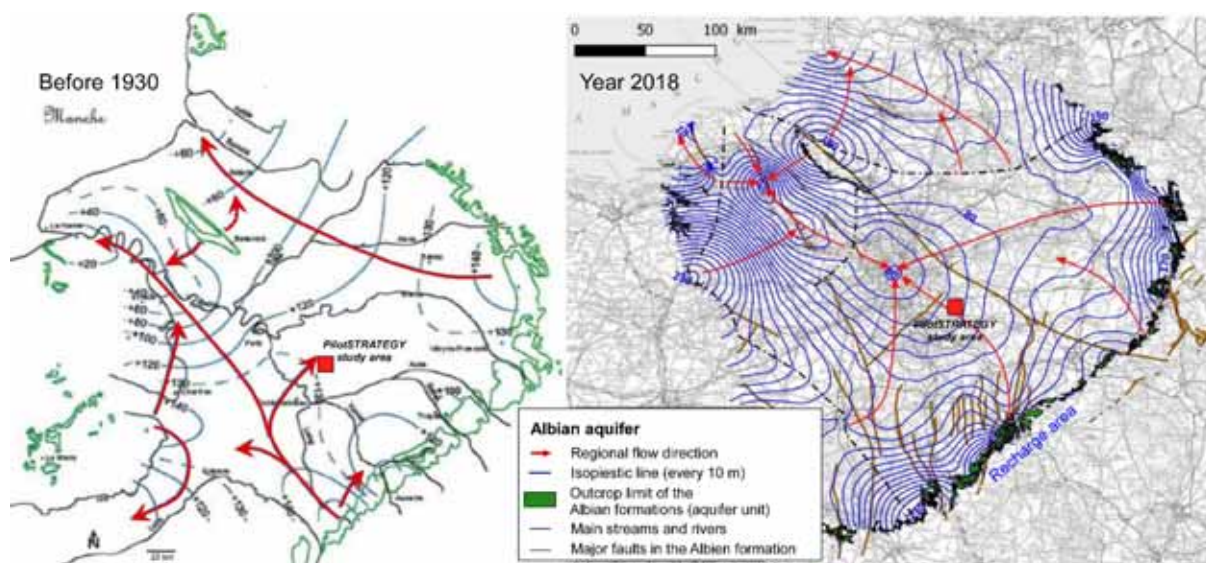


Figure 5-23. Piezometric map of the Albian aquifer : before 1930 (Raoult, 1999) and based on water table level measured in 2018 (Dupaigne et al., 2019).

Most of the recharge of the Albian aquifer occurs at outcrops located on eastern and southeastern edge the basin as well as on the northeast of the basin (Bray anticline; Figure 5-23). This recharge area is located at a minimum distance of 80 km South-East of the PilotSTRATEGY study area. Several hydrogeological studies and models have shown that, depending on location, the Albian aquifer is supplied by the overlying (Late Cretaceous) Cenomanian chinks and by the underlying Neocomian sands and locally the Tithonian limestones (Vernoux et al., 1997; Raoult, 1999; Marti, 2000; Seguin et al., 2015). Recharge from the outcrops and by downward drainage from the overlying (Late Cretaceous) chalk formations are estimated to contribute to 42 – 55% and 31 – 48% of the total recharge, respectively. The recharge of the Albian aquifer by upward drainage from the Neocomian

sands and (locally) Tithonian limestones were estimated as much more moderate, contributing 7 – 8% and 0 – 7% of the total recharge, respectively. Recharge by the Neocomian aquifer is highly variable spatially, with a maximum contribution in the Paris metropolitan area under the influence of the density of groundwater extraction. Geochemical studies suggested an influence of the deeper Upper Jurassic aquifer (Raoult et al., 1997; Raoult, 1999; Innocent et al., 2021), although the extent of this cannot be quantified.

The Albian aquifer naturally discharges into the English Channel and the different main rivers (i.e. Seine, Loire, Somme Rivers) and the associated watercourses (Gonçalvès, 2003; Seguin et al., 2015). Discharge also occurs by natural upward drainage toward the overlying Late Cretaceous chalk in the areas where the Albian aquifer is artesian and away from the influence of groundwater extraction (Dupaigne et al., 2019), i.e. overall, along the valleys of the main river (Figure 5-24).

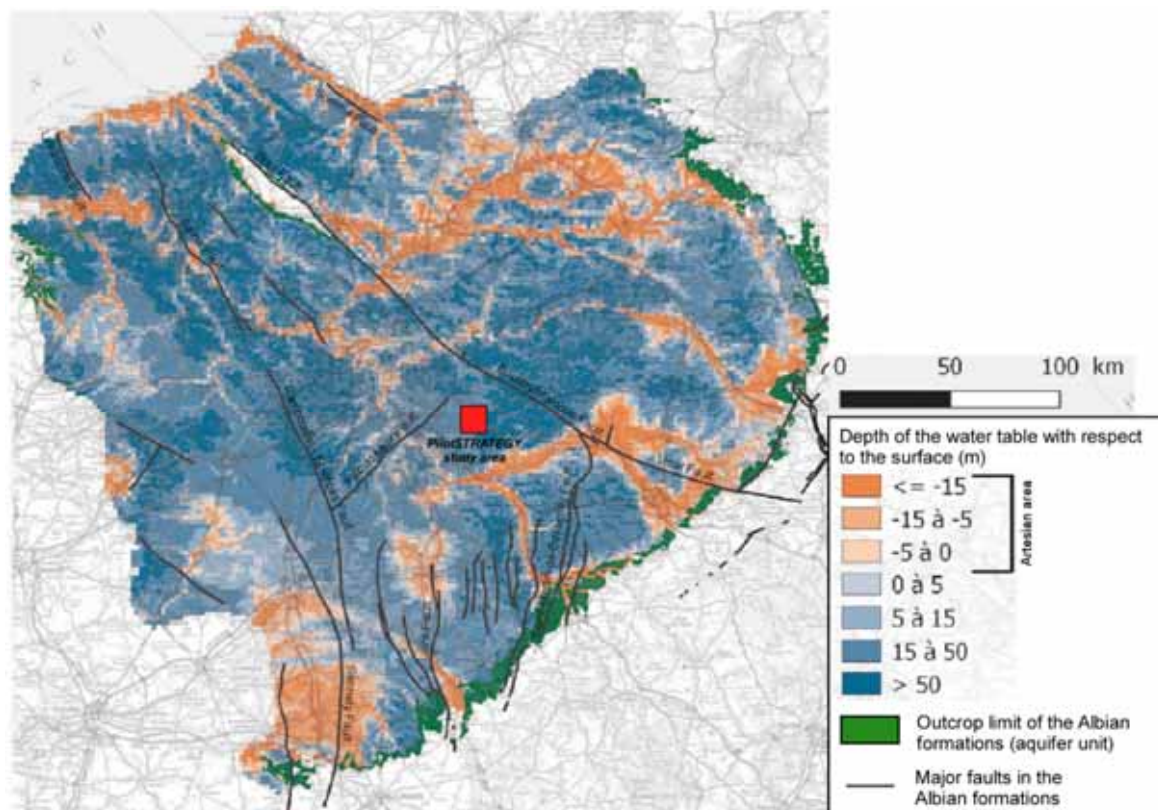


Figure 5-24. Map of the depth of the water table in the Albian aquifer with respect to the surface, and the main faults that intersect the aquifer (adapted from Dupaigne et al., 2019). Negative values (orange - brown) show where the aquifer has artesian potential.

The transmissivity and hydraulic conductivity of the Albian aquifer were mapped across the Paris Basin (Vernoux et al., 1997; Raoult, 1999; Hervé and Ignatiadis, 2007). This approach highlighted a zone of high transmissivity ($> 10^{-3} \text{ m}^2/\text{s}$) extending from the outcrops in the South of basin – near Orleans – toward the north of Paris (Figure 5-25). The Brie area is part of a zone with lower transmissivities, of the order of $10^{-4} \text{ m}^2/\text{s}$ but locally lower, due to the occurrence of clayey sands. From the local thickness of the sandy portions of the aquifer, the hydraulic conductivity of the Albian aquifer ranges from 0.1 to 10^{-6} m/s (Seguin et al., 2015). In the PilotSTRATEGY study area, the hydraulic permeability is estimated around 10^{-6} m/s ($< 30 \text{ m/y}$) based on the hydrogeological model developed by Seguin et al. (2015). An average porosity of 30% is commonly reported for the Albian sands (DHYCA, 1965; Vernoux et al., 1997; Seguin et al., 2015).

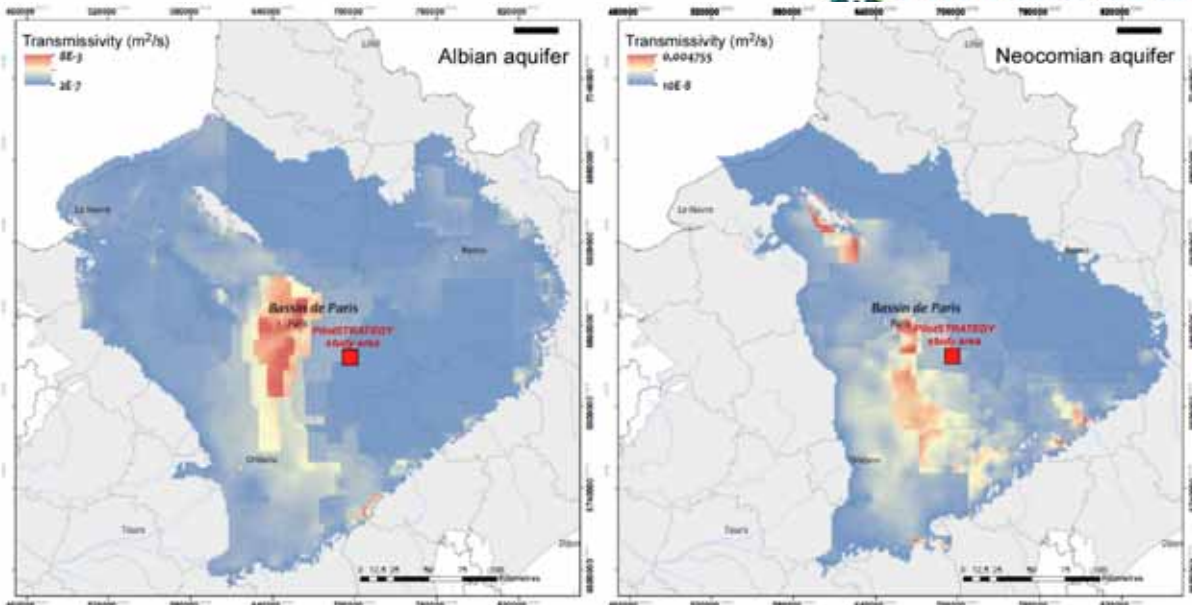


Figure 5-25. Map of the transmissivity of the Albian (left) and Neocomian (right) aquifers (Seguin et al., 2015).

The hydrogeological characteristics of the Neocomian aquifer are influenced by the historical exploitation of the Albian aquifer. Before the exploitation of the Neocomian and Albian aquifers in the Paris metropolitan region, the groundwater naturally flowed in the basin from South-East to North-West. Although the exploitation of the Neocomian aquifer in the center of the basin only began in 1996, a drawdown of its water table was induced by the historical groundwater abstractions in the overlying Albian aquifer. The watertable drawdown of the Neocomian aquifer is more moderate (≈ -50 m in Paris) than that of the Albian aquifer (≈ -100 m in Paris). The occurrence of the induced piezometric cone in the aquifer modified the natural groundwater flow of the aquifer in the center of the basin and reoriented the flow directions from the East and South-East toward the Paris metropolitan area (Figure 5-26; Vernoux et al., (1997)). In the Brie area, the flow direction in the Neocomian aquifer hence slightly differs from that of the Albian aquifer in the center of the basin due to a lower hydraulic gradient (i.e. lower water table drawdown in the Paris metropolitan area), but follows the same regional flow direction. The average natural flow gradient for the Albian aquifer and Neocomian aquifer are estimated to 3 ‰ and 0.4 ‰, respectively (Vernoux and Manceau, 2017).

The sandy Neocomian aquifer does not outcrop on the eastern and southern edges of the basin, where Hauterivian limestone facies are found instead. Accordingly, the recharge of the sandy Neocomian aquifer may come from the Hauterivian limestones and the underlying Early Tithonian/Purbeckian limestones, mainly via the fracture porosity/permeability as these formations are otherwise considered to be aquitards (Seguin et al., 2015). The aquifer naturally discharges into the English Channel and the main rivers (i.e. Seine and Somme Rivers).

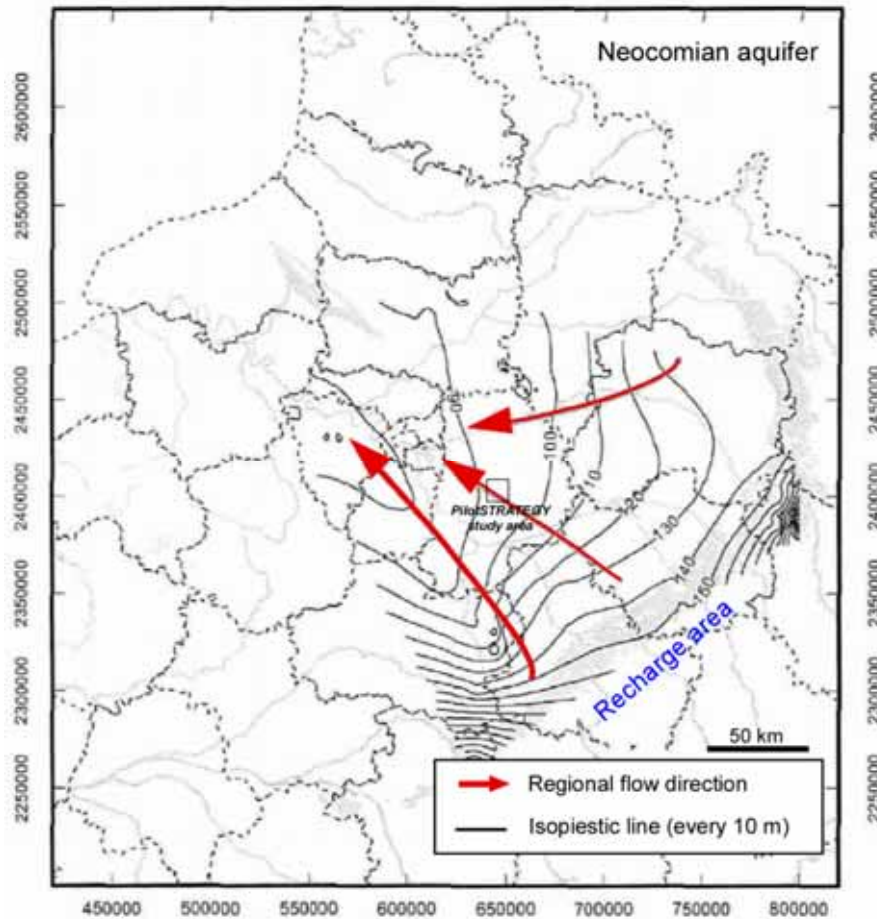


Figure 5-26. Piezometric map of the Neocomian aquifer (Vernoux et al., 1997).

The transmissivity of the Neocomian aquifer does not exceed $4 \times 10^{-3} \text{ m}^2/\text{s}$, and is thus overall lower than that of the Albian aquifer within the basin. This hydrodynamic difference results from the finer grain size of the sands and a slightly higher clay content in the Neocomian aquifer. The transmissivity map displays preferential zones with relatively high permeability, following a North-Northwest – South-Southeast direction in the southern part of the basin until Paris, near to the outcropping zones in the Bray area and in the southeast part of the basin edges (Figure 5-25). The highly variable transmissivity within the sedimentary basin is the result of uneven cementation of the sand beds (Dupaigne et al., 2019). In the Bray area, the transmissivity of the Neocomian aquifer was estimated to be of the order of 10^{-4} to $10^{-5} \text{ m}^2/\text{s}$ (Seguin et al., 2015; Vernoux and Manceau, 2017), equivalent to a hydraulic conductivity of 10^{-6} to 10^{-7} m/s (3 to 30 m/y). An average porosity of 28 % is commonly reported for the Neocomian sands (DHYCA, 1965; Seguin et al., 2015; Vernoux and Manceau, 2017).

Hydrodynamic parameters of the Early Cretaceous clay formations are rarely measured, although of major interest to consider the vertical drainage and resulting recharge or discharge between the successive aquifers or aquitards. Based on the knowledge from storage of domestic gas in the Neocomian and Albian aquifers, vertical permeabilities were measured in the Aptian clay and in the Gault Clay and estimated to $< 0.1 \text{ mD}$ (i.e. nearly equivalent to $< 10^{-9} \text{ m/s}$) and $1 - 17 \text{ mD}$ (i.e. $10^{-9} - 1.7 \times 10^{-7} \text{ m/s}$), respectively (Vernoux et al., 1997). Porosities of the Aptian and Gault clays used in hydrogeological model are generally around 40% (Seguin et al., 2015).

5.5.4 Features of the groundwater

Hydrochemical data for the Neocomian aquifer are very scarce in the Paris Basin, limited to complete analyses for less than 10 boreholes mainly located in the Paris metropolitan area, and salinity measurement from about 50 boreholes covering the central part of the basin. Although the number of wells in the Albian aquifer are relatively more abundant, the knowledge of the chemical properties of Albian waters is still limited at the basin scale as most of the boreholes are located in the Paris metropolitan area and are commonly used for geothermal extraction and so are not subject to water quality monitoring.

The groundwater from the Neocomian aquifer is fresh water, with a mean salinity of 1 g/l in the Paris Basin (Figure 5-27). The highest salinity values reach up to 5 g/l in the eastern part of the basin. Although influenced by the limited dataset (whereby contours are drawn around each borehole, the so-called local nugget effect), the groundwater salinity is generally lower in the southwest part (250 – 870 mg/l) and higher in the eastern and northern peripheral regions around the Paris metropolitan area (Figure 5-27; Vernoux et al., 1997). Chemical analyses indicate a Na-Ca – HCO₃ water type freshwater to a Na – HCO₃-SO₄ type near Melun (south of the Brie area). The temperature of the groundwater follows the general pattern in the central part of the Paris Basin, with a maximum temperature of 45°C in the deepest part of the basin near Coulommiers (Figure 5-28).

The fresh groundwater in the Albian aquifer is overall less mineralized than in the Neocomian aquifer, with salinity lower than 1.5 g/l throughout most of the Paris Basin and lower than 0.6 g/l (61 – 635 mg/l) in the Paris metropolitan area (Hervé and Ignatiadis, 2007), where more data are available (Figure 5-29). The Albian aquifer displays generally lower Na, Mg, F and Sr concentrations than the Neocomian aquifer (Raoult et al., 1997). Overall, the freshwater is of Ca – HCO₃ type and considered of high quality for drinking water supply (Innocent et al., 2021), after treatment of the relatively high iron and manganese concentration (i.e. > threshold values) and locally high fluorine concentration (Hervé and Ignatiadis, 2007). The groundwater temperature ranges from 11°C to 38°C throughout the Paris Basin (Raoult, 1999; Seguin et al., 2015), with a maximal temperature in the center of the basin (Figure 5-28).

Salinities of up to 5 g/l were measured in the Albian aquifer in the northern part of the basin and east of the Paris metropolitan region. These salinity highs are associated with the evolution of the groundwater composition from Ca – HCO₃ type to Na – Cl type, and result from two different phenomena. East of the Paris metropolitan area, the occurrence of evaporites in the Purbeckian (Late Malm) combined with vertical drainage, due to a higher hydraulic head in the Neocomian aquifer, are deemed to explain the salinity highs observed in both the Neocomian (Figure 5-27) and Albian aquifer (Figure 5-29). In the northern part of the basin, the salinity of the aquifer is related to the occurrence of structurally trapped groundwater due to the shape of the Albian deposits, which do not outcrop and end in a wedge to the North where they are overstepped by the Late Cretaceous chalk. The trapped groundwater has a longer residence time and has therefore undergone more intense water-rock interaction than the groundwater flowing in most of the Albian aquifer (Roux, 2006).

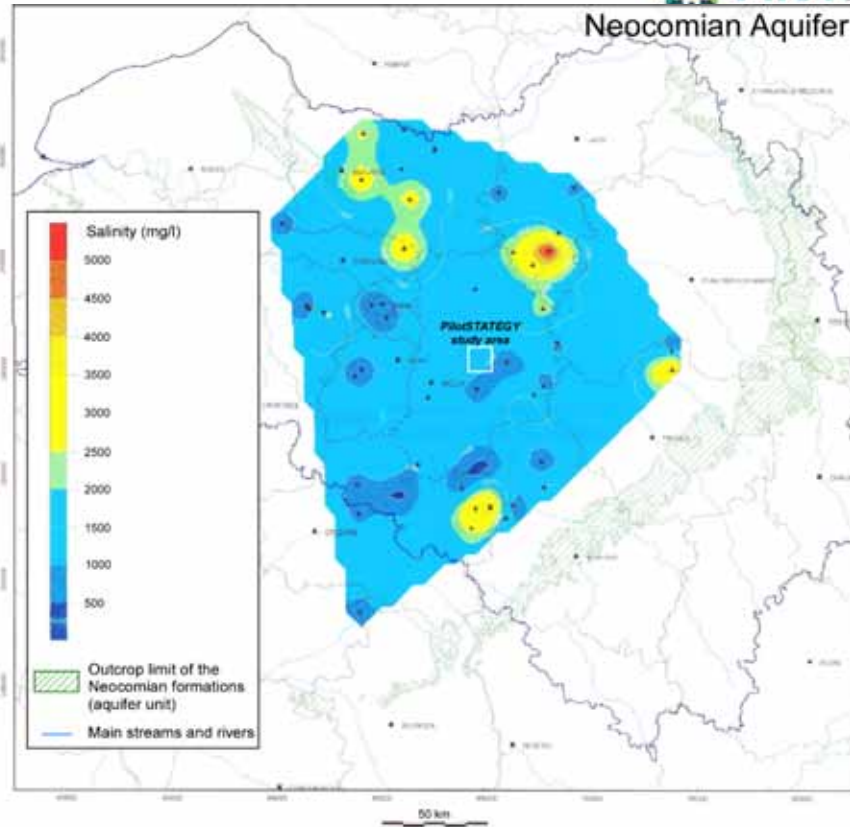


Figure 5-27. Map of the salinity of groundwater in the Neocomian aquifer. The location of wells used for the interpolation are reported to consider local nugget effect due to the spatial distribution of the data (adapted from Vernoux et al., 1997).

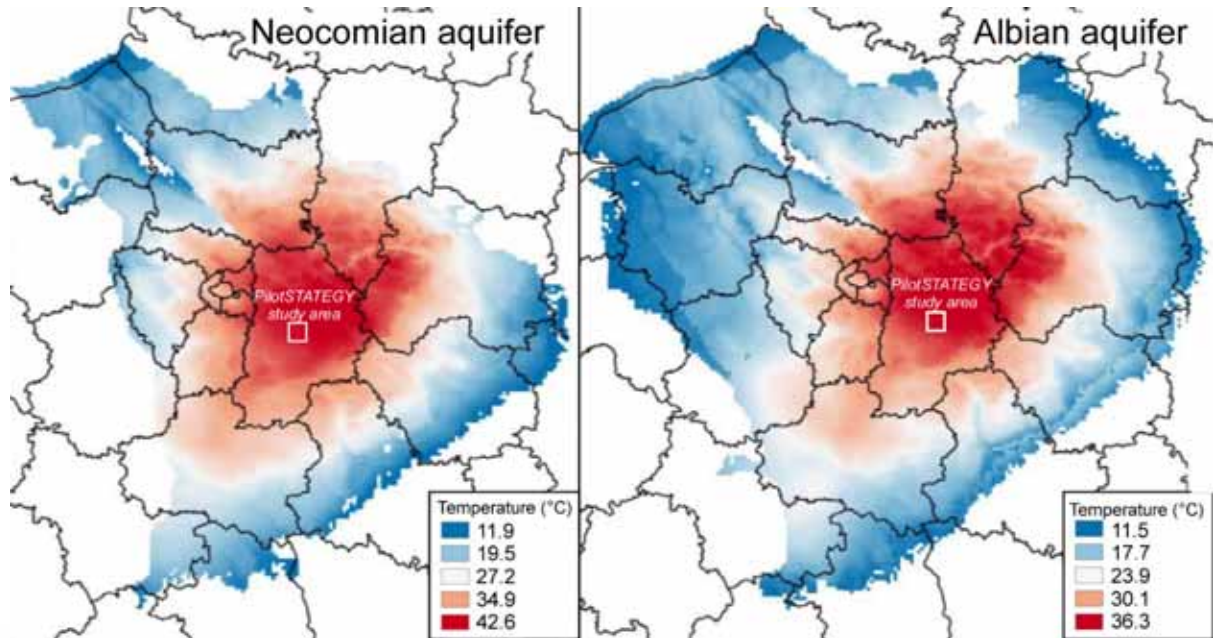


Figure 5-28. Map of the temperature within the Neocomian (left) and the Albian (right) aquifers (adapted from Seguin et al., 2015).

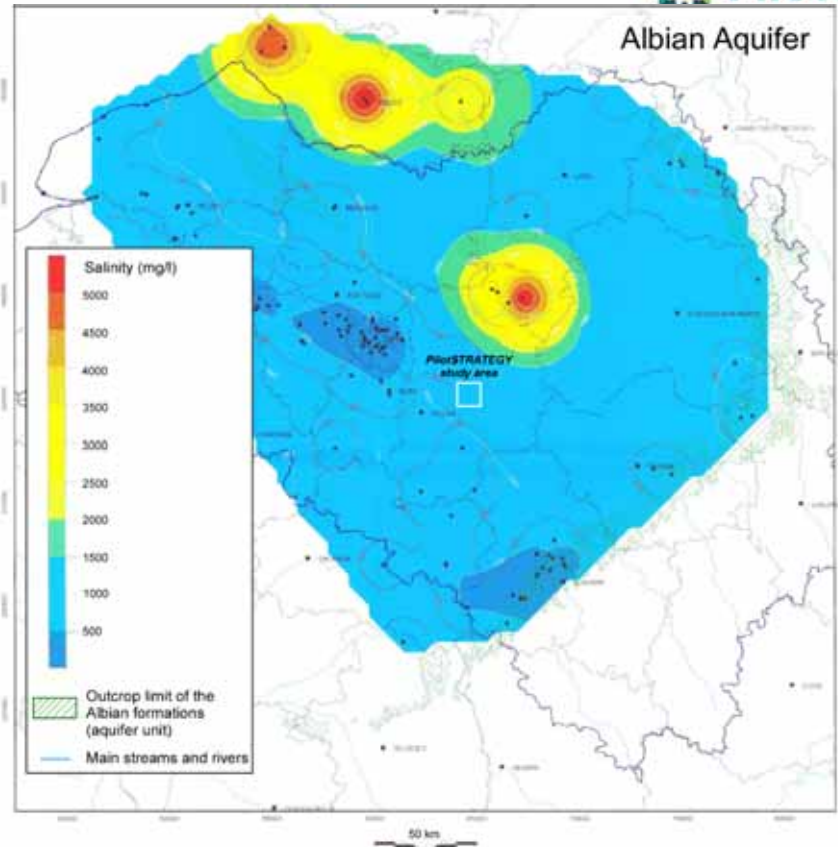


Figure 5-29. Map of the salinity of groundwater in the Albian aquifer. The location of wells used for the interpolation are reported to consider the influence of the spatial distribution of the data on the result (adapted from Vernoux et al., 1997).

5.5.5 Occurrence of faults

All the major faults that intersect the Albian aquifer are illustrated in Figure 5-24, including the regional Bray fault and the Bouchy/Malnoue faults in the southern Brie area. Most of the hydrogeological studies focusing on the Albian aquifer did not report the tectonic structures as potential semi-permeable barriers within the aquifer (Vernoux et al., 1997; Raoult, 1999; Seguin et al., 2015; Dupaigne et al., 2019). Accordingly, these faults appear not to affect the natural sub-horizontal flow (Figure 5-23), which confer (sub-horizontal) permeable properties to the regional tectonic structures within the Albian aquifer at basin scale.

5.5.6 Societal uses of the formation

The Neocomian and Albian aquifers are both considered to be strategic resources for drinking water in the Paris metropolitan region, although the exploitation of the Albian aquifer was historically favored due to its (relatively) shallower depth and higher water quality. Accordingly, management policy has been progressively established since the 1940's to regulate the exploitation, either for drinking and industrial water supply or for geothermal production (Roux, 2006). The Neocomian aquifer is exploited to only a very low extent in the Paris metropolitan region, in order to minimize any potential impact on the water table of the Albian aquifer. As previously mentioned, the Albian aquifer is extensively exploited but with strict regulation of the volume abstracted. No wells exploiting the Neocomian or the Albian aquifers are reported in the Brie area. The nearest wells identified in the extended area of interest are located more than 25 km far from the PilotSTRATEGY study area, i.e. at Evry and Corbeil Essonne to the west and Bougligny, near Melun to the SW (Figure 5-27).

5.6 Late Cretaceous formations

The Late Cretaceous is largely represented by chalk formations, i.e. limestone composed mainly of the tests of microorganisms (coccoliths). The Late Cretaceous chalk is formed by the generally clayey Cenomanian, overlain by the Turonian and Senonian strata. The Late Cretaceous formations crop out at the surface and form a vast halo around the Tertiary sedimentary deposits outcropping in the Paris metropolitan region.

The chalk outcrops over a total area of nearly 75,000 km² (e.g. Figure 5-1). The outcropping chalk formations are extensively exploited for drinking water and irrigation, where the aquifer is unconfined. Knowledge of the hydrogeological and hydrodynamic properties of the chalk formations below the Tertiary deposits in the deep zone of the basin remains limited. In the Paris metropolitan region, outcrops of the Chalk aquifer are spread over a narrow area, mostly in the southeastern and western part of the region. Groundwater abstraction from the confined parts of the Chalk aquifer has been limited to a few zones under a thin overlay of Tertiary deposits (i.e. in rivers valleys), where the permeability remains relatively high (Schomburg et al., 2005). The Brie area is a plateau formed by Tertiary sedimentary deposits, overlying the Turonian and Senonian chalks (Figure 5-30). The Late Cretaceous formations are therefore overlain by Paleogene sediment on the PilotSTRATEGY study area, limiting the local interest and the associated hydrogeological knowledge of the chalk formations.

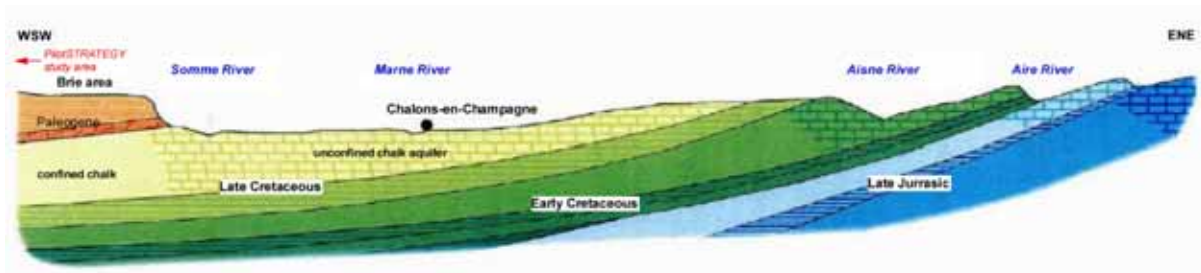


Figure 5-30. Schematic geological cross section of the southeastern and eastern part of the Paris Basin (adapted from Rouxel-David, 2002).

5.6.1 Geological features of the formation

A geological synthesis of the Paris Basin (Mégnyen et al., 1980) provides an overview of the different chalky facies composing the Late Cretaceous formations (Table 5-5), which reach a maximum thickness of nearly 700 m in the basin center.

Table 5-5. Simplified lithostratigraphy of the Late Cretaceous formations in the Paris Basin, showing the Senonian formations as the dominant lithology in the Paris Basin (adapted from Mégnyen et al. (1980)). The color code specifies the overall hydrogeological properties of the geological formations: aquifer (blue), aquitard (light blue) and aquiclude (white). Formations labelled in grey have not been identified beneath the PilotSTRATEGY study area.

Geological period	Chronostratigraphy	Lithological domains	Dominant lithology
Late Cretaceous	Maastrichian	Senonian	flinty chalk
	Campanian		
	Santonian		
	Coniacian		
	Turonian	Turonian	clayey chalk - chalk
	Cenomanian	Cenomanian	glauconitic chalk sandy and chalky marl

The Cenomanian formations are formed of glauconitic chalk and limestone with marl or clay interlayers. In the PilotSTRATEGY study area, the Cenomanian, overlaying the Early Cretaceous Gault Clay, is composed of a lower 40 m thick clay layer and an upper 65 m thick glauconitic chalk layer.

The Turonian formation is described as a compact chalk, grey in the lower part (clayey chalk) becoming whiter (purer chalk) in the upper part and free of any flint. The occurrence of marl in the lower part of the formation can occur locally, but has not been observed in the wells located in the PilotSTRATEGY study area. In the zone of interest, the 230m thick Turonian chalk overlies the Cenomanian clayey and chalky formations.

The Senonian is divided into four stages; from base to top the Coniacian, the Santonian, the Campanian and the Maastrichtian stages (Table 5-5). The Turonian-Senomanian transition occurs with the appearance of massive flint-rich chalk. The three first stages, i.e. only stages identified in the outcropping area nearest to the PilotSTRATEGY study area, are soft-to-compact white chalk, characterised by quasi-systematic presence of flint (Crastres de Paulet et al., 2011). In the center of the Paris Basin only the Santonian and the Campanien stages are present, covered by Tertiary deposits. The Senonian chalk refers hereafter to the flinty chalk of the upper stages of the Late Cretaceous, for which the thickness is estimated as ca. 320 m in the PilotSTRATEGY study area. Overall, the calcium carbonate (calcite) content increases progressively upwards, from 88 % in the Cenomanian to nearly 98 % in the Campanian (Duermael, 1964).

5.6.2 Distribution and extent of the aquifer, aquitard and aquiclude units

During the Paleogene period, the chalk bedrock underwent significant alteration, further accentuated during the Quaternary with the deepening of the present-day valleys. In the outcrop areas, the groundwater flow is predominantly related to the occurrence of joints (fractures) in the chalk, substantially developed beneath the valleys. The fracture density decreases with depth, where the chalk becomes progressively more compact and much less permeable (Panetier, 1966). The fracturing is less developed in the chalk under the plateaus, i.e. where the Cenozoic formations overlay the Senonian chalk, as the distance from the outcrop areas increases.

In the areas where the Turonian or Senonian chalk crops out at the surface, the formation forms a huge unconfined aquifer, due to the large covered surface in the Paris Basin and the large thickness of the chalk strata. If the Turonian and Senonian chalk composes conceptually a single thick aquifer unit, the gradual reduction of the fissuring defines the limit of 'weathering' (surface influence) at depth and the effective thickness of the Chalk aquifer. This limit is closely related to the configuration and extent of the valley and the depth can vary considerably spatially. An average depth of 30 m is reported in the Paris metropolitan area (Schomburg et al., 2005), although the maximum effective thickness reaches up to 60 m locally (Crastres de Paulet et al., 2011). Accordingly, the Turonian and Senonian chalk strata display conceptually mixed hydrodynamic properties in the outcropping area, with an upper part (several tens of meters thick) considered as a productive aquifer and the lower part as an aquitard.

In the Brie area, the top of the late Cretaceous lies at a depth up to 200 m below the Cenozoic formations and between 100 and 150 m depth on the PilotSTRATEGY study area, which is located closer to the local area of outcrop (Figure 5-31). Based on the general knowledge of the hydrodynamic properties of the chalk in the basin, and considering that the prospect area is located nearly 15 km far from the nearest outcrop, the chalk formations are likely to display too low permeability to be considered as a confined aquifer in the PilotSTRATEGY study area. Underlying the Lower Turonian chalk formation, the

Cenomanian glauconitic chalk formation has very low permeability. Accordingly, the Turonian and Senonian chalk shall be considered to be aquitard units in the PilotSTRATEGY study area. Together with the Albian Gault Clays and Brienne Marls, the Cenomanian clayey chalk and marl form locally a thick aquiclude unit, effectively preventing vertical drainage between the Albian aquifer and any local Turonian aquifers.

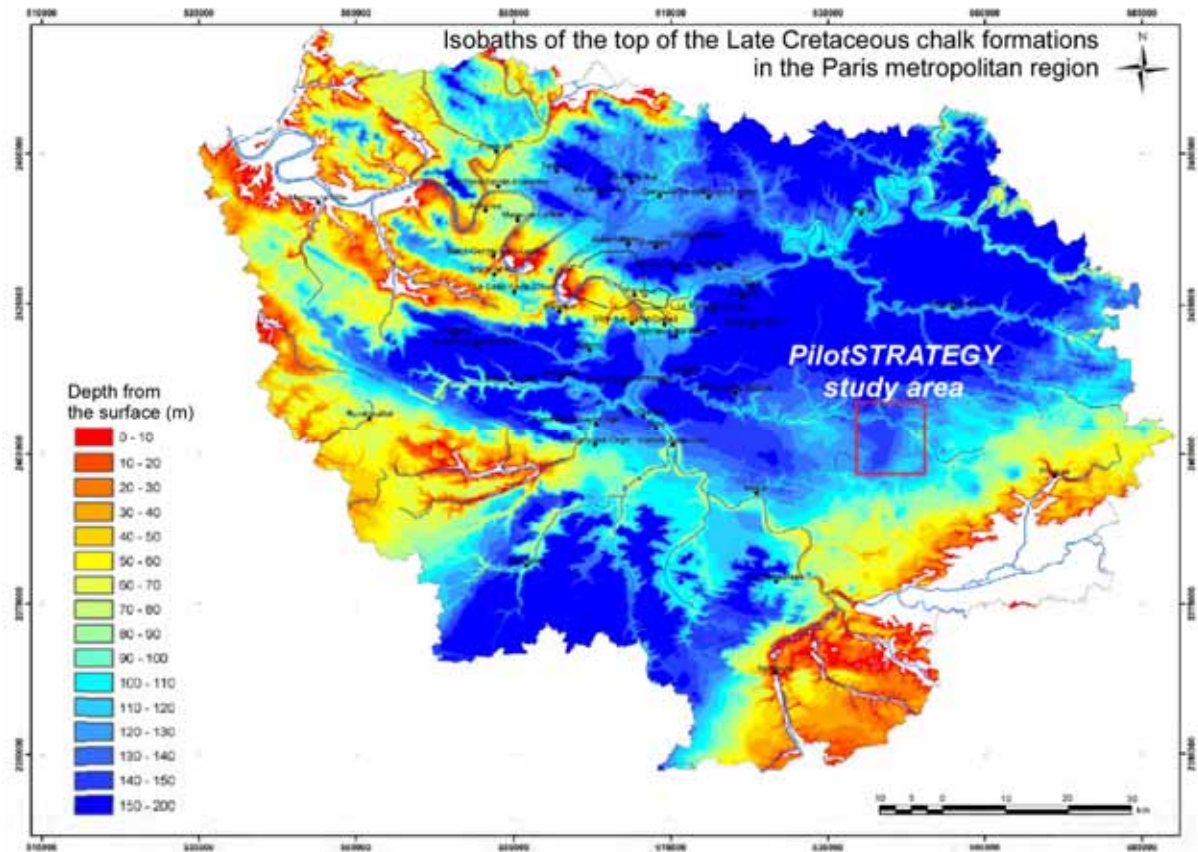


Figure 5-31. Map of depth of the top of the Late Cretaceous chalk formations (isobaths) in the Paris metropolitan region and the geographical area of the PilotSTRATEGY sector (adapted from Crastres de Paulet et al., 2011).

5.6.3 Hydrogeological properties of the aquifer

The Chalk aquifer is generally unconfined, but may be locally captive below the alluvium and the Paleogene formations. The outcropping chalk plateaus represent the aquifer's main recharge zones. Groundwater flows generally towards the center of the Paris Basin and towards the rivers that are the natural outlets for the aquifer units in the valleys. In the center of the basin, underlain by Paleogene formations, the main recharge and discharge of the Chalk aquifer take place locally in the deep valleys, where the aquifer is directly connected to the alluvial deposits and the main rivers (e.g. Seine, Orge rivers). At the edge of the plateau, the Paleogene aquifer unit can be connected to the Chalk water table and contributes to the local recharge of the Chalk aquifer.

The Late Cretaceous chalk is a fine-grained limestone with microporosity varying between 20 and 40% (Mégnyen, 1979). However, groundwater barely flows through the microporosity. If the dual porosity network stores large volumes of groundwater, then it is the fracture porosity of a complex network of joints (fractures and fissures) that governs the main hydrodynamic properties of the aquifer, where hydraulic conductivity can attain up to 5×10^{-3} m/s (Mégnyen, 1979; Amraoui et al., 2002). On the

plateaus, the permeability of the Chalk is lower than in the valleys, in the order of 10^{-6} to 10^{-7} m/s. The area identified by Magnien et al. (1970) with high hydraulic conductivity are highlighted on Figure 5-32. The hydraulic conductivity decreases with depth, reaching values up to 5×10^{-3} m/s in subcropping Chalk aquifer and 5×10^{-5} m/s at depths greater than 30 m (Amraoui et al., 2002). This permeability trend with depth, together with the water table of the Chalk aquifer (effective thickness) significantly influences the transmissivity properties (Figure 5-33). The transmissivity of the subcropping Chalk aquifer is up to 10^{-2} m²/s (due to high effective thickness), whereas the transmissivity decreases to 10^{-3} m²/s when the water table of the aquifer is below 30 m depth.

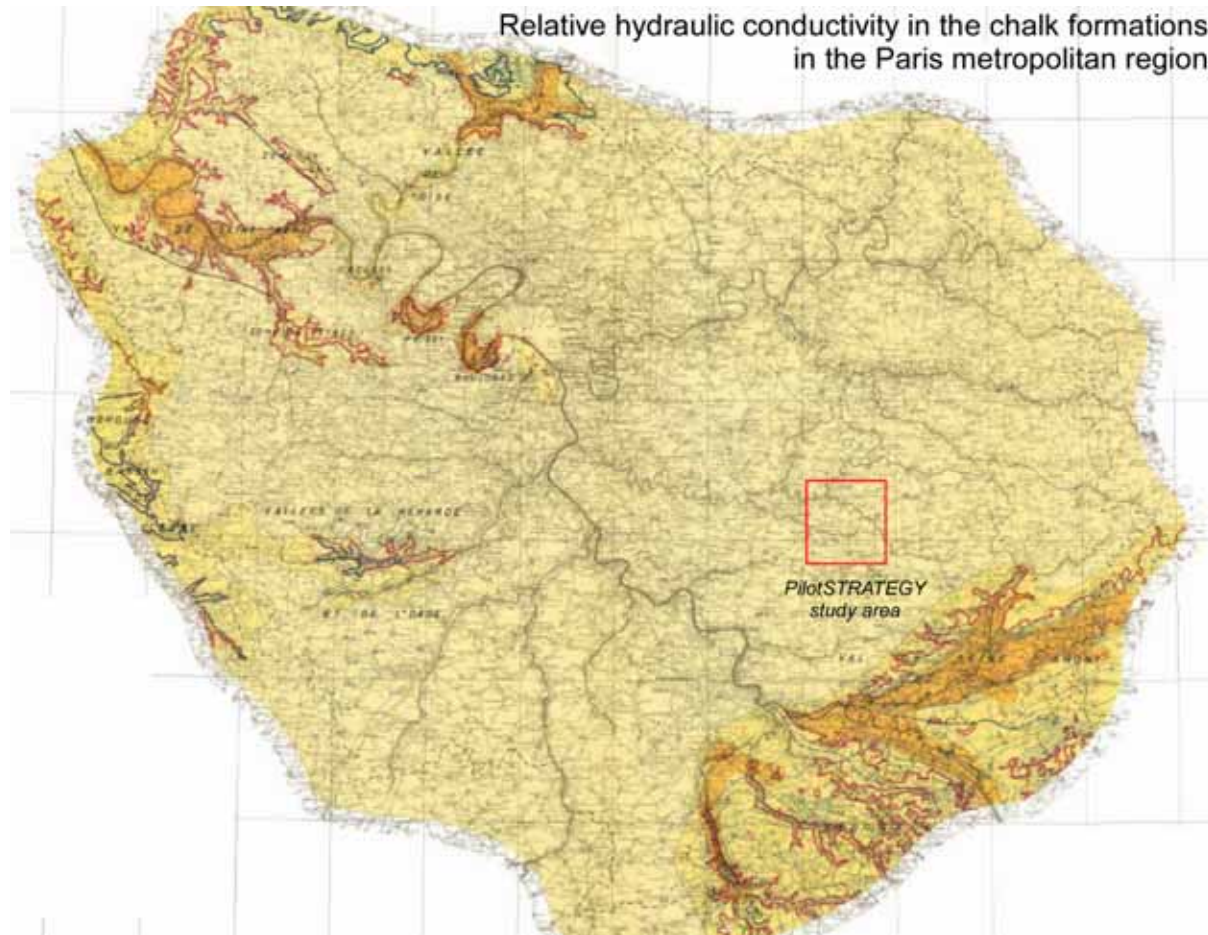


Figure 5-32. Map of the Late Cretaceous chalk in the Paris metropolitan area showing areas identified with higher hydraulic conductivity (orange) that are reliable for groundwater abstraction and water supply (Mégnyen et al., 1970). The Turonian or Senonian chalks generally crop out at the surface in the (orange) areas.

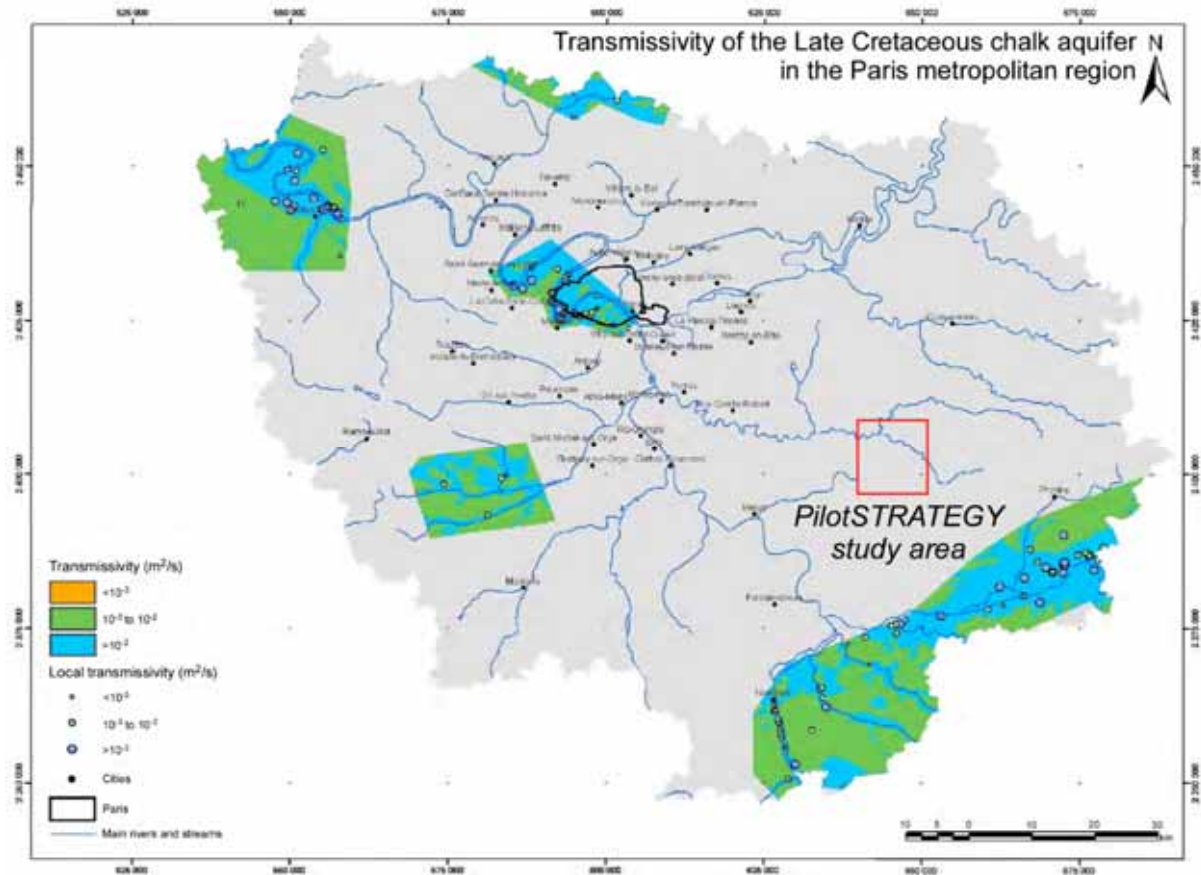


Figure 5-33. Map of transmissivity of the Late Cretaceous chalk in the Paris metropolitan region in areas where the Chalk aquifer is exploited for groundwater abstraction and water supply (adapted from Schomburg et al., 2005).

The hydrodynamic properties of the Late Cretaceous formations remain unknown on and nearby the PilotSTRATEGY study area due to the thick overlaying Paleocène deposits and the 15 km distance of the prospect area from the nearest outcrop. The poor permeability of the Chalk prevents local societal use for water supply and therefore there are no boreholes for hydrodynamic tests. ANDRA's quantitative model, developed for the entire Paris Basin, uses a median hydraulic conductivity of the order of 6.5×10^{-5} m/s for the Late Cretaceous Chalk (ANDRA, 2005).

5.6.4 Groundwater composition

Groundwater analyses are mainly available from the unconfined Chalk aquifer in the areas of outcrop. Due to a moderate depth of the water table (10 to 30 m below ground level) the temperature of the groundwater is relatively low, with a mean temperature of 12°C and season variation of 9 – 16°C (Schomburg et al., 2005). On the edge of the area overlain by Paleogene deposits, the shallow Chalk groundwater is fresh water ($< 500 \text{ mg.l}^{-1}$) of Ca-HCO₃ type (Kloppmann et al., 1998; Gillon et al., 2010; Cao et al., 2023). In the center of the Paris metropolitan area (Figure 5-34), where the aquifer is partly confined, the Chalk groundwater can have a higher salinity ($> 750 \text{ mg.l}^{-1}$) and the composition evolves to Ca-Mg-HCO₃ or Ca-Mg-SO₄-HCO₃ type (Mégnyen et al., 1970; Kloppmann et al., 1998). This hydrogeochemical change results from downward drainage from the Tertiary cover, where gypsum-rich deposit are locally a supplementary source of calcium and sulfate.

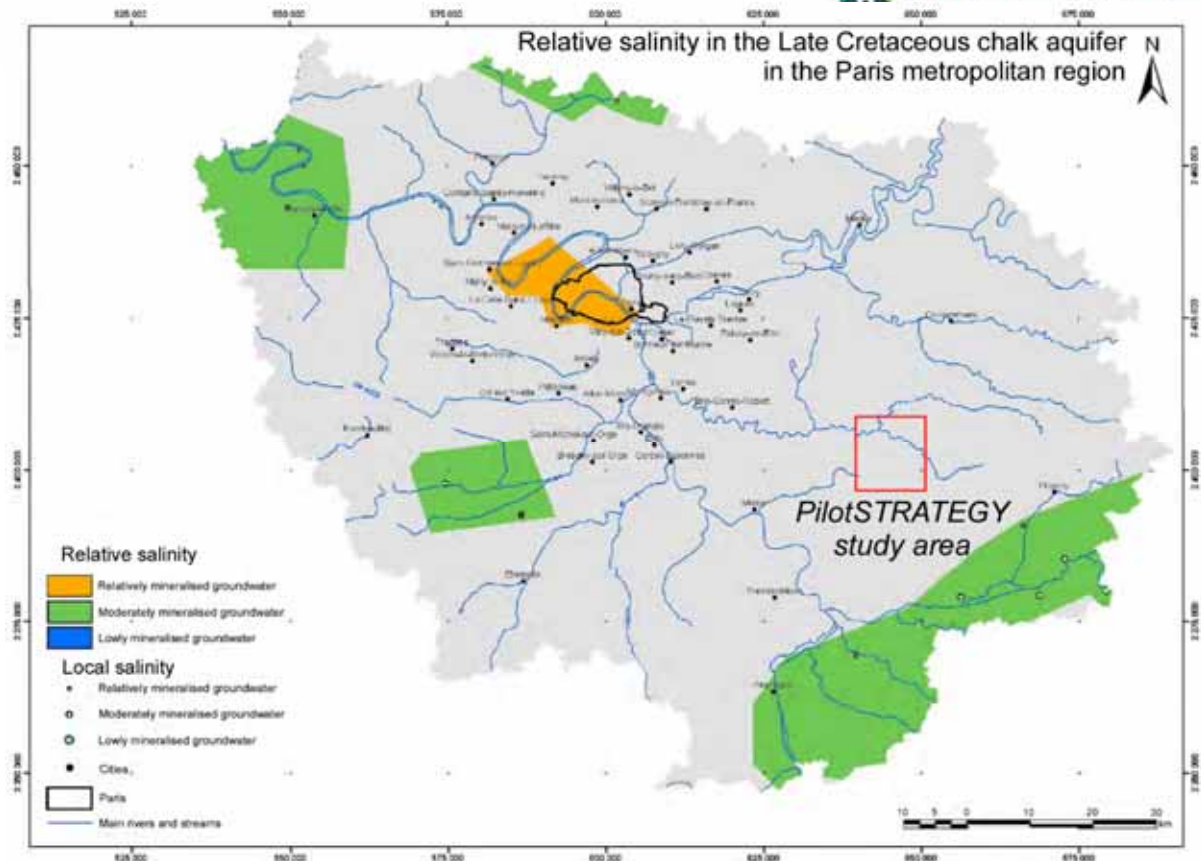


Figure 5-34. Map of relative salinity of the Late Cretaceous chalk in the Paris metropolitan region in areas where the Chalk aquifer is exploited for groundwater abstraction and water supply (adapted from Schomburg et al., 2005).

5.6.5 Occurrence of faults (if any)

Based on the numerous North-South and East-West seismic lines, several major fault systems meet beneath the Brie area in the late Cretaceous formations. These include the North-West – South-East Malnoue Faults, the North-East – South-West Metz Fault and the North – South Saint-Martin-de-Bossenay faults (Figure 5-2). A major phase of deformation has been identified in the Paris Basin at the base of the Paleogene deposits (mainly Thanetian) as a major compressive event, associated with an intense reactivation of North-West – South-East trending lineaments, such as the Bray fault (Hanot and Obert, 1992; Guillocheau et al., 2000; Briais et al., 2016). Accordingly, the regional Bray fault (Figure 5-2) and its southern extension in the Brie area, the North-West – South-East Malnoue faults, certainly offset the Cenomanien, Turonian and Senonian formations near the PilotSTRATEGY study area.

5.6.6 Societal uses of the formations

The groundwater in the Turonian and Senonian chalk are exploited for communal, private and industrial use, where the permeability of the Chalk is suitable for water supply. Because of the low permeability of the Chalk in the Brie area, the Late Cretaceous formations are however not exploited for any societal use in or near PilotSTRATEGY study area. The closest active well for groundwater abstraction takes place at the bottom of the plateau formed by Paleogene formations (Figure 5-33), located about 15 km (i.e. minimum distance) southeastern from the study area.

5.7 Paleogene formations

The Paleogene formations, dating mainly from the Eocene and Oligocene, are present only in the central Paris Basin, where they outcrop and overlie the Senonian chalk. The Paleogene formations are a succession of sedimentary deposits with pronounced variation in both facies and thickness within the Paris metropolitan region. In the Brie area, where the PilotSTRATEGY study area is located, the Paleogene formations form a complex multi-layered aquifer that is an important water resource for the urban, industrial and agricultural activity of the Brie plateau. Given the strategic importance of the aquifer for regional water resources, the AQUI'Brie association was created to federate all regional water stakeholders. The AQUI'Brie association has developed the knowledge of the multi-layered aquifer, including (i) monitoring of the water table, quality and water uses, (ii) numerical modelling of the hydrodynamics of the hydrosystem and (iii) promotion of actions for the protection, improvement and rational use of the groundwater resource in the Brie area. This knowledge focuses mainly on the Eocene formations of the hydrosystem, as the Oligocene formations are vulnerable to surficial anthropic pollution.

5.7.1 Geological features of the formation

The geology and structure of the Paleogene formation in the Brie area were mainly described by Mégnien (1973) and are summarized in Table 5-6. In the southeastern Brie area, the Paleogene formations extend mainly from the Ypresian to the Stampian stage (Mégnien, 1973; Gallois et al., 2015; Edouard, 2019; Blanc, 2020).

Table 5-6. Simplified lithostratigraphy of the Paleogene formations in the Brie area of the Paris Basin, defining the main aquifer in the area of study (adapted from Mégnien (1973)). The color code specifies the overall hydrogeological properties of the geological formation: aquifer properties (blue), aquitard properties (light blue) and aquiclude properties (white). Formations labelled in grey were not identified beneath the PilotSTRATEGY study area.

Geological period	Chronostratigraphy	Lithological domains	Dominant lithology	Aquifer domain (SW Brie area)
Oligocene	Stampian	Fontainebleau sands	unconsolidated sand	Oligocene aquifer (Brie aquifer)
		Brie Limestone	limestone	
		Green Marls	marl	
Late Eocene	Priobunian (Ludian)	Supragypseous Marls		Champigny aquifer
		Champigny Limestones	lacustrine limestone	
		Infraludian marls		
Middle Eocene	Bartonian (Marinesian)	Monceau Sands		
	Bartonian (Auversian)	Saint-Ouen Limestones	lacustrine limestone (locally marly)	
		Beauchamp Sands	sands (locally marly)	
Early Eocene	Lutetian	Marls and pebbles	marl	
		Coarse limestones	lacustrine limestone	
	Ypresian	Cuise sands	glaucconitic sand	Early Eocene aquifer
		Soissoiniais Sands		
		Plastic clays		
Late Paleocene	Thanetian	Thatenian sands		

The Early Eocene formations overlay the Late Cretaceous (Senonian) chalk with the Ypresian sandy-clay formations, or locally the Thanetian Sands. The bottom of the formation consists of (plastic)

lagoonal clay deposits (Sparnacian clay), overlain by predominantly detrital sands, which are generally glauconitic, micaceous, fine grained and relatively well sorted. The Lutetian formations are characterised by the predominance of carbonate deposits. The lagoonal facies, found in the upper part, consists of marls and pebbles with rare intercalation of (more or less) siliceous limestone beds and clay sequences. The thickness of the Lutetian formations is highly variable beneath the Brie plateau, with a maximum of nearly 60 m thick.

The middle Eocene formation comprises mainly the Bartonian formations, differentiating the Auversian sands (Beauchamp Sands) and the Marinesian limestones and sands (Saint-Ouen Limestone and Monceau Sands). The Beauchamp Sands are fine grained white sands, with sandstone and some clay layers, and are relatively thin and more clayey in the southern Brie area. The Saint-Ouen Limestone covers most of the Brie region, but has significant lateral variations in facies. The formations of predominantly lacustrine limestone alternate between compact limestone beds and marl layers containing flints. The Monceau Sands are fine greenish clayey sands with sandstone interlayers, sometimes limestone or gypsum. Beneath the Brie area, the facies of the Monceau Sands becomes distinctly more clayey and its thickness is very limited (< 1 m).

The Late Eocene formations include the Priabonian (mainly Ludian) formations, including the Infragypseous Marls (i.e. *Pholadomya ludensis* marl), the Champigny Limestones and the Supragypseous Marls. The Infragypseous Marls are yellowish marls or compact limestones of marine origin. The lacustrine Champigny Limestones occur as thick beds, although the facies change to gypsum in the north and marly limestone in the south of the Brie area. The Supragypseous Marls are composed of the white Pantin and the blue Argenteuil Marls.

The Oligocene formations, mostly just the Stampian formation in the Brie area, including the Green Marls (Romainville Marl), the Brie Limestones and the Fontainebleau Sands. The Romainville Marls are the bottom of the Oligocene and are an alternation of green marls, limestones and white marls. The Brie Limestones are lacustrine white-to-yellow limestones, occurring over most of the Brie area with ca. 10 m thickness, apart in the river valleys as result of erosion. The Fontainebleau Sands are locally found on hilltops (Figure 5-35) and form the top of the Stampian formation. The Fontainebleau Sands are fine, white or yellowish quartz sands, poorly stratified and are clayey at the base of the formation.

In the South and the South-East of the Brie area, where the PilotSTRATEGY study area lies, the edge of the Paris Basin significantly influences the succession of the Eocene formations and the associated facies variation. The Senonian chalk and the Ypresian sandy-clay formations rise abruptly to the southeast and have induced a gradual thinning of the overlying Eocene formations (Figure 5-35). Therefore, a certain number of Eocene formations – i.e., the thinnest – progressively disappears from the sedimentary sequence in the southern and southeastern Brie area. The Thanetian Beauchamp and Monceau sands or the Infraludian Marls are not found in the border of the basin, making the distinction between the lacustrine Saint-Ouen and Champigny limestones locally difficult (Figure 5-35). To the southeast of the Brie area, the Lutetian marls become significantly thinner, until they disappear and bring the Lutetian and the Saint-Ouen limestones into contact (Figure 5-35).

In the PilotSTRATEGY study area, located on and nearby the Grandpuits-Bailly-Carrois counties (Figure 5-1), the Paleogene formations locally reach a total thickness of 100 to 130 m. Megnier et al. (1973) produced detailed geological cross-sections that illustrate the geological heterogeneity of the Paleogene formation. One of these cross-section passes through Nangis county (Figure 5-36). According to this cross-section, the Eocene formations consist in a sequence of Ypresian sands,

overlaid by the Lutetian limestone in contact with the Saint-Ouen Limestone. The Saint-Ouen Limestone are described locally as a mixed facies (50-70% of marl; Mégnien (1973)). A thin layer of Infraludian Marls lies between the Champigny and the Saint-Ouen limestones. The outcropping Brie Limestones overlay a thick layer of Supragypsaceous and Green marls.

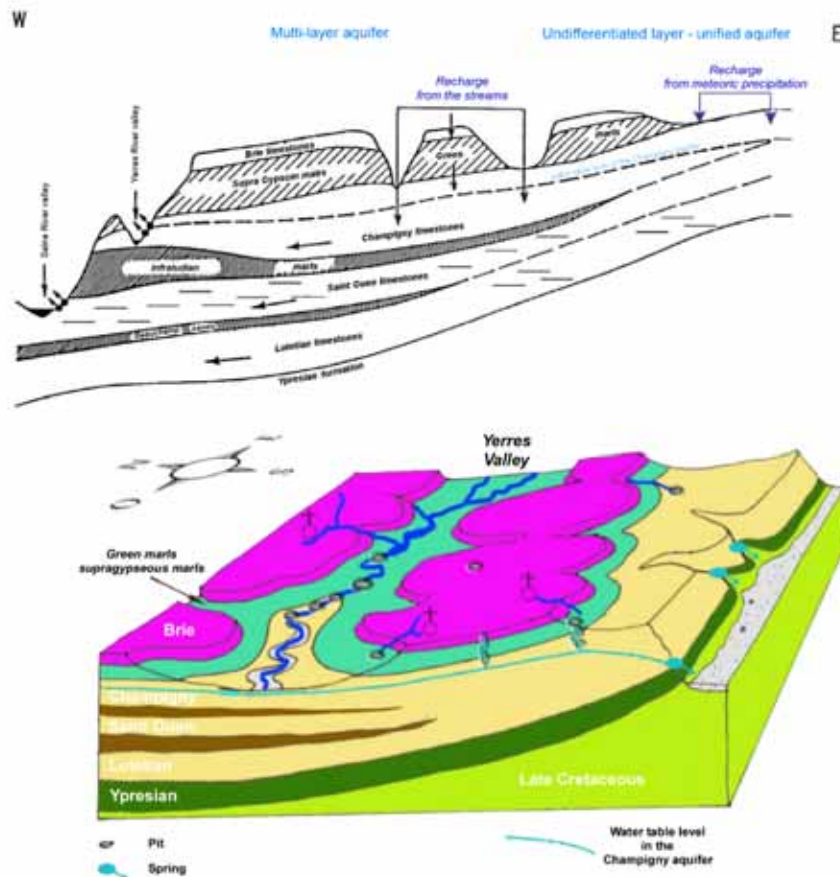


Figure 5-35. Schematic geological cross-section of the Eocene and Oligocene formations, overlying the Senonien chalk, in the southeastern Brie area; (top) West-East cross section (adapted from Mégnien (1973)) and 3D geological view of the southern border of the Brie plateau (adapted from Reynaud A., (2012)) emphasizing the lateral variation of the layout and succession of Paleogene sedimentary deposits.

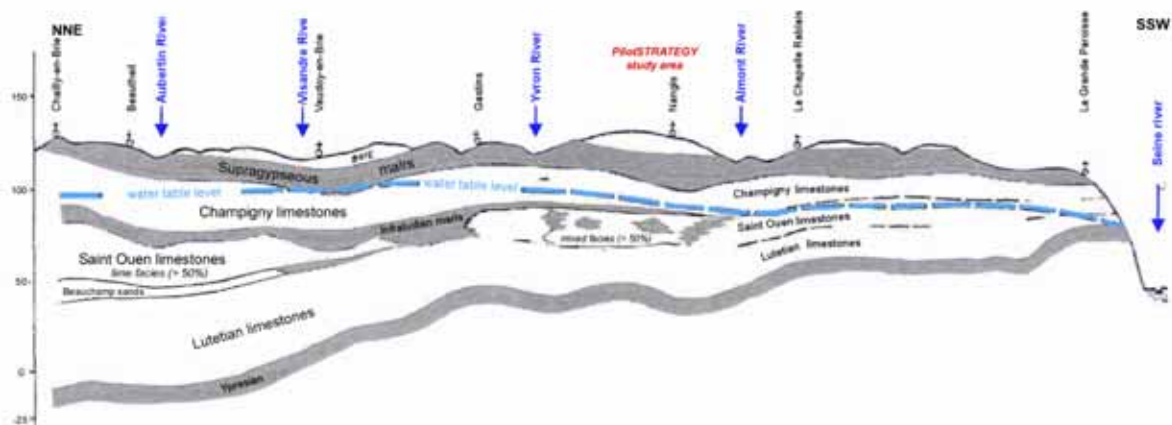


Figure 5-36. North-Northeast – South-Southwest geological cross-section of the Paleogene passing through the Nangis county, near the PilotSTRATEGY study area (adapted from Mégnien (1973)).

5.7.2 Distribution and extent of the aquifer, aquitard and aquiclude units

The sequence of sediments defined by Mégnien (1973) highlights the occurrence of one major Eocene and one minor Oligocene aquifer in the Brie area, namely the Champigny limestone aquifer and the Brie aquifer respectively.

The term “Champigny limestone aquifer” applies to the whole groundwater resource located in the Eocene limestone reservoir. The lateral variations of the lithological facies complicate the delimitation of the aquifer complexes (Figure 5-35). The Champigny limestone aquifer is generally considered as a multi-layered aquifer due to the occurrence of three potential aquitards contributing to a regional-to-local vertical compartmentalization, namely the clayey Beauchamp Sands, the marly Saint-Ouen Limestone (i.e. northwest of the Brie area) and the Infraludian Marls (Mégnien, 1979). If this complex multi-layered aquifer scheme applies to the west and northwest of the Brie area, the Champigny limestone aquifer consists mainly in a unified aquifer composed of the Lutetian, Barthonian and Ludian limestone formations (Table 5-6; Figure 5-36).

Based on the lithological well log of a deep well, the Champigny limestone aquifer is mainly composed of 55 m thick of undifferentiated limestones (i.e. Lutetian, Saint-Ouen, Champigny limestones) beneath the PilotSTRATEGY study area. The facies of the Saint-Ouen Limestone are described as limestone (i.e. not marly limestone), whereas the Infraludian Marls are not reported on the lithological well logs available in Grandpuits-Bailly-Carrois county. The Eocene limestone aquifer unit overlays the Ypresian formations, consisting locally in a 25 m thick clayey formation, overlain by a 25 m thick sandy formation (Cuise and Soissonais). Considering its thickness, the Ypresian clay formation is regarded as an aquiclude, whereas the Ypresian sandy formation is the Early Eocene aquifer, which is connected with the Champigny limestone aquifer. The Champigny limestone aquifer is locally disconnected from the Oligocene Brie aquifer by green marls, 5 m thick. Because of their moderate thickness, the Oligocene Green Marls are considered locally as an aquitard in the prospect area. The limestone Brie aquifer, 18 m thick, crops out at the surface of the PilotSTRATEGY study area.

5.7.3 Hydrogeological properties of the aquifer

The Champigny limestone aquifer is defined as a complex multilayer aquifer in the Paris Basin, due to the marked variation in facies and permeability of both the aquifer and aquitards. In the east and southeast of the Brie area, the Lutetian, Saint-Ouen and Champigny limestones form a single aquifer, meaning that each of the Eocene limestone formations is hydraulically connected to one another. The top water table of the Champigny limestone aquifer mostly lies in the Champigny Limestone, apart from the areas near to the valleys of the main rivers (Figure 5-36). The Champigny limestone aquifer is overall an unconfined aquifer in the southeast Brie area, with the water table only occasionally reaching the base of the overlying Supragypseous and/or Green Marls. The aquifer can be locally confined beneath the Ludian and Stampian marls in synclinal troughs, where the depth of the sedimentary pile increases locally (e.g. Chailly en Brie; Figure 5-36).

In the Eocene aquifer(s), groundwater naturally flows overall from the East to the West on the Brie area, toward the main rivers, i.e. the Seine and Marne Rivers, which form the southern and northern border of the Brie plateau, respectively (Figure 5-37). In the western part of the Brie area, where the Champigny limestone aquifer is vertically compartmentized (Figure 5-35), the piezometric maps slightly change between the Champigny Limestone and the Lutetian Limestone and the Ypresian sands (Figure 5-37), suggesting that the lower and upper compartments of the Champigny limestone aquifer are poorly connected. In the eastern part of the Brie area, where the Lutetian, Saint-Ouen and

Champigny limestones are undifferentiated and connected, the piezometric maps are fairly similar between the lower and upper part of the Champigny limestone aquifer (Figure 5-37).

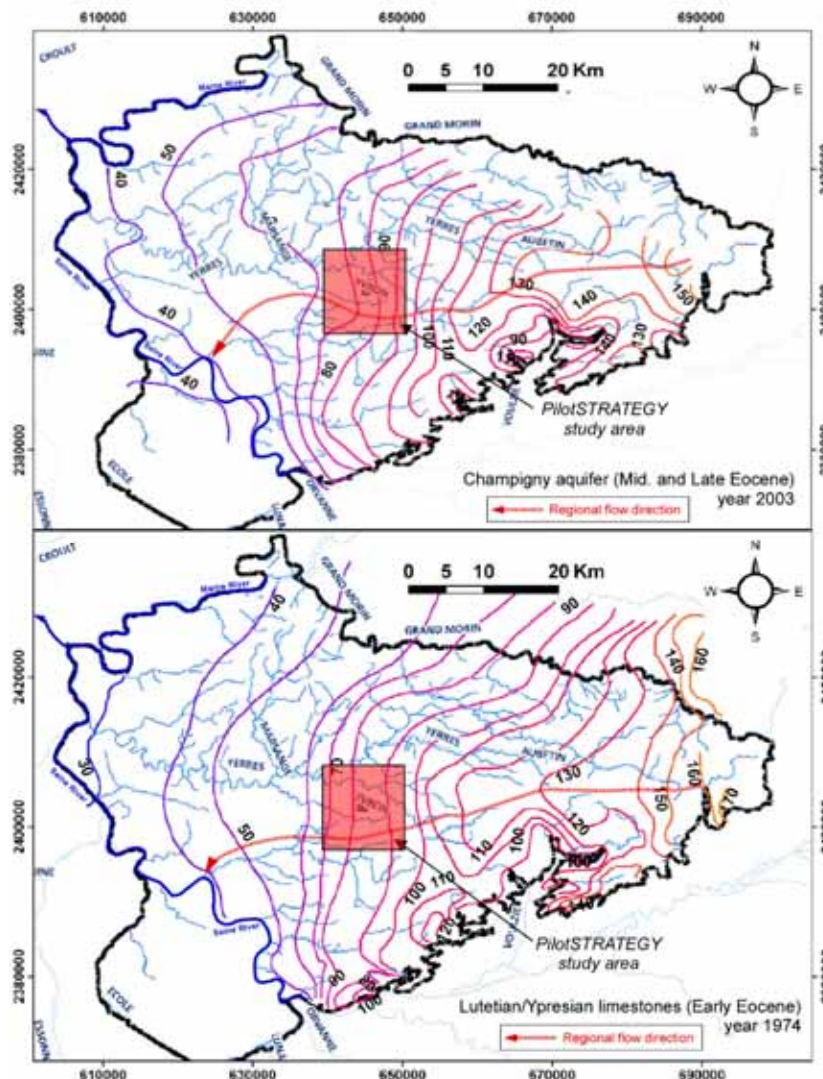


Figure 5-37. Piezometric map of the Eocene aquifers (adapted from Ménégnien (1973) after Bellier (2013)) – top: piezometry in the Champigny Limestones (Late and middle Eocene); bottom: piezometry in the Lutetian/Ypresian limestones (Early Eocene).

The Champigny limestone aquifer recharges mainly from local streams and rain in the bottom of the valleys, where the limestones crop out at the surface (i.e. where overlying marly layers are eroded; Figure 5-35). The wide extent of the Green and Supragypseous marls over almost the entire Brie region does not preclude recharge of the Champigny aquifer from the Brie aquifer because of the occurrence of springs at the base of the Brie limestones (Figure 5-35). Local springs directly recharge the outcropping Champigny Limestones along valley edges. The karstification of the Paleogene limestone has led to the formation of sinkholes in the Brie Limestones, which contribute to the recharge of the Champigny limestone aquifer. The Seine and Marne rivers are the main natural outlets of the Champigny limestone aquifer, together with some local streams and springs. In addition, groundwater withdrawal for water supply contributes to discharges the Eocene aquifer artificially.

The Eocene limestone formations have undergone heterogeneous karstification, moderately advanced but over a wide area, leading to the occurrence of sinkholes, water sinks and groundwater

resurgences. The karstification of the limestone aquifer, together with the facies variation, significantly influences the hydrodynamic properties of the aquifer. The spatial variability in transmissivity can range from 10^{-2} to 10^{-5} m²/s over distances of less than 100 m (Roux, 2006). The upper part of the Champigny limestone aquifer (i.e. the Champigny limestone) displays a spatial variation of the transmissivity in the Brie area with lower transmissivity in the eastern part (1×10^{-3} – 3×10^{-3} m²/s) than in the central and western part (1×10^{-2} – 5×10^{-2} m²/s; Vernoux and Martin, 2003; Bellier, 2013). In the Middle and Early Eocene limestones, the transmissivity is related to the facies type, with mean values of around 10^{-3} m²/s for calcareous facies and 10^{-4} m²/s for marly facies, respectively (Mégnyen, 1973). More specifically, Edouard (2019) and Blanc (2020) estimated the transmissivity of the Saint-Ouen Limestones to 7×10^{-4} – 7×10^{-3} m²/s, the Lutetian limestones to 3.2×10^{-4} – 2×10^{-3} m²/s and the Ypresian sands to 5.4×10^{-3} – 2.3×10^{-3} m²/s in the Brie area. The combined Champigny limestone aquifer has a transmissivity of 2×10^{-2} m²/s in the southern Brie area (Blanc, 2020).

The Brie aquifer is a perched unconfined aquifer above the Early Stampian marls. This Oligocene aquifer is extensive on the Brie plateau but with a low saturated thickness (5 – 6 m; Mégnyen and Turland (1967)). Although no piezometric map exists in the Brie Aquifer in the Brie area, the water table level is close to the surface and therefore follows the topography. In winter, the water table level rises locally above the surface level in topographic low spots on the hilltops, which led to the installation of historical agricultural drains to limit surficial flooding. The Brie aquifer recharges from meteoric precipitation, by percolation through the overlying thin Quaternary silty formations on the hilltops. The aquifer discharges through numerous springs in the valleys. Vertical drainage, both downward and upward, may occur through the Supragypseous and the Green marls contributing to local discharge or recharge of the Brie aquifer according to the hydrogeological conditions. The average transmissivity of the Brie Limestone ranges from 10^{-4} m²/s and 10^{-5} m²/s according to Martin et al. (1999). However, Edouard (2019) estimated an average transmissivity of the Brie Limestone to 5.3×10^{-3} m²/s in the northwestern Brie area and Blanc (2020) an average transmissivity to 1.3×10^{-2} m²/s in the southwestern Brie area.

5.7.4 Groundwater composition

The spatial distribution of the formations that are tapped by boreholes depends on the extent of the geological formations. In the southwestern part of the Brie area, the temperature of the shallow groundwater is relatively low, with a mean temperature of 12°C and season variation of 7.2 – 13.5°C. In the PilotSTRATEGY study area, where the Lutetian, Saint-Ouen and Champigny limestones are undifferentiated and together form the Champigny limestone aquifer, the groundwater is fresh water (< 700 mg/l; mean : 500 mg.l⁻¹) of Ca-HCO₃ type (Berger and Roussel, 1977), slightly magnesium-rich, with a tendency to NO₃ enrichment (< 50 mg.l⁻¹; mean : 35 mg.l⁻¹). In the northwest of the Brie area, where aquitards lie between the Lutetian, Saint-Ouen and Champigny limestones, significant sulphate and iron enrichment is reported in the Lutetian limestones and the underlying Ypresian sands. The high concentrations are mainly due to the occurrence of gypsum minerals in the Lutetian marls combined with an overall low flow rate in these confined aquifers (Schomburg et al., 2005). Sulphate enrichment also occurs in the Champigny limestones where the aquifer is locally confined below the Supragypseous Marls in the Brie area (Figure 5-36).

5.7.5 Occurrence of faults

The latest tectonic event in the Paris Basin was identified at the base of the Paleogene deposits in the Thanetian formations (Hanot and Obert, 1992; Guillocheau et al., 2000; Briaies et al., 2016). No major

faults are reported in hydrogeological studies focussing on the Champigny and Brie aquifers on the Brie plateau. Apart from the karstification of the Eocene limestone along fracture joints and fissures, the Paleogene formations are therefore not affected by any major fault in or near the PilotSTRATEGY study area.

5.7.6 Societal uses of the formation

The Champigny limestone aquifer is intensively exploited for industrial and drinking water supply in the Paris metropolitan region. The Brie plateau is also one of the main agricultural areas of the Paris metropolitan region, using groundwater to irrigate cultivated land. Based on the list of boreholes listed in the Brie region in 2012, most of the groundwater abstracted in or near the PilotSTRATEGY study area is pumped from the Champigny and Saint-Ouen limestones (Figure 5-38a). The average annual abstraction volumes are among the highest in the study area – after the Melun sector – on the Brie plateau (Figure 5-38b). The Brie aquifer is, in general, rarely used for water supply, as the quality of the water has gradually deteriorated over the last few decades. However, few boreholes utilise the Brie Limestones within a 5 km radius around the PilotSTRATEGY study area.

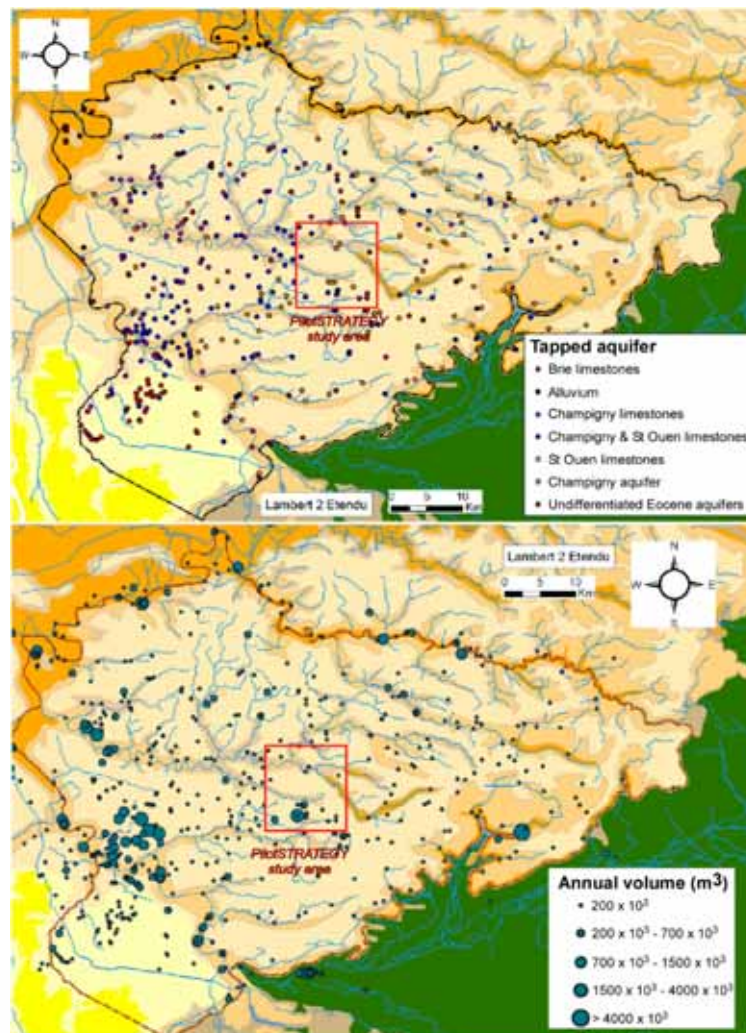


Figure 5-38. Spatial distribution of boreholes in the Brie areas (adapted from Bellier (2013)); the main formation(s) of the aquifer that are pumped are distinguished by the color legend (top); average annual volumes (period 1988 – 2007) taken from the Champigny limestone aquifer independent of the type of water use (bottom).

6. Portugal – Lusitanian Basin

The target area of the PilotSTRATEGY project in Portugal, following a decision process between onshore and offshore possibilities, is located in the offshore part of the Lusitanian basin, 18-20 km from the coast, in a prospect designated as Q4-TV1 (Figure 6-1). The reservoir is a siliciclastic layer of the Early Cretaceous *Torres Vedras Group*. Among the technical criteria for selection of the offshore site was minimising impacts imposed by CO₂ storage to other social-economic activities, including possible impacts (e.g. contamination) to freshwater aquifers utilised for public or private water supply.

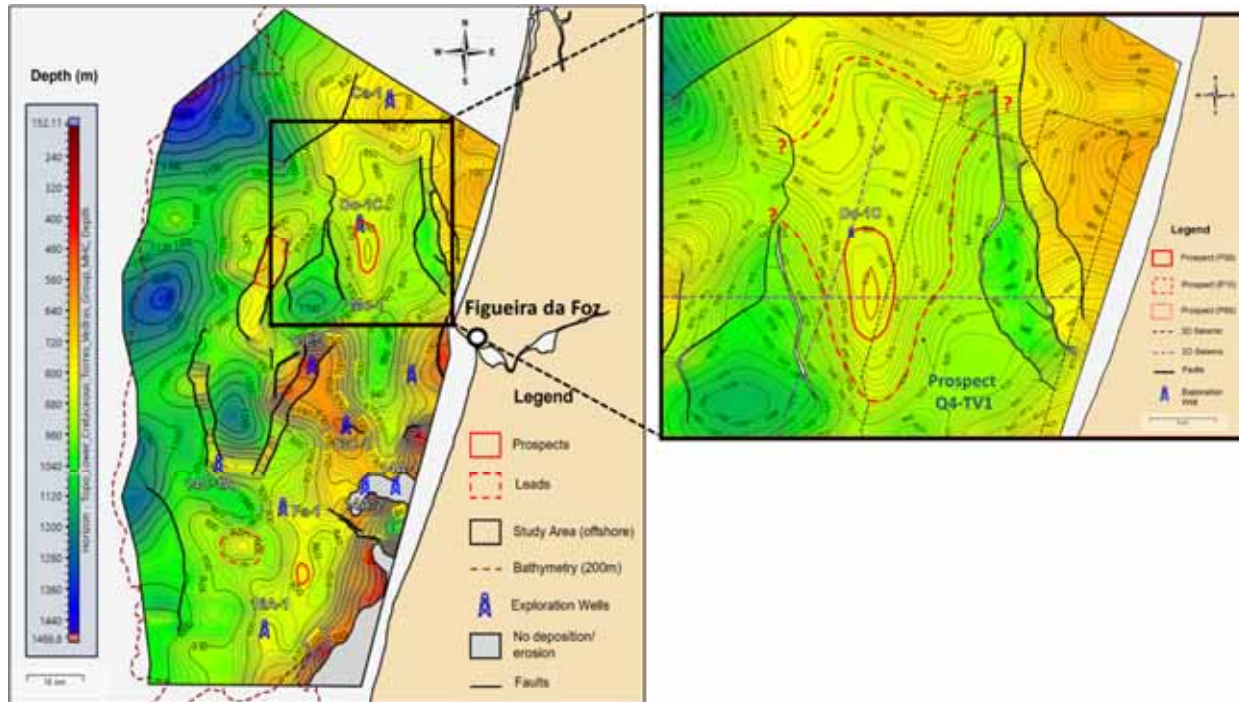


Figure 6-1. Location of the offshore target prospect Q4-TV1, offshore from the Figueira da Foz municipality. The detail shows the P90-P50-P10 closure scenarios. Adapted from Pereira et al. (2023).

Figure 6-1 shows a set of faults to the east of the Q4-TV1 prospect, striking N-S to NW-SE. There is no data about the hydraulic behaviour of those faults, but they may have physically disconnected the onshore and the offshore Torres Vedras Group (Figure 6-2a). In fact, a neotectonic map by Cabral and Ribeiro (1988; Figure 6-2b) identifies a fault that causes the Cretaceous formations to crop at seabed, several kms east from the Q4-TV1 prospect, breaking physical continuity between the onshore and offshore Torres Vedras group.

This geological structure will prevent the possibility of impact from offshore CO₂ injection on the onshore freshwater aquifers due to injection pressure propagation or possible CO₂ leakage. Still, even if negligible, the quantification of those risks will be addressed in WP5 of PilotSTRATEGY.

Nevertheless, a description of the onshore hydrogeological features is still relevant to understand the interaction between the Torres Vedras Group reservoir and any aquifers, aquitards or aquicludes that may overlay it offshore. Information such as groundwater flow pattern and hydrogeochemical facies in the onshore aquifers can help clarify those interactions. Furthermore, given the scarcity of data about the Torres Vedras Group offshore (namely, an almost complete absence of permeability data), some insight can be gained from the onshore data. That is, the onshore hydrogeological characteristics are used as a proxy for the offshore storage complex.

Other hydrogeological characteristics known onshore (i.e. groundwater balance or the societal uses of the aquifer), are less relevant for the offshore area and are presented here only for consistency with the French and Spanish storage sites.

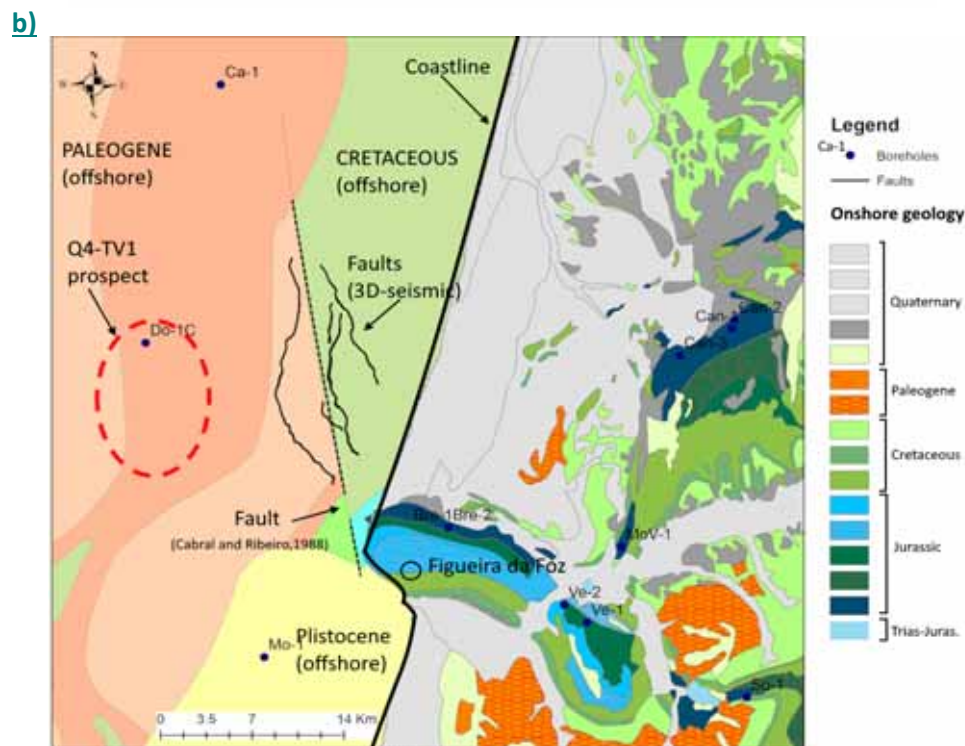
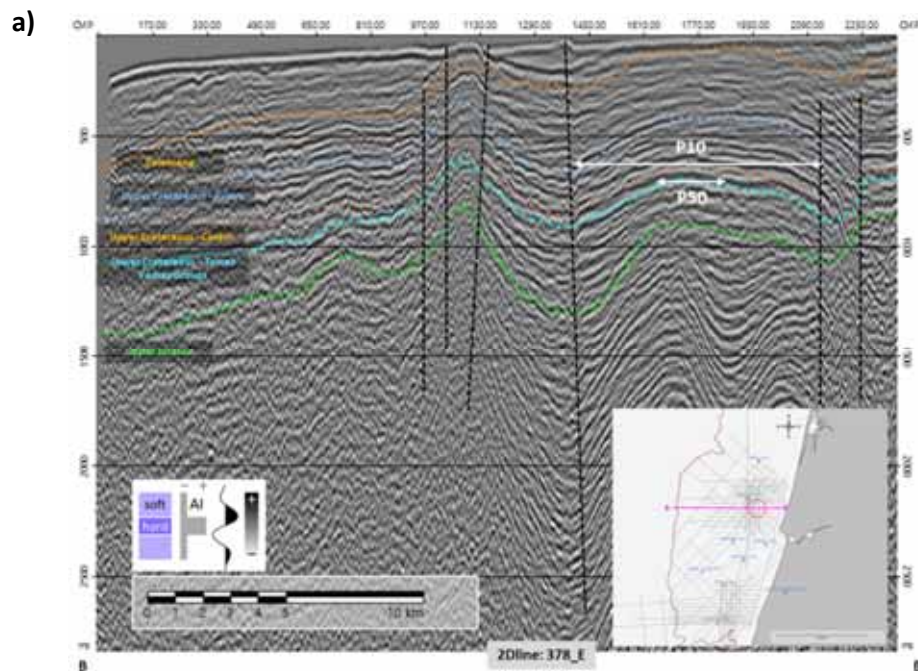


Figure 6-2. a) E-W seismic section crossing the selected prospect Q4-TV1 and illustrating the occurrence of major faults between the prospect and the onshore; see PilotSTRATEGY Deliverable D2.7; b) geological map of the onshore and offshore area around Figueira da Foz, including the faults interpreted in the 3-D seismic block and the location of the Q4-TV1 prospect.

6.1 Overview of the Lusitanian Basin

The onshore part of the Lusitanian Basin (Figure 6-3) is designated in the Portuguese National System for Water Resources (**SNIRH**, in the Portuguese abbreviation) as the **Western Meso-Cenozoic Unit**. This is also the designation commonly used by the hydrogeology community in Portugal, but for consistency with the other deliverables in PilotSTRATEGY, the designation **Onshore Lusitanian Basin** is maintained in this deliverable.

Sedimentary deposition in the Lusitanian Basin coincided with the first stages of the opening of the Atlantic, and resulted in an NNE-SSW elongated basin with a sedimentary thickness of about 5 km (and up to 6 km offshore). To the east, the basin is separated from the Hercynian metamorphic and plutonic rocks by the Porto-Coimbra-Tomar fault, to the south by a branch of this fault striking NNE, which extends to the Setúbal canyon, and to the west by a Hercynian horst, materialized by granites and metamorphic rocks of the Berlengas islands (Almeida et al, 2000; Kullberg et al., 2006).

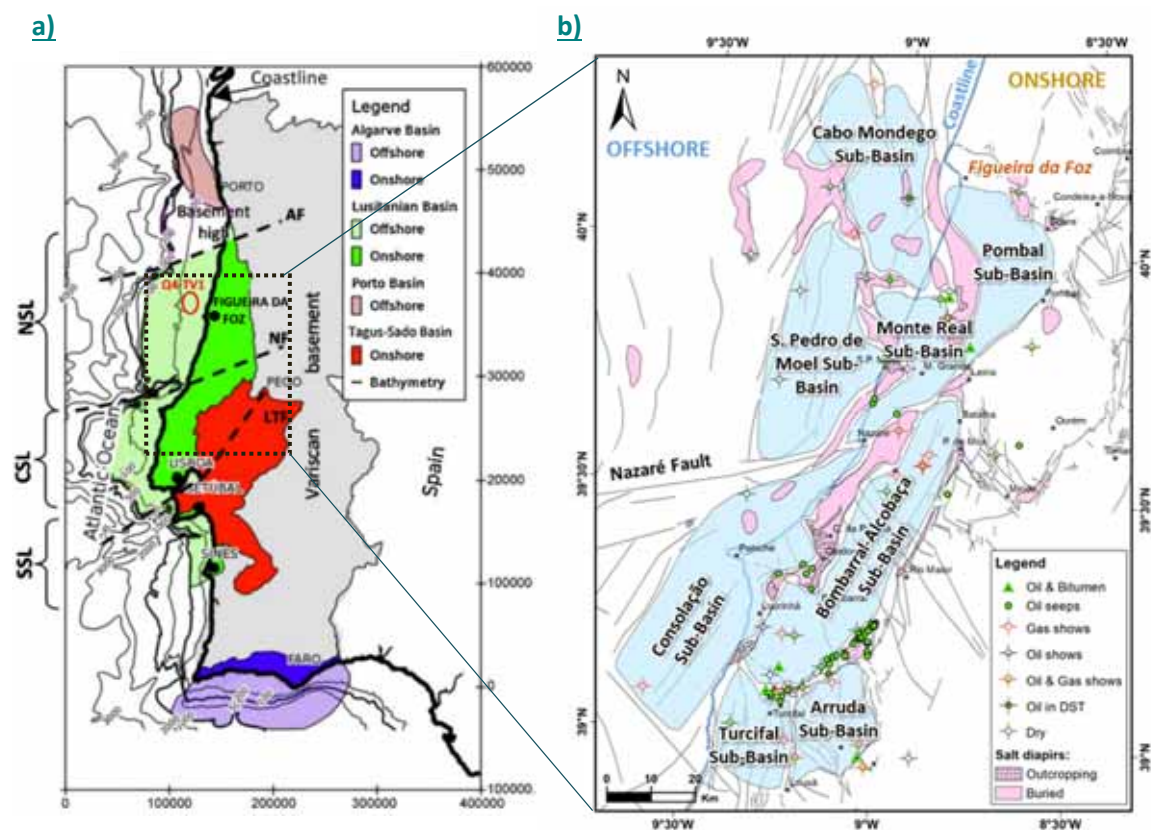


Figure 6-3. a) Geographical setting of the onshore Lusitanian basin and its sectors (NSL - North Lusitanian basin; CSL - Central Lusitanian basin; SSL - South Lusitanian basin). Also shown the major faults (AF- Aveiro fault; NF - Nazaré fault; LTF - Lower Tagus Faults) that subdivide the basin. Prospect Q4-TV1 is located in the north sector (NSL); b) main sub-basins and salt diapirs in the Central/Northern sectors of the basin (adapted from Casacão et al., 2023). Prospect Q4-TV1 is located in the Cabo Mondego sub-basin.

The architecture of the Lusitanian Basin reflects a continuous syn- to post-rift sedimentary record in a proximal margin with mild subsidence. The geometry and lithostratigraphic record of sedimentary packages were largely influenced by salt diapirism and normal faulting throughout the Mesozoic, and later subjected to a major episode of magmatism during the Late Cretaceous. Lastly, there was a

Cenozoic regional-scale tectonic uplift controlled by the Pyrenean and Betic phases of the Alpine orogeny. The reactivation of post-Hercynian faults and the interplay between thick Hettangian evaporites that were already developed at that time caused the reactivation of salt diapirs throughout the different compressional phases (Ribeiro et al., 1990; Wilson et al., 1989; Pinheiro et al., 1996; Alves et al., 2002).

Structurally, the Lusitanian basin is sometimes divided into three sectors (Alves et al., 2002) separated by structural lineaments that formed major transfer zones during the Mesozoic rifting (Figure 6-3).

- **North sector.** The North sector of the Lusitanian Basin is bounded by the Aveiro Fault and by the Nazaré Fault. Two important horst and graben structures exist, with a NW-SE strike: the Monte Real Graben and the Berlengas Horst. Mesozoic deposition is dominated in this sector by clastic Cretaceous formations.
- **Central sector.** The Central sector of the Lusitanian Basin is limited by the Nazaré fault and by the Lower Tagus fault. Compared to the North sector, fractured Jurassic carbonate deposits are more extensively developed than the clastic Cretaceous.
- **South sector.** The South sector of the Lusitanian basin, bounded to the north by the Lower Tagus fault, is the smallest sector of the Lusitanian basin with its onshore extension limited to a narrow strip less than 30km wide (Figure 6-3). Some authors include the southern part of the basin as the Santiago do Cacém sub-basin, separated from the Lusitanian basin by the Grândola fault.

The target area of the PilotSTRATEGY project is located in the north sector of the Lusitanian basin.

Apart from the subdivision in sectors, the salt diapirism during the Late Jurassic resulted in the development of the main sub-basins: Arruda, Turcifal, Bombarral-Alcobaça and Consolação, in the central sector, and the Monte Real, Rio Maior, Pombal and Cabo Mondego and São Pedro de Moel sub-basins in the northern sector of the LB (Figure 6-3b).

6.1.1 General sedimentary sequence

The Triassic *Grés de Silves Group* is the oldest sequence deposited in the Lusitanian basin, which unconformably overlies the Hercynian basement (Figure 6-4). This is followed by the *Dagorda Formation*, composed of layers of gypsum, salt and chalc-dolomitic intercalations. This formation is often associated with salt domes and contains important evaporite layers, sometimes hundreds of meters thick.

The Jurassic formations overlying the *Dagorda Formation*, are mostly carbonate rocks. They consist of dolomitic limestones, mottled limestones, compact limestones and marls from the Sinemurian and the Aalenian. The Malm (Upper Jurassic) begins with a sequence of marls and limestones, with some intercalations of bituminous limestones, at the top, followed by a thick sequence of a detrital nature. The sedimentation became progressively more detrital to the top of the Jurassic (clayey, grey, yellowish, brownish sandstones, etc., with some calcareous, clayey and mottled intercalations).

Sedimentation throughout the Early Cretaceous was impacted by the existence of salt diapirs that constrained the sediment transport routes resulting in variations in thickness and lithological types of the fluvial-deltaic deposits. An important part of the onshore Lusitanian basin is covered by the Albian - Aptian sandstones, the *Torres Vedras Group*, sandstones more or less conglomeratic, clays and marls, laying unconformably on the Jurassic. This siliciclastic formation and its lateral equivalents have been

given various names, depending on its geographical distribution: Torres Vedras sandstones, Carrascal Sandstones, Requeixo Sandstones, Palhaça Sandstones, etc.

The *Torres Vedras Group* was followed by a carbonate series (upper Cenomanian and Turonian) consisting of hard compact limestones, marly limestones, marls, etc, generally designated as the *Cacém formation*. Its thickness generally does not exceed 50 m. This formation has multiple names including the Costa de Arnes limestones.

To the north of Leiria, in the area closest to the offshore target of PilotSTRATEGY, overlaying the *Cacém Formation*, a detrital sequence was deposited, consisting of sandstones, sometimes micaceous, fine to very fine, followed by coarse sandstones and clayey passages – *Aveiro Group*. The sequence ends, in the Aveiro region, with an essentially clayey formation, the *Aveiro sandstones and clays* (Santonian – Maastrichtian).

The Tertiary and Quaternary are represented mainly by clastic deposits. The oldest tertiary deposits are relatively thin, consisting of conglomerates, sandstones, marls and Paleogene limestones. The Miocene is almost always of a continental nature, represented by clays, marls, clayey sandstones, more or less coarse, with intercalations of lignite. The maximum thickness is around 200 m. The Pliocene is represented by marine deposits made up of fine sands and fossiliferous clays, and continental deposits, (clayey sandstones, sands and gravel with intercalations of clays and lignite’s. The Quaternary is represented by beach deposits, terraces, dunes and alluvium. The dunes and sand dunes form a very extensive outcrop along the coast, reaching a maximum width of 20 km in the region of Aveiro.

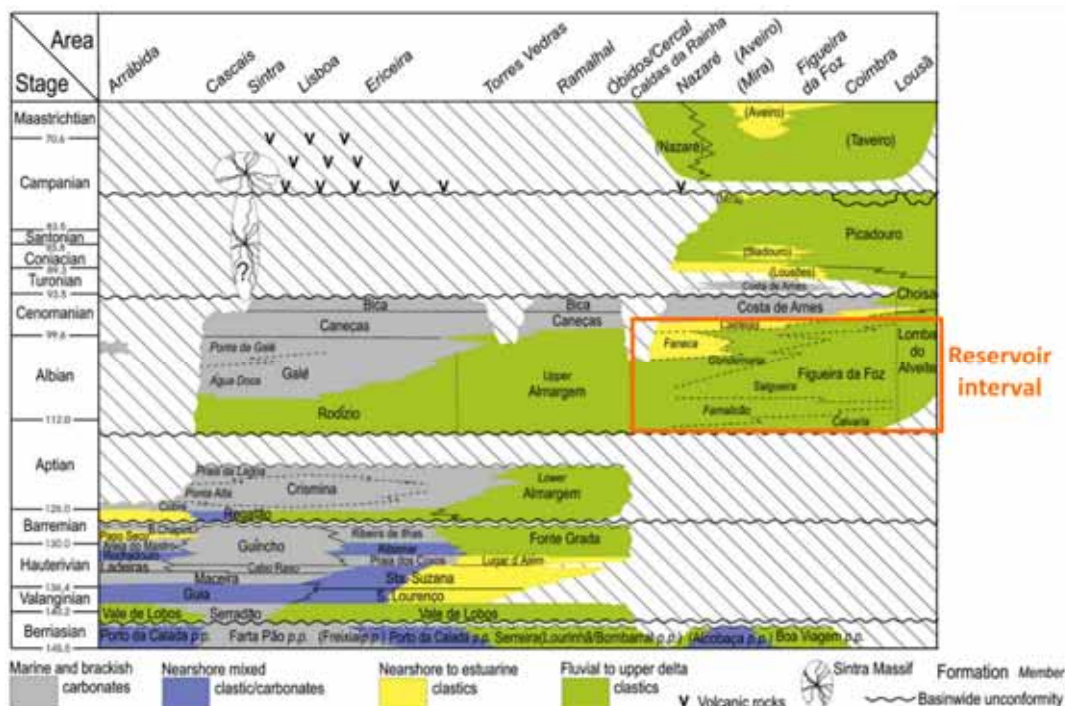


Figure 6-4. Regional stratigraphy in the Lusitanian basin (see deliverable D2.7), adapted from Dinis et al., 2008. Several designations are often used for lateral equivalents of the same geological formation, e.g., the reservoir interval (Torres Vedras Group) occurring in the northern sector of the Lusitanian Basin is often referred as Carrascal Sandstones or the lateral equivalent to the *Cacém formation* is called the *Costa de Arnes limestones*.

6.1.2 Aquifer systems in the north sector of the Lusitanian basin

The national system for water resources information (SNIRH) lists several aquifers (Table 6-1) in the onshore north Lusitanian basin, based on the lithostratigraphy of the geological sequence, and explained by the structural complexity of the basin, that imposes discontinuities between layers that could otherwise have been included in the same aquifer system.

The Jurassic aquifer systems in Table 6-1 are part of the underburden of the storage complex in the offshore target area, while the Plio-pleistocenic aquifer systems occurring along the coast are localised and do not provide insight into the hydraulic behaviour of the storage complex offshore.

As for the Cretaceous aquifers systems in Table 6-1, all of them rely essentially on the same geological formations: i) the siliciclastic unit of the Early Cretaceous (Carrascal sandstones); ii) the carbonate formation from the Late Cretaceous (Costa de Arnes limestones); and iii) the Late Cretaceous sandstones (the Lousões sandstones). This sequence is always capped by the Aveiro sandstones and clays formation (or the Taveiro clays) that act as aquicludes. This sequence has a direct correspondence (and lateral equivalence) to the geological formations identified offshore (Figure 6-4): i) the Carrascal sandstones corresponding to the targeted Torres Vedras Group; ii) the Costa de Arnes limestones corresponding to the Cacém formation and the Lousões sandstones and; iii) the Aveiro sandstones and clays composing the Aveiro Group. In fact, much of the difference in the designations is just a reflection of different disciplines, with Table 6-1 showing the designations adopted in the hydrogeology community and Figure 6-4 the designations used in petroleum exploration activities.

Knowledge about the regional groundwater system of the Cretaceous aquifers is relevant for understanding the hydraulic parameters of the offshore reservoir, and the importance of the overlying aquitards and aquicludes to define and characterise the CO₂ storage complex. Describing the characteristics of all the Cretaceous aquifers systems in Table 6-1 would be somewhat repetitive, and therefore it was decided to focus the remainder of this section of the report on those aquifers closest to the offshore location, i.e. those nearest the Figueira da Foz coastal area. These aquifer systems are perceived to be “proxies” to the offshore storage complex. From north to south, the following aquifer systems are described:

- **Aveiro Cretaceous (O2*)**, which is the most well-studied of all Cretaceous aquifers and the only one known to extend to the offshore;
- **Figueira da Foz – Gesteira (O7)**, of local importance for public and private water supply
- **Louriçal (O29)**, which despite occupying a very large area is less utilised for groundwater supply, and its characteristics are less known, especially for the deepest Cretaceous aquifer layers. Nonetheless, it is included to characterise all the productive sequence from the Lower Cretaceous to the Plio-pleistocenic.

The next sections describe these three aquifers, not because the offshore CO₂ storage poses any risk to the groundwater quality or availability, but to take advantage from the knowledge gathered from the hydrogeologic studies about the hydraulic behaviour, at shallower onshore depth, of the geological formations that form the CO₂ storage complex offshore.

** SNIRH uses a code to designate the aquifer systems. The code used for the aquifers in the western meso-cenozoic hydrogeologic unit is composed by the letter O and a number.*

Table 6-1. Aquifer systems in the onshore north Lusitanian basin. See Figure 6-5 for location of the aquifer systems. Shaded lines indicate the aquifer systems described in this chapter.

Hydrogeologic sub-system	Aquifer systems	Stage	Geological formation	Predominant lithologies	Aquifer type	
Tertiary and quaternary subsystems	Aveiro Quaternary (O1)	Pliocenic to Plistocenic	Fluvial terraces, dunes and alluvium	Sand, sand dunes, alluvium	Porous	
	Leirosa – Monte Real (O10)	Pliocenic to Plistocenic	Complex of sands and sand dunes	Sand and sand dunes	Porous	
	Veiria de Leiria– Marinha Grande (O12)	Recent	Sand dunes	Undiff. Plio-Plistocenic	Sandstones, sand and sand dunes	Porous, multilayer
		Pliocenic to Plistocenic	Undiff. Plio-Plistocenic	Miocene deposits		
	Louriçal (O29)	Miocene	Late Cretaceous	Cacém formation	Sandstones, with minor limestones. Sands	Porous, multilayer
		Early Cretaceous	Early Cretaceous	Torres Vedras Group		
		Plio-quaternary	Plio-quaternary	Plio-quaternary deposits		
		Miocene – Paleogene	Miocene – Paleogene	Undiff. Miocene/Paleog.		
	Cretaceous subsystems	Tentúgal (O5)	Cenomanian/Lower Turonian	Lousões sandstones	Sandstones, with minor limestones	Porous, multilayer
			Cenomanian	Costa de Arnes limestones		
Figueira da Foz – Gesteira (O7)		Turonian	Carrascal sandstones	Sandstones, with minor limestones	Porous, multilayer	
		Cenomanian	Furadouro sandstones			
Viso – Queridas (O30)		Upper Cenom. – Turonian	Tentúgal limestones	Sandstones, with minor limestones	Porous, multilayer	
		Upper Cenom. – Turonian	Carrascal sandstones			
Condeixa- Alfarelos (O31)		Cenoman./Lower Turonian	Costa de Arnes limestones	Sandstones, with minor limestones	Porous, multilayer	
		Cenomanian	Carrascal sandstones			
Aveiro Cretaceous (O2)		Upper Cenom. – Turonian	Furadouro sandstones	Sandstones, with minor limestones	Porous, multilayer	
		Cenomanian/Turonian	Tentúgal limestones			
Jurassic subsystems	Ançã-Cantanhade (O4)	Upper Cenom. – Turonian	Upper Coarse sandstone	Sandstones, with minor limestones	Porous, multilayer	
		Cenomanian	Lousões sandstones			
	Verride (O8)	Aptian / Cenomanian	Costa de Arnes limestones	Limestones	Karstic	
		Senonian	Carrascal sandstones			
	Sicó-Alvaiázere (O11)	Middle/upper Domerian	Andorinha limestones	Limestones and marls	Karstic	
		Sinemurian-Lotaringian	Ançã limestones			
Bairrada karstic (O3)	Middle/upper Domerian	Limestones and marls	Limestones / dolomites	Karstic		
		Sinemurian-Lotaringian	Lemede marly-limestone Coimbra formation	Limestones, marly limestones	Karstic	

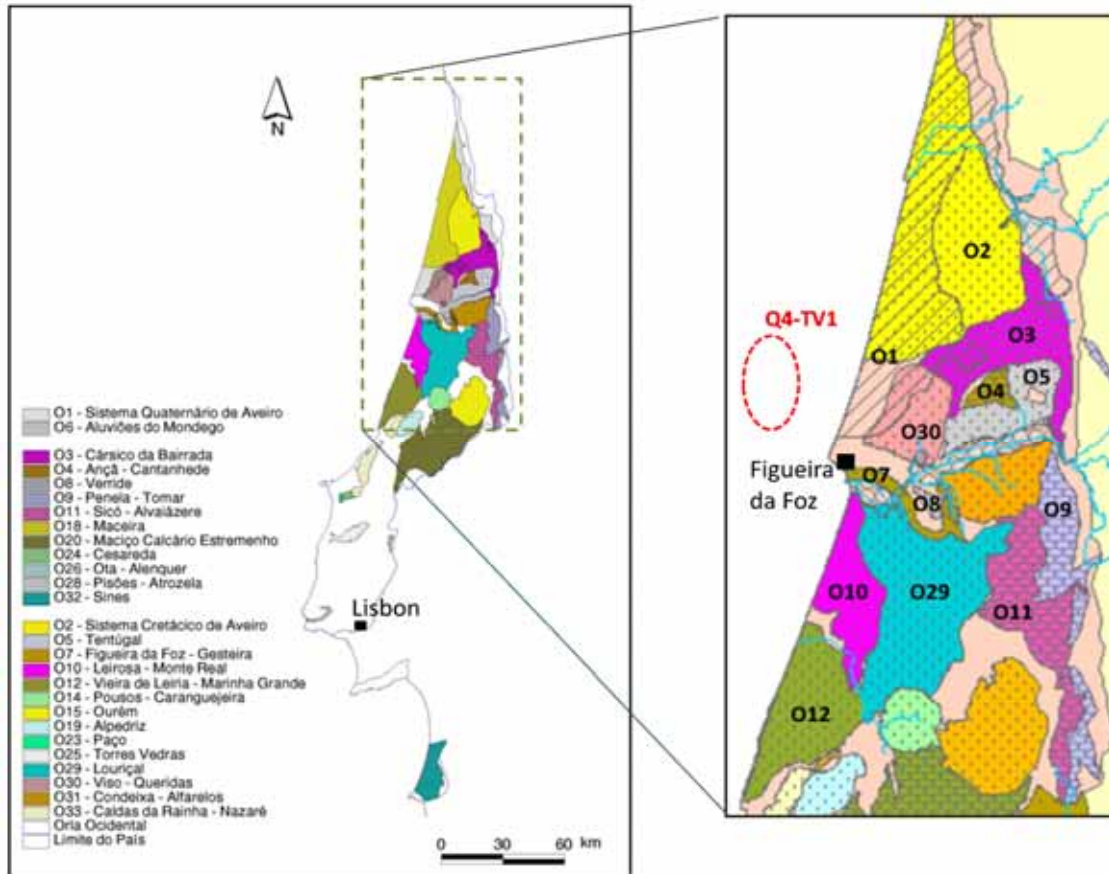


Figure 6-5. Aquifer systems in the Lusitanian basin and in the north sector of the Lusitanian basin (adapted from Alenida et al, 2000). This report describes only the Cretaceous aquifers at the coastal region, closer to the Q4-TV1 prospect, namely aquifers systems O2, O10 and O29.

6.2 Aveiro Cretaceous aquifer System – O2

The Aveiro Cretaceous aquifer system (O2) is mostly siliciclastic sediments, clayey and/or siliceous sandstones from continental to transitional depositional environment (Figure 6-6). The only exception are the carbonate rocks deposited during the Cenomanian transgression. Within the sedimentary sequence, there are several productive layers separated by aquitards or aquicludes, but often groundwater wells produce simultaneously from multiple layers, so that in practice the Aveiro Cretaceous aquifer is a multi-layered aquifer system.

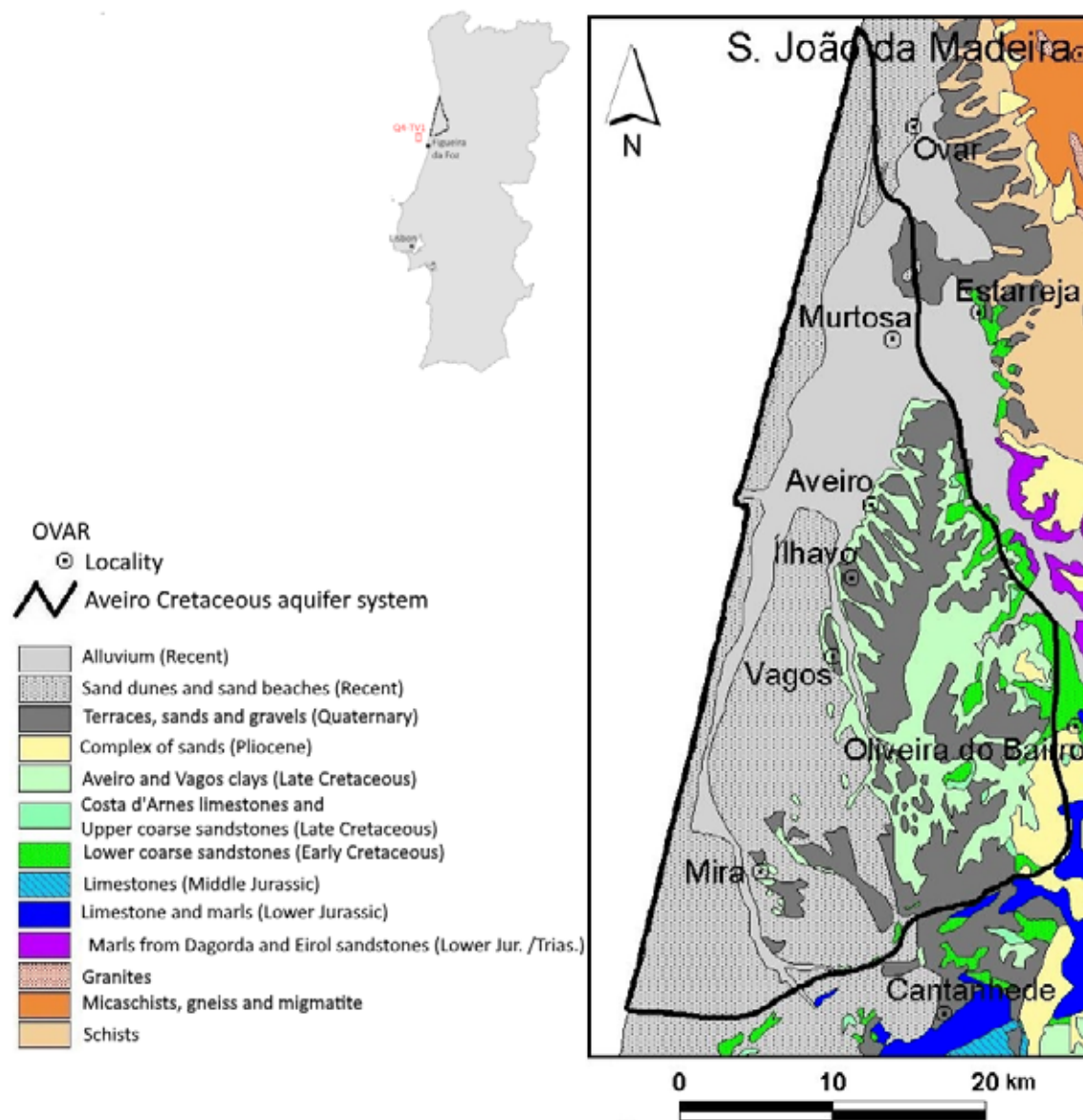


Figure 6-6. Physical and geological setting of the Aveiro Cretaceous aquifer system. Adapted from Almeida et al. 2000.

6.2.1 Geological features of the aquifer

The Aveiro Cretaceous multi-layered aquifer system extends over an area of 893.7 km² in the northernmost part of the Lusitanian basin (Figure 6-7). Throughout most of the area the aquifer rests on Precambrian shales, except in a small sector of the basin, where Triassic and Jurassic formations occur (Marques da Silva, 1990).

The Aveiro Cretaceous aquifer outcrops along its eastern edge, and its thickness increases slightly to the sea, dipping gently to the west, towards the offshore (Figure 6-7). There is also a slight plunge to the NW under the current coastline. Faults striking approximately N–S affect the sequence of Cretaceous sediments and compartmentalize the aquifer. To the east the aquifer behaves as an unconfined water-table aquifer, and the absence of the otherwise confining Aveiro Clays formation in the eastern zone of the aquifer defines the recharge zone. Nevertheless, through most of the area, the hydraulic behaviour is that of a confined aquifer (Carreira Paquete, 1998). The aquifer system is composed of five lithostratigraphic units (Table 6-2).

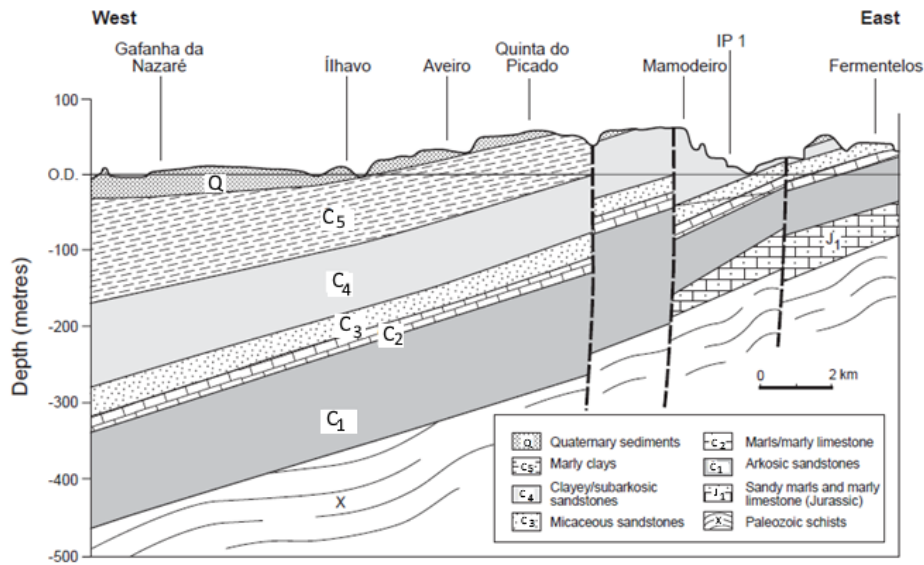


Figure 6-7. Cross section of the Aveiro Cretaceous aquifer system. Adapted from Condesso de Melo et al., 2009.

Table 6-2. Lithostratigraphic units in the Cretaceous Aveiro multi-layered aquifer system. Adapted from Condesso de Melo, 2002.

Unit	Stage	Designation	Permeable zone*	Hydraulic behaviour	
C ₅	Campanian-Maastrichtian	Aveiro Sandstones and Clays	Confining unit 1	Aquiclude	
C ₄	Coniacian-Santonian	Upper Coarse sandstones	Permeable zone 2 / 3	Main Aquifer	
C ₃	Upper Turonian-Lower Coniacian	Micaceous Sandstones (Furadouro Formation)	Permeable zone 4		
C ₂	Upper Cenomanian - Turonian	Carbonate Formation (Costa d'Arnes limestones)	Permeable zone 5		
C ₁	Aptian / Albian – Lower Cenomanian	Lower Coarse sandstones (Carrascal sandstones)	Top		Permeable zone 6
			Intermediate	Permeable zone 7	Confining unit
			Bottom		Intermediate aquifer
				Confining unit	
				Lower Aquifer	

Lower Coarse Sandstones - C₁

Often called the Carrascal sandstones (Albian-Aptian), these are the lateral equivalent of the Torres Vedras Group targeted at the Q4-TV1 prospect. The unit has a maximum thickness of 120 m. The chemical and piezometric features, as well as the permeability characteristics, show this is a very heterogeneous unit that can be subdivided into three sub-units:

- i. A lower sequence composed of coarse, well-cemented sandstones;
- ii. A middle sequence consisting of sandstones less coarse than the previous sequence, with interlayered clayey levels. Permeability is also lower than in the underlying sequence, while the water is more mineralized. It is bounded at the base and top by clay layers;
- iii. An upper sequence, underlying the carbonate formation (C₂). This sequence has higher permeability than the previous ones, but also more saline waters (Marques da Silva, 1990). The lower part of the sequence is bounded by a clayey impermeable layer – an aquiclude.

This division of C₁ units in three sequences is most striking along the coastal area (Marques da Silva, 1992) and is expected to extend into the offshore.

Carbonate formation - C₂

Also named the Costa de Arnes limestones, this is a lateral equivalent of the Cacém formation identified in the offshore oil exploration wells, capping the Torres Vedras Group. The unit has fairly high facies variation throughout the region, decreasing in thickness from south to northeast. Onshore the thickness is only about 15 m, but oil exploration boreholes showed thicknesses increasing to the offshore (see deliverable D2.7). In the eastern part of the onshore area, this unit has good hydraulic and hydrochemical properties, but in the central part of the region and in the recharge area of the system, the unit is of low permeability. The oil exploration boreholes offshore showed that the base of the sequence has a higher clay and marly composition that can provide the first cap-rock of the targeted Torres Vedras Group reservoir (i.e. unit C₁).

Micaceous sandstones - C₃

Also called the Furadouro Formation and the Lousões sandstones, it is fine to very fine quartz sand. It is bounded by micaceous clays layers, usually with organic matter. This unit is the most permeable and productive of the entire Aveiro Cretaceous aquifer system (Marques da Silva, 1990). The thickness of the unit varies between 10 and 30 m. A high mica content can sometimes cause groundwater quality issues due to the presence of very fine particles.

Upper coarse Sandstones - C₄

This unit consist of alternating layers of clays and sandstone, with an average thickness of about 150 m, with a predominance of clays at the top of the unit. The middle and upper zone of this formation are characterized by very low permeability, with an increase in water mineralization. Due to the marked anisotropy and low transmissivity, unit C₄ is considered to be an aquitard (Marques da Silva, 1990).

Aveiro Sandstones and clays - C₅

This unit caps the Aveiro Cretaceous system. It is mostly clays and/or marls, so is considered an aquiclude. There is an increase in thickness from east to the coast and from the north to the south, reaching average values of 140 m (Saraiva et al., 1983, *in* Amaral, 2013). This formation overlaps a large part of the other Cretaceous units, isolating this multi-aquifer system from the overlying Quaternary aquifer system. This unit is a secondary seal to the C₁ aquifer layers.

6.2.2 Hydrogeological properties of the aquifer

The five Cretaceous lithostratigraphic units, as defined in the previous chapter, have distinct hydrogeological behaviors. In fact, according to Marques da Silva (1990) and Condesso de Melo (2002), the system consists of three superimposed aquifers that are distinguished by different piezometry and chemistry (Table 6-2):

- The main aquifer, which has good quality water and is also the most productive, includes the upper sequence of the Lower Coarse Sandstones (C_1), the Carbonate Formation (C_2), the Micaceous Sandstone (C_3) and the lower part of the Upper Coarse Sandstones (C_4), and is hence a multilayer aquifer.
- An intermediate aquifer, characterized by higher salinity groundwaters, and higher piezometry than the main aquifer, but with low permeability. It is located in part of the lower Coarse Sandstones (C_1) and separated from the main aquifer by clay layers that bound the middle sequence of the C_1 unit;
- At the base there is a third aquifer, the lower part of the lower Coarse Sandstones (C_1), which has even more mineralized waters than the previous one, and is less permeable. Again, it is separated from the intermediate aquifer by the clay layers that bound the middle sequence of the C_1 unit. It has high piezometric levels and in some cases free-flowing artesian wells.

6.2.2.1 Hydraulic Parameters and Productivity

Marques da Silva (1990) and Condesso de Melo (2002) present data about the productivity and hydraulic parameters of the reservoir system. Marques da Silva (1990) shows aggregated data, not distinguishing between the several aquifer layers (Table 6-3), while Condesso de Melo (2002) provides values for the individual layers of the multilayered aquifer system (the “permeability zones” identified by the same author and shown in Table 6-4).

Table 6-3. Statistics of main hydraulic parameters in the Aveiro Cretaceous aquifer. Adapted from Marques da Silva (1990)

Parameter	Mean	Stand. Dev.	Min	Q1	Median	Q3	Max.
Flow rate (l/s)	16.3	12.3	0.2	5.0	15.0	25.0	50.0
Transmissivity (m^2/d)	338	178	11	216	340	420	850
Storage coefficient	3.1×10^{-3}	1.2×10^{-2}	4.5×10^{-6}	4.8×10^{-5}	1×10^{-4}	7×10^{-4}	8.2×10^{-2}

The main aquifer, which includes units from the top of C_1 , C_2 to C_4 , has the highest hydraulic conductivities (18 to 22 m/d) and is where most groundwater flow should occur, with the C_3 micaceous sandstones, likely being the main contributing unit. The hydraulic conductivity values decrease significantly up and downwards from the main aquifer to values of 1 to 5 m/d. The storage coefficients are characteristic of a confined aquifer with values varying between 10^{-5} and 10^{-4} .

The offshore reservoir corresponds to Permeable zones 6 and 7, which have an average hydraulic conductivity of 5 m/d, and average transmissivity of $68 m^2/d$ and storativity of 6.5×10^{-5} . There are no hydraulic conductivity data available for the confining unit (C_5 – Aveiro sandstones and clays), permeable zone 1.

Condesso de Melo (2002) presented a transmissivity map, with the proviso that it should be used with caution, since it included pumping-test data from different productive layers. Still, it provides an overall picture of the spatial distribution of the transmissivity (Figure 6-8). The central part of the aquifer (around Ílhavo, Aveiro and Cacia) has the highest transmissivity values, while for all other

areas this decreases considerably. Very low transmissivities ($< 50 \text{ m}^2/\text{d}$) were recorded in the recharge area, at the eastern edge of the aquifer system.

Table 6-4. Statistics of main hydraulic parameters in the Aveiro Cretaceous aquifer, by permeable zone. For identification of the permeable zones see Table 6-2. From Condesso de Melo (2002).

Aquifer layers tested	Permeable zone 6 & 7			Permeable zone 5, 6 & 7			Permeable zone 4, 5, 6 & 7			Permeable zone 3, 4, 5, 6 & 7		
	T	K	S	T	K	S	T	K	S	T	K	S
Hydraulic parameters												
Total no. of data values	15	15	2	8	8	0	104	104	16	90	90	10
Missing values	1	1	14	0	0	0	0	0	88	1	1	81
Minimum	2	0.1	3.2E-05	1	0.1		0.1	0.004	9.6E-12	0.4	0.02	4.5E-06
Maximum	275	25	3.2E-05	166	13		8165	255	3.6E-01	896	46	4.3E-03
Average	68	5	3.2E-05	40	3		388	15	2.3E-02	265	10	7.6E-04
Median	15	1	3.2E-05	13	0.5		256	11	9.8E-05	235	8	3.5E-05
1st Quartil	7	0.5	#N/A	2	0.1		168	6	4.4E-05	117	4	7.7E-06
3rd Quartil	91	6	#N/A	61	5		415	16	6.9E-04	361	12	2.0E-04
Standard deviation	95	8	0.0E+00	57	4		803	25	8.9E-02	198	9	1.5E-03

Aquifer layers tested	Permeable zone 3 & 4			Permeable zone 3, 4 & 5			Permeable zone 4 & 5			Permeable zone 2, 3, 4, 5, 6 & 7		
	T	K	S	T	K	S	T	K	S	T	K	S
Hydraulic parameters												
Total no. of data values	16	16	3	10	10	2	8	8	1	19	19	5
Missing values	1	1	14	0	0	8	0	0	7	0	0	14
Minimum	66	4	2.8E-05	182	10	1.6E-05	180	11	4.7E-03	16	1	1.1E-05
Maximum	838	43	3.9E-04	877	32	2.2E-05	757	47	4.7E-03	575	21	6.0E-05
Average	413	22	1.5E-04	427	20	1.9E-05	427	24	4.7E-03	200	7	3.2E-05
Median	368	18	3.6E-05	429	21	1.9E-05	441	22	#N/A	161	6	3.6E-05
1st Quartil	253	15	#N/A	220	12	#N/A	300	19	#N/A	63	2	1.3E-05
3rd Quartil	571	28	#N/A	530	27	#N/A	499	25	#N/A	239	9	4.4E-05
Standard deviation	220	11	2.0E-04	213	8	4.1E-06	177	11	#N/A	181	6	2.0E-05

Aquifer layers tested	Permeable zone 2			Permeable zone 2 & 3			Permeable zone 2, 3 & 4			Permeable zone 2, 3, 4 & 5		
	T	K	S	T	K	S	T	K	S	T	K	S
Hydraulic parameters												
Total no. of data values	5	5	0	6	6	0	2	2	0	2	2	0
Missing values	0	0	0	0	0	0	0	0	0	0	0	0
Minimum	9	0.2		1	0.05		645	25		452	13	
Maximum	84	7		461	15		693	27		454	13	
Average	41	3		140	5		669	26		453	13	
Median	37	3		64	4		669	26		453	13	
1st Quartil	11	0.3		20	1		#N/A	#N/A		#N/A	#N/A	
3rd Quartil	69	6		230	8		#N/A	#N/A		#N/A	#N/A	
Standard deviation	33	3		178	6		34	1		1	0	

Legend: #N/A - Not applicable T - Transmissivity in $\text{m}^2 \text{d}^{-1}$ K - Permeability in m d^{-1}
 S - Storage coefficient



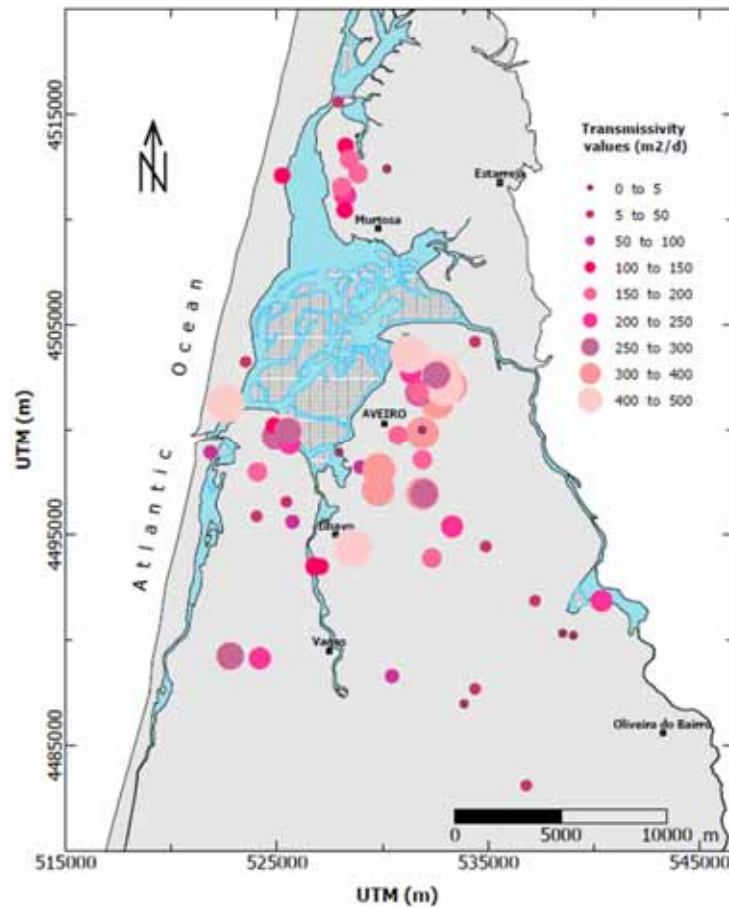


Figure 6-8. Spatial distribution of transmissivity values for the Aveiro Cretaceous aquifer. From Condesso de Melo, 2002.

6.2.2.1 Spatio-temporal Analysis of Piezometry

Groundwater exploitation in this system began in the late 1950's. The first wells drilled had a strong artesian behaviour, especially along the coastal area. As more groundwater wells were drilled, the piezometric levels naturally declined. However, the situation of free-flowing behaviour continued, with confinement guaranteed by the aquiclude Aveiro Sandstones and Clay formation. Serrano and Garcia (1997) presented a piezometric map for 1986 that shows a generalized decrease in piezometric levels, with zones (Aveiro – Gafanha – Ílhavo) where drawdowns were increasing on the order of 1.5 m/year.

Despite the continuous groundwater depletion in the aquifer, only limited signs of seawater intrusion or salt mobilization were observed in studies conducted until the early 2000's. The local water supply company of the Aveiro region (AdRA) has observed high chloride concentration (300 – 750 mg/L) in some boreholes at the northern and central parts of the aquifer. With the onset of operations of the Carvoeiro water system (pumping from the Vouga alluvium) a recovery of piezometric levels began to take place.

Currently the piezometric map of the Aveiro Cretaceous aquifer (Figure 6-9) is influenced by groundwater extraction, showing a depression in the central part of the groundwater body to which the main flow directions converge.

The aquifer currently shows piezometric levels below sea level throughout its northern and central zone. This situation encourages seawater intrusion, and locally, to the west of Vagos and Murtosa, a groundwater flow from sea to land. However, no seawater intrusion effects have yet been detected, either because the saline wedge has not yet reached the groundwater wells or because the hydraulic conditions in the offshore part of the Cretaceous prevent or hinder its advance.

In the southern and easternmost parts of the aquifer, coinciding with the recharge zone, piezometric levels above mean sea level still exists and around Vagueira there are still some free-flowing groundwater wells.

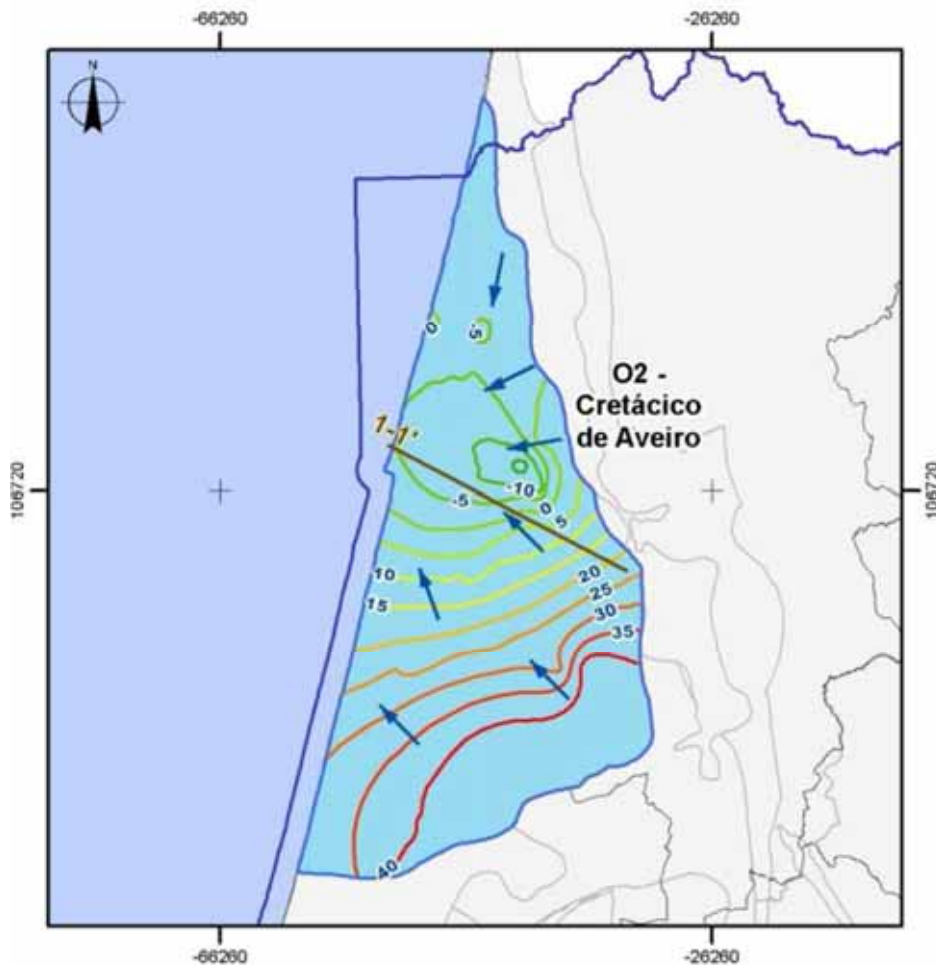


Figure 6-9. Piezometric map (in metres) and groundwater flow directions. Adapted from ARH Centro (2012).

6.2.2.2 Groundwater balance

The simplest hydrogeological conceptual model has recharge in the eastern part, where the permeable units of the Cretaceous outcrop or lie under Quaternary terraces. In this sector, recharge is provided directly by rainfall, by drainage from the terraces, and possibly by induced recharge from the Vouga River or other smaller water courses. Marques da Silva (1990) estimates about 10 hm³/year of inputs in the unconfined eastern sector.

On the other hand, the piezometry of the region indicates the possibility of groundwater inflow from the Bairrada Karst aquifer system to the Cretaceous, in the southern edge where the two aquifers

come in contact. Peixinho de Cristo (1985) estimates a 1 hm³/year for this inflow, so that the total recharge can reach 11 hm³/year.

In 2012 the administrative body (ARH Centro) regulating water supply in the region calculated the groundwater balance for this aquifer water. They used an estimated value of annual groundwater availability (6.9 hm³/year) and the calculated value of groundwater extraction (11 hm³/year) and reached a groundwater balance of -3.8 hm³/year. This confirms that extractions are higher than the groundwater availability ($\approx 155\%$), indicating overexploitation of the aquifer (Figure 6-10).

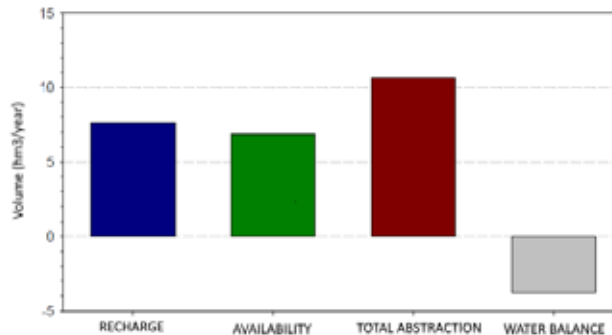


Figure 6-10. Groundwater balance at the Aveiro Cretaceous aquifer. Adapted from ARH Centro (2012).

6.2.3 Features of the groundwater

Groundwater in the Aveiro Cretaceous aquifer system usually show low electrical conductivities (median values 442 mS/cm), while pH varies from values below 7.0 in the recharge zone to close to 8.0, or even 8.5 near the coast, but slightly alkaline groundwaters (median pH \approx 7.6) predominate.

Measurable nitrate was found only in the recharge zone. The median nitrate value of around 2 mg/l is well below the allowable value for human consumption, but there is a maximum value of 43 mg/l. This reflects the great sealing that the C₅ unit provides to the system, decreasing the vulnerability to contamination of the main aquifer, plus the existence of very slow groundwater flow, confirmed by C¹⁴ dating. This leads to a classification as paleowaters (Carreira, 1996; 1998).

With regards to the trace elements, the most abundant are iron and manganese, with medians of 0.1 and 0.015 mg/L respectively, but with maximum recorded values of 7.9 and 0.28 mg/L, which are above the allowable values for human consumption. Lead and nickel have median values corresponding to the limits of detection, always well below the allowable values for human consumption (Figure 6-11a).

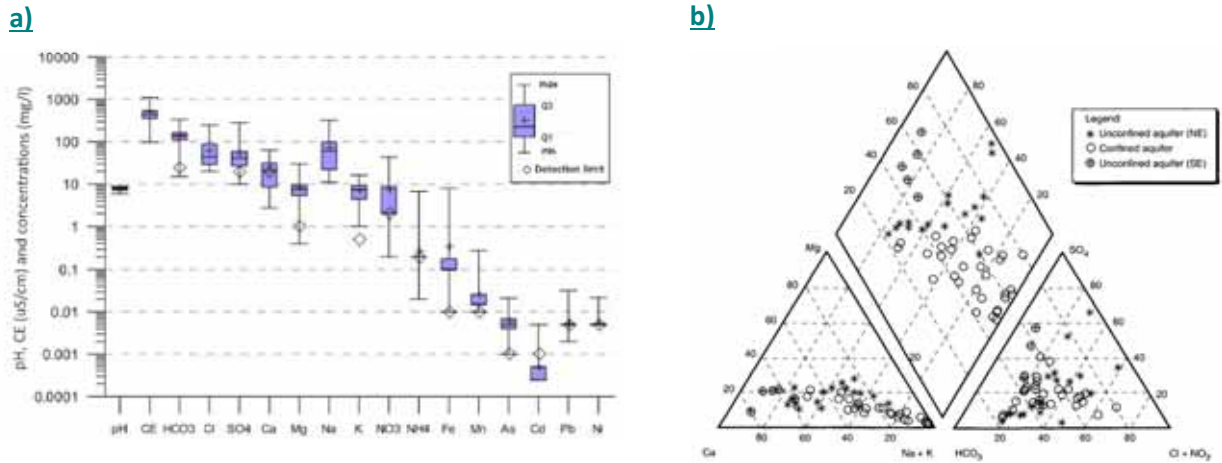


Figure 6-11. a) Hydrochemical features of the Aveiro Cretaceous aquifer. Adapted from ARH Centro (2012) b) Piper diagram. Adapted from Almeida et al. (2000)

Regarding the hydrochemical facies, calcium bicarbonate and sodium bicarbonate waters predominate, but the occurrence of Na–Cl waters is also relevant (Figure 6-11b and Figure 6-12a).

As a measure of groundwater salinity, most of the aquifer had reasonably low Electrical Conductivity (EC) from 250 to 1000 $\mu\text{S}/\text{cm}$ in 2018 (Figure 6-12b). Waters with EC higher than 1000 $\mu\text{S}/\text{cm}$ were found in four boreholes. The distribution of saline boreholes was apparently random and did not show any trend of being close to the coast. Dissolved Oxygen (DO) in groundwater was present only in the unconfined part of the aquifer, which is obviously due to the influence of modern recharge. DO was absent in the saline boreholes.

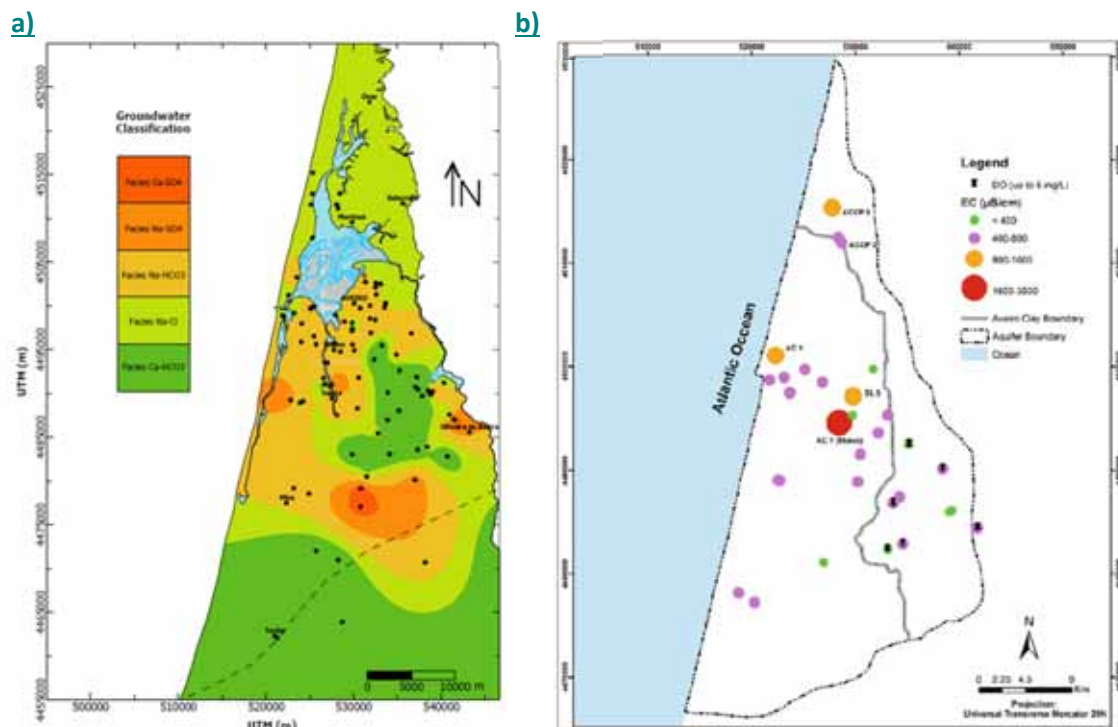


Figure 6-12. a) Hydrogeochemical facies. Adapted from Condesso de Melo (2002); b) Electrical conductivity (EC) distribution. After Rahman et al. (2022).

Evidence of a strong decrease in the piezometric levels in the past led to the hypothesis of seawater intrusion along the coastline. Findings from numerical modelling by Rahman et al. (2022) indicates a potential inland movement of the freshwater–seawater interface which could be the reason for increased salinity. However, boreholes affected with high salinity in the northern and central parts showed a scattered distribution. Some of the boreholes closer to the coast showed remarkably low salinity (<50 mg/L) compared to some boreholes located further inland (**Erreur ! Source du renvoi introuvable.b**). Such discrete distribution of salinity cannot be explained by the movement of freshwater–seawater interface from offshore and may result from mixing of groundwater from the high salinity intermediate and base aquifers with the groundwater from the main aquifer.

6.2.4 Conceptual model and occurrence of faults

The tectonic setting of the formations in the Aveiro Cretaceous aquifer is controlled by the reactivation of the Late Hercynian fracture network that defined a set of blocks, inside which the sedimentary cover has limited deformation. The main fault strikes are:

- N-S direction, parallel to the western edge of the Hesperian Massif. This is present as an extensive fault that runs from the Serra de Montemor to Mamodeiro and Carrajão;
- NNW-SSE direction, mainly in the terminal part of the Vouga river, although covered by the most recent formations.

The Cretaceous formations themselves are not very deformed. In the Aveiro area, they form a very open syncline that dips gently towards the coast. In certain parts, a series of synclines and anticlines are drawn, but always with very small dips, as a rule less than 5 – 10°. It is not known if these faults and fold defined blocks have some degree of independent hydrogeological features.

Geophysical studies carried out in the region of Aveiro have identified two major faults that cut through the Cretaceous formations. These faults, however, do not seem to act as hydraulic barriers, with the Eastern sector of the N-S striking fault, having a higher hydraulic head than that of the Western sector (Figure 6-13).

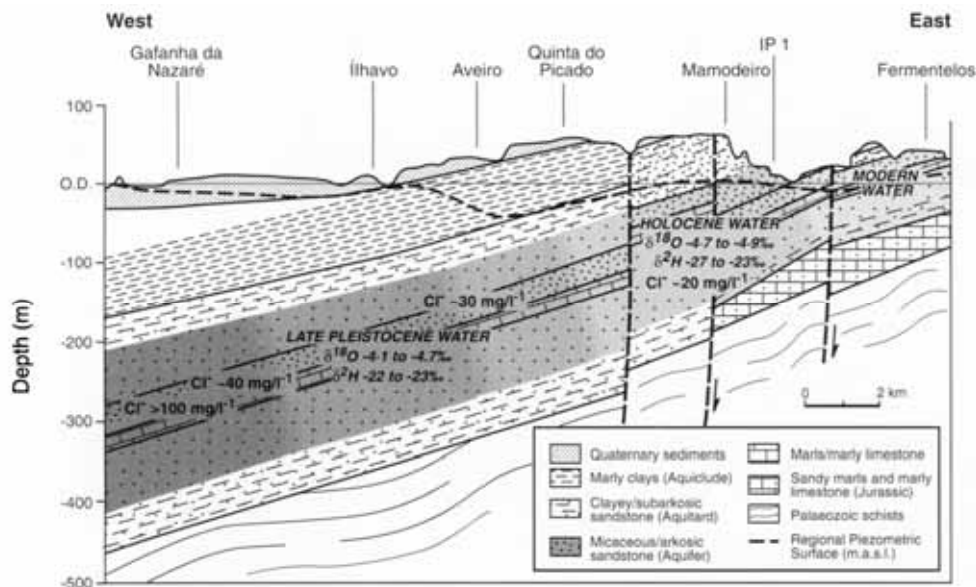


Figure 6-13. Diagram showing the regional groundwater flow in the aquifer and the influence of faults on it. Adapted from Condesso de Melo et al. (2001).

6.3 Figueira da Foz – Gesteira aquifer system (O7)

The Figueira da Foz – Gesteira aquifer system covers an area of 64 km², located south of the Aveiro Cretaceous aquifer system (O2). The aquifer system is formed by two main sectors (Figure 6-14): i) north of the river Mondego; a monoclinical structure that forms the Serra da Boa Viagem and Alhadas; ii) south of the river Mondego; around the flanks of the Verride anticline.

This aquifer system is a much less important groundwater source than the Aveiro Cretaceous aquifer, and data about it is much scarcer, with SNIRH only listing five public water supply wells (four groundwater quality monitoring wells and one piezometric level monitoring well), for which detailed information exists. The watershed management authority lists 181 private wells, the vast majority (128) of which are for irrigation, but information about them is absent in the public domain or in published references.

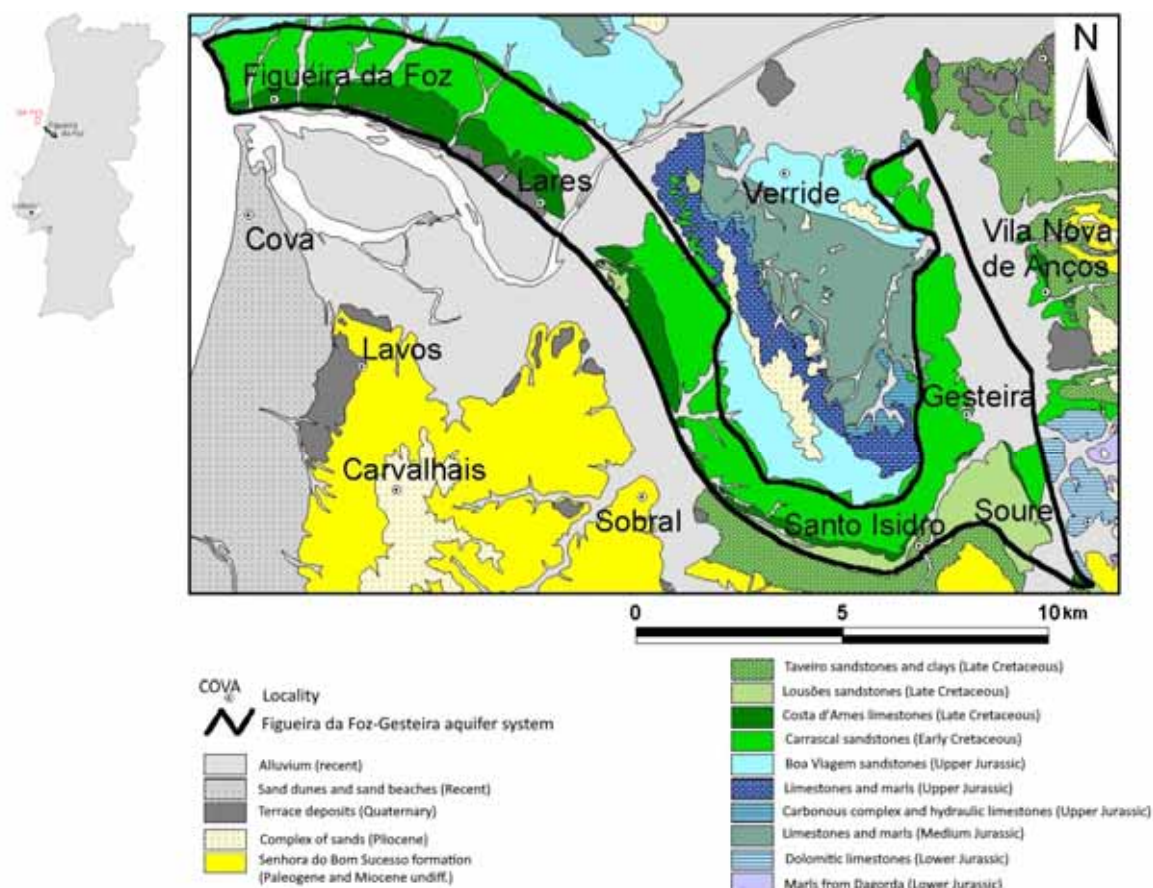


Figure 6-14. Physical and geological setting of the Figueira da Foz – Gesteira aquifer system. Adapted from Almeida et al. 2000.

6.3.1 Geological features of the aquifer

The aquifer system is composed of a Cretaceous sequence that mimics part of the sequence described for the Aveiro Cretaceous aquifer, and comprises:

- Carrascal sandstones (Aptian/Albian) - these are more or less clayey sandstones, fine to coarse, conglomeratic, with gravel and pebbles. The formation decreases in grain size from the bottom to the top. It rests unconformably on the Jurassic. It corresponds to unit C₁ in the

Aveiro Cretaceous aquifer, and it is the lateral equivalent of the Torres Vedras Group targeted offshore for CO₂ storage;

- Costa de Arnes limestones (Cenomanian) – limestones, mottled limestones, marls. This is equivalent to the C₂ unit in the Cretaceous Aveiro aquifer system. The transition to the underlying Carrascal sandstones unit is through a sequence of increasing marly and clayey components, known to be thicker offshore and to compose the first seal of the Torres Vedras Group.
- Lousões sandstones (Cenomanian / Lower Turonian) – Made up of very fine micaceous sandstones, passing into coarse to very coarse sub-arkose sandstones. Equivalent to the C₃ unit in the Cretaceous Aveiro aquifer.

In the river valleys, alluvium of the Mondego river, and on the western flank of the Verride anticline of the river Arunca, cover the aquifer system (Figure 6-14).

6.3.2 Hydrogeological properties of the aquifer

The Figueira da Foz-Gesteira aquifer, much like the Aveiro Cretaceous aquifer, can be regarded as a multilayered aquifer system, with multiple productive layers, separated by aquitards and aquicludes. However, the multiple aquifer layers are often exploited together, with wells screened in the several producing layers, so that there is no information about the hydraulic properties and groundwater quality of the different layers. Also, there is a complete absence of data (even in terms of thickness) for the aquitards and aquicludes separating the productive layers. According to Velho (1989), a full thickness of 273 m is known for entire set of productive layers.

The three above mentioned formations can be regarded as productive aquifers, with the Carrascal sandstones representing the bulk of the outcropping formations (Figure 6-14). This is the productive formation in direct contact with the Jurassic substrate. When at the surface, together with the Lousões Sandstones and the Costa de Arnes Limestones, they are an unconfined aquifer. The overlying Costa de Arnes Limestones show a karstic to porous aquifer character, it is an unconfined aquifer in the areas where it outcrops, but a semi-confined to confined aquifer when underlying the Lousões sandstones, presumably due to aquitards / aquicludes present at the base of the Lousões sandstones.

The Lousões sandstones outcrops in the monoclinical structure at shallower depths (sector north from river Mondego) and in the southern area of the Verride anticlinal (sector south from the Mondego River) where it shows a water-table behaviour (Figure 6-14). The aquifer system has a lower boundary provided by the Boa Viagem sandstones formation (Upper Jurassic) and an upper boundary composed by the Taveiro Sandstones and Clays (Late Cretaceous), which is the lateral equivalent of the C5 unit in the Aveiro Cretaceous aquifer system, which behaves as an aquiclude to the aquifer system.

6.3.2.1 Hydraulic Parameters and Productivity

Due to the grain size variability of the siliciclastic layers, the hydraulic characteristics also vary significantly across the aquifer. Overall, the aquifer system shows an average aquifer productivity of 14.7 l/s.

Table 6-5 lists the statistics of some hydraulic parameters estimated from analysis of pumping tests. The most productive wells are located in the sector north of the Mondego River. The transmissivity values increase with depth, there is a relatively strong correlation between the depth of the wells and

the flow rate. As a rule, all the perforated thickness is productive, with the increase in transmissivity given by the increase in the screened thickness.

In the sector north of the Mondego River, the average transmissivity is 118.6 m²/d. In the sector south of the river, Velho (1989) mentions the interpretation of pumping tests in only two wells: one with transmissivity estimated between 1.3 – 3.1 m²/d; while the other gave estimated values between 44.8 – 65.5 m²/d.

Table 6-5. Statistics of main hydraulic parameters in the Figueira da Foz - Gesteira aquifer. Adapted from Almeida et al. (2000)

Parameter	Mean	Stand. Dev.	Min	Q1	Median	Q3	Max.
Flow rate (l/s)	14.7	10.6	1.7	4.5	12.5	25.0	30.0
Transmissivity (m ² /d)	118.6	83	33.5	62.9	108.4	133.0	330.0

6.3.2.2 Spatio-temporal Analysis of Piezometry

There are not enough data from wells and boreholes to allow the spatio-temporal analysis of piezometry, but general flow directions are provided by the watershed management authority and indicated in Figure 6-15.

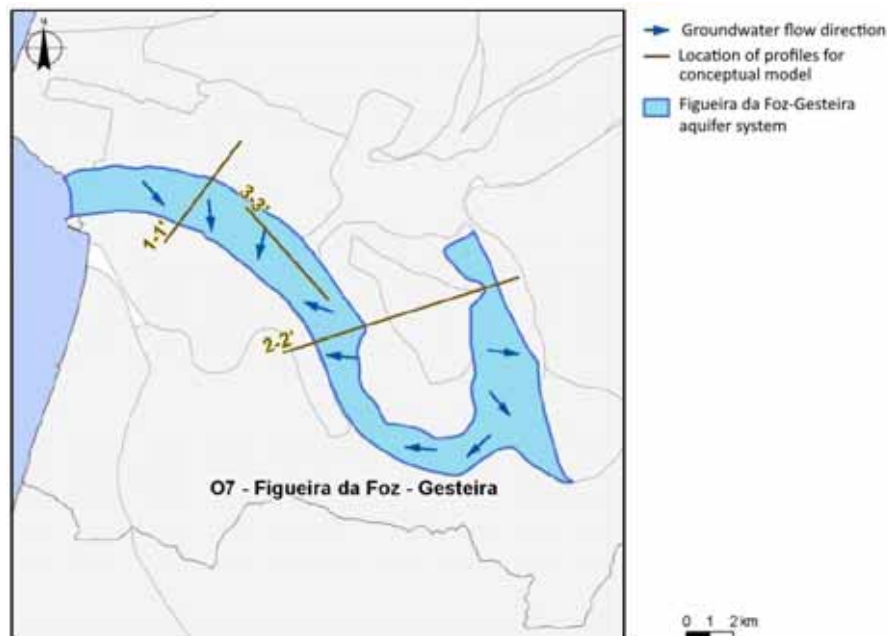


Figure 6-15. Estimated flow directions in the Figueira da Foz -Gesteira aquifer system. Adapted from ARH Centro (2012).

In terms of flow directions, the north and south of the Mondego River should be regarded as two different regions. The sector north of the river has a monoclin structure dipping to the south and a general flow direction also to the south. South of the Mondego River, along the flanks of the Verride anticline, flow diverges away from the anticline.

6.3.2.3 Groundwater balance

Direct recharge by precipitation in the outcropping area of the aquifer is of the order of 150 mm/year, equating to 9.5 hm³/year for the entire aquifer system (Figure 6-16). The alluvium in the Mondego river valley, which separates the north and south sector, and the streams that cross it, are drainage structures of the most shallow layers, although occasionally they can also recharge the aquifer system.

The groundwater balance was estimated by subtracting from the annual water availability (8.6 hm³/year), the calculated value of groundwater extraction (1.7 hm³/year). The groundwater balance estimated by the ARH Centro, the watershed management authority, is 6.8 hm³/year, which puts yields at around 20% of the annual availability.

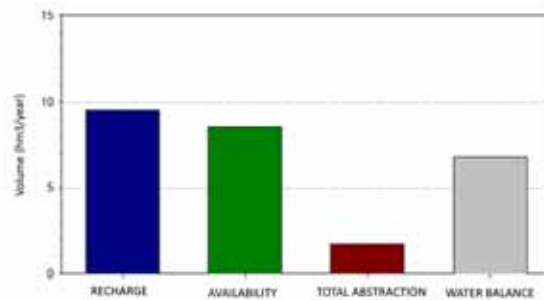


Figure 6-16. Groundwater balance components for the Figueira da Foz – Gesteira aquifer system. Adapted from ARH Centro 2012)

6.3.3 Groundwater composition

The Figueira da Foz – Gesteira groundwaters are chemically characterized by low electrical conductivities (median values 451 mS/cm) and pH with median value on the order of pH≈7.1. The median nitrate value of around 5.3 mg/l is well below the limiting value for human consumption. All minor elements have medians values below the recommended values for human consumption. Iron, manganese and lead have only one measurement exceeding the limits for human consumption (Figure 6-17a).

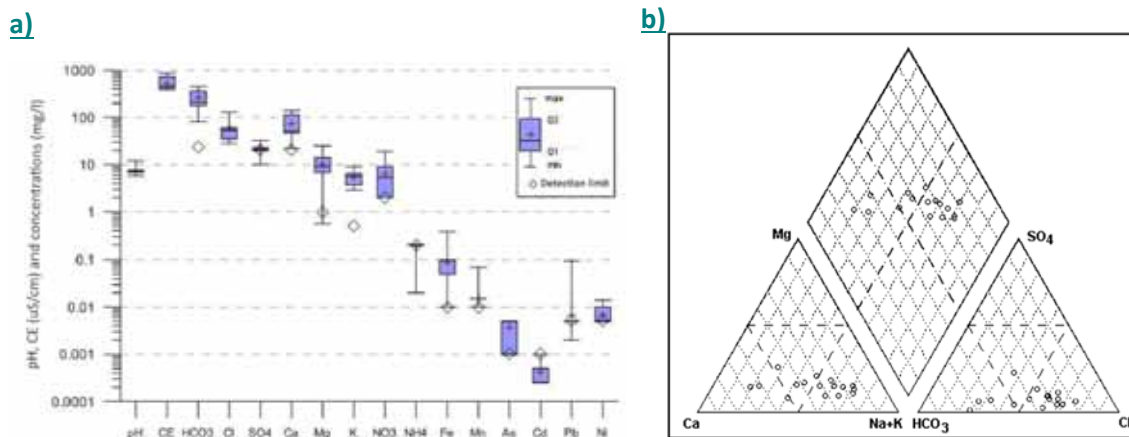


Figure 6-17. a) Statistics of hydrogeochemical features of the Figueira da Foz – Gesteira aquifer. Adapted from ARH Centro (2012). b) Piper diagram. Adapted from Almeida et al. (2000).

Groundwater facies vary between Na–Cl and Ca–HCO₃ (Figure 6-17b) waters. Sulfate and magnesium are systematically present in low concentrations. In the sector north of the Mondego river, chloride and sodium are predominant. South of the Mondego river, the groundwaters show a predominance of bicarbonate and calcium, probably due to longer circulation time in the limestones. One well located near Marujal, on the NE flank of the Verride anticline shows much higher mineralization, with the groundwater being of Na-Cl facies, probably related to circulation in contact with the evaporites in the Verride anticline.

6.3.4 Conceptual model and occurrence of faults

The outcrops of the aquifer system are distributed on the southern flank of a salt diapir structure, extending from NW to SE. Standing out north of the Mondego River is the monoclinical that extends between the mountains of Boa Viagem and Alhadas, while south of the Mondego, the flanks of the anticlinal of Verride are exposed.

The fracture system in the Verride anticlinal is intense and comprises fault systems striking N-S, NNW-SSE, WNW-ESE and NE-SW. According to the neotectonics maps by Cabral and Ribeiro (1988) some seismically active faults occur: i) the previously mentioned salt diapir structure; ii) the faults that limit it on the NE and SW flanks; iii) the Buarcos-Verride anticline complex.

Figure 6-18 depicts the conceptual model and the influence of the geological structure and main faults on it.

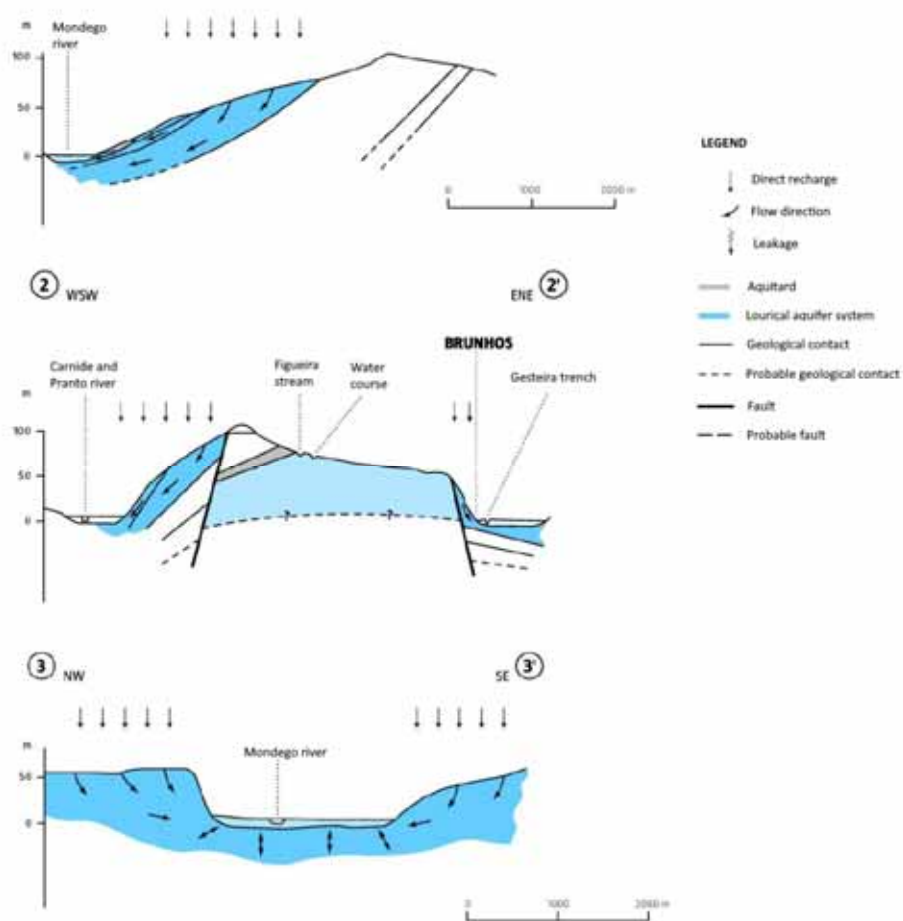


Figure 6-18. Conceptual model of the Figueira da Foz – Gesteira aquifer system, showing the influence of geological structure and main faults. Adapted from ARH Centro (2012). See Figure 6-15 for location of sections.

6.4 Lourical aquifer system (O29)

The Lourical Aquifer System is located in a subsidence basin, often designated as the Lourical basin or Pombal sub-basin (Figure 6-3, Figure 6-9). It is a multilayered aquifer system composed of three subsystems: Cretaceous, Miocene and Plio-Quaternary. Unlike the previous two aquifer systems,

which are only Cretaceous formations, the Louriçal aquifer may show the full sequence that represents the lateral equivalent of the overburden in the Q4-TV1 offshore storage target.

The basin, with a total area of 588km², has as its limits to the west the Jurassic formations of the Serra do Sicó, to the east the salt diapir of Monte Real (Figure 6-19). It lies south of the Figueira da Foz aquifer system previously described.

The groundwater management authority ARH Centro listed fifteen public water supply wells in 2012, for which some detailed data exists, in a total of 2566 groundwater wells. Most of the wells, 1683, provides irrigation water. The vast majority are shallow wells intercepting the upper layers of the multilayered aquifer system, seldom reaching the Cretaceous aquifer layers.

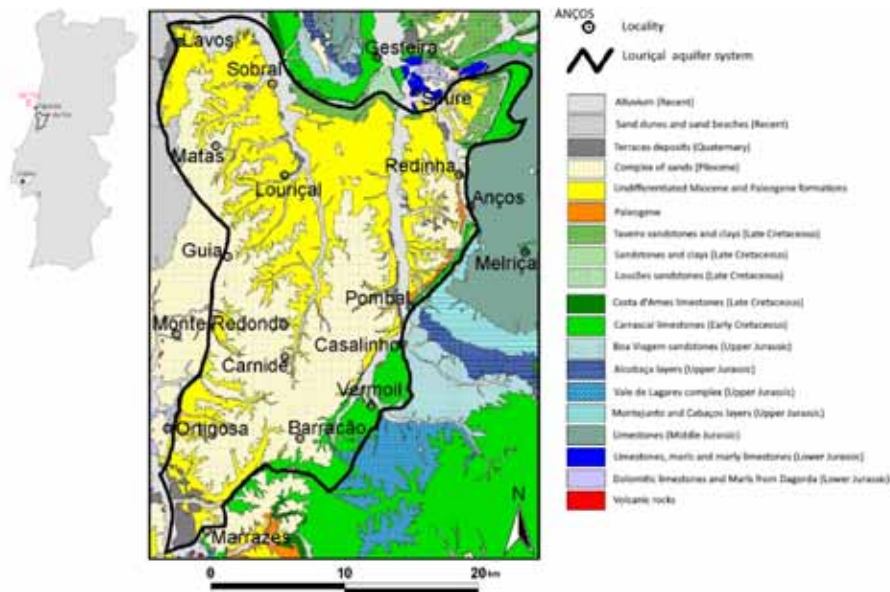


Figure 6-19. Physical and geological setting of the Louriçal aquifer system. Adapted from Almeida et al. 2000.

6.4.1 Geological features of the formation

In most of the Louriçal basin, thick Paleogene and Miocene deposits of continental origin are covered by a Pliocene sedimentary sequence, marine at its base, continental at the middle and the upper part composed by sandy-clayey and conglomeratic deposits. Overall, three different subsystems are present:

Plio-Quaternary Subsystem

This subsystem is composed of the Plio-quaternary deposits that partially cover the surface of the Louriçal basin. They are clayey sands and gravels. In the upper part, there are several clayey intercalations, more or less developed, and the sequence ends in sands with well-rounded pebbles. The outcrops are of two types: small isolated patches, crowning the hills of the undifferentiated Miocene and Paleogene terrains; and spatial continuous outcrops, forming extensive plateaus and which, to the west, extend to the deposits of the Leirosa-Monte Real aquifer system. This subsystem is not representative of seabed sediments in the offshore target area, and are of negligible interest for understanding the offshore storage complex.

Undifferentiated Miocene and Paleogene Subsystem

The Miocene formations are separated from the Cretaceous by a sequence comprising a thick, predominantly clayey, ensemble of the Late Cretaceous Taveiro Sandstones and Clays and the

Paleogene. These are more or less clayey sandstones and clays, in alternating layers, reaching thicknesses around 400 m in the central part of the basin.

Cretaceous subsystem

This comprises three formations, from the top to the bottom: the Lousões Sandstones, the Costa de Arnes Limestones and the Carrascal Sandstones. This is the same sequence in the Cretaceous Aveiro aquifer (O2) and the Figueira da Foz-Gesteira aquifer (O7) previously described. From base to top:

- Carrascal sandstones - generally sandstones more or less clay-rich, fine to coarse, conglomeratic, with gravel and pebbles and clays. The formation decreases in grain size from the base to the top. It rests unconformably on the Jurassic. It corresponds to the C₁ sequence in the Aveiro Cretaceous aquifer.
- Costa de Arnes limestones - the intermediate unit. Composed of limestones, marly limestones, and marls. The transition to the Carrascal Sandstones is through marls and clays. It corresponds to the C₂ sequence in the Aveiro Cretaceous aquifer;
- Lousões sandstones – these form the upper unit, with very micaceous arkosic fine sandstones at the base that evolve to subarkosic coarse to very coarse sandstones. It corresponds to the C₃ sequence in the Aveiro Cretaceous aquifer.

The Cretaceous only outcrops at the edges of the Lourical basin and in small, scattered outcrops, between Monte Redondo and Guia and on the eastern edge of the Monte Real salt diapir (Figure 6-19). The total thickness of the Cretaceous sequence is greater than 200 m.

The Late Cretaceous Taveiro Sandstones and Clays and the Paleogene formations confine the Cretaceous formations and act as aquicludes, again replicating the behavior of Unit C₅ in the Aveiro Cretaceous and the Figueira da Foz-Gesteira aquifer systems.

6.4.2 Hydrogeological properties of the aquifer

6.4.2.1 Hydraulic Parameters and Productivity

The hydrogeological properties of the multilayered aquifer reflect the existence of the three subsystems separated by aquitards and aquicludes. Data is very scarce for detailed statistical analysis, but the watershed authority ARH Centro presents the range of hydraulic properties in Table 6-6.

Plio-Quaternary Aquifer Subsystem

The Plio-Quaternary subsystem is generally an unconfined porous aquifer that may show some confined and/or suspended aquifer behaviour in the upper part due to the presence of several clayey intercalations. There is an almost complete lack of information regarding the hydraulic parameters and productivity of this subsystem.

Miocene Aquifer Subsystem

The porous, confined to semi-confined, Miocene subsystem consists of multiple productive layers (low to medium productivity) separated by layers with aquitard/aquiclude behavior. Each productive layer is usually thin, with seemingly unrelated piezometric levels that show a significant increase with depth (Peixinho de Cristo, 1998).

Although the size of the samples is small, it seems that the productivity of the western flank of the Lourical syncline is the most heterogeneous. In general, groundwater wells have low productivity and yields. In the eastern flank, the Pombal region, the flows are weak, of the order of few liters per

second, even for wells that exceed three hundred meters depth. The specific flow rates are low in the entire Miocene subsystem: only one well has a value above 1 l/s/m.

According to Peixinho de Cristo (1998), there is not enough data to make a precise characterization of the hydraulic characteristics of this subsystem; however, it can be stated that, as a whole, the subsystem has variable mean transmissivity between 100 and 200 m²/d and storage coefficient of the order of 10⁻⁵.

Paleogene Aquitard

In the eastern part of the basin, where these formations outcrop, the Paleogene may act as an aquitard that locally confines the Cretaceous Aquifer Subsystem.

Upper Cretaceous aquitard (Taveiro Sandstones and Clays)

These are the upper layers of the Cretaceous series, which act as an aquitard. The N and NE areas of the water body area are confined where the formations of the Cretaceous Aquifer Subsystem as defined by Velho (1998) are also confined.

Cretaceous Aquifer Subsystem

The porous Cretaceous aquifer subsystem exhibits unconfined behavior in the outcrop areas, becoming rapidly confined as soon as the layers dip away from the outcrops. Layers of a clayey nature separate the various productive layers giving the subsystem a multilayer character. The transition from the Costa de Arnes Limestones, the intermediate unit, to the Carrascal Sandstones is made through marly and clayey beds, giving aquitard characteristics. The productivity of the subsystem ranges from 27 and 40 l/s.

The depth of the Cretaceous formations has been a major uncertainty in exploration efforts and production from this subsystem. Thus, the hydrogeological information available is very limited, with information only on the shallower part, east of Leirosa, where four wells are known, with transmissivities ranging from 86 to 1007 m²/d (Table 6-6).

Table 6-6. Summary of hydraulic properties of the components of the Lourical multilayered aquifer system (Source : ARH Centra, 2012)

Formation	Hydrogeologic behaviour	Transmissivity (m ² /d)	Specific flow rate (l/s/m)
Plio-quadernary subsystem	Unconfined porous aquifer.	-	-
Paleogene	Aquitard	-	-
Miocene subsystem	Confined to leaky porous aquifer. Locally aquitard/aquiclude	100 to 200	0.11
Late Cretaceous (Taveiro Sandstones and Clays)	Aquitard	-	-
Cretaceous Subsystem	Unconfined / confined porous aquifer. Locally an aquitard.	86 to 1007	0.85 to 5.2

6.4.2.2 Spatio-temporal Analysis of Piezometry

Given the scarcity of information it is not possible to draw a piezometric map for the different subsystems of the Lourical aquifer. Circulation is long, deep and slow towards the sea, where it discharges at the northwestern end of the Lourical aquifer system (Peixinho de Cristo, 1998; Figure 6-20). The fact that the flowing is relatively weak may mean that there is some fluid exchange with the adjacent units. There may also be flow up the most important faults, such as those of the valleys of the Arunca and Pranto rivers, which may act as draining structures with upward flow.

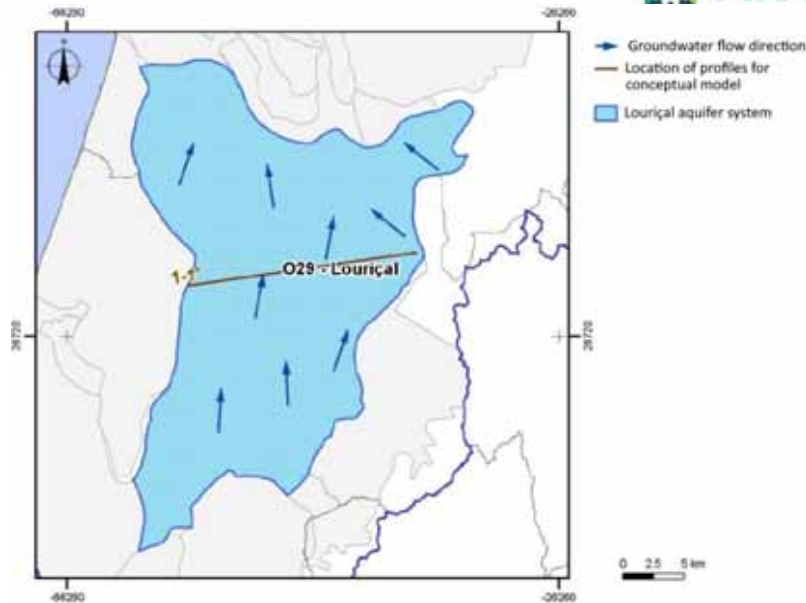


Figure 6-20. Piezometric map and main flow direction in the Lourical aquifer system.

6.4.2.3 Groundwater balance

Cretaceous subsystem

Direct recharge of the Cretaceous subsystem occurs by precipitation in the outcrops to the east, north and west boundaries of the basin. In the latter sector, recharge can also occur through Plio-quaternary cover. The total set of outcrops, with an area of 65 km², result in an average annual recharge of 10 hm³. Rivers drain the surface and outcrop zones of the aquifer system, but the alluviums in the Arunca and Anços rivers, during the high waters season, also recharges the Cretaceous subsystem. On average, it is expected that the system outputs balance the inputs.

Miocene Subsystem

Recharge of this subsystem is through precipitation that infiltrates directly in the outcrops of the most permeable layers, at the edges of the basin. Peixinho de Cristo (1998) estimates that the average annual recharge of the subsystem is on the order of 30 to 40 hm³, but if the total area of the subsystem is considered, 450 km², a recharge value of 45 hm³/year is obtained. The discharge of the subsystem is mainly to the sea, in the northwestern part of the Lourical basin, but the superficial aquifer layers discharge to the hydrographic network: the Arunca and Carnide rivers and its tributaries.

Plio-Quaternary Subsystem

The recharge of this subsystem is through precipitation on the outcrops. It is estimated that this recharge is of the order of 220 mm/year, that is, the equivalent to 46 hm³/year, for an area of 210 km². But since leakage to the underlying Miocene subsystem is estimated at 100 mm, the renewable groundwater resources are in the order of 25 hm³/year. Discharge is exclusively to the watercourse network.

The groundwater balance presented by the watershed management authority ARH Centro has an estimated value of annual water availability (60 hm³/year) and the calculated value of groundwater extraction (3.8 hm³/year). According to ARH Centro the water balance is 57 hm³/year (Figure 6-21), a

value that confirms that the abstractions are only around 6% of the average annual groundwater availability.

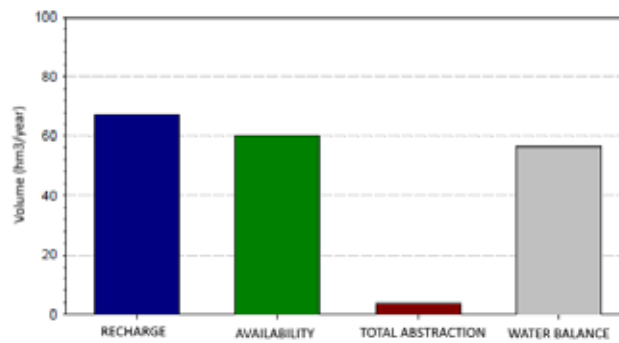


Figure 6-21. Groundwater balance components for the Louriçal aquifer system. Adapted from ARH Centro (2012).

6.4.3 Groundwater composition

Groundwaters with low electrical conductivities (median values 225 mS/cm) and slightly acidic pH (median pH≈6.2) predominate. The median nitrate value is around 9.4 mg/l, well below the legislated limit for human consumption. In relation to the smaller elements, all elements have median values below the legislated value for human consumption (Figure 6-22a). However, iron and arsenic have maximum values of 0.5 mg/l and 0.32 mg/l, respectively, exceeding the legislated values for human consumption.

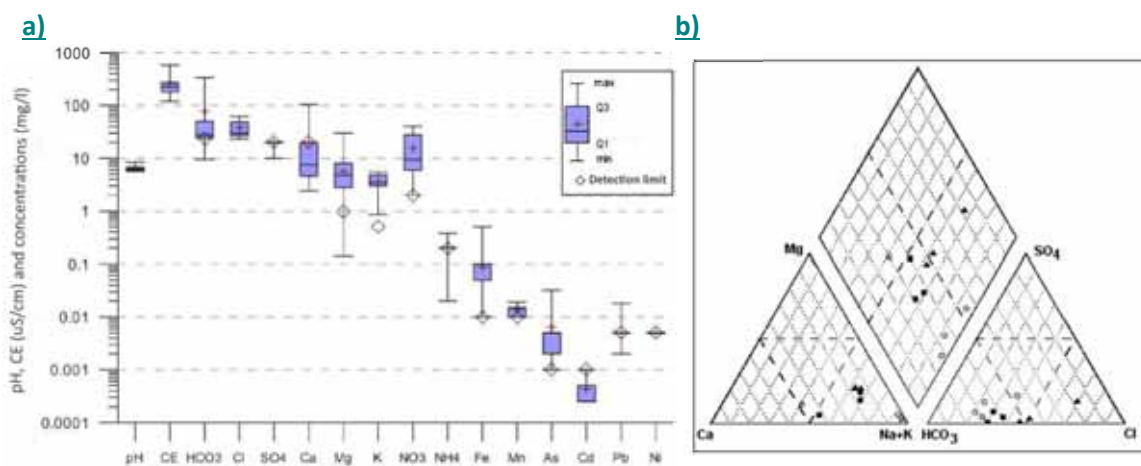


Figure 6-22. a) Statistics of hydrogeochemical features of the Louriçal aquifer. b) Piper diagram.

In two of the four inventoried wells in the deep Cretaceous subsystem, groundwaters are high mineralized and are unsuitable for domestic supply and industrial, with a sodium bicarbonate facies (Figure 6-22b).

In the Miocene subsystem, near Pombal, groundwaters are also mainly sodium bicarbonate type, but in the western flank of the Louriçal syncline the geochemical types are Na–HCO₃-Cl and Na–Cl.

No information is available on the water quality of the Plio-Quaternary Subsystem.

6.4.4 Conceptual model and occurrence of faults

The analysis of a few 2-D seismic sections the basin reveals:

- The Louriçal syncline, with a NW-SE axis plunging to the SE. The flanks are approximately symmetrical, associated with the Figueira da Foz-Soure salt dome, in the north, and the Monte Real salt dome in the south.
- An asymmetrical syncline parallel to the Jurassic formations of the Serra do Sicó and extending to the region of Leiria, with NE-SW direction.

As well as the salt domes, including the NNE oriented Monte Real salt dome, the basin is crossed by some major faults. The NE-SW Lousã-Pombal-Leiria fault crosses the eastern boundary of the basin. There are also the faults that limit, to the NE and SW, respectively, the Serra da Boa Viagem and the Verride anticline, and which control the valleys of the Arunca and Pranto rivers (Figure 6-23).

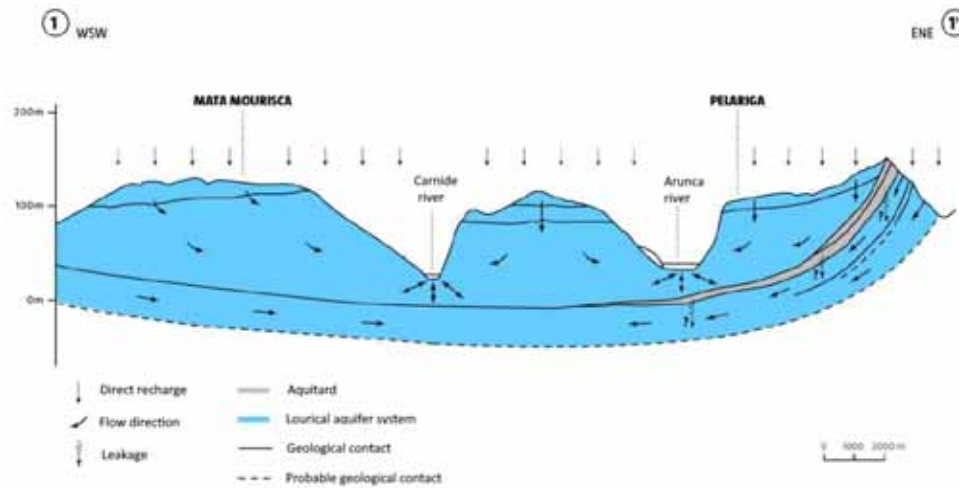


Figure 6-23. Conceptual model and geological structure of the Louriçal aquifer.

7. Spain – Ebro Basin

The Lopín structure, the target for CO₂ storage in the onshore Spanish region, is located in the Ebro Basin (

Figure 7-1). From a hydrogeological point of view, two overlapping and independent systems are present here: 1) a shallow Quaternary to Lower Jurassic system; 2) a deep Middle to Lower Triassic system. In the Lopín structure, both the storage and the seal formations are part of the deep Triassic system (Figure 7-2 and Figure 7-3).

The sequence of aquifer-aquiclude-aquitard is shown in **Erreur ! Source du renvoi introuvable.** Three aquifer formations are identified in the Triassic deep system under the Keuper facies. With respect to the Jurassic main regional aquifer, it lays on the Lower Liassic clay-anhydrite-marl Lecera formation. The Cenozoic, although it is an alternation of clay-gypsum-conglomerate-sand, it is generally considered as an aquitard, at a regional scale.

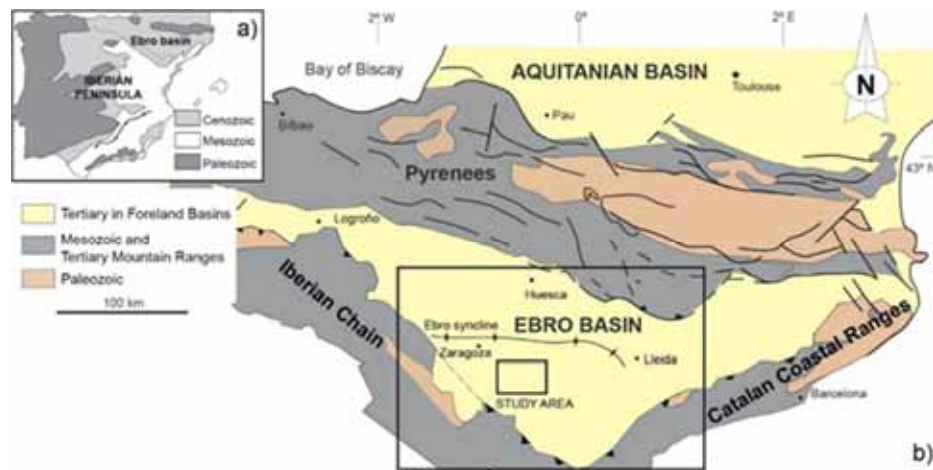


Figure 7-1. a) Simplified geological sketch of the Iberian Peninsula (from Soto et al., 2009). b) Geological sketch of the northeastern part of Iberia showing the study area in the central part of the Ebro basin and the Alpine ranges (modified from Soto et al., 2016).

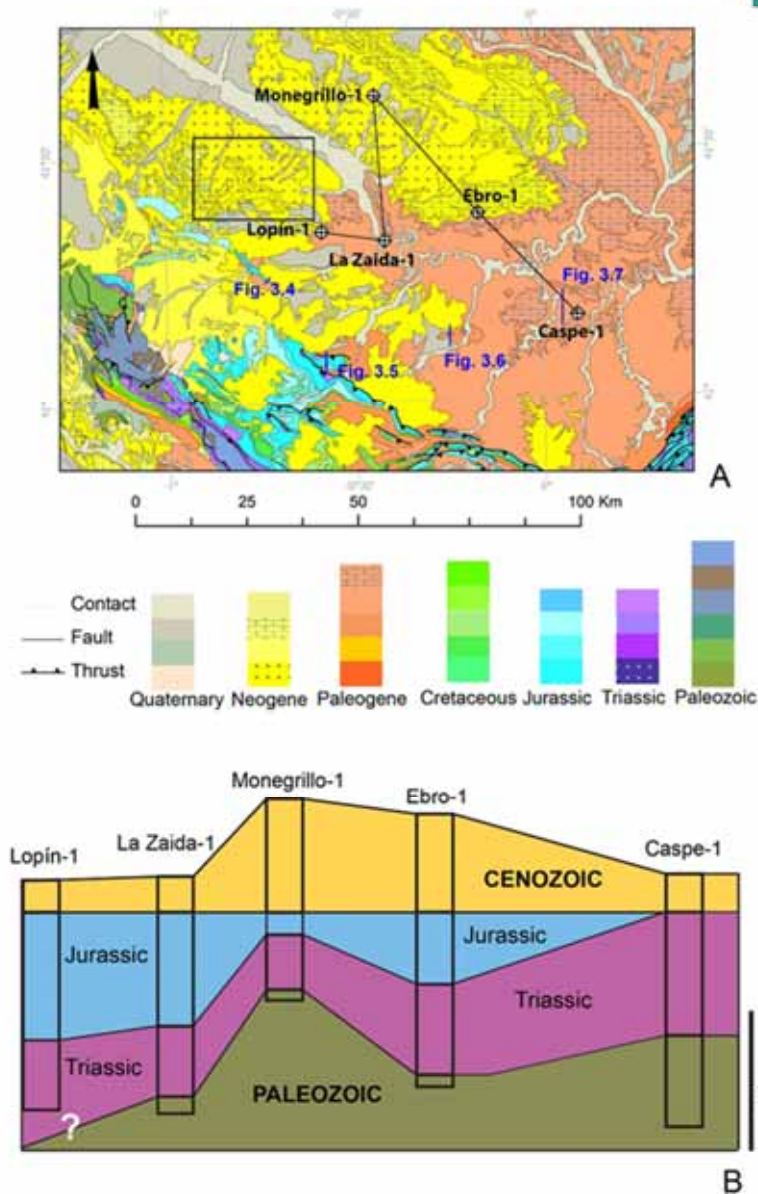


Figure 7-2. Geological map of the southern Ebro basin showing the location of the study area and the location of wells Lopin-1, La Zaida-1, Monegrillo-1, Ebro-1 and Caspe-1. b) Sketch showing the rocks in terms of age crossed by the above mentioned wells. See Figure 9-2a) in the PilotSTRATEGY Deliverable 2.7 Conceptual Geological Models Report (Wilkinson 2023). The Triassic hosts the deep hydrogeological system. The Jurassic and Cenozoic are the shallow system. The Jurassic is the main regional aquifer supporting most of the extractions. The Cenozoic formations are quite poor from a hydrogeological point of view because they are clayey and evaporitic.

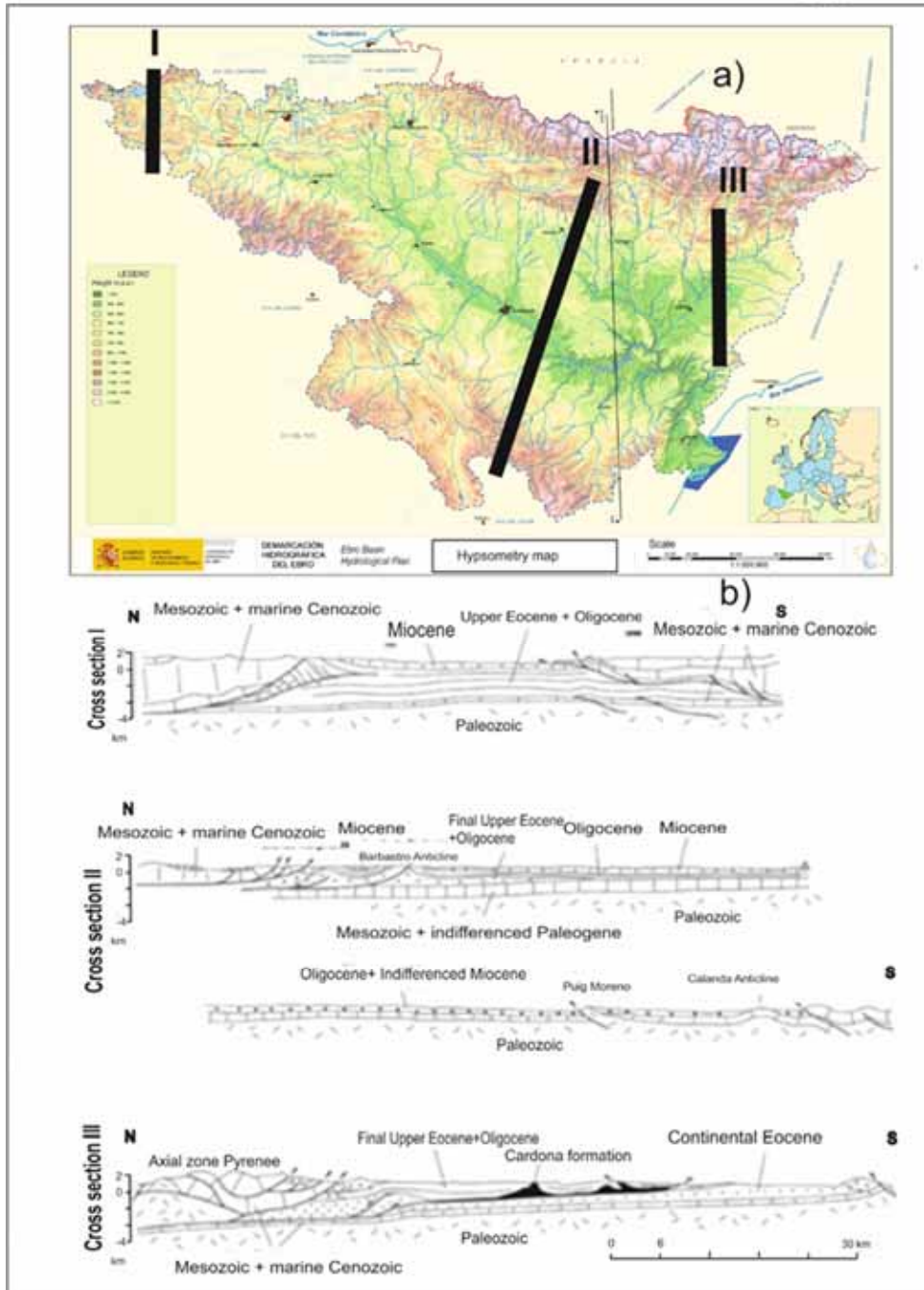


Figure 7-3. a) Hypsometric map of the Ebro Basin (Modified of Hydrological Planning of the Ebro Basin, CHE,2023). b) Three regional geological cross sections, for location see (a) (Pardo et al., 2004).

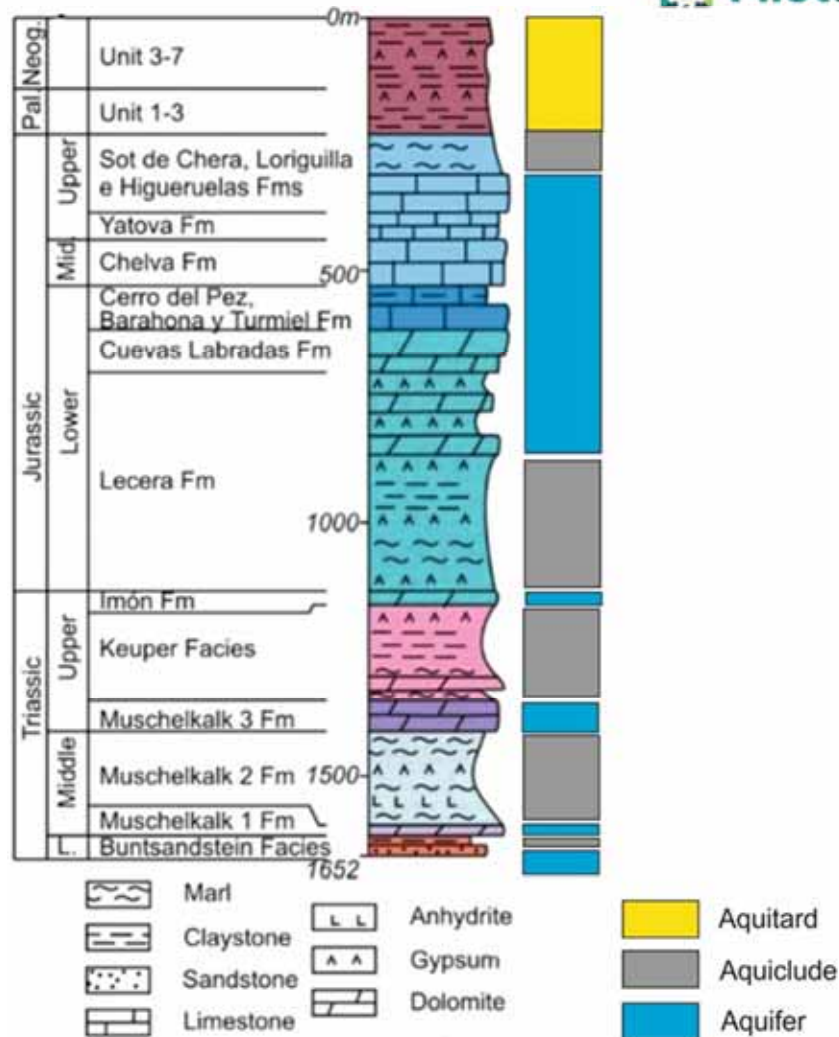


Figure 7-4. Stratigraphic column of Lopín-1 well. Modified from Figure 6.2 in PilotSTRATEGY Deliverable 2.7 Conceptual Geological Models (Wilkinson, 2023).

7.1 Overview of the Ebro Basin

The Ebro Catchment Basin is located on the Northeast quadrant of the Iberian Peninsula covering 85,534 km². It is, indeed, the biggest hydrographic basin in Spain representing the 17% of the territory, and one of the most important Mediterranean Catchment Basins.

The main drainage artery is represented by the Ebro River that flows from NW to SE. Its main tributary rivers are: Aragón, Gállego, Cinca and Segre on the north riverbank, and Oia, Iregua, Jalón, Huerva and Guadalope on the south riverbank.

The climate is Mediterranean type, although some Atlantic influences are effective on the NW edge; Continental and mountain traits are present on the inner sectors. Maximum rainfall, up to 1000 mm/year, occurs in the Pyrenees, while the driest semi-arid conditions, normally not reaching 400 mm rainfall a year, are predominant in the central sectors of the Ebro Valley.

The population in the basin is 3,200,000 inhabitants, what means a density of 37 inhabitant/km², which is quite low with respect the European norm.

From a geological point of view, the Ebro Cenozoic Sedimentary Basin does not coincide with the Ebro catchment basin (hydrographic). This is because the sedimentary basin is limited to just the Cenozoic sedimentary infill, while the catchment has a hydrographic framework involving different geological domains (the Cenozoic basin itself, part of the Pyrenees Range, part of the Iberian Range and part of the Coastal Catalan Range). The sedimentary basin represents the final evolutionary stage of the Southern Pyrenean foreland basin. The geological limits of the basin are: the Pyrenees Range to the North; the Iberian Range to the South East; the Coastal Catalan Range and the Mediterranean Sea to the East; and the Cenozoic Duero Basin to the West.

The current structure and the limits of the Cenozoic basin were established between the Upper Oligocene and the Lower Miocene, when the southern Pyrenean foreland-thrusts became inactive. The bottom of the Cenozoic sedimentary infill is located 3,000 meter below sea level at the Pyrenean edge. Resting on an erosive basal surface, the Cenozoic sediments onlap southwards, meaning that the oldest sediments are found at the Pyrenean margin, and the sediments that directly overlie the erosive surface become progressively younger towards the Iberian Range margin in the south.

A part of the sedimentary infill, especially at the northern margin, are allochthonous marine and continental formations that overthrust the Ebro Basin.

Three main domains may be identified in the Cenozoic Ebro Basin, based on the structure, the subsidence and the age of the outcropping sediments.

- a) Western sector, affected by thrusts that were active until the late Miocene accompanied by deep subsidence, reaching a total thickness of 5,000 m (Cross section I, Pardo *et al.*, 2004) figure 6.2. Geología de España, in IGME-SGE, 2004))
- b) Central sector, is wider and has subsided less than the western sector. The structure is basically tabular. A progressive southwards displacement of sedimentation towards the Iberian margin has been identified, until the sector acted as a passive basin margin. The pre-Cenozoic strata, closest to the Iberian passive margin, is affected by NW-SE trending and N vergent thrusts rooted in the Upper Triassic (Keuper facies). Those thrusts controlled Paleogene sedimentation and even affected the Neogene infill. They also cause the Mesozoic basement to outcrop locally, surrounded by Miocene sediments (Cross section II, figure 6.2. in Geología de España, IGME-SGE, 2004).
- c) Eastern sector. No Neogene sedimentary record is present, but the area was clearly subsiding during the Paleogene. E-W to ESE-WNW and NE-SW fold structures are identified close to the Southern Pyrenean front (cross section III, figure 6.2 in IGME-SGE, 2004). Those folds are related with some detachment planes linked to the Southern Pyrenean front and Paleogene diapiric evaporitic formations.

The Lopín structure is located in the Central sector. From a hydrogeological point of view, two overlapping and independent systems are identified in the Ebro Basin: 1) A shallow Quaternary to Lower Jurassic system; 2) A deep Middle to Lower Triassic system. In the Lopín storage structure, both the storage and the seal formations are part of the deep Triassic system.

The hydrogeological behavior of the Ebro Basin shallow system is deeply linked to the Ebro River, which acts as a recharge inductor or a drainage axis, depending on the piezometer stage. Normally, recharge is produced through the direct infiltration of rainfall and snow, infiltration from the Ebro river channel, the storage in the riverbanks during flooding and lateral underground recharge from the surrounding formations from the Iberian Range to the South, and the Pyrenees Range to the North. In general, the knowledge of the hydrogeological dynamics of the shallow system is quite satisfactory

since it is the one studied and exploited. Groundwater masses of the Ebro Basin were defined in this shallow system and they were properly characterized as it was mandatory from the European Framework Directive 2000/60/CE. The Ebro River Basin Authority has a wide monitoring network established for both piezometry and quality.

However, the deep Triassic hydrogeological system, lying under the Keuper facies, is poorly known. Triassic strata do not outcrop inside the sedimentary Cenozoic Ebro Basin. The only access to the middle and lower Triassic formations is through some scarce oil investigation boreholes.

According with this hydrogeological model, the proposed hydrogeological column is summarized in Figure 7-5. The components of the model are described in the remainder of this report, from oldest (deepest) to youngest (shallowest).

QUATERNARY	GW DEFINED MASSES (EBRO BASIN) Detrital multilayer (Tertiary) & Carbonated aquifers (Jurassic) Hydraulic connection among GWM (vert. & lat.) Upwards flow in discharge zones Regional flow towards Ebro River (regional discharge)	SHALLOW SYSTEM
NEOGENE		
PALEOGENE		
JURASSIC		
TRIASSIC KEUPER FAC.	Regional Base Aquifuge	DEEP SYSTEM (Reservoir&Cap formations)
TRIASSIC MUSCH. BUNT. FAC	Deep and confined hydrog. System. Slow flow/high salinity (Oil Exploration Wells) Undefined recharge and discharge areas	

Figure 7-5. Simplified hydrogeological sketch of the Lopín area. Two systems are identified: 1) Deep Triassic system; 2) Shallow Jurassic to Quaternary system.

7.2 Hydrogeology of the Triassic system

Most information of the Triassic system information was obtained from the project ALGECO2, carried out by IGME in 2010 (IGME, 2010). The Triassic system was considered as a single hydrogeological unit, although it is composed of pairs of storage and sealing formations which are described in more detail in sections 7.2.1 to 7.2.3:

- 1) Storage formation: Buntsandstein (Cañizar, Prades and Rillo de Gallo formations), sandstones 17 to 532 m thick. Seal formation: Buntsandstein (Röt facies and Eslida Formation), clays and anhydrite, 16 to 325 m thick.
- 2) Storage formation: Muschelkalk I, dolomites 11 to 105 m thick. Seal formation: Muschelkalk II, clays and anhydrite 17 to 323 m thick.
- 3) Storage formation: Muschelkalk II, sandstones. Seal formation: Muschelkalk II, clays and anhydrite. The thickness is very variable, ranging from 17 to 323 m.
- 4) Storage formation: Muschelkalk III, dolomites 45 to 200 m thick. Seal formation: Keuper facies clays and evaporites, 15 to 895 m thick. Keuper facies is also a part of the regional aquiclude for the shallow system.

From a tectonic point of view, the Triassic system under the Ebro basin is an autochthonous unit. No Triassic outcrops are present inside the Ebro basin itself. The closest are those in other surrounding

units including the Iberian Range to the south, and the Catalan Coastal Range to the East. This unit continues to the north, reaching the base of the Pyrenees at 4000 m depth. From a conceptual hydrogeological point of view, the Triassic system is associated with deep and very slow groundwater flows and no identified recharge areas inside the Ebro Basin itself. Oil boreholes show salinities higher than 65,000 NaCl ppm, considered to be deep brines, with the only exception of Lérida-1 and Fraga-1, with salinities of 6,000 and 30,000 ppm respectively. The supposed recharge areas are located outside the Ebro Basin limits, in the Iberian Range and the Pyrenees, where the groundwater flow is vertical and descending. The supposed discharge zone is located around Lleida city, 90 kilometers away to the NE from Lopín structure, where a numerical flow model shows an ascending groundwater flow (Figure 7-6).

Some numerical simulations were performed in the ALGECO2 project (IGME, 2010) using finite element codes, GMS 6.5 (EMRL, 2006) for gridding (60,863 elements and 31,155 nodes) and pre-processing, and Feflow 5.4 (Diersch, H.J. F., 2005) to calculate flow and transport. The following model was used:

- The shallow system includes all the stratigraphic series from Quaternary to the top of the Triassic Keuper facies. Most of this system is Cenozoic sediments but there is also some Jurassic at the base.
- The Keuper facies forms the basal regional aquiclude of the shallow system, and the underlying Triassic formations are the deep hydrogeological system.
- The lateral boundaries were considered to be impervious (no flow), and for the upper limit the piezometric level was coincident with the topography.
- The hydraulic parameters were obtained from the boreholes logs.
- The vertical hydraulic conductivity was ten times the horizontal hydraulic conductivity.
- The hydraulic conductivity values used were:
 - ✓ Ebro basin shallow system= 1.6×10^{-2} m/d
 - ✓ Keuper (three scenarios: base case, variant #1, variant #2) = 8.6×10^{-6} m/d; 8.6×10^{-5} m/d; 8.6×10^{-4} m/d
 - ✓ Triassic deep system= 1.25×10^{-1} m/d

Two simulations were carried out:

- a) Steady regime and constant density, to evaluate the hydraulic behavior of the Keuper facies in the deep flow, assuming the equivalent to fresh water pressures in the whole domain (the mean density of the brine in the basin is 1.23 gr/cm^3);
- b) Transient regime and variable density, to estimate the effect of varying the density in the deep flow. It has explained the stratification of the salinity observed in the Ebro Basin, where it is almost impossible to find fresh water below 500 m depth.

The results of the deep system flow and salinity distribution are synthetized in Figure 7-6 where the conceptual hydrogeological model is illustrated.

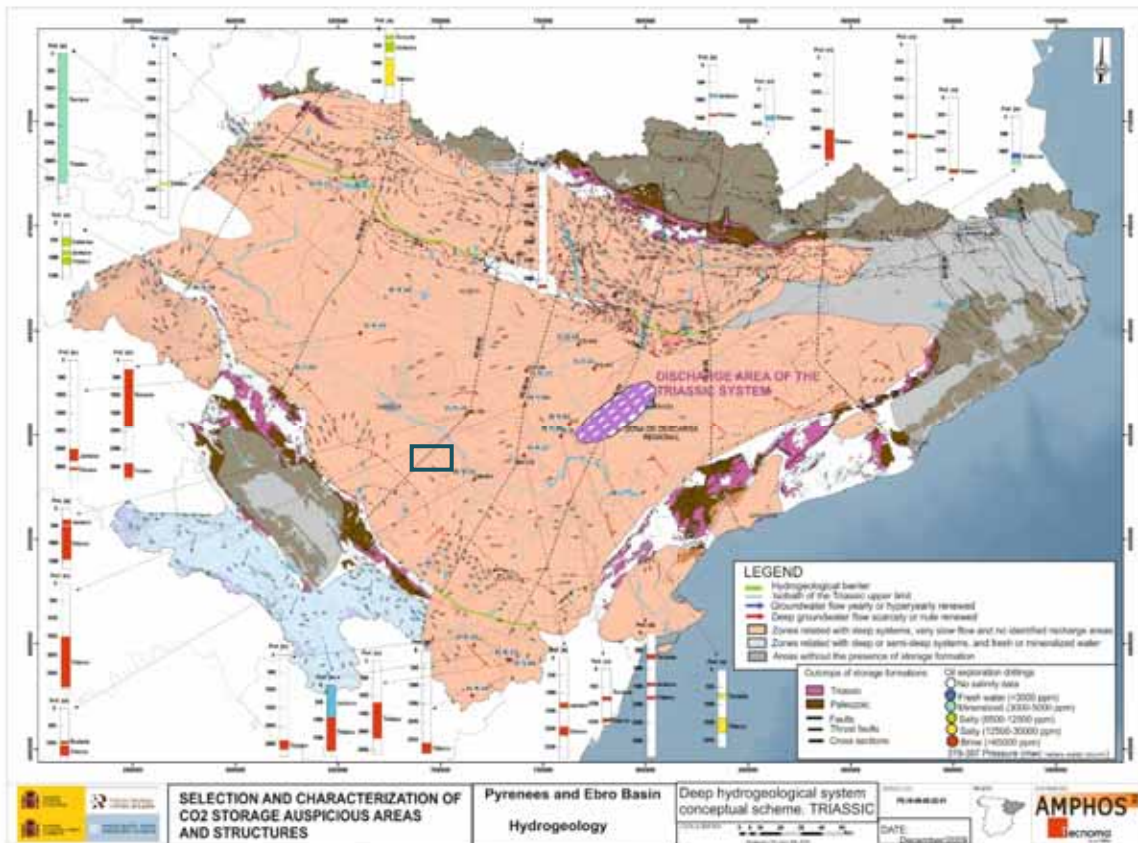


Figure 7-6. Hydrogeological conceptual model obtained by mean of a 2D numerical flow model in ALGECO2, (IGME 2010). The black rectangle shows the studied area.

With respect to the deep system, two areas are identified as recharge zones: Pre-Pyrenees zone (to the North) and the Iberian Bond zone (to the South). The flow converges towards the middle of the Ebro Basin. For a median scenario, it is supposed that most of the recharge water flows through the Cenozoic sediments, although at the recharge zones, a part of it is supposed to pass through the Keuper reaching the Triassic deep system. In the area of Lleida city, towards the east, the modelling shows an ascending regional discharge zone. This should mean that the Keuper may periodically allow some vertical circulation (recharge and discharge). If the hydraulic conductivity of the Keuper is increased, as in scenarios #1 and #2 (above), the geometry of the discharge zone does not change substantially but the recharge rate of the Triassic system increases.

The transient numerical model with variable density was carried out to study the stratification of high salinity (NaCl) waters. The initial conditions assumed that the Triassic formations are saturated with high salinity water (200 g/L of NaCl), and the recharge water that infiltrates from the overlaying zones have a concentration lower than 1 mg/L of NaCl). Simulating for 1000 years, it could be observed that fresh water is rarely found deeper than 500 m, what is similar to the data obtained in oil boreholes. Also, from 500 to 1000 m depth the salinity reaches a pseudo-stationary regime, and no important variations are expected.

With the aim of validating these results, calculated pressures were compared with the pressure in some oil boreholes (Fraga, Esplús and Monzón; Figure 7-7 and Figure 7-8). The units of the measured pressures are meters of water column (mwc); the numerical model units are meters of salt water column (mswc), which are corrected by multiplying by the density of salt water 1.23 g/cm^3 .

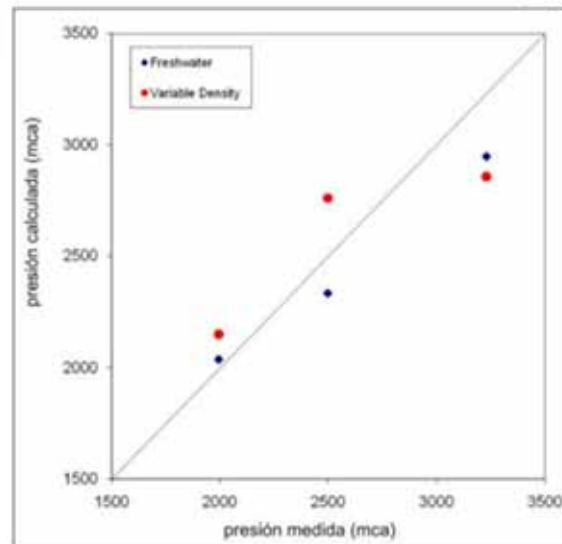


Figure 7-7. Comparative graphs of measured pressure in boreholes (x-axis) and modelled pressure (y-axis) for freshwater and variable density models. Good correlations are observed. Pressure units: meters of water column (mca).

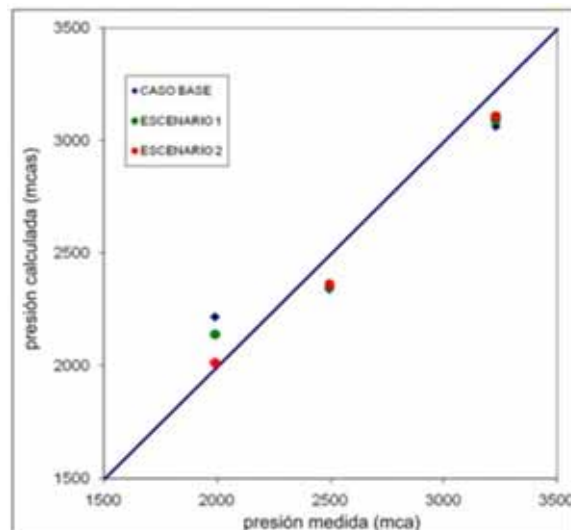


Figure 7-8 Comparative graphs of measured pressure in boreholes (x-axis) and modelled pressure (y-axis) for variants of the variable density model. Good correlations are observed. Pressure units: meters of water column (mca).

7.2.1 Buntsandstein formation: the target reservoir

7.2.1.1 Geological features of the formation

The target formation for CO₂ storage is in the Triassic series, and more specific in the continental siliciclastic lower Triassic Buntsandstein facies. In the Ebro Basin it is the first Triassic sequence overlaying the Paleozoic basement as an angular unconformity. Sedimentation is related with the infill of some small troughs that were generating during the Permian-Triassic tectonic extension. That has resulted in some notable thickness differences, although they are largest in the more subsidence-prone Pyrenees Range.

Generally, these facies are one or more fining-upwards mega-sequences, starting with conglomerates, then sandstones and finally clay – claystone and occasionally evaporites as well. The sediments were deposited in a continental environment, such as braided river systems, that evolve upwards to flood

plains with marine influence when, finally, the sedimentary troughs are completely filled.

This Buntsandstein does not outcrop in the Ebro basin since the whole Mesozoic basement is covered by Cenozoic sediments. The closest outcrops are situated about 50 km southwards, on the Iberian Range, in the north flank of the Montalbán anticline structure, where two stratigraphic columns were studied in Peñarroyas and Torre de las Arcas. Inside the basin, however, some access points to the Buntsandstein formations are located in deep oil exploration boreholes, like Chiprana-1 (30 km east of the Lopín structure) and Ebro-2 (45 km northeast of the Lopín structure). The stratigraphic Triassic series was completely penetrated in Ebro-2, and partially in the Chiprana-1 borehole. From the literature, the total thickness of the Buntsandstein is quite variable, from 17 to 532 m. However, in Ebro-2 it is 135 m and in Chiprana-1 at least 90 m. Taking into account that the stratigraphic columns from outside the basin, Peñarroyas and Torre de las Arcas, show 118 m and 136 m of Buntsandstein, respectively, a good average should be around 127 m thick.

From PilotSTRATEGY Deliverable 2.7 Conceptual Geological Models (Wilkinson, 2023), a more detailed stratigraphy of the Lower and Middle Triassic is shown in

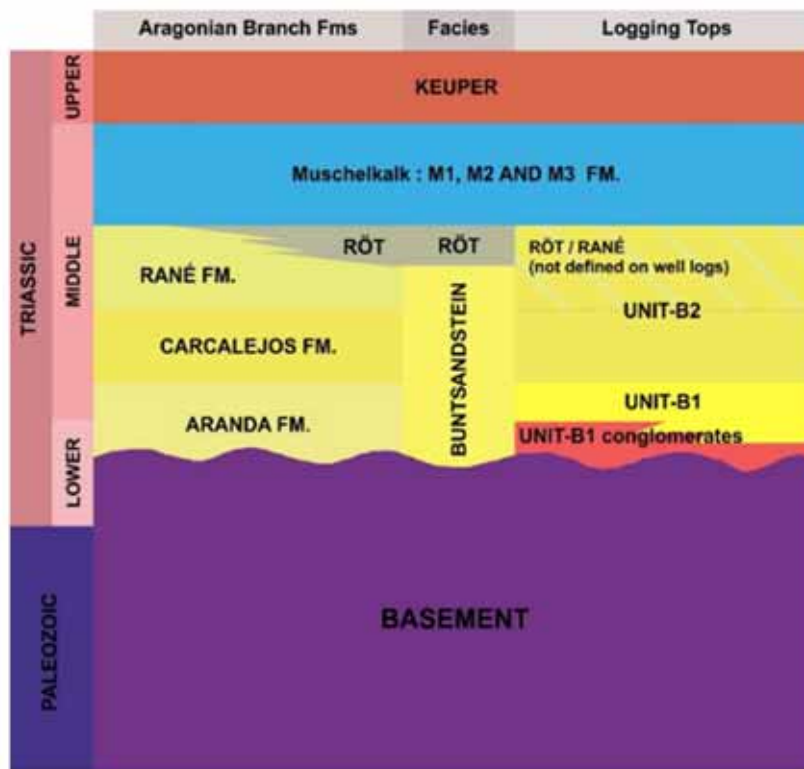


Figure 7-9. So, from bottom to top the Buntsandstein Facies is made up of the Aranda Formation (Lower Triassic) which is sandstone interbedded with thin (centimetre) shales, red and, occasionally, green (Díez et al., 2007). The overlying Carcalejós Formation (Anisian age - Díez et al., 2007) is alternating red sandstones and shales, and sometimes contains levels of microconglomerates. The Rané Formation (Anisian age - Díez et al., 2007) is alternating shales and fine-grained red sandstones. In borehole log analysis the Aranda Formation is unit B-1, unit B-2 corresponds to the Carcalejós Formation, as they are usually named in the oil and gas industry in this area (Aurell et al., 2001). The B-2 unit passes upwards gradually into Rané formation so no clear marker has been used to define this formation boundary. The estimated depth of Buntsandstein inside the Ebro basin ranges between 2,700 and 4,500 m.

With respect to the structural features, gravity modelling supports the interpretation of the Lopín structure as a succession of horsts and grabens where the faults that limit those structures only affect the Paleozoic basement, Buntsandstein and M1 of the Muschelkalk (Figure 7-10 and



Figure 7-11).

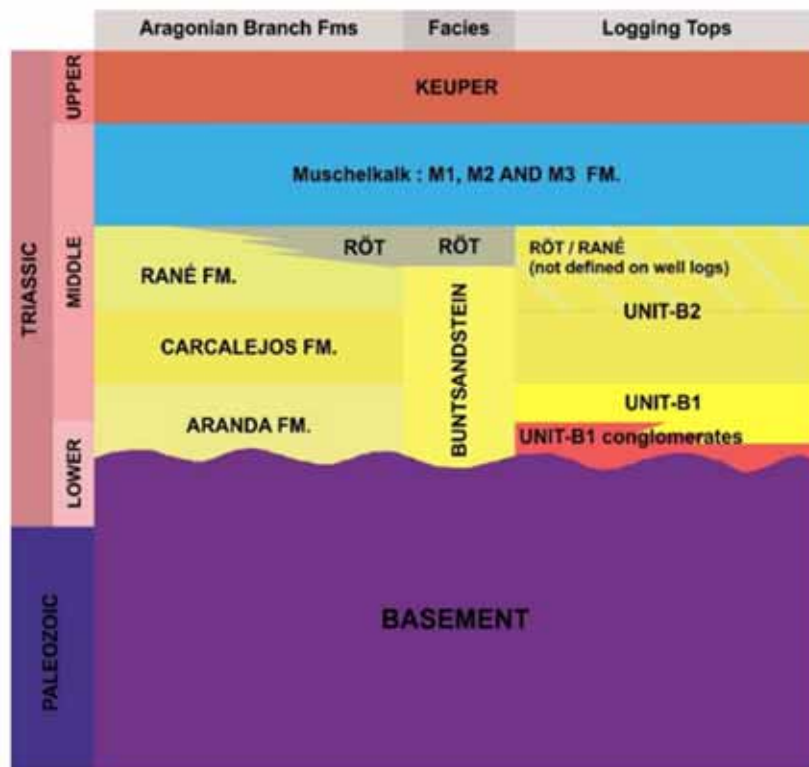


Figure 7-9. Correlation table between formations defined from outcrops in this area and in boreholes. Triassic Formations from Arche et al. (2004). From PilotSTRATEGY Deliverable 2.7 Conceptual Geological Models (Wilkinson, 2023).

No specific recharge areas of the Buntsandstein aquifer have been identified inside the Cenozoic Ebro basin. It is supposed to be hydraulically connected with Triassic outcrops in the Pyrenees, in the northern rim, and those located in the South rim, in the Iberian Range. No discharge zones are identified either, except one inferred from numerical simulations carried out during ALGECO2 project (IGME, 2010). In the surroundings of Lleida city, about 80 km to the East of the Lopín structure, one vertical ascending discharge zone was inferred.

The seal unit is the Rané Member (the top of the Rané Formation), the Röt facies (Formation Cálvena) and the Formation Trasobares (basal Muschelkalk Facies). They are mainly clays, marls and anhydrites. In Ebro-2 borehole they are 98 m thick, in Lopin-1 borehole they are just 5 m thick and in Chiprana-1 they are 63 m thick.

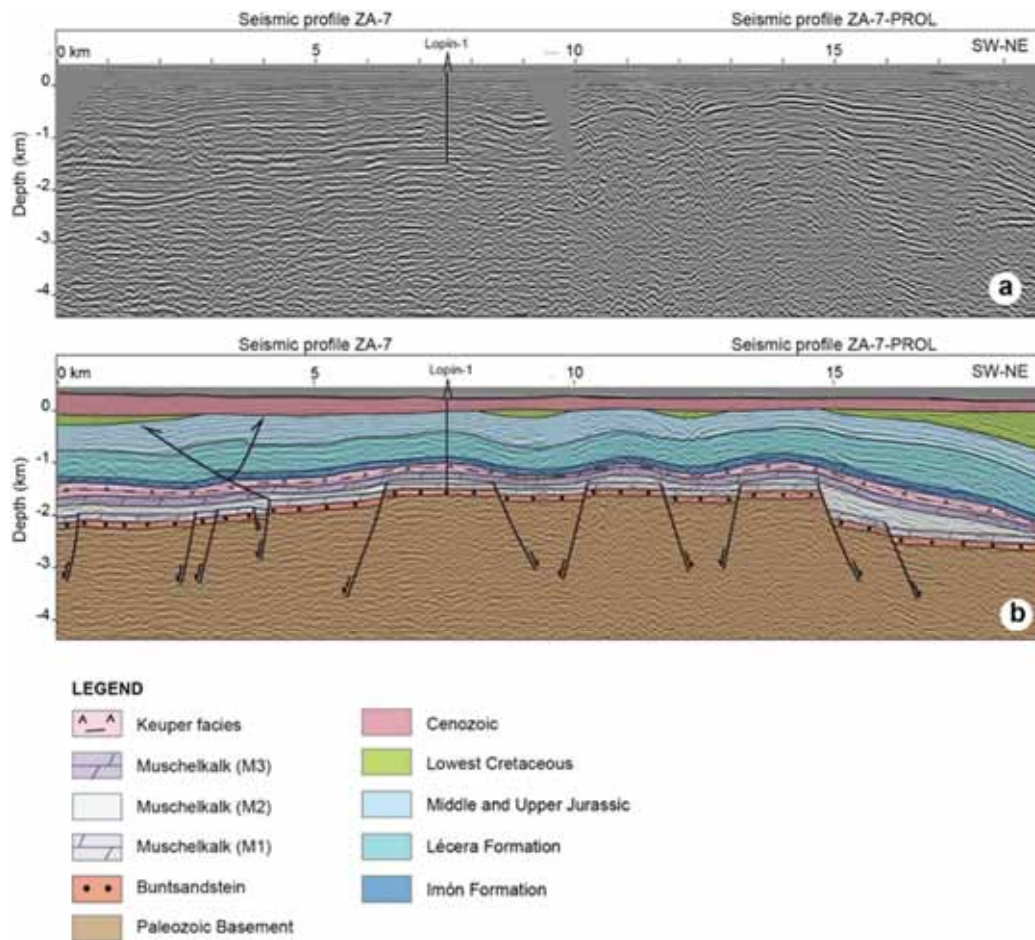


Figure 7-10. Initial geological cross section obtained from the interpretation of the seismic profile ZA-07. Deliverable 2.7 Geological Model (Wilkinson, 2023).

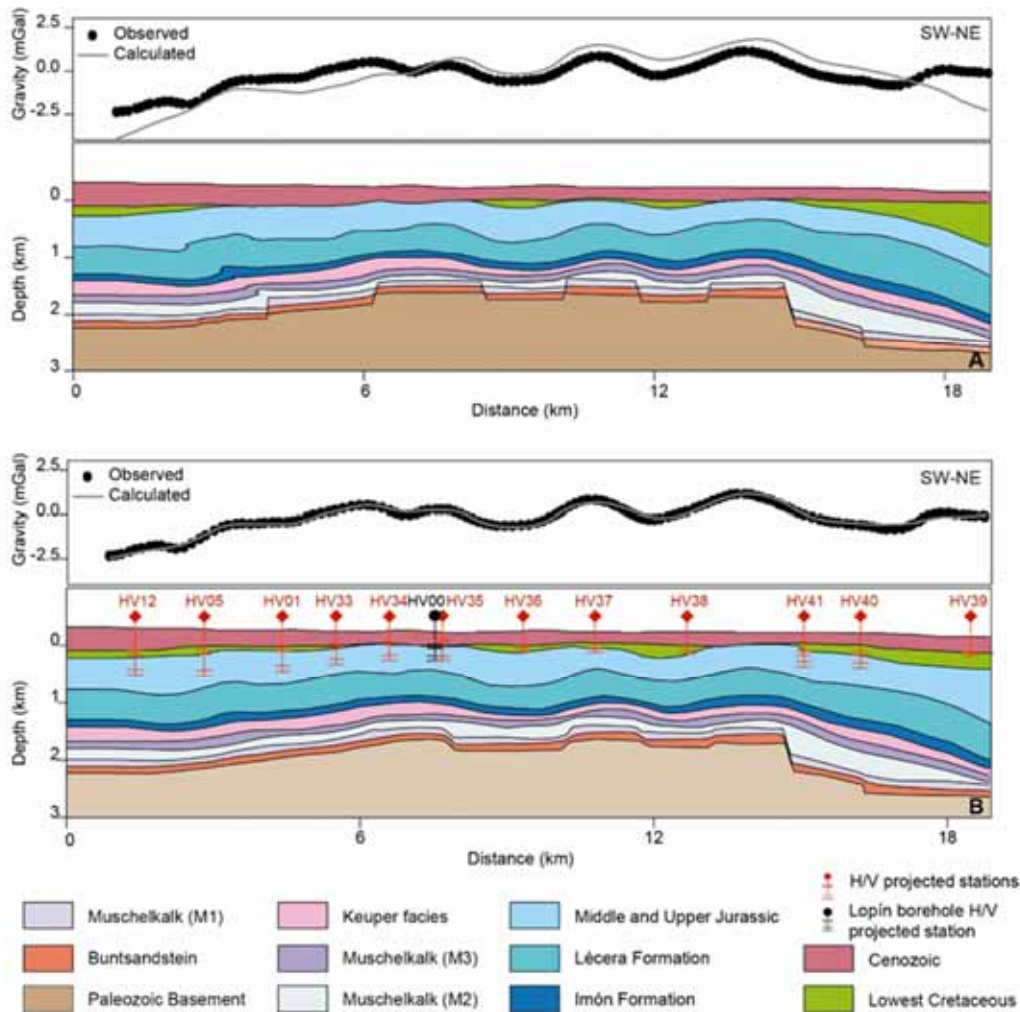


Figure 7-11. Initial geological cross section based on the interpretation of the depth-converted seismic profiles ZA-7 and ZA-7-PROL. Please note that the corresponding observed and calculated gravity anomalies do not match. (B) Gravity-consistent geological cross section taking into account the H/V data and petrophysical data (density data used in the model is displayed in the units' boxes). See figure 9-30 (A) in the Deliverable 2.7 Geological Model WP2 (Wilkinson, 2023).

7.2.1.2 Hydrogeological properties

The available data of petrophysical parameters were calculated from log records in boreholes (Marina Rueda, 2022) and from petrographic analyses of samples from exposures at Peñarroyas and Torre de las Arcas where stratigraphic columns were measured (Daniel Marcos, 2022).

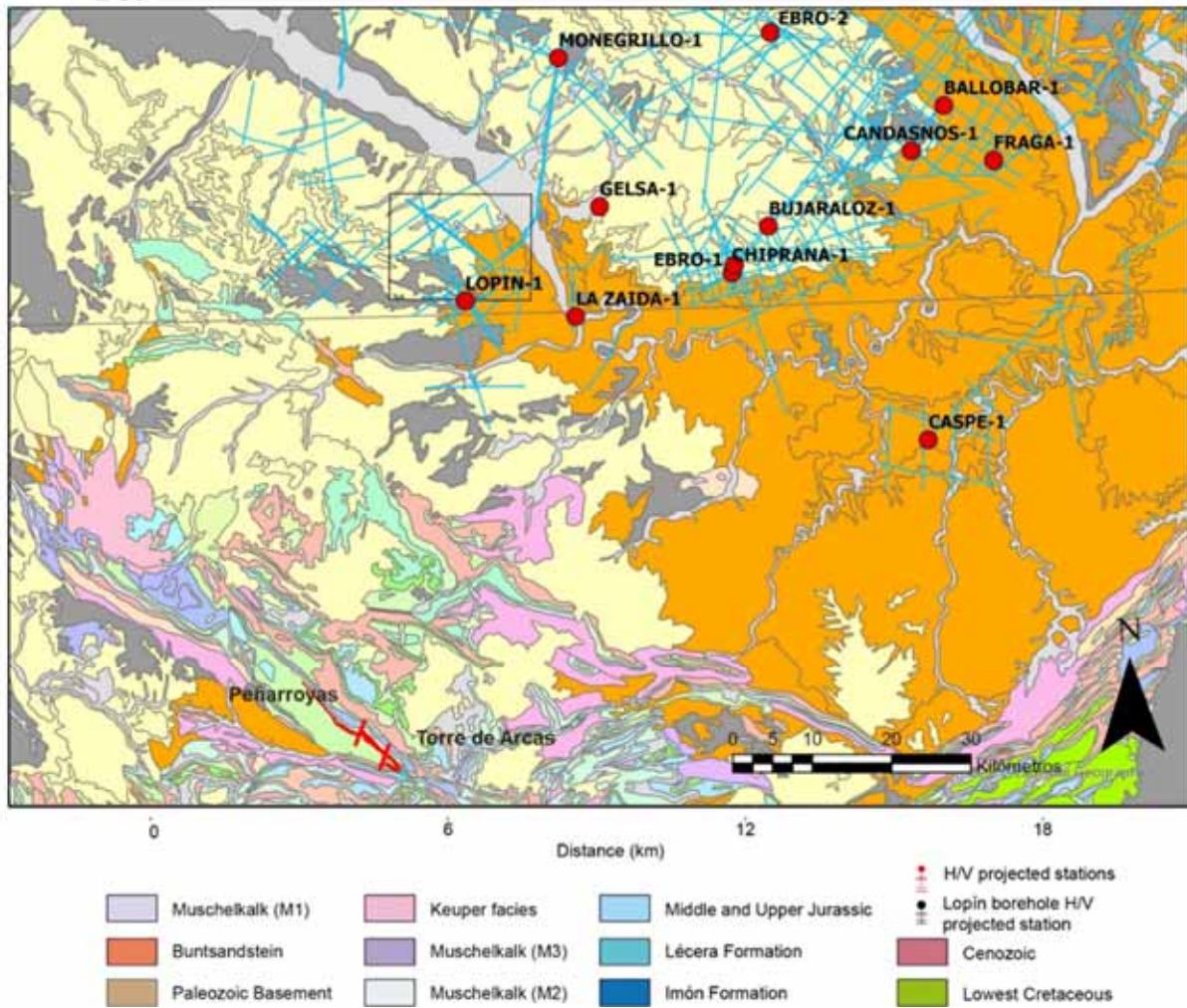


Figure 7-12. Location of the oil exploration boreholes, seismic lines and the location of the closest outcrops (Peñarroyas and Torre de Arcas). The Lopin structure is shown by the black rectangular outline.

Table 7-1. Coordinates of the oil exploration boreholes, and distance from Lopín-1 borehole.

Well	YUTM (m)	XUTM (m)	Z (m) KB	Distance from LOPÍN-1 (Km)
LOPÍN-1	4580522	702543	227.45	0
LA_ZAIDA_1	4578553	716464	165	14.06
MONEGRILLO-1	4611180	714284	378	32.83
CHIPRANA-1	4584099.7	736141	315	33.79
EBRO-1	4585150	736510	332.7	34.28
EBRO-2	4614391.1	740962.6	471	51.22
ZUERA-1	4633160	678138	354	58.02
CANDASNOS-1	4599395.6	758735.7	282.4	59.28
CASPE-1	4562906.7	760904.7	284.4	60.96
SARIÑENA-1	4630812.9	741839.3	354.15	63.82
BALLOBAR-1	4605165.6	762843.7	281	65.14
FRAGA-1	4598244	769125	301	68.9
MAYALS-1	4582376.5	796257.2	359.7	93.73

Preliminary data of mean volumes of shales (Vsh) and effective porosity (Marina Rueda, 2022) were made using available scanned paper copies of logs: Caliper (CALI), Spontaneous Potential (SP), Gamma Ray (GR), Induction (ILD), Dual Laterolog (LL), Microlaterolog (MLL), Microresistivity (Micronormal Resistivity MNOR & Microinverse Resistivity MINV), Density (RHOB), Neutron (NPHI), Sonic (DT). Data was processed with Techlog software. The calculated parameters are shown in Table 7-2 (Vsh) and

Table 7-3 (effective porosity).

Table 7-2. Mean volumes of shales (Vsh) of each geological unit in every borehole. Chiprana-1 does not include the values from the Tierga formation because the Gamma Ray log did not reach sufficient depth (Marina Rueda, 2022).

		Vsh (%)							
		EBRO-2	BALLOBAR-1	FRAGA-1	EBRO-1	CHIPRANA-1	LA ZAIDA-1	CASPE-1	
Fm Trasobares		11,2	17,8	31,7	33,1	34,9	28,2	31,4	
Fm Cálcena		76,7	86,3	85,7	68,9	58,7	81,1	66,9	
Fm. Tierga	Mb. Rané	67,1	87,0	85,6			76,0		
	Mb. Carcajeos	37,3	26,3	34,4	27,7		39,9	30,0	
	Mb. Aranda	Aranda 3	22,1	11,0	12,4	13,5		9,2	17,1
		Aranda 2	35,6	16,7	23,8	18,8		35,5	19,4
		Aranda 1	29,3	18,6	21,0	16,8		12,2	18,3

Table 7-3. Effective mean porosity (%) of each geological unit in every borehole. In grey boxes are shown the units whose mean porosity is lower. In yellow those with higher values. In borehole Chiprana-1, the porosities of the Tierga Formation were obtained by mean of Hg porosimetry (Marina Rueda, 2022).

		POROSIDAD (%)														
		EBRO-2		BALLOBAR-1		FRAGA-1		EBRO-1		CHIPRANA-1		LA ZAIDA-1		CASPE-1		
Fm. Tierga	Fm Trasobares	1,00		1,46		1,89		0,22	1,07	1,23	2,94	2,74		1,10	3,26	
	Fm Cálceña	0,75	1,56	1,09	1,59	1,69	1,42	1,30	1,07	3,73	2,94	1,62	1,71	4,63	3,26	
	Mb. Rané	2,77		2,51		0,67						1,19				
	Mb. Carcajejos	7,34		6,89		8,06		9,15		8,32		6,92		12,74		
	Mb. Aranda	Aranda 3	7,69	6,63	11,83	9,18	11,03	11,14	10,88	9,16	9,95	10,77	12,44	9,56	18,13	17,76
		Aranda 2	5,44		11,13		12,23		8,98		7,19		8,32		21,17	
		Aranda 1	3,52		8,58		13,11		5,98		17,51		9,44		18,46	

However, some later and more precise recalculations (see PilotSTRATEGY Deliverable 2.7. Conceptual Geological Models; Wilkinson, 2023) were made of volume of shales (Vsh) based on Gamma Ray logs with anomalies corrected for, and matched with spectral GR and Thorium content in Chiprana-1 cores (see Table 7-4).

Table 7-4. Vsh based on GR index and Th content in shales. Chiprana-1 core. PilotSTRATEGY Deliverable 2.7. Conceptual Geological Models (Wilkinson, 2023).

Chiprana-1 well	Vsh (GR index)	Vsh (Th) core
Average	56.92%	60.11%
Median	61.44%	60.95%
Standard Deviation	23.13%	22.52%
P10	26.56%	28.16%
P50	61.44%	60.95%
P90	84.18%	89.65%

To estimate porosity from the sonic logs (DT), two alternatives were considered (see PilotSTRATEGY Deliverable 2.7, Conceptual Geological Models), the so called Wyllie's equation and the RHG simplified equation (Raymer et al. 1980). In the Chiprana-1 well there was a chance to compare the DT curves with the porosity data taken from the core samples. The results are shown in Table 7-5.

Table 7-5. Porosity estimated by Willie equation, the RHG simplified equation and porosity in cores. Chiprana-1 well. From PilotSTRATEGY Deliverable 2.7. Conceptual Geological Models (Wilkinson, 2023).

Chiprana-1	Porosity Wyllie Sonic	Porosity RHG simplified Sonic	Porosity-cores
Average	10,03%	12.78%	9.32%
Median	8,59%	10.79%	9.11%
Standard Deviation	5,70%	9.10%	4.00%
P10	5,76%	8.21%	
P50	8,59%	10.79%	9.11%
P90	15,97%	17.37%	

Resistivity logs were also used to calculate porosities, using Archie equation (Archie, 1942), as well as Neutron Porosity (NPHI)/Bulk Density (RHOB) (see Deliverable 2.7. Geological Model WP2; Wilkinson

2023). The results in Ebro-1 well and the compared methods are shown in Table 7-6. Notice that the Sonic-RHG method gives higher porosity than the other methods, as with the Chirrana-1 well.

Table 7-6. Compared different porosity methods in Ebro-1 well. Deliverable 2.7. Geological Model WP2 (Wilkinson, 2023)

Ebro-1 Buntsandstein B1 Formation Porosity evaluation					
	Archie-Res	RHG-Sonic	Wyllie-Sonic	RHOB PHIE	PHIE NPFI/RHOB
median	11.29%	13.39%	11.47%	10.90%	11.05%
Average	11.75%	13.23%	11.35%	10.37%	10.77%
Stan Dev	0.02	0.02	0.03	0.04	0.03
P10	8.81%	10.98%	8.83%	5.51%	6.21%
p50	11.65%	13.39%	11.47%	10.90%	11.05%
p90	14.94%	15.70%	14.13%	14.92%	15.12%

As the Buntsandstein has been divided in three parts: base conglomerates, middle mainly clean sandstone sequences (B1) and shaly top formation (B2), calculations were made for those different sections.

7.2.1.2.1 Basal Conglomerates

Calculated properties of the Basal Conglomerates (Figure 7-13) are in Table 7-7 and Table 7-8. For methods, see PilotSTRATEGY Deliverable 2.7, Conceptual Geological Models.

Table 7-7. Volume of shale (Vsh) in Buntsandstein basal conglomerates calculated by different methods in well Ebro-1, Ebro-2, Caspe-1, Fraga-1 and Ballobar-1. For methods see PilotSTRATEGY Deliverable 2.7, Conceptual Geological Models (Wilkinson, 2023).

Buntsandstein Conglomerates	Vsh-N/D Ebro-1	Vsh-GRI Ebro-1	Vsh-N/D Ebro-2	Vsh-GRI Ebro-2	Vsh-GRI Caspe-1	Vsh-GRI Fraga-1	Vsh-GRI Ballobar-1
median	41.26%	13.61%	18.87%	19.10%	3.31%	5.42%	61.46%
Average	44.58%	16.51%	24.81%	24.80%	4.90%	7.58%	50.15%
Standard Deviation	0.26	0.14	0.20	0.16	0.09	0.07	0.23
P10	10.52%	4.39%	5.14%	10.27%	0.00%	1.10%	14.60%
p50	41.26%	13.61%	18.87%	19.10%	3.31%	5.42%	61.46%
p90	80.97%	28.99%	60.80%	56.24%	7.15%	20.33%	73.55%

Table 7-8. Porosity in Buntsandstein basal conglomerates calculated by different methods in well Ebro-1, Ebro-2, Caspe-1, Fraga-1 and Ballobar-1. From PilotSTRATEGY Deliverable 2.7, Conceptual Geological Models (Wilkinson, 2023).

Buntsandstein Conglomerates	PHIE-N/D Ebro-1	PHIE-N/D Ebro-2	Wyllie-DT Caspe-1	Wyllie-DT Fraga-1	Wyllie-DT Ballobar-1
median	5.23%	6.71%	9.41%	11.09%	2.98%
Average	5.35%	6.04%	10.18%	10.20%	2.67%
Standard Deviation	0.03	0.03	0.04	0.04	0.015
P10	1.35%	1.30%	6.04%	5.45%	0.00%
p50	5.23%	6.71%	9.41%	11.09%	2.98%
p90	9.09%	8.95%	15.80%	14.58%	4.40%

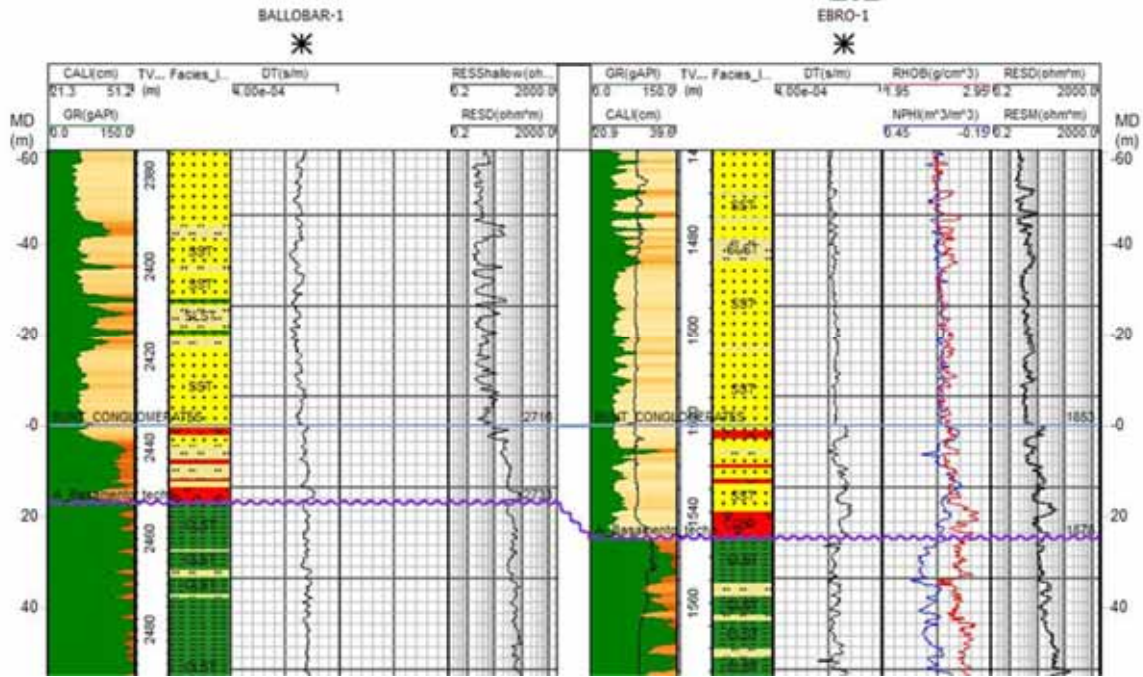


Figure 7-13. Example of logs response in the Buntsandstein basal conglomerate in wells Ballobar-1 and Ebro-1. From PilotSTRATEGY Deliverable 2.7. Conceptual Geological Models (Wilkinson, 2023).

7.2.1.2.2 Buntsandstein sandstones (B1)

This formation presents a quite homogeneous log signature; it is a thick sequence of sandstones with rare shale intercalations.

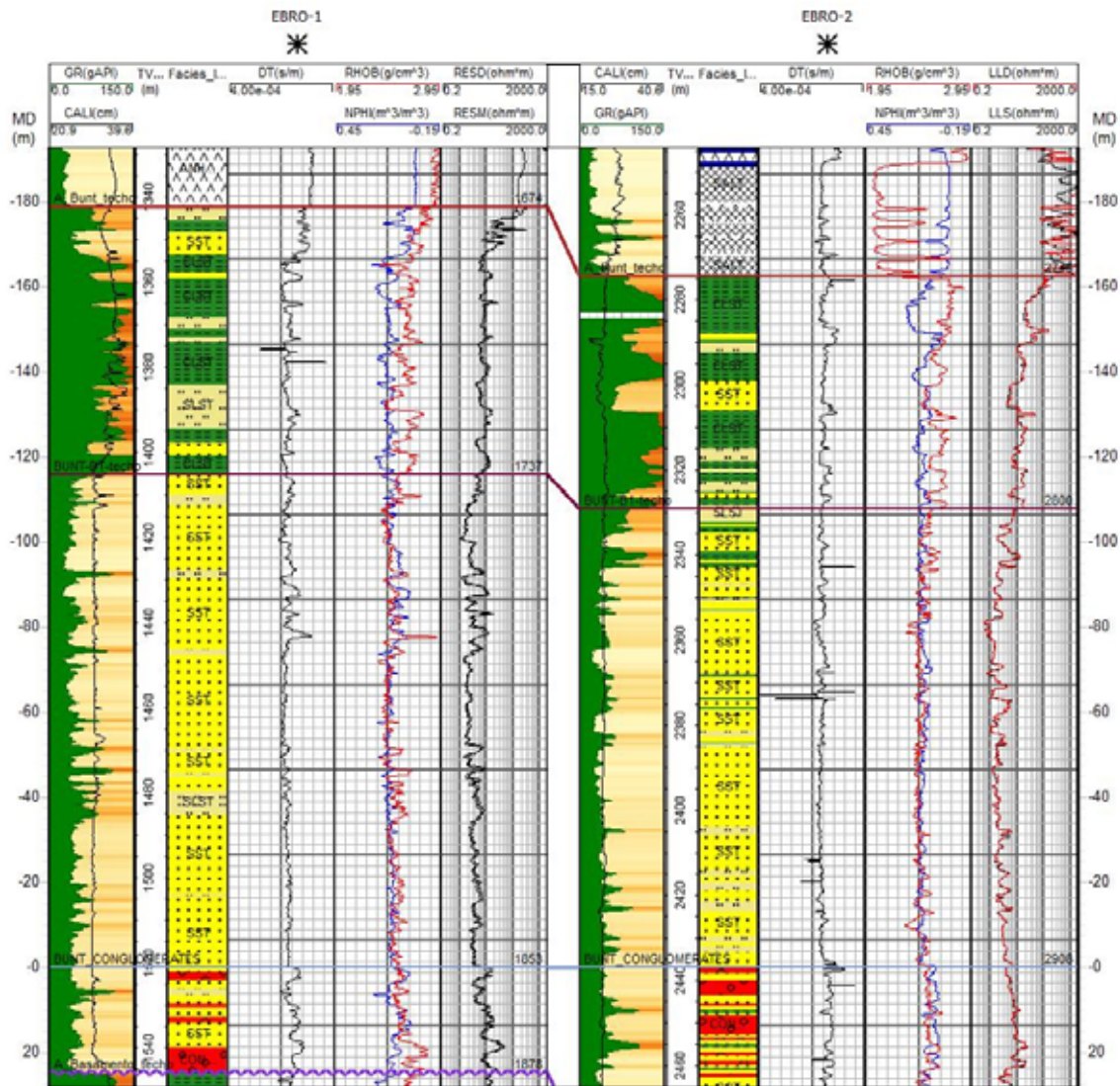


Figure 7-14. Ebro1 and Ebro-2 suite of wireline logs. Buntsandstein B1 formation appears to be fairly homogeneous. The top formation, B2, is much more argillaceous and presents some thick sandy intercalations. From PilotSTRATEGY Deliverable 2.7, Conceptual Geological Models (Wilkinson, 2023).

Table 7-9. Vsh in Buntsandstein B1 calculated by different method in well Ebro-1, Ebro-2, Caspe-1, Fraga-1 and Ballobar-1

Buntsandstein B1	Vsh-N/D Ebro-1	Vsh GRi Ebro-1	Vsh-N/D Ebro-2	Vsh GRi Ebro-2	Vsh GRi Caspe-1	Vsh GRi Fraga-1	Vsh GRi Ballobar-1
median	26.51%	11.06%	24.76%	12.90%	5.01%	9.79%	6.38%
Average	28.72%	15.02%	26.52%	16.45%	7.19%	15.33%	11.71%
Standard Deviation	0.15	0.14	0.14	0.13	0.09	0.17	0.16
P10	10.21%	1.31%	11.06%	5.57%	0.00%	0.00%	0.00%
P50	26.51%	11.06%	24.76%	12.90%	5.01%	9.79%	6.38%
P90	48.51%	33.14%	43.57%	31.18%	15.82%	40.15%	32.77%

Table 7-10. Porosity in Buntsandstein B1 calculated by different method in well Ebro-1, Ebro-2, Caspe-1, Fraga-1 and Ballobar-1.

Buntsandstein B1	PHIE-N/D Ebro-1	PHIE-N/D Ebro-2	Wyllie-DT Caspe-1	Wyllie-DT Fraga-1	Wyllie-DT Ballobar-1
median	10.93%	11.87%	22.75%	16.78%	10.22%
Average	10.69%	11.23%	22.37%	15.90%	9.76%
Standard Deviation	0.03	0.03	0.03	0.032	0.03
P10	6.08%	7.21%	18.73%	12.46%	5.15%
P50	10.93%	11.87%	22.75%	16.78%	10.22%
P90	14.90%	14.09%	25.74%	18.79%	13.52%

7.2.1.2.3 Buntsandstein Sandstones and Shales (B2)

This formation overlays the main reservoir and it is considered to be, so far, a primary seal. It is a very argillaceous formation with some interbedded sandstones. These sandy levels could be porous but the Net to Gross ratio of this formation is very low in general. The Table 7-11 Table 7-10 and Table 7-12 show the Vsh and the calculated porosities in the very argillaceous sandstones.

Table 7-11. Vsh in Buntsandstein B2 calculated by different method in well Ebro-1, Ebro-2, Caspe-1, Fraga-1 and Ballobar-1.

Buntsandstein B2	Vsh N/D Ebro-1	Vsh GRi Ebro-1	Vsh N/D Ebro-2	Vsh GRi Ebro-2	Vsh GRi Caspe-1	Vsh GRi Fraga-1	Vsh GRi Ballobar-1
median	61.23%	71.43%	73.20%	75.09%	69.09%	81.36%	92.04%
Average	61.44%	66.86%	69.79%	68.79%	60.33%	72.37%	81.87%
Standard Deviation	0.21	0.27	0.27	0.27	0.32	0.25	0.22
P10	33.31%	30.81%	32.78%	31.32%	11.56%	34.01%	47.66%
p50	61.23%	71.43%	73.20%	75.09%	69.09%	81.36%	92.04%
p90	92.38%	100.00%	100.00%	100.00%	89.30%	100.00%	100.00%

Table 7-12. Porosity in Buntsandstein B2 calculated by different method in well Ebro-1, Ebro-2, Caspe-1, Fraga-1 and Ballobar-1.

Buntsandstein B2	PHIE-N/D Ebro-1	PHIE-N/D Ebro-2	Wyllie-DT Caspe-1	Wyllie-DT Fraga-1	Wyllie-DT Ballobar-1
median	5.78%	7.08%	19.33%	9.28%	0.81%
Average	5.84%	6.24%	19.62%	10.24%	2.74%
Standard Deviation	0.04	0.03	0.06	0.06	0.04
P10	0.30%	1.19%	12.99%	2.23%	0.02%
p50	5.78%	7.08%	19.33%	9.28%	0.81%
p90	11.29%	9.71%	26.27%	19.36%	10.78%

Independently of the log data, porosity has also been estimated from surface samples, collected in two stratigraphic sections, Peñarroyas and Torre de las Arcas, situated 50 km southwards of Lopín structure, in the Iberian Range, on the north flank of the Montalbán anticline structure (see location in

Figure 7-11). Table 7-13 and

Table 7-15. Point-counted porosity of Buntsandstein samples from the Torre de las Arcas exposures (Daniel Marcos, 2022).
show the results.



Table 7-14. Point-counted porosity of Buntsandstein samples from the Peñarroyas exposures (Daniel Marcos, 2022).

Peñarroyas				
Position (m)	Samples	Facies	Grain size	Porosity (%)
68	PS-P 5	St	fine	11.16
46	PS-P 4	St		12.46
37	PS-P 3	Sp		9.65
12	PS-P 2	Sp		9.65
2	PS-P 1	Sp		8.99

Table 7-15. Point-counted porosity of Buntsandstein samples from the Torre de las Arcas exposures (Daniel Marcos, 2022).

Torre de las Arcas				
Position (m)	Samples	Facies	Grain size	Porosity (%)
46	PS-TA 5	St	fine	15.6
39	PS-TA 4	Sp		7.9
31	PS-TA 3	Sp		10.8
12	PS-TA 2	Sp	medium	10.8
11	PS-TA 1	St		13.48

7.2.1.3 Hydraulic pressure mapping

The conceptual hydrogeological map (Figure 7-6) of the Triassic system was built from data in oil exploration boreholes reports. Those data were also used to build a numerical groundwater flow model ALGECO2 (IGME, 2010) using the code Feflow 5.4, (Diersch, H.J. F., 2005). Here, recharge areas were located in the surrounding Triassic outcrops, and an upwards discharge zone was predicted in the proximity of Lleida city. Although it is not a hydraulic pressure map *sensu stricto*, it is an approach to the conceptual flow scheme.

As a first approach to evaluate the reservoir pressure, well reports have been studied. The Drill String Tests (DST's) have proven to be very useful since they provide reservoir fluid temperatures and, usually a reservoir pressure measurement. Other data used are the mud weights used during drilling operations and the reported mud losses or gains while drilling, as well as any gas peaks. Unfortunately, these latter data give only a minimum pressure. The results are shown in Table 7-16.

Table 7-16. Buntsandstein formation pressure obtained in wells Monegrillo-1, Chiprana-1 and Ebro-1. (1) - from mud density data. See Deliverable 2.7. PilotSTRATEGY Conceptual Geological Models (Wilkinson, 2023)

Wells	Distance from Lopín	Equivalent fluid density gradient at Buntsandstein	Formation Pressure at Buntsandstein	Top Buntsandstein
MONEGRILLO-1	32.83 Km	1.26 g/cm ³	162 bar	909m SS
CHIPRANA-1	33.79 Km	1.25 g/cm ³	217 bar	1392m SS
EBRO-1	34.28 Km	1.22 g/cm ³ (1)	205 bar (1)	1341m SS

7.2.1.4 Features of the pristine fluid

Salinity of the fluids during the drilling operations was calculated from the electrical resistivity logs

$$\text{TDS [mg/L]} = k_e \times \text{EC [\mu S/cm]}$$

where:

EC – Electrical conductivity of the water at 25 °C; and

k_e – Multiplier or conversion factor.

The value of k_e increases along with the increase of ions in water. It ranges from 0.5 to 0.8, but usually, 0.67 is used.

Using this procedure, the obtained results are shown in Table 7-17.

Table 7-17. Salinity (TDS) obtained in Ebro-1, Monegrillo-1 and Caspe-1 wells.

WELLS	Resistivity (Ohm*m) 25°C	Conductivity (S*m) 25°C	Ke	TDS (mg/L)	Formation
EBRO-1	0.04094475	24.42315569	0.67	163635.1431	Bunt.
MONTEGRILLO-1	0.064535168	15.49542717	0.67	103819.362	Bunt.
CASPE-1	0.171249602	5.839429644	0.67	39124.178	Bunt.

With respect to the composition of fluids in the Buntsandstein formation, only Monegrillo-1, Sariñena-1 and Ebro-2 have any representative samples and physio-chemical parameters (Table 7-18).

Table 7-18. Some physical-chemical parameters obtained in, Monegrillo-1, Sariñena-1 and Ebro-2 wells.

BOREHOLE	Interval (m)	Cl ⁻ (ppm)	Ca ²⁺ (ppm)	pH	Density (g/cm ³)	T (°C)	Formation
MONTEGRILLO-1	1290-1308	77,000					Bunt.
SARIÑENA-1	2874.8-2893.2	249,000					Bunt.
EBRO-2	2871-2950	274,520	4000	6.5	1.2	85	Bunt.

Wells reports and log header data have been used to estimate downhole temperatures (See Deliverable 2.7. Geological Model WP2; Wilkinson, 2023). The temperatures recorded in the wells, probable maximum temperatures and temperature gradients are shown in

Table 7-19 and Table 7-20.



Table 7-19. Formation temperatures in different wells.

WELLS	Thermometer depth SS	Measured Temp.	Assumed HORNER-PLOT Temp	Geological Formation
Max rec temp Ebro02-DST01	793.00	92.22	92.22 (*)	Above Keuper
Max rec temp Ebro02-DST02	1623.00	72.22	72.22	M3
Max rec temp Ebro02-DST03	2400.00	85.00	85.00	M2
Max rec temp Ebro02-WL01	1343.00	65.55	71.81	KEUPER
Max rec temp Ebro02-WL02	1332.00	68.33	71.81	KEUPER
Max rec temp Ebro01-WL01	232.00	34.00	37.70	TERTIARY
Max rec temp Ebro01-WL02	1147.00	55.00	61.57	M3
Max rec temp Ebro01-WL03	1634.00	68.00	74.57	PALEOZOIC
Max rec temp Lopín01-WL01	1398.20	56.70	61.91	BUNT
Max rec temp CASPE01-WL01	1524.60	55.55	64.46	PALEOZOIC
Max rec temp MAYALS01-WL01	1041.30	58.33	64.90	??
Max rec temp MONEGRILLO01-WL01	762.00	56.00	59.70	Above Keuper
Max rec temp CADASNOS1-DST1	970.60	59.00	59.00	Above Keuper
Max rec temp CADASNOS1-DST2	1240.60	70.00	70.00	Above Keuper
Max rec temp CADASNOS1-WL01	1277.60	63.00	69.57	KEUPER
Max rec temp SARIÑENA1-WL01	1695.85	70.00	76.57	KEUPER
temp CHIPRIANA-1 DST	566.00	60.00	60.00	Above Keuper
temp CHIPRIANA-1 DST	594.90	53.00	53.00	Above Keuper
temp CHIPRIANA-1 DST	1257.20	60.00	60.00	M2
temp CHIPRIANA-1 DST	1310.70	65.00	65.00	M1
temp CHIPRIANA-1 DST	1331.50	68.30	68.30	M1
temp CHIPRIANA-1 DST	1351.20	67.70	67.70	M1
temp CHIPRIANA-1 DST	1382.80	75.55	75.55	M1
temp CHIPRIANA-1 DST	1440.70	70.00	70.00	BUNT
temp CHIPRIANA-1 DST	1457.20	68.30	68.30	BUNT
temp CHIPRIANA-1 DST	1471.20	70.00	70.00	BUNT

(*) Most likely wrong data

Table 7-20. Temperature gradients

Gradient EBRO-2	31.6	Celsius/km
Gradient EBRO-1	30.5	Celsius/km
Gradient LOPÍN-1	29.2	Celsius/km
Gradient CASPE-1	27.6	Celsius/km
Gradient MAYALS-1	36.0	Celsius/km
Gradient MONEGRILLO-1	40.4	Celsius/km
Gradient CADASNOS-1	36.5	Celsius/km
Gradient SARIÑENA-1	30.3	Celsius/km
Gradient CHIPRIANA-1	31.1	Celsius/km

7.2.1.5 Occurrence of faults

Overall, gravity modelling supports the interpretation of the Lopín structure as a succession of horsts and grabens where the normal faults that limit those structures only affect the Paleozoic basement, the Buntsandstein reservoir and unit M1 of the Muschelkalk (Figure 7-15). No faults are identified passing through the overall Triassic seal unit (Keuper), as shows the geological model. No connection with the surface is known either.

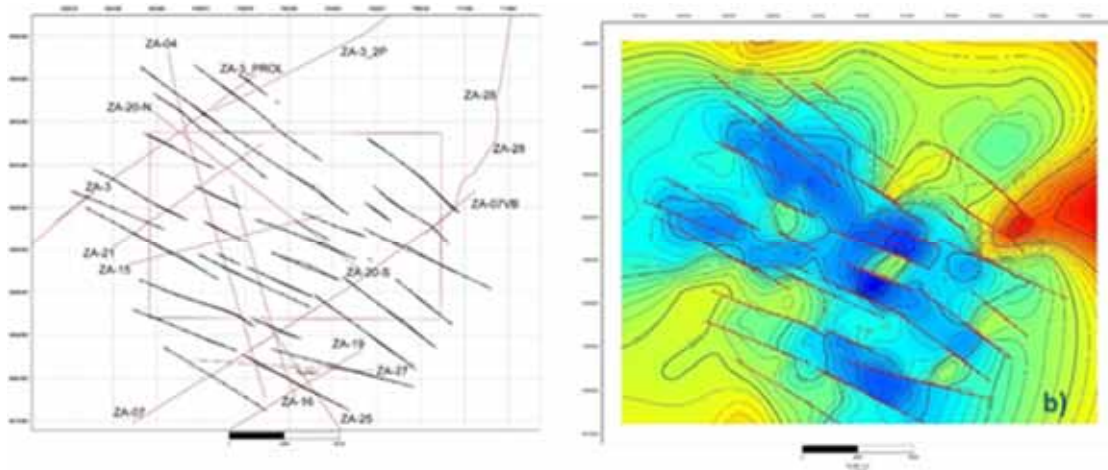


Figure 7-15. (a) Map showing the orientation of interpreted normal faults (black lines) and the location of interpreted seismic lines (red lines). The red square shows the study area. (b) Isobath map of the top of the Buntsandstein facies. From PilotSTRATEGY Deliverable 2.7, Conceptual Geological Models (Wilkinson, 2023).

7.2.1.6 Societal uses of the formation

The target unit is not used for water supply in the area. No geothermal uses are known either. It may be observed in Figure 7-16 and

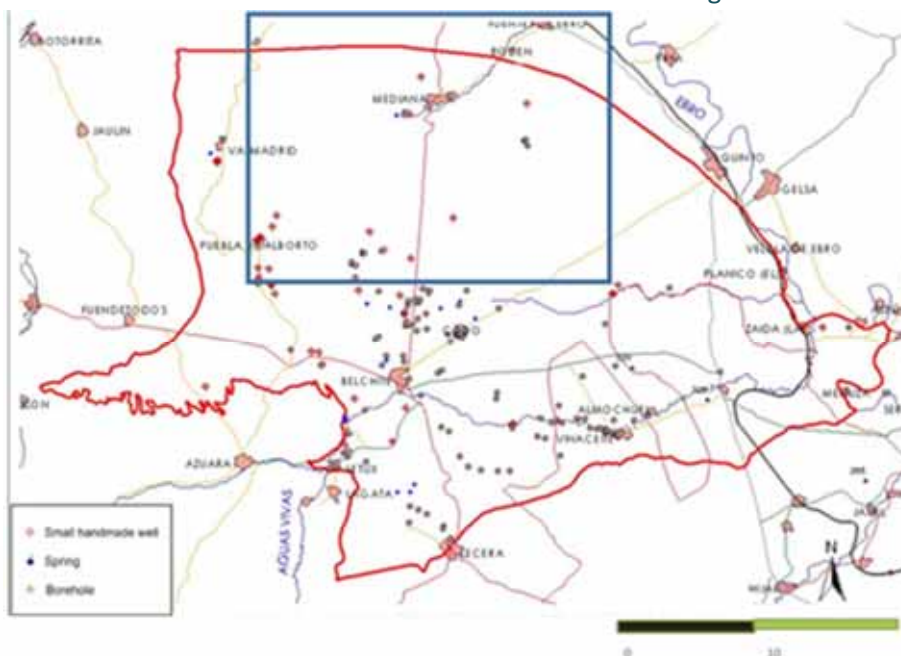


Figure 7-17, that groundwater uses are very scarce in the area. Exploitation is restricted almost exclusively to the Jurassic regional aquifer, because Cenozoic aquifers have very limited resources and

poor

hydraulic



characteristics (see 7.4 section).
resources are also available from the Ebro River.

Surface

Figure 7-16. Water uses in the studied area (blue rectangle), in Campo de Belchite groundwater mass ES091079. Most of them correspond with boreholes that exploit the Jurassic regional aquifer and handmade shallow wells that exploit the Cenozoic aquifer. None of them exploits the deep Triassic system. IGME-DGA (2009).

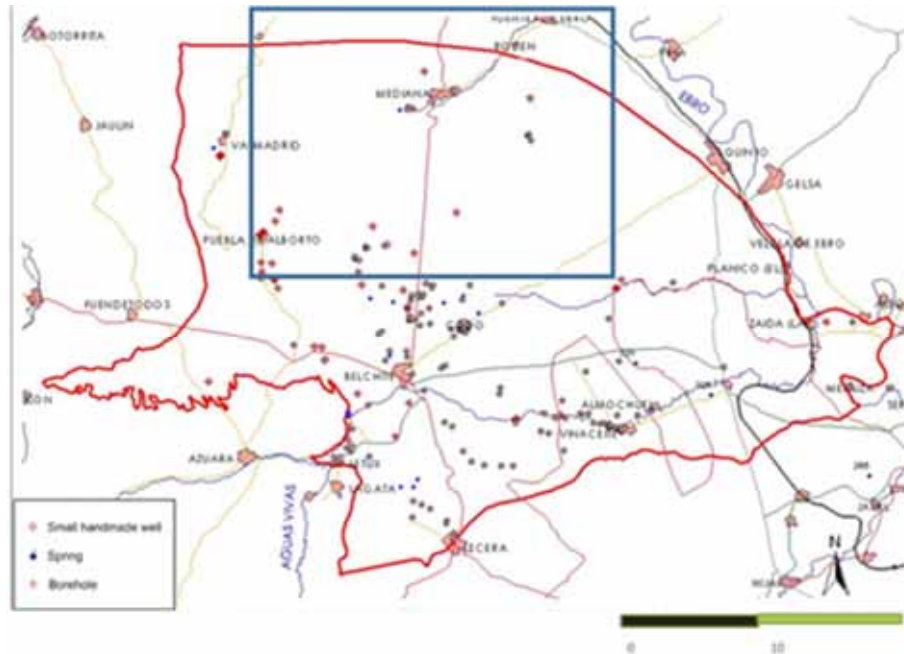


Figure 7-17. Groundwater installations. The studied area is the blue rectangle. Most of them are located inside Campo de Belchite groundwater mass ES091079. Boreholes utilise the Jurassic regional aquifer. Handmade shallow wells utilise the Cenozoic aquifer. None of them uses the deep Triassic system. IGME-DGA (2009).

7.2.2 Muschelkalk M1 formation

7.2.2.1 Geological features of the formation

The Muschelkalk M1 is the lowest carbonate unit of the Triassic Muschelkalk facies, also known as Muschelkalk I (M1). The age of this formation is Anisien (middle Triassic). It is dolomitic with some intercalations of anhydrites or salts, and/or marls/limestones, and with a thickness of 11 to 105 meters. M1 is affected by the same structures and deformational style as the target Buntsandstein unit. It is overlain by a seal of clays and anhydrites known as Muschelkalk II (M2), also Anisien in age, whose thickness ranges from 17 to 323 m. Both M1 and M2, are present in the Ebro basin at depths from 590 (borehole Caspe-1) to 3,250 m.

M1 and M2 form a part of the deep hydrogeological Triassic system. There is the same lack of hydrogeological data as with the Buntsandstein aquifer, since they do not outcrop inside the basin and no known useage of these units either. So, the same conceptual model can be applied to the M1 as the Buntsandstein. It means that the recharge areas are supposed to be those in the northern (Pyrenees), southern (Iberian range) and eastern (Coastal-Catalonian range) rims, where the Muschelkalk formations outcrop. Hence the closest recharge areas to the PilotSTRATEGY study area are located 50 km south, in the Iberian Range, in the north flank of the Montalbán anticline structure. The

groundwater flow map of the Triassic hydrogeological system, obtained by means of a numerical model developed during the project ALGECO2 (IGME, 2010) is presented in Figure 7-6.

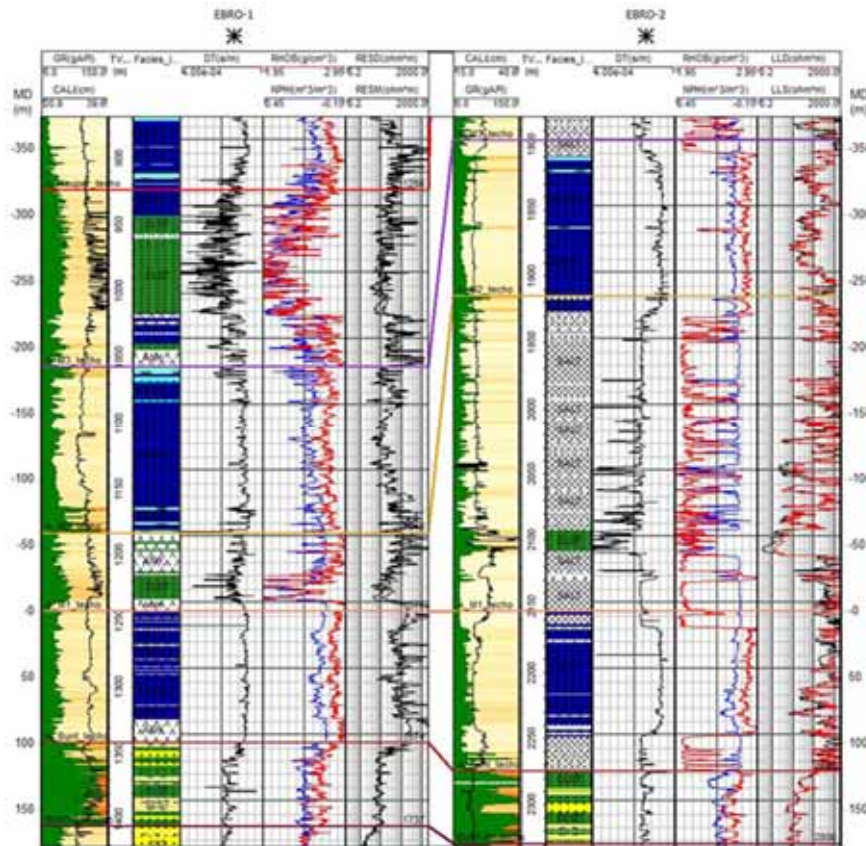


Figure 7-18. Muschelkalk in the Ebro-1 and Ebro-2 wells, M1 and M3 are dolomitic in general with some caved zones, M2 is clearly an evaporitic level that presents big thickness variations. PilotStrategy Deliverable 2.7. Geological Model WP2 (Wilkinson, 2023).

7.2.2.2 Hydrogeological properties

The Table 7-21 summarises calculated porosity for the M1 formation in the Ebro-1 well.

Table 7-21. Calculated porosity of M1 in the Ebro-1 well, from borehole logs (for methods see PilotStrategy Deliverable 2.7 Conceptual Geological Models; Wilkinson, 2023). DT = sonic log; RHOB = bulk density log

	DT-Wyllie (Dolomite)	RHOB (Dolomite)
median	3.88%	2.21%
Average	4.12%	2.42%
S-Deviation	0.0295	0.0172
P10	2.52%	0.29%
p50	3.88%	2.21%
p90	6.02%	4.99%

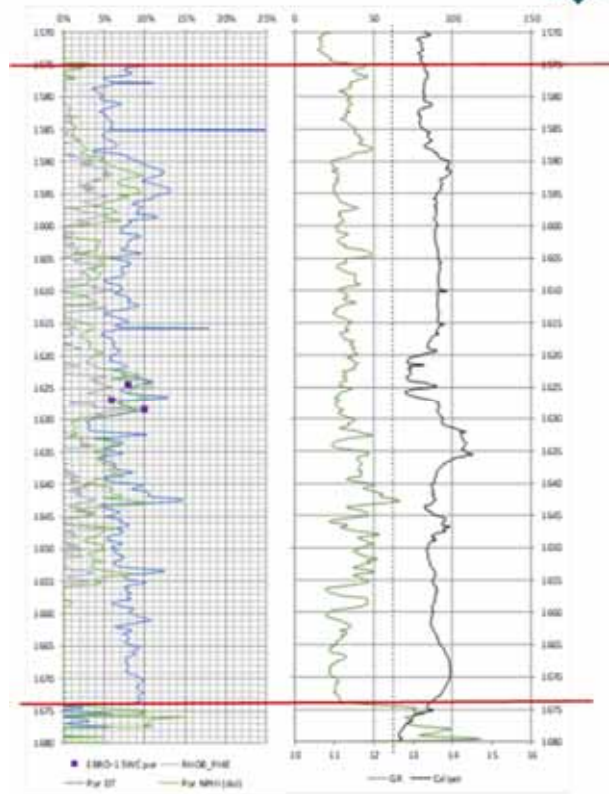


Figure 7-19. Dolomites porosities in the Ebro-1 well with sonic transit time (DT), neutron porosity (NPHI, corrected to dolomite porosity) and bulk density (RHOB) curves. On the right hand are gamma ray (GR) and caliper data, the bit diameter in this well section is 12.5 inches (dash line). Three points in the left-hand chart are the porosities of 3 side wall core samples that were reported in Ebro-1 Final Report and correspond with the top of M1. From PilotStrategy Deliverable 2.7. Conceptual Geological Models (Wilkinson, 2023).

7.2.2.3 Features of the pristine fluid

No salinity data for M1 are available, but general salinity for the whole Muschelkalk set was calculated by means of the logs (spontaneous potential, SP and from drill string tests, DST). Table 7-22 shows calculated data in five wells.

Table 7-22. Salinity of the whole Muschelkalk interval calculated from log data. SP = spontaneous potential, DST = drill string test

BOREHOLE	Interval (m)	LOG	Salinity (ppm)
EBRO-1	Muschelkalk	SP	104,154
MONEGRILLO-1	Muschelkalk	SP	90,902
MONEGRILLO-1	Muschelkalk	DST	76,000
SARIÑENA-1	Muschelkalk	DST	237,000
CASPE-1	Muschelkalk	SP	90,902
EBRO-2	Muschelkalk	DST	200770

No composition data for fluids is available for the M1 porewaters. The known temperatures from boreholes are listed in Table 7-23.

Table 7-23. M1 temperature measured in Chiprana-1 well.

BOREHOLE	Interval (m)	T (°C) Measured	Gradient °C/km	Formation
CHIPRANA-1	1646.50	65.0	31.1	M1
CHIPRANA-1	1666.20	68.3	31.1	M1
CHIPRANA-1	1697.80	75.55	31.1	M1

7.2.2.4 Occurrence of faults

On the overall, gravity modelling supports the interpretation of the Lopín structure as a succession of horsts and grabens where the normal faults that limit those structures only affect the Paleozoic basement, Buntsandstein and M1. Figure 7-20 and Figure 7-21 show fractures affecting the top of M1 and M2 formations, note that there are less mapped faults at the M2 level. However, none of these faults are identified as passing through the Keuper formation, as it will be seen later. No connection with the surface is known either.

7.2.2.5 Societal uses of the formation

M1 unit is not utilised for water supply in the area. Notice in Figure 7-16 and

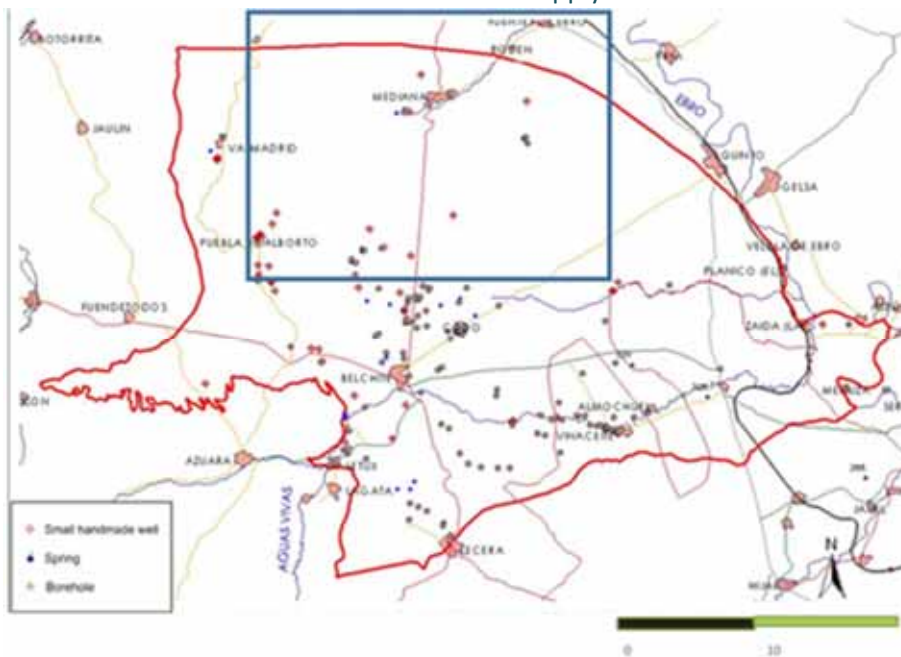


Figure 7-17 that groundwater wells are scarce in the area and there are no boreholes that exploit the Triassic system. Exploitation is restricted almost exclusively to the Jurassic regional aquifer. There is also availability of surface resources from the Ebro River. No geothermal uses are known either.

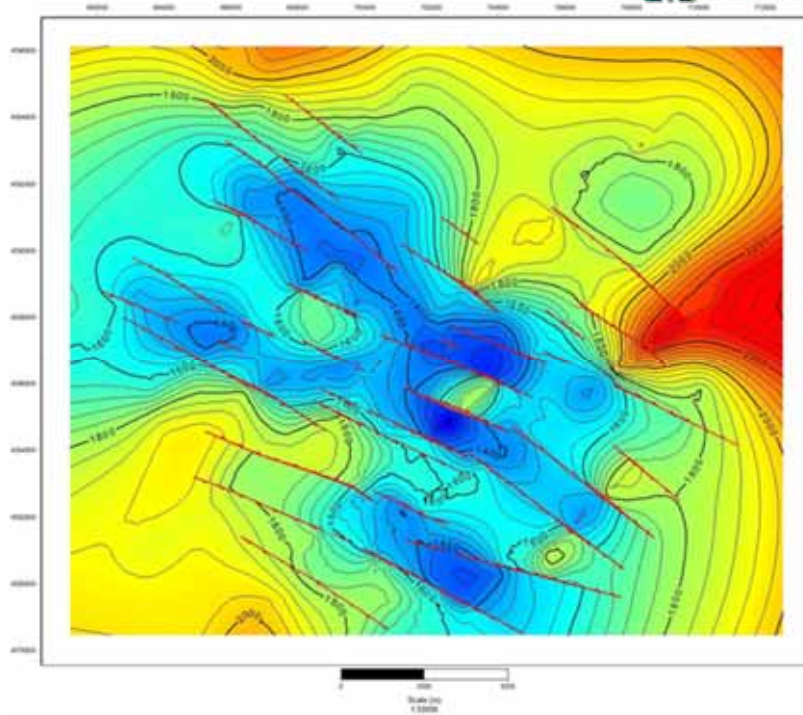


Figure 7-20. Isobath map of the top of the M1 facies. From PilotStrategy Deliverable 2.7. Conceptual Geological Models (Wilkinson, 2023).

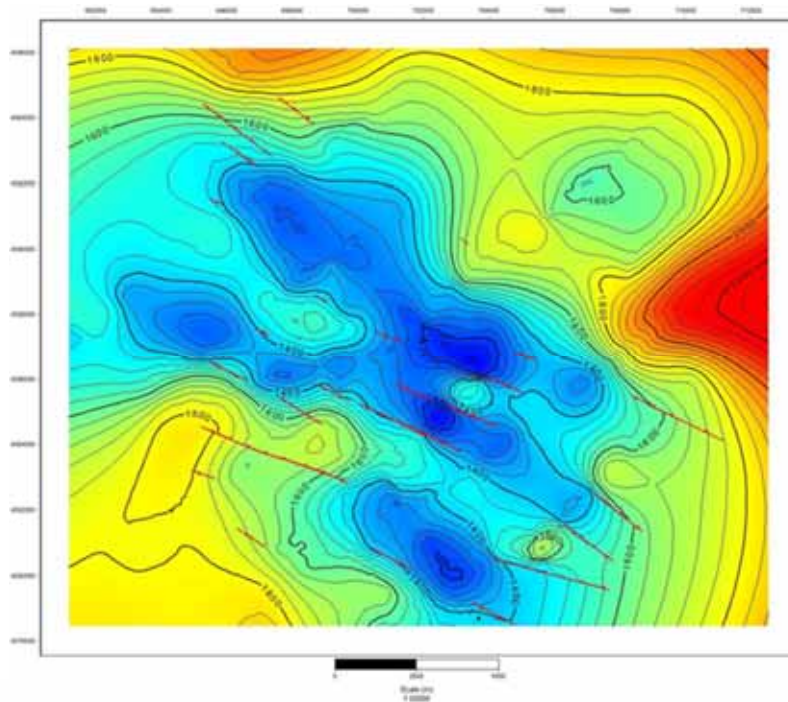


Figure 7-21. Isobath map of the top of the M2 facies. From PilotStrategy Deliverable 2.7. Conceptual Geological Models (Wilkinson, 2023).

7.2.3 Muschelkalk M3 formation

7.2.3.1 Geological features of the formation

Muschelkalk M3 is the top carbonate unit of the Triassic Muschelkalk facies, also known as Muschelkalk III (M3). The age of this formation is Ladinian (middle Triassic). It is dolomitic with some intercalations of anhydrites or salts, and/or marls/limestones with a thickness ranging from 45 to 200 meters.

M3 is affected by the same structures and deformational style as the target Buntsandstein unit. On top, there is a seal of the evaporates and clays of the Keuper facies, whose thickness ranges from 15 to 895 m. M3 is present in the Ebro basin at depths from 425 (borehole Caspe-1) to 4,880 meters.

M1 and M3 form a part of the deep hydrogeological Triassic system, as above, with the same lack of hydrogeological knowledge as the Buntsandstein aquifer, because it does not outcrop inside the basin and there no known use either. Hence, the same conceptual scheme may be applied to the M3 as M1 and the Buntsandstein. The recharge areas are supposed to be those in the northern (Pyrenees), southern (Iberian range) and eastern (Coastal-Catalonian range) rims, where the Muschelkalk formations outcrop. The closest recharge areas are located 50 km south, in the Iberian Range, in the north flank of the Montalbán anticline structure.

7.2.3.2 Hydrogeological properties

Table 7-24 summarises the porosities calculated for M3 formations in the Ebro-1 well.

Table 7-24. Calculated porosity of M3 in the Ebro-1 well, from borehole logs (for methods see PilotStrategy Deliverable 2.7. Geological Model WP2; Wilkinson, 2023). DT = sonic log; RHOB = bulk density log.

	DT-Wyllie (Dolomite)	RHOB (Dolomite)
median	5.83%	5.91%
Average	6.21%	6.04%
S-Deviation	0.0310	0.0393
P10	3.14%	0.87%
p50	5.83%	5.91%
p90	9.76%	10.33%

Groundwater flow map of the Triassic hydrogeological system, obtained by means of a numerical model developed during the project ALGECO2 (IGME, 2010) is presented in Figure 7-6.

7.2.3.3 Features of the pristine fluid

No specific data of the salinity of the porewaters in M3 are available, but general salinity for the whole Muschelkalk set was calculated by means of the spontaneous potential borehole logs and from drill stem tests), see Table 7-22.

The composition and temperature of fluids was obtained for M3 from samples in two boreholes (Table 7-25). Temperature of fluids was measured in situ in wells Ebro-1 and Ebro-2 (Table 7-26).

Table 7-25. Composition of M3 fluids obtained in samples from boreholes Sariñena-1 and Ebro-2

BOREHOLE	Interval (m)	Cl ⁻ (ppm)	Ca ²⁺ (ppm)	Methane (ppm)	T (°C)	Formation
SARIÑENA-1	2348.8-2429.0	237,000				M3
EBRO-2	2094.0-2144.0	200,770	2080	5400	72	M3

Table 7-26. M3 measured temperature in boreholes Ebro-1 and Ebro-2

BOREHOLE	Interval (m)	T (°C) Measured	Gradient °C/km	Formation
EBRO-2	1958	72.2	31.6	M3
EBRO-1	1480	55.0	30.5	M3

Occurrence of faults

No relevant faults have been identified affecting the top of unit M3 top in the Lopín structure, but four small fractures are present, though those do not affect the overlying Keuper facies. See

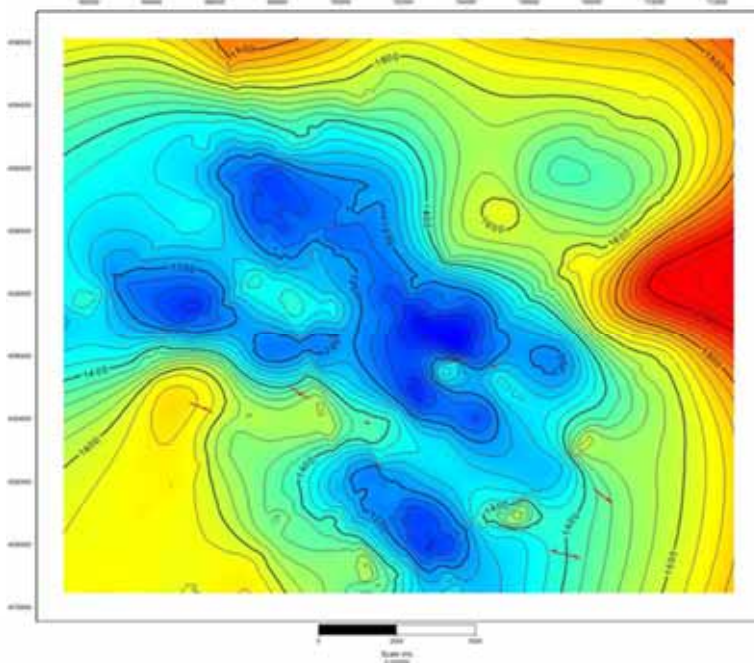


Figure 7-22 and Figure 7-23.

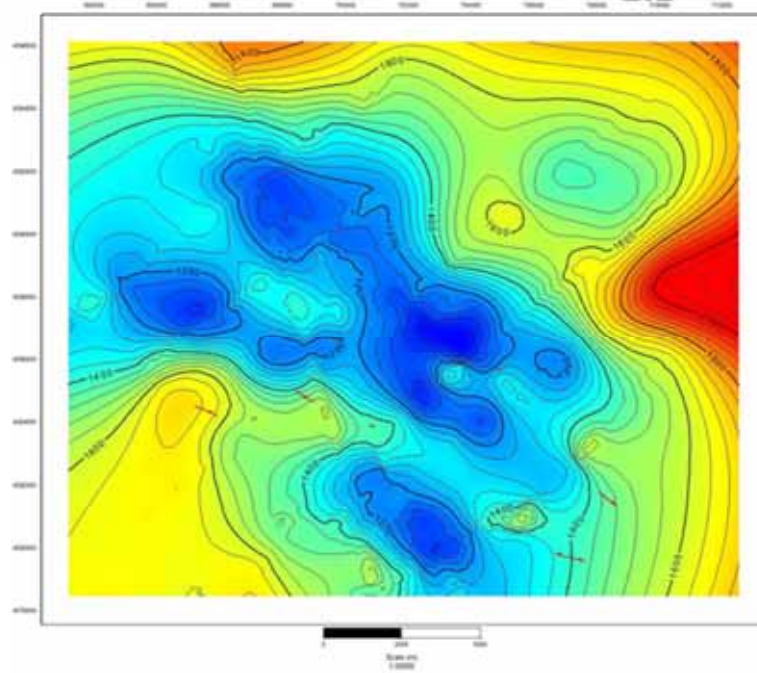


Figure 7-22. Isobaths map of the top of the M3 facies. From PilotSTRATEGY Deliverable 2.7 Conceptual Geological Models (Wilkinson, 2023)

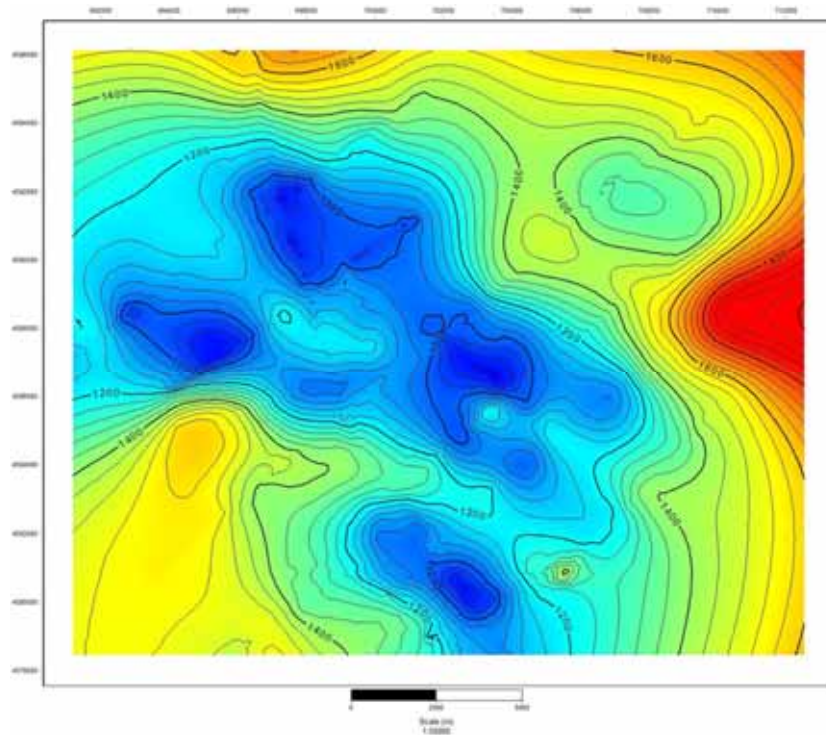


Figure 7-23. Isobaths map of the top of the Keuper facies. From PilotSTRATEGY Deliverable 2.7 Conceptual Geological Models. No faults are detected affecting the top of the Keuper facies.

7.2.3.4 Societal uses of the formation

M3 unit is not used for water supply in the area. Notice in Figure 7-16 and

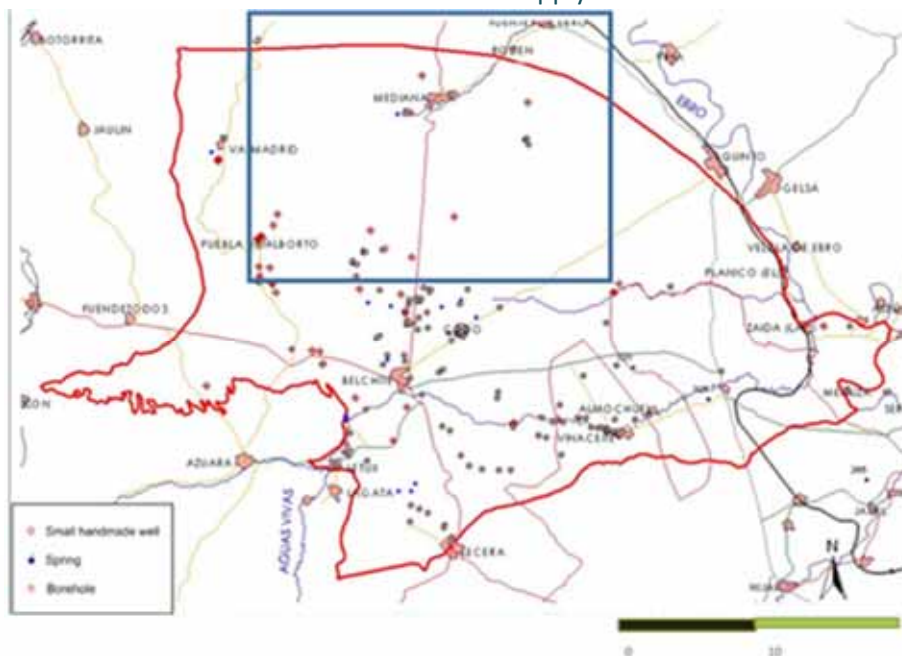


Figure 7-17 that groundwater uses are very scarce in the area and there are no wells that use the Triassic system. Exploitation is restricted almost exclusively to the Jurassic regional aquifer (see 7.3

section). There is also availability of surface resources from the Ebro River. No geothermal uses are known either.

7.3 Jurassic Formations

7.3.1 Geological features of the formation

Karstic and fissured marine Jurassic carbonates form the main regional aquifer system in the south central Ebro basin. Similar to the Aragonese Branch of the Iberian Range, the Jurassic lies on the impervious clays and evaporites of the Keuper facies.

The Jurassic aquifer is composed of Lower Jurassic (Liassic) carbonate formations (Cortes de Tajuña carniolos and Cuevas Labradas dolomite; 300 m thick), and Middle-Upper Jurassic (Upper Dogger-Malm) formations (Chelva and Higuera carbonates; 80 m thick). These aquifers are vertically separated by 300 m of marl-anhydrite formations (Cerro del Pez, Turmiel and Sot de Chera formations). The upper limit of the Jurassic aquifer is Paleogene red gypsum-clays acting as the confining formation. According with this stratigraphic scheme two confined Jurassic aquifers are present, a lower aquifer (Liassic) and an upper aquifer (Dogger-Malm).

The lower aquifer only outcrops in the Belchite anticline, 10 km south of the Lopín structure. It is hydrogeological confined in the rest of the studied area. It is possible that there is hydraulic connectivity at outcrop between the lower Jurassic and the Dogger-Malm aquifers due to a lateral hydraulic connection. The Dogger-Malm aquifer outcrops in the Aguilón and La Lomaza areas. It is also hydraulically confined in the rest of the studied area.

Natural recharge of the Jurassic hydrogeological system comes from infiltration of precipitation (rain and snow); infiltration from river beds flowing on Jurassic outcrops, such as the Aguavivas river on the Belchite anticline; and also through underground inflow coming from the south (Iberian Range). As above, in the Belchite anticline, the transfer of water between the Liassic formations and the upper aquifer is possible due to a lateral hydraulic connection.

Some discharge areas are identified linked to the regional Jurassic aquifer. The most important is La Virgen de la Magdalena spring, located in Mediana de Aragón, with an average flow of 125 L/s. Another discharge zone is identified in Codos locality, with an average flow of 25 L/s. Some minor leakage is also present in the Aguasvivas and Lopín creeks, interpreted as upwards diffuse discharge zones through Neogene low permeability formations. (IGME-DGA, 2009; IGME-DGA, 2010; MITECO-CHE, 2021)

7.3.2 Hydrogeological properties

The Liassic aquifer displays the best hydraulic properties, having transmissivities up to 1,000 m²/day, and exploitation flows of 100 L/s. The storage coefficient is estimated to be 5x10⁻⁵. (IGME-DGA, 2009; IGME-DGA, 2010).

The Malm-Dogger aquifer, and particularly the Higuera formation, shows lower values, with average transmissivities of just 38 m²/day. (IGME-DGA, 2009; IGME-DGA, 2010).

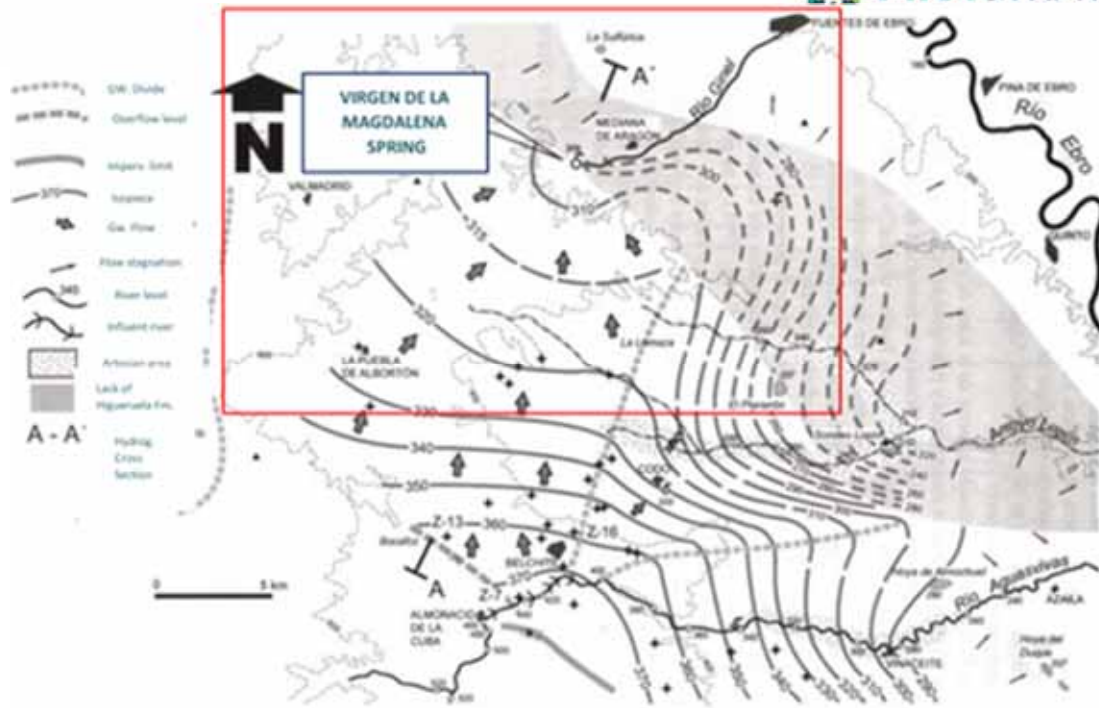


Figure 7-24. Piezometric map of the Jurassic aquifer. The red rectangle shows the studied area. (Modified from Coloma et al., 1997). The position of the main discharge point, Virgen de la Magdalena Spring, is shown. A Cross section is shown in Figure 7-25.

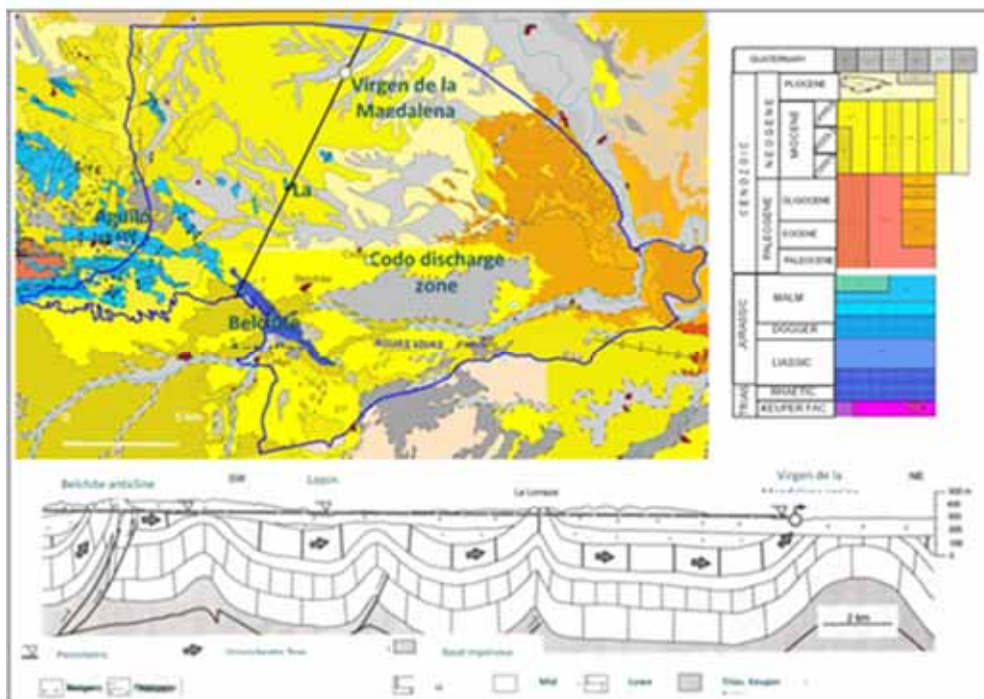


Figure 7-25. Conceptual flow model of the Jurassic upper aquifer on a NE-SW cross section. One main recharge zone is located in the SW (Belchite anticline) and here the Liassic and the upper aquifer have hydraulic connection. To the W in the Aguilón area the Malm-Dogger aquifer outcrops and is also a major recharge zone. The Lomaza area is also an outcrop of the upper Jurassic aquifer. The main discharge zone is the Virgen de la Magdalena spring, on the N edge of the cross section. Modified from IGME-DGA, 2010

7.3.3 Features of the groundwater

The composition and temperature of fluids were obtained for the Liassic and Rhaetic (Sub-Liassic) aquifer, from measurements and samples obtained in boreholes (Table 7-27).

Table 7-27. Composition of Liassic and Rhaetic fluids obtained in samples from boreholes.

BOREHOLE	Interval (m)	Cl ⁻ (ppm)	Ca ²⁺ (ppm)	pH	T (°C)	Formation
MONEGRILLO-1	944-965	125,000				LIASSIC
SARIÑENA-1	1996-2040	269,000				SUB-LIASSIC (Rhaetic)
CADASNOS-1	1499-15424	254,000			70.0	SUB-LIASSIC (Rhaetic)
EBRO-2	1551-1600	211,176	6400	6	92.0	SUB-LIASSIC (Rhaetic)

Temperature was measured in wells Chiprana-1, Ebro-2 and Cadasnos-1 (Table 7-28).

Table 7-28. Temperature measured in boreholes.

BOREHOLE	Interval (m)	T (°C) Measured	Gradient °C/km	Formation
CHIPRANA-1	881	60	31.1	DOGGER
	910	53		LIASSIC
EBRO-2	1260	92.2	31.6	LIASSIC
CADASNOS-1	1252	59.0	36.5	LIASSIC
	1522	70.0		SUB-LIASSIC (Rhaetic)

7.3.4 Occurrence of faults

None of the faults that intersect the Triassic (Buntsandstein or Muschelkalk) are identified in the geological model as intersecting the Jurassic in the Lopín area. As it is shown in Figure 7-26 and Figure 7-27 no faults are interpreted either affecting the Rhaetic or the base of the Tertiary cover.

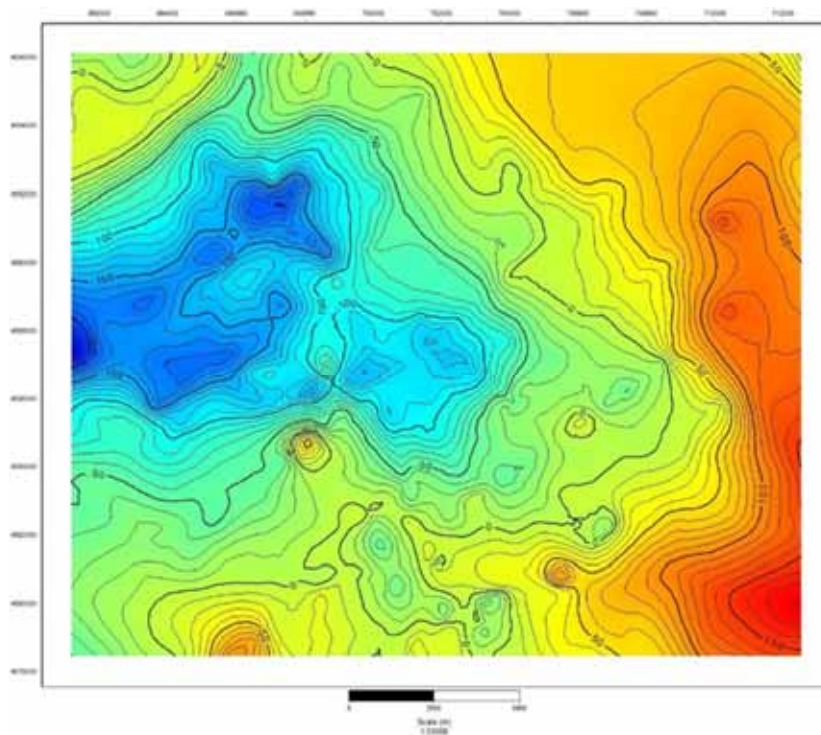


Figure 7-26. Isobath map of the top of the Imón Formation (Subliassic-Rhaetic). From PilotSTRATEGY Deliverable 2.7 Conceptual Geological Models (Wilkinson, 2023). None of the faults intersecting the Triassic (Buntsandstein and Muschelkalk) are identified at the top of the Rhaetic (Imón formation).

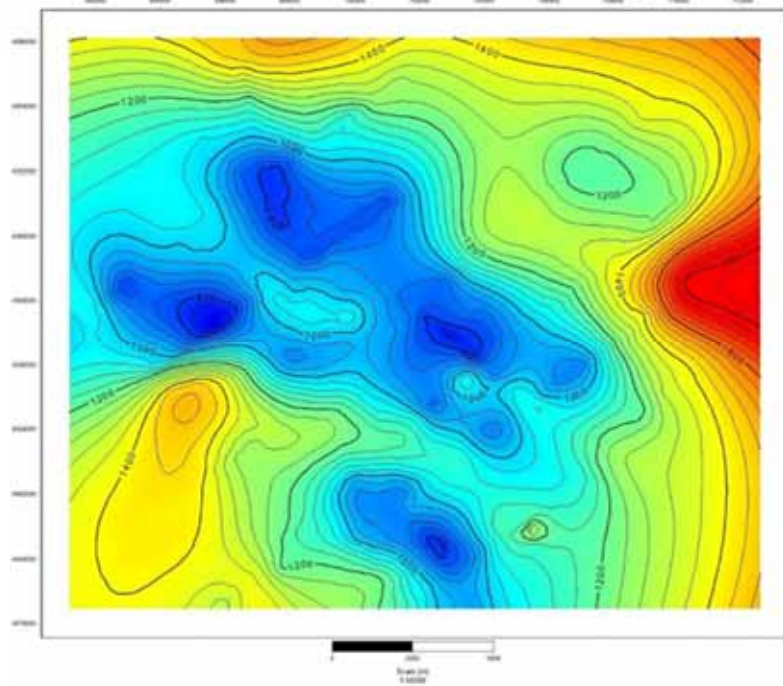


Figure 7-27. Isobath map of the base of the Cenozoic rocks. None of the faults intersecting the Triassic (Buntsandstein and Muschelkalk) are identified at the base of the Cenozoic sedimentary infill. From PilotSTRATEGY Deliverable 2.7 Conceptual Geological Models (Wilkinson, 2023).

7.3.5 Societal uses of the formation

No geothermal uses of groundwater have been identified. However most of the main boreholes in the area exploit the Jurassic regional aquifer. The main use of groundwater in the area is irrigation for agriculture. Most of the installations are located inside the Campo de Belchite groundwater mass ES091079.

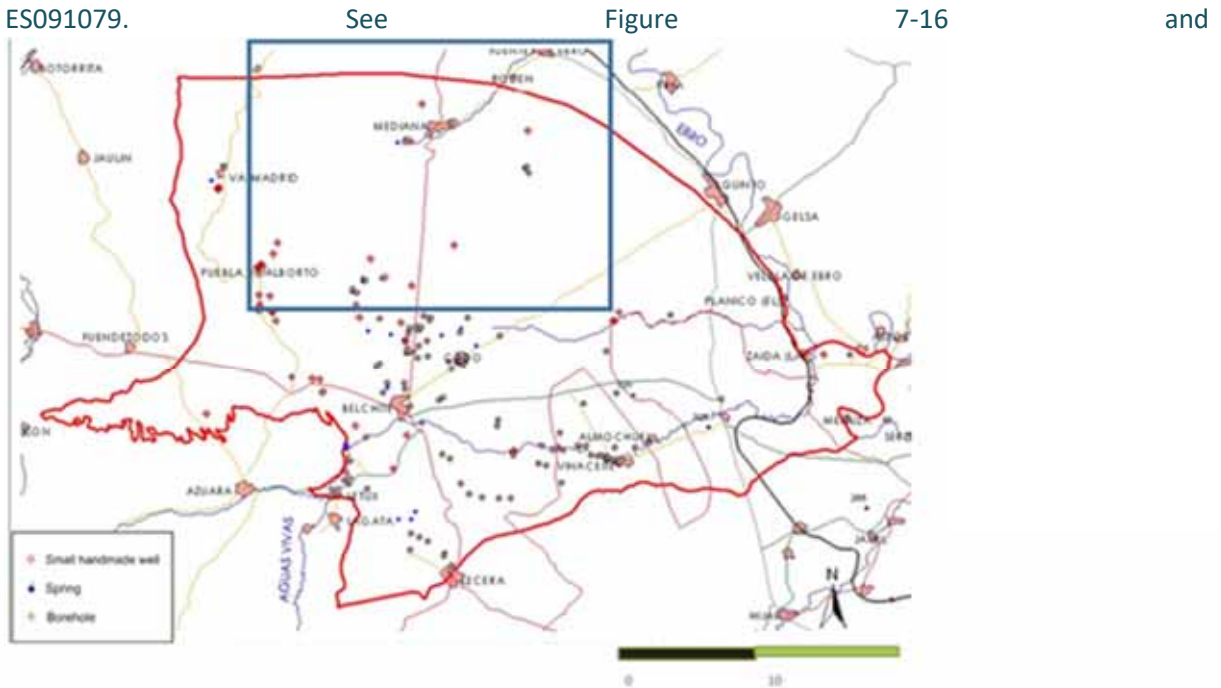


Figure 7-17.

7.4 Cenozoic and Quaternary formations – a multilayer detrital aquifer

7.4.1 Geological features of the formations

The Cenozoic formations overlie the Jurassic carbonates. They are continental Oligocene to Miocene formations, alternating conglomerates, clays, gravels, evaporites and carbonates. From a hydrogeological point of view, they collectively form a sub-horizontal multilayer aquifer of low to medium permeability. Some of those more transmissive layers may be utilised as local aquifers although they are of relatively small output due to their limited dimensions and the hydraulic parameters. Conglomerates predominate in the Oligocene, however the Miocene is more clay-rich, although lateral facies changes are quite frequent. The top of Miocene is normally represented by carbonates, these form geomorphological plains called “Muelas” due to differential erosion.

The Cenozoic aquifer has transmissivity values lower than 100 m²/day even in the most favorable cases, and an average total thickness of 200 m. To the north of the Lopín structure, no groundwater masses have been defined in Cenozoic formations due to the scarce water resources herein and the minor role that they play in the general hydrogeological behavior of this sector of the Ebro central basin. In fact, only the Quaternary sediments associated with the Ebro, Jalón, Aguas Vivas and Barranco de Lopín fluvial systems are modest aquifers, lying on Cenozoic low permeability formations.

The vertical hydraulic head gradient is a downward trend between the Jurassic and the Cenozoic aquifer, except in discharge areas like in Virgen de la Magdalena and Codos springs, where groundwater flow moves upwards from the Jurassic. In this last case the Jurassic aquifer acts as a basal drain. Recharge comes from direct precipitation and the return of irrigation water by infiltration. No discharge zones are known associated with the Cenozoic formations but are assumed to be diffuse discharge to streams.

With respect to the Quaternary alluvial formations, they form aquifers associated with the main streams and the Ebro, Jalón, Aguas Vivas and Lopín Rivers (e.g. Figure 7-28). The predominant lithologies are gravels, sands and silts corresponding with fluvial terraces, channels and alluvial plains. The thickness of the Quaternary aquifer ranges from 5 to 80 m but an average of 20 m in quite representative (CHE, 2021). The underlying units are the low permeability Cenozoic detrital formations. Transmissivity show a distribution according with the thickness of sediments, from 100 to 12,000 m²/day. The lower values are found near the contact with the Cenozoic formations and the higher ones in fluvial troughs. The storage coefficient is 0.06 to 0.12, according with pumping test (DGA-IGME, 2006). Permeability values range from 15 to 1500 m/d, although a good average value is 280 m/d (MITECO-CHE, 2021).

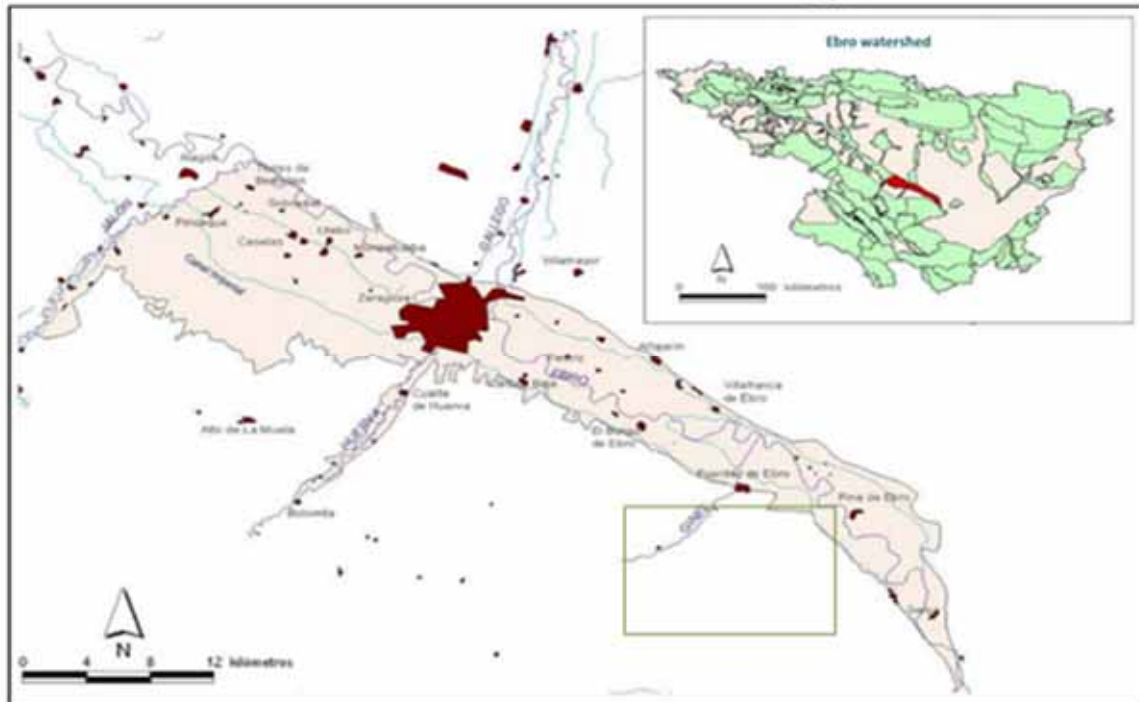


Figure 7-28. The extent of the Quaternary Ebro Alluvial aquifer. The green rectangle shows the location of the study area. The overlap of this aquifer and the study area is small. (Modified of MITECO-CHE, (2021).

The hydrogeological behavior is linked to the rivers that deposited the sediments. Recharge occurs along the whole extent of the alluvial and the fluvial terraces, mainly from the infiltration of rain water and returns from irrigation. Discharge happens into the river bed and also through extraction.

Groundwater flow coincides approximately with surface water direction, converging from the alluvial edges to the main streams. In periods of flood the flow direction may be reversed, giving place to temporary water storage in the river banks.

7.4.2 Hydrogeological properties

No hydrophysical test have been carried out in these formations, but estimation of average effective porosity and permeability (López Gutiérrez, 2015) may be established.

For the Cenozoic interbedded formations, effective porosity of the clay layers may be assumed to be 0.1% and permeability 6.3×10^{-4} m/d. For alluvial conglomerates the average effective porosity is 9% and permeability 1.6 m/d. For clays and gypsum the effective porosity is 0.4% and permeability 3.3×10^{-4} m/d. Only conglomerate layers are considered to be aquifers, but the formations are predominantly clay-rich layers, so the utility of the whole sequence is quite limited from the point of view of water supply.

With respect to the Quaternary alluvial formations, there is a predominance of gravels (terraces) and silts (river floodplain). For the first, an average effective porosity may be 18% and a permeability of 1.1×10^3 m/d. In the case of floodplain silts the average effective porosity may be 2% and the permeability of 5.6×10^{-3} m/d.

No piezometric maps of the Cenozoic formations are available, since these formations are considered to be of low-medium permeability and the important regional aquifer is the Jurassic. So there is no representative data to draw reliable piezometric maps.

With respect to the Quaternary formations, they have more favourable hydrogeological conditions and there is some data that allows to the drawing of a piezometric map upstream of the Lopín structure (Figure 7-29).

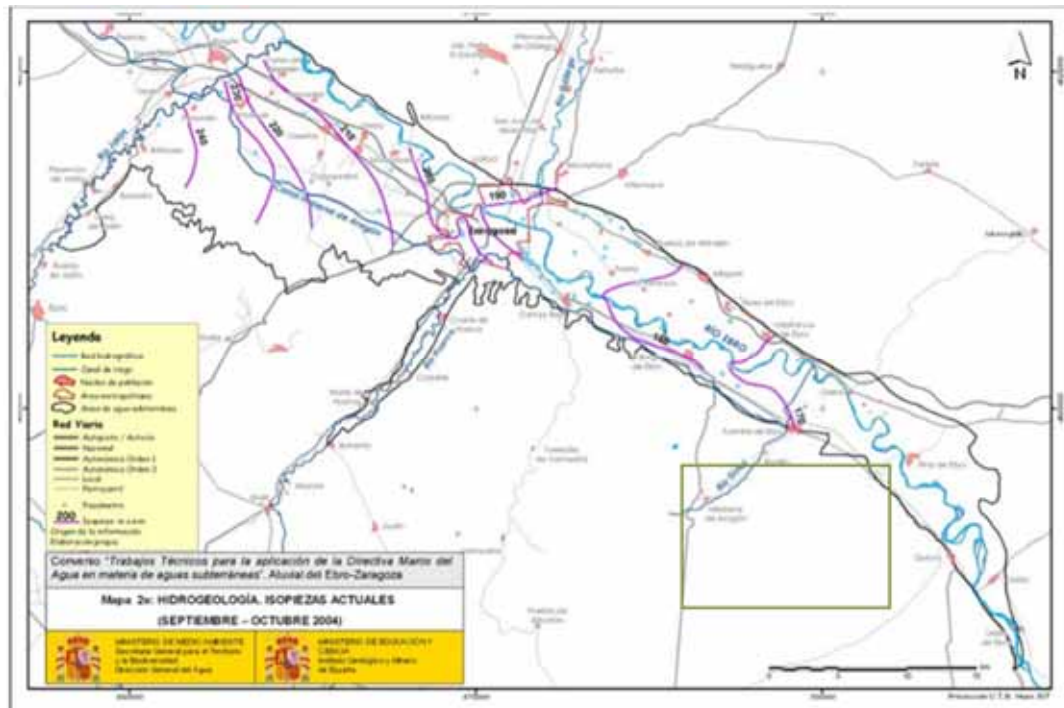


Figure 7-29. Piezometry of the Quaternary Ebro Alluvial aquifer. The green rectangle shows the location of the study area. (Modified of IGME-DGA, 2021).

7.4.3 Occurrence of faults

No faults have been detected cutting the Cenozoic sediments.

7.4.4 Societal uses of the formation

No geothermal uses of groundwater have been identified. Most of the boreholes in the area are located inside the Campo de Belchite groundwater mass (ES091079). They correspond with wells that catch the Jurassic regional aquifer IGME-DGA (2009). Some former small handmade wells used to catch Cenozoic conglomerate levels for agrarian uses although many of them are abandoned at

present.

See

Figure

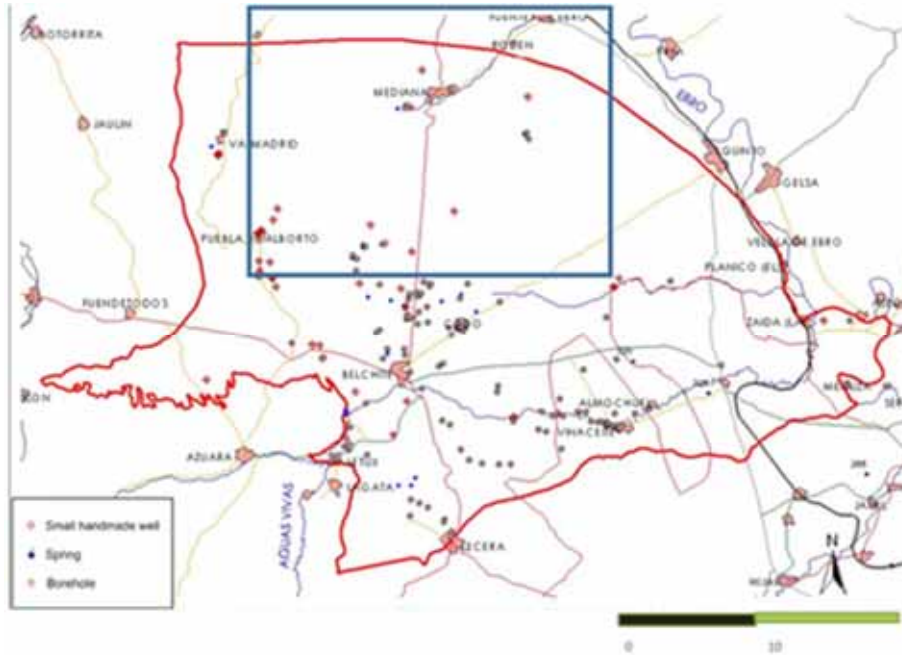


Figure 7-17.

7.5 Aquicludes in the Ebro Basin

According with the stratigraphic sequence, see Figure 7-4, four aquicludes are defined. From the bottom to the top they are: 1) Röt facies (Rané formation), 2) Muschelkalk #2, 3) Keuper facies, 5) Anhydrite Lower Lias unit.

- 1) Röt facies (Rané formation): this is the top seal of the Bundsandstein storage formations B1 and B2 (Arche et al., 2004). It is fine-grained red sandstones, red siltstone-mudstone, shales and salts. The shales tend to be thicker towards the top. This transition zone from continental to marine sedimentation also includes minor gypsum horizons. The thickness of this heterolithic unit reaches 15 – 40 m, from the SW basin limits to the centre. The percentage of shale (Vsh%) ranges between 67.1 and 87.0; and effective porosity between 0.67% and 2.77%. Hydraulic conductivity (k) was not analytically evaluated but an estimate can be made on the basis of lithology (López Gutiérrez, 2015). $K = 2.0 \times 10^{-3}$ m/day seem to be a reasonable average value for this seal formation.
- 2) Muschelkalk 2 (M2). This is a succession of Middle Triassic evaporites and shales, whose thickness in the Ebro basin ranges between 17 and 323 m. In the Lopín-1 well it is 200 m thick. No values of Vsh, effective porosity or hydraulic conductivity have been obtained analytically. Hence, the only resource is a lithology-based estimate (López Gutiérrez, 2015). Depending on the proportion of anhydrite in the stratigraphic succession the effective porosity may range between lower than 0.01% and 0.1%. Hydraulic conductivity (k) may be considered between 8.36×10^{-9} m/day if anhydrite is predominant and 3.15×10^{-4} m/day if shale is predominant. An average value of 10^{-6} m/d may be realistic.
- 3) Keuper facies. This is the main regional seal formation of the area. Across the whole basin the thickness varies from 15 to 895 m. In the Lopin-1 well the Keuper is 445 m thick. In this well, from bottom to top, the lithology is formed by shales with some thick levels of salts, thick level

of shales with some thin anhydrites and finally anhydrites with some dolomitic intercalations. No specific petro-physical data has been obtained, but some estimates can be made based on lithology. An average value of effective porosity, for the whole sequence, may be around 0.4% (López Gutiérrez, 2015). With respect to the hydraulic conductivity, the values used for numerical model have considered three scenarios: 8.6×10^{-6} m/d; 8.6×10^{-5} m/d; and 8.6×10^{-4} m/d. According with the lithology, an average value between shales and evaporites would be 3.15×10^{-4} m/day (López Gutiérrez, 2015), which is close to the upper limit of the values used in the numerical model, in scenario 2.

- 4) Anhydrite Lower Lias unit. It is a thick package of anhydrite with dolomitic interbeds (Lécera Fm) with a total thickness of 200 – 450 m (Jurado, 1990; Gómez et al., 2007). Although pure anhydrite is considered to have null effective porosity, the presence of fine interbeds of dolomite suggests a more realistic value of 0.1%. With respect to hydraulic conductivity (k), the predominance in this formation of anhydrite with null effective porosity suggests a value close to 10^{-9} m/day. However, the presence of the dolomitic interbedding may make a more realistic value between one and two orders of magnitude higher at 10^{-7} m/d to 10^{-8} m/d for the whole sequence.
- 5) Lacustrine marls Upper Malm. It is the 50m thick Sot de Chera Formation, a marl.

Taking into account the hydrogeological properties of the formations and the lack of fractures that pass through the upper and thickest seal, the Keuper facies, then no natural vertical drainage to the overlaying aquifers is expected to happen at the PilotSTRATEGY storage structure. But in the case of an accidental leak caused by a failure of the installations (i.e. boreholes), then the Jurassic regional aquifer and the less important Cenozoic aquifer would be negatively affected with respect water quality, and consequently the use of the water in these aquifers waters would be endangered.

8. Hydrogeological boundaries of the storage sites and storage complexes

Knowledge of the regional hydrogeological systems in the prospect areas for the deployment of pilot facilities is one of the key components of the multi-disciplinary geo-characterisation required to define the prospective storage sites and storage complexes. The PilotSTRATEGY project targets three different deep saline aquifers for geological storage of CO₂. Compared to other type of geological formations capable to store CO₂, the deep aquifer displays the most substantial CO₂ storage capacities and their wide geographical distribution generally favors a shortening of the distance between industrial CO₂ sources and storage sites. Apart from the key viability criteria of the reservoir (i.e. storage capacity and injectivity) and caprock (i.e. integrity) to support the deployment of the storage operation, the injection and propagation of CO₂ in the target formation must also be predictable. The geological storage of CO₂ must comply with certain requirements to ensure a negligible impact of the storage operation on the environment, natural resources and human health and safety over hundreds or thousands of years.

With these respects, dynamic models based on the 3D static geo-characterisation of the storage sites and storage complexes are developed and applied to predict and optimize the fate of the CO₂ in the target geological formations. This requires a good knowledge of the hydraulic connection between the different formations in the target and the surrounding areas, where the CO₂ plume may spread. Accordingly, the definition of the storage site and the storage complex for each region is a prerequisite for the boundary of the dynamic modeling, the safety and performance assessment and more generally for the legal and technical documents. The definition of the storage site and storage complex might evolve during the preparation of the legal and technical documents and the duration of the storage site operation. However, the current understanding of regional hydrogeological system, combined with the geological characterisation (PilotSTRATEGY Deliverable D2.7; Wilkinson (2023)), allow the definition of conceptual boundaries of the storage site and storage complex for each target region in the Paris Basin, the Lusitanian Basin and the Ebro Basin.

The **storage site** is defined as the storage area where the injected CO₂ will naturally flow from the lower injection point in the target reservoir to the primary caprock below which the injected CO₂ permanently accumulates and spreads laterally. Potential leakage through the caprock due to integrity failure is not considered within the conceptual storage sites defined from the geo-characterisation (WP2) as the caprock integrity and leakage risk scenarios will be studied in other work packages of the PilotSTRATEGY project (WP3 and WP5, respectively). Only any natural faults identified in the study area are integrated in the conceptual definition of the storage site, as faults intersecting the primary caprock may be regarded as potential pathways for upward CO₂ migration through and above the primary caprock sealing the reservoir. Therefore, the definition of the boundaries of the storage site relies hereafter on (i) the prospect area initially defined by the research teams, (ii) the shape of the CO₂ plume in the reservoir and below the primary caprock, and (iii) the potential or current exploitation and associated facilities in the reservoir.

The **storage complex** is defined as the extended area of the target reservoir and structural trap, and includes the potential secondary reservoir(s) and secondary seal unit(s), up to the ultimate caprock/seal unit. In other words, natural faults, if any, in and more distant from the storage site, are considered as preferential paths for upward CO₂ migration in the formations above the storage site. In case of connection with the intermediate-to-shallow aquifers, the uppermost boundary of the

storage complex is defined as the ultimate formation (i.e. ultimate seal) above which the upward migration of CO₂ would induce a negative environmental impact on the key natural resources and/or the human health and safety. In the case of connection to the surface, the intersection of the natural faults defines the lateral boundary in the reservoir that the CO₂ plume should not reach. In a similar way to the storage site, the potential or current exploitation and associated facilities in the surrounding area shall be considered not only in the primary reservoir but also in the above formations, where the CO₂ plume may potentially migrate, for the definition of the lateral extent of the storage complex.

8.1 Storage complex in the Paris Basin

In the Paris Basin, the main reservoir of the prospect region for the French pilot site is located in the Dogger (Middle Jurassic) formations, where the prospective injection is in the *Oolithe Blanche* aquifer unit. From a hydrogeological point of view (Figure 8-1), the reservoir includes the *Oolithe Blanche* (Dogger main aquifer), the Comblanchian (overall aquitard unit) and the *Dalle Nacrée* formations (heterogeneous aquifer-aquitard units). Conceptually, the injected CO₂ will accumulate and partly spread at the bottom of the Comblanchian Formation, which slows down the upward migration toward the *Dalle Nacrée* Formation. In the area, the *Dalle Nacrée* Formation forms a secondary reservoir, which is considered as part of the main reservoir. The Callovo-Oxfordian marls, a 120 m thick formation in the PilotSTRATEGY study area, are the first massive aquiclude above the reservoir formations and are hence the primary caprock of the storage site. No faults were identified in the defined study area. Therefore, the French storage site considered in the project is mainly composed of the reservoir (*Oolithe Blanche*, Comblanchian and *Dalle Nacrée* formations) and the Callovo-Oxfordian caprock (marls), also regarded as the primary reservoir – seal unit (Figure 8-1).

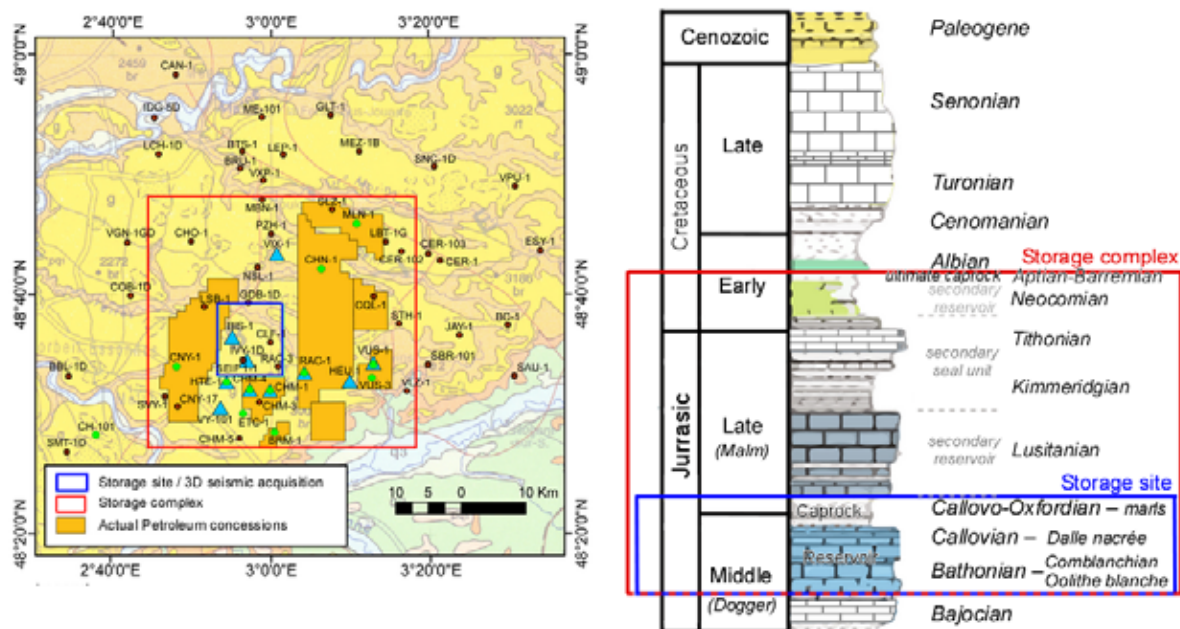


Figure 8-1. Definition of the geographical (left) and vertical (right) boundaries of the storage site and storage complex in the Paris Basin, based on the knowledge of the regional hydrogeological system. Only major aquifers are colored (right).

In terms of local flow, the occurrence of the SEIF 1-1 well currently injecting fluids down to the *Oolithe Blanche* formation impacts the natural flow of the aquifer in the study area. If the SEIF 1-1 well remains

in use during and after the envisaged CO₂ injection, the fluid injection will influence the direction and the shape of the CO₂ plume in the primary reservoir. This feature will depend on the location and depth of the CO₂ injection in the *Oolithe Blanche* formation. These technical key aspects are studied in other WPs of the PilotSTRATEGY project and are thus out of the scope of this deliverable.

The petrophysical properties of the reservoir, and more specifically the fracture porosity and the network of connected fractures in the Dogger limestones, will strongly influence the lateral and possibly the vertical migration of the CO₂ plume within the different units of the reservoir. This identified gap in the current knowledge requires differentiating the boundaries of the storage site and the boundaries of the storage complex, with respect to potential natural migration above the Callovo-Oxfordian caprock. In addition, the oil concessions surrounding the PilotSTRATEGY study area and the Malnoue faults and Conquillie fault located northeast of the extended area are potential features with known natural (faults) or anthropic (wells) pathways for the possible upward migration of the CO₂ plume toward the Cretaceous formations and the surface.

Oil extraction takes place from the upper Comblanchian and mostly in the *Dalle Nacrée* formations, resulting in only a limited-to-moderate influence on the natural flow in *Oolithe Blanche* main reservoir. The presence of both production and injection wells in the oil concessions suggests options to impose artificial flow in the reservoir formation to prevent or limit the migration of the CO₂ plume toward the production wells of the oil concessions, if required. From a hydrogeological point of view, the storage complex should be considered to extend laterally to include the oil field concessions. Such lateral extension allows integrating the production and injection activities in the dynamic models and studying their impact on the long-term migration and fate of the CO₂ plume in the storage site.

Although faults are located at some distance from the PilotSTRATEGY study area (i.e. 15 km minimum), the major subvertical Malnoue faults, which intersect the Dogger formation up to the uppermost Late Cretaceous formations (Figure 8-1), shall be considered in term of the risk assessment of the extended area. The major faults are the main natural path for upward CO₂ migration directly from the *Oolithe Blanche* main reservoir to the Malm and Cretaceous formations and therefore provide the rationale to extend the boundaries of the storage complex vertically. Considering the regional hydrogeological context, the main natural resource(s) above the primary Callovo-Oxfordian caprock are the freshwater aquifers used in the Paris metropolitan area. Among the aquifer units overlying the Callovo-Oxfordian caprock, the Neocomian and Albian aquifers (Early Cretaceous) are the deepest freshwater aquifers to be first impacted by a potential upward migration of CO₂ from the reservoir. As the Neocomian aquifer is only exploited to a low extent for water supply in the Paris Basin, it is highly recommended to extend the storage complex up to the top of the Aptian formation, underlying the strategic freshwater Albian aquifer, to ensure the safety of the prospective CO₂ storage site.

Within the defined storage complex (Figure 8-1), the Malm and Early formations, overlying the Dogger (main) reservoir and the Callovo-Oxfordian primary caprock and underlying the Albian aquifer, compose the “secondary caprock”, following the definition of the geologists (PilotSTRATEGY Deliverable D2.7: Wilkinson (2023); Bordenave and Issautier (2023)). More specifically, considering their hydrogeological properties, the Lusitanian aquifer forms a potential secondary reservoir above the primary caprock, whereas the Kimmeridgian and Thithonian formations (Malm) would act as a thick secondary seal unit, to limit or prevent any potential upward migration of CO₂ toward the Neocomian and Albian aquifer (Figure 8-1). In turn, the Neocomian aquifer and the Late Barmian and Aptian clayey and marly formations compose the ultimate secondary reservoir and ultimate caprock/seal unit of the conceptual storage complex, respectively.

The conceptual storage complex indicates that any potential upward CO₂ plume must not reach the top of the Aptian formation to ensure the safety of the prospective CO₂ storage site. However, the possibility of an upward flow of CO₂ from the primary reservoir up to the Neocomian aquifer must be precluded in order to prevent any potential negative environmental impacts on the strategic fresh groundwater resource. Considering the limited amount of the CO₂ planned to be injected into the pilot site, or even with a full-scale industrial scale injection, it is highly improbable that the CO₂ plume will reach the remote subvertical major faults in the main reservoir, which may act as preferential upward flow path within the storage complex. The hydrodynamic properties of the Manoue faults remain poorly characterised, but have been considered to have semi-permeable properties by Gonzalves (2003), which considerably slows down the upward migration if the subvertical major faults are not sealed within the Malm and Early Cretaceous formations. The large vertical extension of the storage complex is therefore defined based on the most pessimistic scenario, identified from the gap analyses in the data and current knowledge, mainly from a perspective of risk assessment.

8.2 Storage complex in the Lusitanian Basin

Given that the proposed CO₂ storage pilot is located in the offshore part of the Lusitanian basin, more specifically in the Cabo Mondego sub-basin (see Figure 6-3b), the definition of the storage complex has to consider primarily the information obtained by the offshore petroleum exploration activities. Deliverable 2.7 of PilotSTRATEGY (Report of Conceptual Geological Models; Wilkinson (2023)) and the storage complex proposed (Figure 8-2) reflect this approach.

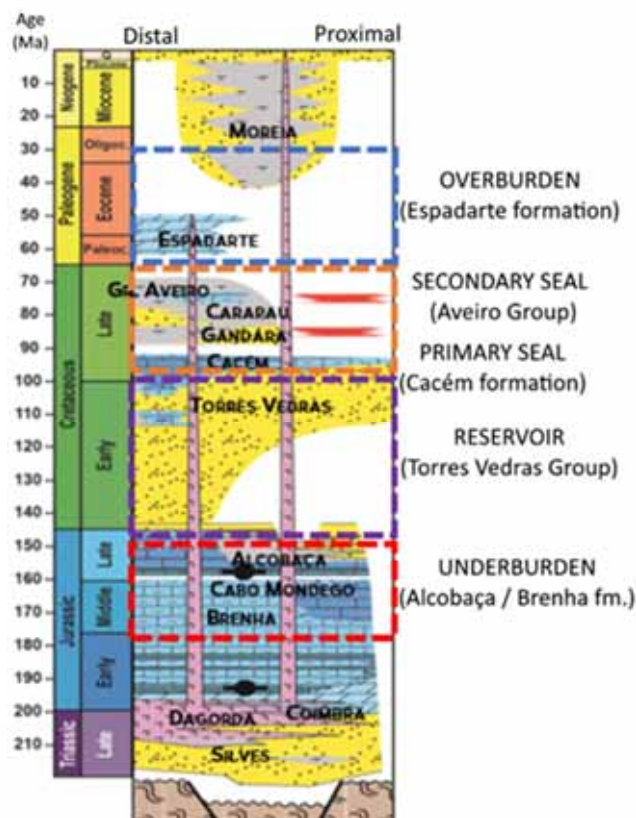


Figure 8-2. Lithostratigraphic chart of the offshore Lusitanian Basin and the main tectono-stratigraphic units, based on the petroleum exploration boreholes. Adapted from Pereira et al. (2023).

However, it is acknowledged that the petroleum exploration activity in offshore Portugal was very limited and existing data is from surveys conducted several decades ago. In that respect, and despite the structural complexity of the Lusitanian basin, the onshore groundwater exploration and exploitation activities can provide some insights about the expected role of some of the layers that make up the structural complex.

Table 8-1 summarizes the aquifer layers, aquitards and aquicludes in the aquifers previously described, but also including some other Cretaceous /Tertiary aquifer system occurring in the north sector of the Lusitanian basin, more distant from the coast and from the offshore target area. The table was simplified by adopting the designations used in the offshore sector for the stratigraphically equivalent formations occurring onshore. For instance, the Cenomanian/Turonian carbonate formations that appear under several names in the onshore (the most frequent being Costa de Arnes Limestones) is here named as the Cacém Formation. The Early Cretaceous siliciclastic formation (onshore most often called Carrascal Sandstones) is named the Torres Vedras Group.

Table 8-1 -Summary of occurrence of aquifers (indicated with x), aquitards and aquicludes in the Cretaceous and Tertiary aquifer systems in the north sector of the onshore Lusitanian basin.

Unit	Series / Stage	Designation	Hydraulic behaviour	Aveiro Cretaceous aquifer (O2)	Figueira da Foz-Gesteira aquifer (O7)	Louriçal aquifer (O29)	Tentúgal aquifer (O5)	Viso – Queridas aquifer (O30)	Condeixa- Alfarelos aquifer (O31)	
	Miocene	Undifferentiated Miocene subsystem	Aquifer, locally aquitard			x				
	Paleogene	Undifferentiated Paleogene subsystem	Aquitard			x				
C ₅	Campanian-Maastrichtian	Aveiro Sandstones and Clays / Taveiro Sandstones and clays	Aquiclude	x		x	x	x		
C ₄	Coniacian-Santonian	Upper Coarse sandstones	Aquifer	x						
C ₃	Upper Turonian-Lower Coniacian	Micaceous Sandstones (Lousões Formation)	Aquifer	x	x	x	x	x	x	
C ₂	Upper Cenomanian - Turonian	Cacém Formation (Costa de Arnes limestones)	Aquifer / Aquiclude	x	x	x	x	x	x	
C ₁	Aptian / Albian – Lower Cenomanian	Torres Vedras Group (Carrascal sandstones)	Top	Aquifer	x	x	x	x	x	x
			Intermediate	Aquitard	x	?	?	?	?	?
				Intermed. aquifer	x	x	x	x	x	x
				Aquitard	x	?	?	?	?	?
Bottom	Lower Aquifer	x	x	x	x	x	x			

Another important assumption in Table 8-1 is the subdivision of the C₁ unit, i.e., the lateral equivalent of the offshore Torres Vedras Group, into three sequences. This subdivision is only described in the Aveiro Cretaceous (O2) aquifer, by far the most well-studied aquifer in the north Lusitanian basin. It is possible that such sequence does not exist in the other Cretaceous aquifers, or that simply not enough information was ever collected to distinguish the sequence. In the Aveiro Cretaceous aquifer the importance of that subdivision is demonstrated by the existence of a **Lower aquifer** and an **Intermediate aquifer**. These aquifers have higher salinity than the **Main aquifer** from which they are separated by aquitards or aquicludes at the base and top of the intermediate sequence of the C₁ unit. Demonstrating if this sequence occurs in the offshore petroleum exploration wells is relevant for the definition of the storage complex.

The role of the Cenomanian / Turonian carbonated formation (the Costa de Arnes or Cacém formation) is ambiguous, in that this formation is often mentioned as productive when outcropping or at shallow depth, but as aquitard or as aquiclude closer to coast or at large depths (in the Aveiro Cretaceous aquifer). It is also often mentioned in groundwater exploration studies that the base of this formation has a more clayey and marly nature, granting it better qualities as a seal. The evolution of this formation to the offshore is essential to understand its role as the primary seal for the offshore reservoir.

The Upper Cretaceous sandstones provide a secondary reservoir in case of leakage. More importantly for the safety of the CO₂ storage is the role of the Aveiro Sandstones and Clays formation, which together with the Paleogene formations, can provide excellent secondary seal properties, judging from the role that these formations play in confining the onshore Cretaceous aquifers. The storage complex in the offshore should attempt to distinguish the subdivisions of the Aveiro Group and the possibly of the Paleogene Espadarte formation (Figure 8-2).

8.3 Storage complex in the Ebro Basin

In the Ebro Basin, the target region for the Spanish pilot site is located in the Buntsandstein facies (Lower Triassic) formations, where the prospective injection will be in the B1 (*Aranda* formation; lower) and B2 (*Carcalejos* formation; upper) units. From a hydrogeological point of view (Figure 8-3), the reservoir includes heterogeneous conglomerates and sandstones. The top seal is composed of the Röt facies (*Rané* formation) shales, marls and anhydrite at the top of the Buntsandstein facies, which are the primary aquiclude caprock of the storage site. Conceptually, the injected CO₂ will accumulate and partly spread at the bottom of the *Rané* formation, which will stop the upward migration toward the Muschelkalk M1 formation. In the area, the Muschelkalk carbonate units M1 and M3 have aquifer properties as well, and could form possible secondary carbonate reservoirs, although the storage site is defined as only the Buntsandstein Formation. Some normal faults were identified affecting the Buntsandstein target formation, the primary caprock and the M1 formation. However, from a hydrogeological regional point of view, the whole Triassic hydrogeological system (B1, B2, M1 and M3) is considered to be hydraulically isolated from the overlying strata by the Keuper facies (Upper Triassic) as regional aquiclude and seal formation. None of those identified normal faults pass through the Keuper facies. In this way, the Triassic highly saline and deep hydrogeological system is hydraulically disconnected from the regional hydrogeological system within the overlying Jurassic and Cenozoic formations.

The regional flow is established to be east-northeastwards from the study area. Using the superposition of the flow direction and the presence of those detected normal faults, the storage site limit is defined as a 15 km long rectangle elongated in an ENE direction (Figure 8-3).

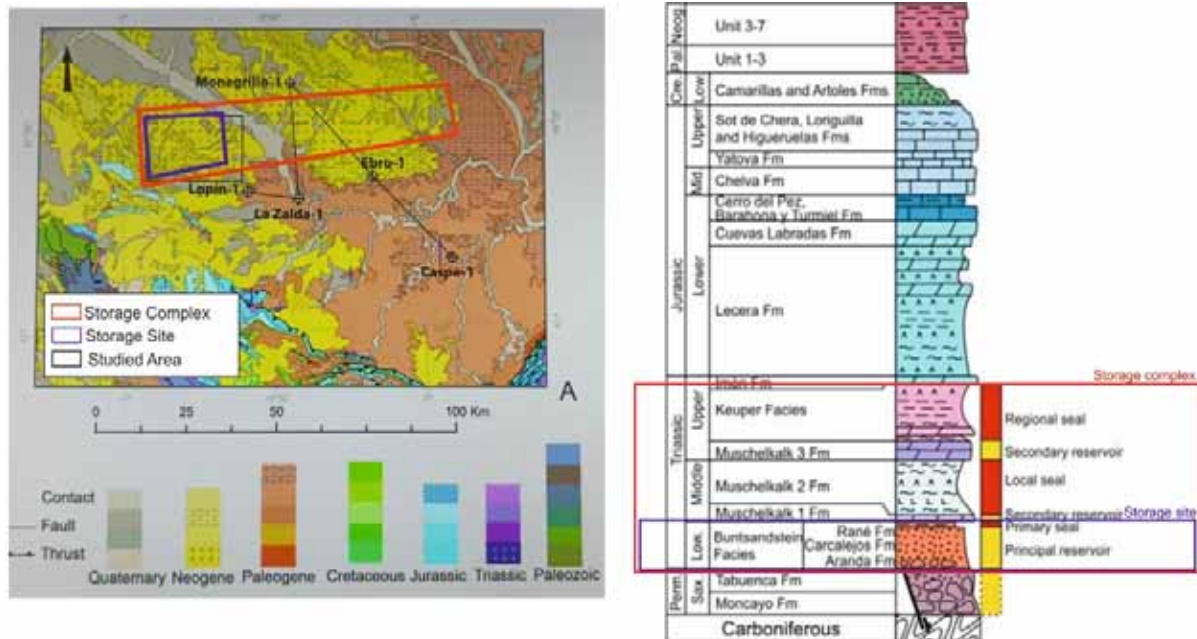


Figure 8-3. Definition of the geographical (left) and vertical (right) boundaries of the storage site and storage complex in the Ebro Basin, based on the knowledge of the regional hydrogeological system.

The petrophysical properties in the reservoir, are quite variable from one borehole to another and from B1 to B2, indicating a high heterogeneity and possible anisotropy. Additionally, considering the mineralogy of Units B1 and B2, dominated by quartz, feldspar and muscovite, the high salinities found in the Buntsandstein storage formation, only can be expected if the transit period is extremely high, almost stationary, as an available Feflow numerical model of the Ebro basin deep system concludes.

In order to define the vertical limit of the storage complex, the Keuper facies have been considered to be the upper regional caprock that prevents the possibility of the overlying regional aquifers (Jurassic and Cenozoic) to be negatively affected. With respect to the lateral limit of the storage complex, it has been considered necessary to be defined pessimistically, allowing for a (rather unlikely) lateral migration of a CO₂ plume from the injection site to the regional discharge area, located 90 km NE, in the region of Lérida (Lleida) city. Although an almost stationary flow regime is interpreted (in simulations over 1000 years), the storage complex shall be extended laterally to include the discharge area.

Considering the limited amount of the CO₂ allowed to be injected in framework of a pilot site, and the characteristics explained above, it is quite highly improbable that the CO₂ plume will reach either the discharge area or the overlying regional aquifer.

8.4 Conclusion

To conclude, the definition of the conceptual storage sites and storage complexes provide the primary framework required for the other WPs of the PilotSTRATEGY project and the preparation of legal and technical documents for the development of the respective pilot sites. The static and dynamics models

developed in the WP3 of the project and associated simulation scenarios to be tested will provide integrative results to further either refine or validate the boundaries of the storage site and storage complex of each of three studied regions.

9. References

- AdRA, 2023, Águas da Região de Aveiro, 2033. Website available at <https://www.adra.pt/home> accessed 16 July 2023.
- Almeida, C., Mendonça, J., Jesus, M.R. & Gomes, A., 2000, Sistemas Aquíferos de Portugal Continental. Instituto da Água/Centro de Geologia da Universidade de Lisboa, 3 Volumes, 671 pp.
- Alves, T., Gawthorpe, R.L., Hunt, D.W., & Monteiro, J.H., 2002, Jurassic tectono-sedimentary evolution of the Northern Lusitanian Basin (offshore Portugal). *Marine and Petroleum Geology*, 19, pp. 727-754
- Amaral, J.P., 2013, Monitorização da massa de águas subterrâneas Cretácico de Aveiro. MSc Thesis. Universidade de Aveiro. 162pp.
- Amraoui N., Golaz C., Mardhel V., Negrel Ph., Petit V., Pinault J. L. and Pointet Th., 2002, *Simulation par modèle des hautes eaux de la Somme.*, Rapport final BRGM/RP-51827-FR, 184 p., 83 fig., 11 tabl., 5 ann.
- ANDRA, 1999, Référentiel géologique du site de Meuse/Haute-Marne, tome 4, le callovo-oxfordien, ANDRA Report A RP ADS 99-005. Châtenay-Malabry, France, Châtenay-Malabry, France.
- ANDRA, 2005, Référentiel du site de Meuse / Haute-Marne. Tome 1 : Le site de Meuse / Haute-Marne : histoire géologique et état actuel., Dossier Argile 2005. 713 p.
- Andre G., 2003, Caractérisation des déformations méso-cénozoïques et des circulations de fluides dans l'Est du Bassin de Paris. Phd thesis, Université Henri Poincaré - Nancy 1.
- André L., Audigane P., Azaroual M. and Menjot A., 2007, Numerical modeling of fluid-rock chemical interactions at the supercritical CO₂-liquid interface during CO₂ injection into a carbonate reservoir, the Dogger aquifer (Paris Basin, France). *Energy Conversion and Management* 48, 1782–1797.
- Arche, A., Gómez, J. L., Marzo, M., & Vargas, H., 2004, The siliciclastic Permian-Triassic deposits in Central and northeastern Iberian Peninsula (Iberian, Ebro and Catalan basins): a proposal for correlation. *Geologica Acta*, 305-305.
- Archie, G.E., 1942, The Electrical Resistivity as an Aid in Determining Some Reservoir Characteristics. *J. Pet. Tech.* (Jan) 5, No. 1.
- ARH Centro, 2012, Plano de Gestão das Bacias Hidrográficas dos rios Vouga, Mondego e Lis Integradas na Região Hidrográfica 4. Parte 2 – Caracterização Geral e Diagnóstico. 1.4.2 – Caracterização das Massas de Águas Subterrâneas Relatório Final, 267 pp.
- Arribas, J., 1985, Base litoestratigráfica de las facies Buntsandstein y Muschelkalk en la Rama Aragonesa de la Cordillera Ibérica (Zona Norte). *Estudios Geológicos* 41, 47-57.
- Aubertin G. and Ballin F., 1984, Analyse des écoulements naturels dans l'aquifère géothermique du Dogger du centre du bassin de Paris., Institut mixte de recherches géothermiques. BRGM/84 SGN 79 GTH-IRG.
- Aurell, M., Bádenas, B., Casas, A., & Alberto, S., 2001, La Geología del Parque Cultural del Río Martín. Asociación Parque Cultural del río Martín.
- BDLISA, 2023. Base de Donnée des Limites des Systèmes Aquifères. Version 3 accessed 20 June 2023, <<https://bdlisa.eaufrance.fr/>>
- Bellier S., 2013, Modélisation de la contamination nitrique de la nappe des calcaires de Champigny. Application à la protection des captages prioritaires de la fosse de Melun et de la basse vallée de l'Yerres. Thèse de doctorat, Mines ParisTech. 359 p.

- Belmokhtar M., Delage P., Ghabezloo S. and Conil N., 2018, Active porosity in swelling shales: insight from the Callovo-Oxfordian claystone. *Géotechnique Letters* 8, 226–230.
- Berger G. and Roussel Ph., 1977, Etude hydrochimique de la nappe des calcaires de Champigny en Brie. Constitution d'un réseau de surveillance., BRGM/77 SGN 546 BDP, 98 p.
- Blanc H., 2020, Interpretation des pompages d'essai et bancarisation des paramètres hydrosynamiques sur le secteur de la Brie., Rapport final BRGM/RP-70151-FR, 83 p., 20 ill., 7 tabl., 13 ann.
- Bordenave, A. & Issautier, B. 2023. Geological Conceptual Model of Paris Basin, Grandpuits area, France. Deliverable 2.7. PilotSTRATEGY project (grant agreement: 101022664)
- Bouniol B., 1985, Etude d'un réservoir géothermique carbonaté : le Lusitanien de la Région Parisienne. Université Pierre et Marie Curie - Paris VI. Institut Mixte de Recherches Géothermiques. BRGM 85 SGN 053 IRG. 223 p.
- Bouniol B. and Magnet Ph., 1983, Ressources géothermiques au Lusitanien dans le bassin de Paris., BRGM/83 SGN 045 GTH, 52 p.
- BRGM, 1983, Potentiel géothermique "basse température" en France., rapport BRGM 83 SGN 375 SPG.
- Briais J., Guillocheau F., Lasseur E., Robin C., Châteauneuf J. J. and Serrano O., 2016, Response of a low-subsiding intracratonic basin to long wavelength deformations: the Palaeocene–early Eocene period in the Paris Basin. *Solid Earth* 7, 205–228.
- Brosse É., Badinier G., Blanchard F., Caspard E., Collin P. Y., Delmas J., Dezayes C., Dreux R., Dufournet A., Durst P., Fillacier S., Garcia D., Grataloup S., Hanot F., Hasanov V., Houel P., Kervévan C., Lansiard M., Lescanne M., Menjot A., Monnet M., Mougin P., Nedelec B., Poutrel A., Rachez X., Renoux P., Rigollet C., Ruffier-Meray V., Saysset S., Thinon I., Thoraval A. and Vidal-Gilbert S., 2010, Selection and Characterization of Geological Sites able to Host a Pilot-Scale CO₂ Storage in the Paris Basin (GéoCarbone-PICOREF). *Oil Gas Sci. Technol. – Rev. IFP* 65, 375–403.
- Cabral; J. e Ribeiro, A., 1988, - Carta Neotectónica de Portugal Continental. Serviços Geológicos de Portugal, Lisboa.
- Cao F., Jaunat J. and Ollivier P., 2023, A conceptual model of hydrogeological function and perchlorate transfer in the unconfined Champagne Chalk aquifer (NE France). *Geological Society, London, Special Publications* 517, SP517-2020–153.
- Caritg S., Bourguin B., Foissard D. and Lopez S., 2014, Projet LUSITANIEN - Evaluation du potentiel géothermique du Lusitanien du bassin de Paris pour la production de chaleur : mise en adéquation entre ressource et besoins. Rapport final. BRGM/RP-63244-FR, 147 p., 43 fig., 13 tabl., 8 ann.
- Carreira Paquete, P.M.M., 1998, Paleoáguas de Aveiro. PhD thesis, Universidade de Aveiro, Portugal, 377 pp.
- Carreira P.M.M., Soares A.M.M., Marques da Silva M.A., Araguás L.A., Rozanski K., 1996, Application of environmental isotope methods in assessing groundwater dynamics of an intensively exploited coastal aquifer in Portugal. *Isotopes in Water Resources Management* 2:45–58
- Carreira, P. M.; Monge Soares, A. M.; Marques da Silva, M. A.; Peixinho de Cristo, F.; Gonfiantini, R. P., 1994, Caracterização Físico Química e Isotópica do Aquífero Cretácico de Aveiro-Resultados Preliminares. 2º Congresso da Água. Lisboa. Tomo II. pp. 205-215.
- Casacão, J., Silva, F., Rocha, J., Almeida, J. and Santos, M., 2023, Aspects of salt diapirism and structural evolution of Mesozoic–Cenozoic basins at the West Iberian margin. *AAPG Bulletin*, Volume 107(1), pp. 49–85.
- Castro M. C., Jambon A., de Marsily G. and Schlosser P., 1998, Noble gases as natural tracers of water circulation in the Paris Basin: 1. Measurements and discussion of their origin and mechanisms of vertical transport in the basin. *Water Resources Research* 34, 2443–2466.
- CHE, 2023. Plan Hidrológico del Ebro tercer ciclo, 2022-2027, Real Decreto 35/2023, de 24 de enero

- Crastres de Paulet F., Dufrenoy R., Pira K., Polez K., Petrignet M., Guizouam G. and Demangeon G., 2011, Carte piézométrique de la Craie séno-turonienne dans le Sud-Est du Bassin parisien - Basses eaux d'octobre 2011., Rapport final BRGM/RP-60712-FR, 49 p., 25 fig., 6 tabl, 4 ann.
- Coloma López, P., Sánchez Navarro, J.A., Martínez Gil, F.J., y Pérez, A., 1997, El drenaje subterráneo de la cordillera Ibérica a la depresión terciaria del Ebro. *Revista Sociedad Geológica de España* 10: 205-218.
- Condesso de Melo M.T., Carreira Paquete P.M.M., Marques da Silva M.A., 2001, Evolution of the Aveiro cretaceous aquifer (NW Portugal) during the late pleistocene and present day: evidence from chemical and isotopic data. In: Edmunds WM&Milne C J (eds). *Palaeowaters in Coastal Europe: evolution of groundwater since the Late Pleistocene*; Geological Society, London, Special Publications, 189, pp 139–154. <https://doi.org/10.1144/gsl.sp.2001.189.01.09>
- Condesso de Melo M.T., Marques da Silva M.A., 2009, The Aveiro quaternary and cretaceous aquifers Blackwell Publishing Portugal. *Natural Groundwater Qual*, 233–262
- Condesso de Melo, 2002, Modelo matemático de fluxo e transporte de massa do sistema multiaquífero Cretácico da região de Aveiro (Portugal). PhD thesis, Universidade de Aveiro, 206pp.
- Daniel Marcos, 2022, Máster universitario en Exploración de Hidrocarburos y Recursos Minerales de la Universidad Complutense de Madrid (UCM). Curso 2021-2022
- Delmas J., Brosse E. and Houel P., 2010, Petrophysical Properties of the Middle Jurassic Carbonates in the PICOREF Sector (South Champagne, Paris Basin, France). *Oil Gas Sci. Technol. – Rev. IFP* 65, 405–434.
- Delmas J., Houel P. and Vially R., 2002, *Paris Basin, Petroleum potential*. IFP regional report.
- Dewolf Y. and Pomerol C., 2005, The Parisian Basin. In *The Physical Geography of Western Europe* (ed. E. A. Koster). Oxford University Press.
- Dezayes Ch., 2007, Réseau de fractures dans le Dogger de Bourgogne. Données pour le calcul de perméabilité équivalente., Rapport final BRGM/RP-54955-FR, 77 p., 35 fig., 7 tabl., 2 ann.
- DGA-IGME, 2006, Trabajos técnicos para la aplicación de la Directiva Marco del Agua en materia de aguas subterráneas. Caracterización adicional del Aluvial del Ebro-Zaragoza. Convenio de colaboración entre la Dirección General del Agua (DGA) y el Instituto Geológico y Minero de España, 112 pag.
- DHYCA, 1965, *Contribution à l'étude hydrogéologique de la nappe albienne dans le Bassin de Paris.*, rapport SG-RJM.
- Diersch, H.-J.G., 2005, FEFLOW Software —Finite Element Subsurface Flow and Transport Simulation System— Reference Manual. WASY GmbH, Berlin.
- Díez, J. B., Bourquin, S., Broutin, J., & Ferrer, J., 2007, The Iberian Permian Triassic 'Buntsandstein' of the Aragonian Branch of the Iberian Range (Spain) in the West-European sequence stratigraphical framework: a combined palynological and sedimentological approach. *Bulletin de la Société Géologique de France*, 178(3), 179-195.
- Dinis, J.L., Rey, J., Cunha, P.P., Callapez, P., and Pena dos Reis, R., 2008, Stratigraphy and allogenic controls of the western Portugal Cretaceous: an updated synthesis. *Cretaceous Research*, v. 29 (5-6), p. 772-780
- Duermael G., 1964, Problèmes hydrogéologiques en Champagne crayeuse entre la Marne et l'Aube. Rapport BRGM/64-DSGR-A-006. Master Thesis, Université de Paris.
- Dupaigne T., Bault V. and Meire B., 2019, Réalisation d'une carte piézométrique synchrone de la nappe de l'Albien et nouvelles thermométries du Bassin parisien., Rapport final BRGM/RP-68536-FR, 85 p., 52 ill., 5 ann.
- Edouard H., 2019, Bancarisation et synthèse des propriétés hydrodynamiques des aquifères du secteur de Brie, projet RGF - PRODHYGE., Rapport final BRGM-RP-70150-FR, 78 p., 19 ill., 14 ann.

- Enssle C. P., Cruchaudet M., Croisé J. and Brommundt J., 2011, Determination of the permeability of the Callovo-Oxfordian clay at the metre to decametre scale. *Physics and Chemistry of the Earth, Parts A/B/C* 36, 1669–1678.
- Espitalie J., Marquis F., Sage L. and Barsony I., 1987, Géochimie organique du bassin de Paris. *Rev. Inst. Fr. Pét.* 42, 271–302.
- Fleury M., Pironon J., Le Nindre Y. M., Bildstein O., Berne P., Lagneau V., Broseta D., Pichery T., Fillacier S., Lescanne M. and Vidal O., 2011, Evaluating sealing efficiency of caprocks for CO₂ storage: An overview of the Geocarbone Integrity program and results. *Energy Procedia* 4, 5227–5234.
- Gallois N., Viennot P. and Verjus P., 2015, Modélisation mathématique du comortement hydrogéologique des formations tertiaires du bassin parisien., ARMINES/MINES ParisTech, Fontainebleau.
- Gillon M., Crançon P. and Aupiais J., 2010, Modelling the baseline geochemistry of groundwater in a Chalk aquifer considering solid solutions for carbonate phases. *Applied Geochemistry* 25, 1564–1574.
- Gomez, J.J., Goy, A. and Barron, E., 2007, Events around the Triassic-Jurassic boundary in northern and eastern Spain. A review. *Palaeogeography, Palaeoclimatology, Palaeoecology*, 244, 89-110, DOI: <http://dx.doi.org/10.1016/j.palaeo.2006.06.025>
- Gonçalvès J., 2003, Modélisation 3D de l'évolution géologique du bassin de Paris : implication diagenétiques et hydrogéologiques. Thèse de doctorat, Université Paris VI - Pierre et Marie Curie, 351 p.
- Graciansky P. and Jacquin T., 2003, Evolution des structures et de la paléogéographie au passage Lias-Dogger dans le bassin de Paris d'après les données de la subsurface. *Bulletin De La Societe Geologique De France*.
- Grenet B., Haeffner H., Samson A. and Suzanne P., 1995, Stratégie d'exploitation des nappes de l'Albien et du Néocomien en région parisienne. In *Connaissance et valorisation des nappes profondes* colloque d'hydrotechnique, 152e session du Comité Scientifique et Technique de la SHF.
- Guillocheau F., Robin C., Allemand P., Bourquin S., Brault N., Dromart G., Friedenber R., Garcia J.-P., Gaulier J.-M., Gaumet F., Grosdoy B., Hanot F., Le Strat P., Mettraux M., Nalpas T., Prijac C., Rigollet C., Serrano O. and Grandjean G., 2000, Meso-Cenozoic geodynamic evolution of the Paris Basin: 3D stratigraphic constraints. *Geodinamica Acta* 13, 189–245.
- Hanot F. and Obert D., 1992, Tectonique du Bassin parisien par les déformations du toit de la Craie. In: La tectonique du Bassin parisien; séance conjointe. *AGPB-SGF. Bull. Inf. Géol. Bassin Paris* 29, 47–55.
- Hervé J. Y. and Ignatiadis I., 2007, Nappes de l'Albien et du Néocomien. Définition des conditions d'accès à la ressource géothermique en Île-de-France., Rapport final BRGM/RP-55990-FR, 55 p.
- Houel P., 2008, Description géologique et hydraulique préparatoire à l'interprétation de la zone PICOREF (SE du bassin de Paris). Project PICOREF., Rapport IFP n°60269.
- Housse B. and Maget P., 1976, Potentiel Géothermique du bassin parisien., BRGM - elf aquitaine BRGM/RR-29146-FR, 155 p.
- IGME, 2010, Plan de selección y caracterización de áreas y estructuras favorables para el Almacenamiento Geológico de CO₂ en España, Plan ALGECO2.
- IGME-DGA, 2009, Memoria de la actividad 2: apoyo a la caracterización adicional de las masas de agua subterránea en riesgo de no cumplir los objetivos medioambientales en 2015. Demarcación Hidrográfica del Ebro. 2009. Proyecto: encomienda de gestión para la realización de trabajos científico-técnicos de apoyo a la sostenibilidad y protección de las aguas subterráneas. Servicio de Información Documental del IGME. Código 63809. http://info.igme.es/SidPDF/139000/918/139918_0000031.pdf
- IGME-DGA, 2010, Encomienda de gestión para la realización de trabajos científico-técnicos de apoyo a la sostenibilidad y protección de las aguas subterráneas. Actividad 4: Identificación y caracterización de la interrelación que se presenta entre aguas subterráneas, cursos fluviales, descargas por manantiales,

zonas húmedas y otros ecosistemas naturales de especial interés hídrico Demarcación Hidrográfica del EBRO. Servicio de Información Documental del IGME.

Código 64040. http://info.igme.es/SidPDF/148000/21/148021_0000002.pdf

- Innocent C., Kloppmann W., Millot R. and Vaute L., 2021, A multi-isotopic study of the groundwaters from the Lower Triassic Sandstones aquifer of northeastern France: Groundwater origin, mixing and flowing velocity. *Applied Geochemistry* 131, 105012.
- Jurado, M.J., 1990, El Triásico y Liásico basal evaporíticos del subsuelo de la cuenca del Ebro. In: Ortí, F., Salvany, J.M. (Eds.), Formaciones evaporíticas de la Cuenca del Ebro y cadenas periféricas y de la zona de Levante. Enresa, pp. 21–28.
- Kloppmann W., Dever L. and Edmunds W. M., 1998, Residence time of Chalk groundwaters in the Paris Basin and the North German Basin: a geochemical approach. *Applied Geochemistry* 13, 593–606.
- Kullberg, J.C., Rocha R.B., Soares A.F., Rey J., Terrinha, P., Callapez, P. & Martins, L., 2006, A Bacia Lusitaniana: Estratigrafia, Paleogeografia e Tectónica. In R. Dias, A. Araújo, P.
- Lasseur E., Barthélémy Y., Le Nindre Y., Hubert G., Labat K., Nauroy J. F., Wertz F. and Bény C., 2009, Géocarbone - Intégrité volets 1 et 2 : synthèse des travaux de géologie., Rapport détaillé BRGM/RP-56926-FR, 545 p.
- Lerouge C., Grangeon S., Gaucher E. C., Tournassat C., Agrinier P., Guerrot C., Widory D., Fléhoc C., Wille G., Ramboz C., Vinsot A. and Buschaert S., 2011, Mineralogical and isotopic record of biotic and abiotic diagenesis of the Callovian–Oxfordian clayey formation of Bure (France). *Geochimica et Cosmochimica Acta* 75, 2633–2663.
- Lopez S., Hamm V., Le Brun M., Schaper L., Boissier F., Cotiche C. and Giuglaris E., 2010, 40 years of Dogger aquifer management in Ile-de-France, Paris Basin, France. *Geothermics* 39, 339–356.
- López Gutiérrez, J., 2015, Estimación de parámetros petrofísicos mediante criterio de experto. Servicio de recursos energéticos. Departamento de Investigación en Recursos Geológicos. Instituto Geológico y Minero de España. Servicio de Documentación.
- Maget P., 1991, SMAERC, Forage au Dogger de Saint Florent sur Cher, Programme complémentaire pour la détermination du potentiel., Rapport BRGM, R33148 CEN 4S/91, 19 p.
- Marina Rueda Fort, 2022, Caracterización a partir de diagrfias del posible almacén de CO2 de Lopín. Well log characterization of the possible Lopín CO2 store. Facultad de Ciencias Geológicas Universidad Complutense de Madrid Máster Universitario En Exploración De Hidrocarburos Y Recursos Minerales Curso 2021-2022
- Marques da Silva M.A., 1990, Hidrogeologia del sistema multiacuifero cretacico del Bajo Vouga - Aveiro (Portugal). PhD Thesis, Universitat de Barcelona, Barcelona, Spain.
- Marques da Silva, M.A., 1992, Camadas Guia do Cretácico de Aveiro e sua Importância Hidrogeológica. *Geociências, Rev. da Universidade de Aveiro*, Vol. 7, fasc. (12). pp. 110-124.
- Marti A., 2000, Agence de l'eau Seine-Normandie - Réalisation d'un modèle de gestion des aquifères de l'Albien et du Néocomien., *Hydroexpert. Rapport final de PHASE 3*, 113 p.
- Martin J., Giot D. and Nindre Y. L., 1999, Etudes préalables à la réalisation d'un modèle de gestion de la nappe de Beauce. Géométrie du réservoir et limites de la nappe de Beauce., BRGM/RR-40571-FR, 123p., 6tabl., 98 fig., 1 ann.
- Mas P., Calcagno P., Caritg-Monnot S., Beccaletto L., Capar L. and Hamm V., 2022, A 3D geomodel of the deep aquifers in the Orléans area of the southern Paris Basin (France). *Sci Data* 9, 781.
- Matray J.-M., Lambert M. and Fontes J. Ch., 1994, Stable isotope conservation and origin of saline waters from the Middle Jurassic aquifer of the Paris Basin, France. *Applied Geochemistry* 9, 297–309.
- Matray J.-M. and Fontes J.-C., 1990, Origin of the oil-field brines in the Paris basin. *Geology* 18, 501–504.

- Maurel C., Bugarel F. and Hamm V., 2020, Retour d'expérience des opérations de géothermie à l'Albien et au Néocomien du Bassin de Paris., Rapport final BRGM/RP-69437-FR, 134 p., 41 fig., 28 tab., 2 ann.
- Mégnyen C., 1979, Hydrogéologie du centre du bassin de Paris., BRGM Mémoire, 532 p.
- Mégnyen C., 1973, Premiers résultats de l'étude géologique et structurale du réservoir aquifère de la nappe des calcaires de Champigny en Brie., Bureau des Recherches Géologiques et Minières, Service géologique régional Bassin de Paris. Brie-Comte-Robert. Rapport BRGM 73-SGN-289 BDP.
- Mégnyen C., Diffre Ph. and Rampon G., 1970, Atlas des nappes aquifères de la région parisienne. BRGM Paris., Paris.
- Mégnyen C., Mégnyen F., Courel L., Durand M., Maget P., Maiaux C., Ménillet F. and Pareyn C., 1980, Synthèse géologique du bassin de Paris. Mémoire du BRGM n°101, 102, 103.
- Mégnyen C. and Turland M., 1967, Atlas des nappes aquifères du district de la région de Paris., BRGM.
- Michard G. and Bastide J.-P., 1988, Etude géochimique de la nappe du dogger du bassin parisien. *Journal of Volcanology and Geothermal Research* 35, 151–163.
- Miteco-Che, 2021a, Caracterización Adicional de las Masas de Agua Subterránea. MSBT: ES091MSBT058 - Aluvial del Ebro: Zaragoza. <https://www.chebro.es/documents/20121/420100/ES091MSBT058.pdf>
- Miteco-Che, 2021b, Caracterización Adicional de las Masas de Agua Subterránea. MSBT: ES091MSBT079 - Campo de Belchite. <https://www.chebro.es/documents/20121/420100/ES091MSBT079.pdf>
- Panetier J.-M., 1966, *Carte de la surface piézométrique de la nappe de la craie du Sénonais et du Gâtinais. Notice Explicative.*, Centre de Recherches et d'expérimentation du Génie rural. BRGM/66-DSGR-A113, 11 p., 1 carte., Centre de Recherches et d'expérimentation du Génie rural.
- Pardo, G., Arenas, C., González, A., Luzón, A., Muñoz, A., Pérez, A., Pérez-Rivarés, F.J., Vázquez-Urbez, M., y Villena, J., 2004, La cuenca del Ebro. En: *Geología de España* (J.A. Vera, Ed.), SGE-IGME, Madrid, 533-543.
- Peixinho de Cristo, F., 1985, Estudo hidrogeológico do sistema aquífero do Baixo Vouga. Divisão de Geohidrologia, Direção-Geral dos Recursos e Aproveitamentos Hidráulicos, Ministério do Equipamento Social, Coimbra, 57 pp.
- Peixinho de Cristo, F., 1998, Águas Subterrâneas no Baixo Mondego. Project Praxis XXI 2/2.1/CTA - 156/94.
- Pellenard P., Deconinck J.-F., Marchand D., Thierry J., Fortwengler D. and Vigneron G., 1999, Contrôle géodynamique de la sédimentation argileuse du Callovien-Oxfordien moyen dans l'Est du bassin de Paris: influence eustatique et volcanique. *Comptes Rendus de l'Académie des Sciences - Series IIA - Earth and Planetary Science* 328, 807–813.
- Pereira, P., Caeiro, M.H., Carneiro, J., Ribeiro, C., Silva, F., Casacão, J., Pina, B., Marques da Silva, D., 2023, Screening offshore geological structures for implementing a CO2 injection pilot in Portugal. The 12th Trondheim Conference on CO2 Capture, Transport and Storage, June 19 - 21, 2023.
- Pinheiro, L.M., Wilson, R.C.L., Reis, R.P., Whitmarsh, R.B. & Ribeiro, A., 1996, The western Iberian margin: A geophysical and geological overview. *Proceedings of the Ocean Drilling Program Scientific Results*, 149, p. 3-23
- Rachez X., 2007, Calcul de perméabilités directionnelles d'un milieu stratifié fracturé., Rapport final BRGM/RP-55470-FR, 61 p.
- Rahman, M.S., de Melo, M.T.C., 2022, Application of Numerical Model Coupled with Field Sampling to Investigate Increased Salinity in a Coastal Aquifer at Aveiro, Portugal. In: Arthur, S., Saitoh, M., Pal, S.K. (eds) *Advances in Civil Engineering. Lecture Notes in Civil Engineering*, vol 184. Springer, Singapore. https://doi.org/10.1007/978-981-16-5547-0_41

- Raoult Y., 1999, La nappe de l'Albien dans le bassin de Paris, de nouvelles idées pour de vieilles eaux. Thèse de doctorat, Université Pierre et Marie Curie - Paris VI.
- Raoult Y., Boulegue J., Lauerjat J. and Olive P., 1997, Geochemistry of the Albian aquifer in the Paris Basin area contributes to understanding complex hydrogeological behaviour. , 419–425.
- Raoult Y., Boulegue J., Lauerjat J., Violette S., De Marsily G. and Levassor A., 1999, La nappe de l'Albien dans la Bassin de Paris : de nouvelles idées pour de vieilles eaux. *Sciences Géologiques, bulletins et mémoires* Transferts dans les systèmes sédimentaires : de l'échelle du pore à celle du bassin, 117–119.
- Raymer, L.L., Hunt, E.R., and Gardner J.S., 1980, An improved sonic transit time-to-porosity transform. Paper presented at the SPWLA 21st Annual Logging Symposium, Lafayette, Louisiana, July 1980
- Reynaud A., 2012, Synthèse des mesures de terrain et des données de la chimie de l'eau 2003-2011., rapport AQUI'Brie, 232 p., 180 fig.
- Ribeiro, A., Kullberg, M. C., Kullberg, J. C., Manuppella, G., & Philipps, S., 1990, A review of Alpine tectonics in Portugal: Foreland detachment in basement and cover rocks. *Tectonophysics*, 184, p. 357-366
- Robin C., 1995, Mesure stratigraphique de la déformation : application à l'évolution jurassique du bassin de paris. These de doctorat, Rennes 1.
- Rojas J., Giot D., Le Nindre Y.-M., Criaud A., Fouillac C., Brach M., Menjoz A., Martin J.-C. and Lambert M., 1989, Caractérisation et modélisation du réservoir géothermique du Dogger Bassin Parisien, France., BRGM/IRG SNG 89/R 30 169, 251 p.
- Roux J. C., 2006, Aquifères & eaux souterraines en France. Ouvrage collectif sous la direction de J.C. Roux et sous le parrainage de l'Académie des Sciences., Tome 1. brgm édition, 479 p, BRGM.
- Rouxel-David E., 2002, Cartographie de la piézométrie de la nappe de la craie en Champagne-Ardenne., Rapport final BRGM/RP-52332-FR, 31 p., 4 pht.
- Saïag J., 2016, Caractérisation des hétérogénéités sédimentaires et pétrophysiques d'un réservoir carbonaté microporeux : le cas de la Craie (Crétacé supérieur, Bassin de Paris). These de doctorat, Dijon.
- Saraiva, M.P.S., Barradas, J. & Marques da Silva, M.A., 1983, Aquífero Cretácico de Aveiro – subsídios para a sua caracterização hidrogeológica. *Hidrogeologia y Recursos Hidráulicos*, VII, AEHS, Madrid, 41-49.
- Sarrochi C. and Levy-Lambert H., 1966, La nappe aquifère de l'Albien dans le bassin de Paris., *Annales des Mines*, 1-21 p.
- Schomburg S., Gateau Ch., Goyénèche O., Vernoux J. F. and Denis L., 2005, Guide d'aide à la décision pour l'installation de pompes à chaleur su nappe aquifère en région Ile-de-France - Atlas hydrogéologique., Rapport final BRGM/RP-53306-FR, 94 p., 10 fig., 28 cartes, 31 pl.h.t.
- Seguin J. J., Castillo C. and Arnaud L., 2015, Modélisation des nappes de l'Albien et du Néocomien., Rapport final BRGM/RP-64873-FR, 271p., 152 fig., 21 tabl., 8 ann.
- Serrano, J.A.P.F., Garcia, P.C.S, 1997, Piezometria da Região Centro. Direcção Regional do Ambiente do Centro. Coimbra. 108 pp.
- SNIRH, 2023, Sistema Nacional de Informação de Recursos Hídricos. Available at the website: <https://snirh.apambiente.pt/index.php?idMain=1&idItem=1.4&uh=O>. Accessed 16 July 2023
- Velho, J.A.G.L., 1989, Hidrogeologia do Anticlinal de Verride. MSc thesis. Universidade de Lisboa. 163 pp.
- Vernoux J. F., Maget P., Afzali H., Blanchin R., Donsimoni M. and Vairon J., 1997, Synthèse hydrogéologique du Crétacé inférieur du bassin de Paris., rapport DSGR/IDF BRGM/RR-39702-FR,.
- Vernoux J. F. and Manceau J. C., 2017, Risques de pollution des nappes de l'Albien et du Néocomien par les forages profonds du bassin parisien., Rapport final BRGM/RP-66820-FR, 98 p., 31 ill., 16 tabl., 2 ann.

- Vernoux J. F. and Martin J., 2003, Etude de la délimitation des zones d'alimentation des captages contaminés par les nitrates en Seine-et-Marne., Rapport final BRGM/RP-52561-FR, 54p., 10fig., 6tabl., 4ann., 2 planches.
- Wei H. F., 1986, Circulation du fluide géothermal du Dogger dans le bassin de Paris. Mémoire de DEA, Rapport du CIG. LHM/RD/86/67, Ecole des Mines de Paris.
- Wei H. F., Ledoux E. and De Marsily G., 1990, Regional modelling of groundwater flow and salt and environmental tracer transport in deep aquifers in the Paris Basin. *Journal of Hydrology* 120, 341–358.
- Wilkinson, M. 2023. Deliverable 2.7 - Conceptual Geological Models of the Portugal, Spain and France. PilotSTRATEGY project. <https://pilotstrategy.eu/about-the-project/work-packages/geo-characterisation>
- Wilson, R. C. L., Hiscott, R. N., Willis, M. G., & Gradstein, F. M., 1989, The Lusitanian basin of west-central Portugal: Mesozoic and Tertiary tectonic, stratigraphy, and subsidence history. In *Extensional Tectonics and Stratigraphy of the North Atlantic Margins*, edited by A. J. Tankard and H. R. Balkwill, AAPG Mem., 40, p. 341 – 361
- Worden R. H. and Matray J.-M., 1995, Cross formational flow in the Paris Basin. *Basin Research* 7, 53–66.
- Yven B., Sammartino S., Géraud Y., HOMAND F. and Villiéras F., 2007, Mineralogy, texture and porosity of Callovo-Oxfordian argillites of the Meuse/Haute-Marne region (eastern Paris Basin). *Bulletin de la Societe Geologique de France* Mém. Soc. géol. France, 73–90.

